Running the Gauntlet of the Bacterial Cell Wall

Amirah Alofi

A thesis submitted for the degree of **Doctor of Philosophy.**

Newcastle University

Institute for Cell and Molecular Biosciences

July 2024

Abstract

In nature, bacteria have a variety of shapes, from simple cocci and rods to more complicated spiral or appendage structures. In their life, they need a strong exoskeleton that can maintain their shape during growth and protect them from changes in environmental conditions. This rigid structure is generally provided by the cell wall and is considered an essential component in the bacterial cell. However, the cell wall represents a complex logistical problem in terms of the controlled synthesis and degradation that is required to maintain shape, permit enlargement, and prevent lysis. Significant advances have been made in understanding wall synthesis, and in Gram-negative bacteria synthesis can be integrated with degradation. But, for Gram-positive bacteria the regulation of cell wall degradation is poorly characterised. Genetically the genes encoding the key enzymes are known and the expression of these enzymes are known to be highly regulated. However, understanding how the biochemical activity of these enzymes is restricted and regulated, presumably within the cell wall or on the outside surface of the cell is not clear. The results obtained in this laboratory have indicated that altered cell wall composition or media components modulate the level of the hydrolysis enzyme activity in some way during vegetive growth. This study aimed to extend our understanding of the autolytic systems and how the enzymatic activity may be regulated by components of the cell envelope or minor modifications of the cell wall material.

Acknowledgments

I would like to express my deepest gratitude to the many people in my life who have made this amazing journey possible.

First, I would like to thank my mentor and supervisor, Richard Daniel, for his support, guidance, and valuable advice that always kept me on the right path. Whenever I encountered challenges or had questions arise during the experiments or the writing process, he made himself readily available to provide his guidance and expertise. His dedication to simplifying the complicated issues I faced throughout my PhD has been invaluable to me. For Richard Daniel group, past and present, thank you for your generous help and for creating a nice working environment.

A special thanks to my parents (Hanan and Muaweed) for their sacrifices to ensure my happiness and success. Their unconditional love and unwavering trust have been a source of my strength and determination. Thank you for supporting me and believing in me during my academic journey. Words cannot fully express the depth of my appreciation for everything you have done. I also extend a heartfelt thank you to my brothers and sisters for always being by my side and for their constant encouragement.

My deepest thanks are extended to my best friends, Alaa and Taghreed. Alaa, you are the one who encouraged me to start this journey. I am deeply grateful that we have been on this journey together from the beginning until the very end. Your support through this has been invaluable. Alaa and Taghreed, I feel incredibly fortunate to have you, both of you are amazing, highly motivated, and wonderful friends. Thank you for always being around for encouragement, sharing the hard times, and making the most of the good times.

I would like to acknowledge the entire faculty in the Centre for Bacterial Cell Biology (CBCB) specially the 4th floor for their help when needed. An additional thank you goes to Dr. Aurelie Guyet and Dr. Stepan Fenyk for the invaluable advice they have provided to me during my experiments. Thank you also to Dr. Andrew Porter and Dr. Pawel Palmowski for their assistances with Mass spectrometry and analysing the data.

I remain forever appreciative for every individual I had the opportunity to meet during my academic journey, from whom I have gained new insights, inspiration, and skills. Last but not least, I would like to express my gratitude for government of Saudi Arabia for their financial support, which enabled me to complete this amazing educational journey.

Contents

List of Tables

List of Figures

List of Abbreviations

Amp	Ampicillin
ATP	Adenosine triphosphate
B. subtilis	*Bacillus subtilis*
bp	Base pair
BSA	Bovine serum albumin
$CaCl_2$	Calcium chloride
CAA	Casamino acids
°C	Degree centigrade
dH_{2O}	Deionized water
Cam	Chloramphenicol
C	C-terminal
E. coli	*Escherichia coli*
EDTA	Ethylenediaminetetraacetic acid
Erm	Erythromycin
FM5-95	*N*-(3-trimethylammoniumpropyl)-4-(6-(4-(Diethylamino)phenyl) hexatrienyl)Pyridinium Dibromide
G	Glucose
Glc*N*Ac	*N*- acetylglucosamine
IPTG	Isopropyl-b-D-thiogalactopyranoside
Kan	Kanamycin
Kb	kilobase
kDa	Kilo Dalton
L	Litre
LB	Luria-Bertani broth
LiCl	Lithium chloride
LTA	Lipoteichoic acid
Log	Logarithmic
MW	Molecular weight
M	Molar
mM	Millimolar
mg	Milligram
mg/ml	Milligram per millilitre

$MgSo_4$/Mg	Magnesium sulphate
ml	Millilitre
min	Minute(s)
Mur*N*Ac	*N*- acetylmuramic acid
N	N-terminal
NA	Nutrient agar
NaCl	Sodium Chloride
NB	Nutrient broth
OD_{600}	Optical density measure at (600nm)
O/N	Overnight
PBS	Phosphate buffer saline
PAB	Penassay broth (Antibiotic media No.3)
PCR	Polymerase chain reaction
pH	Potential hydrogen
PG	Peptidoglycan
PVDF	Polyvinylidene difluoride
rpm	Revolutions per minute
spec	Spectinomycin
SMM	Standard minimal media
SDS-PAGE	Sodium dodecyl sulphate-polyacrylamide gel electrophoresis
SDS	Sodium Dodecyl Sulphate
SSC	Saline sodium citrate
SpA	Protein A
SpA’	Protein A lacking LysM and LPXTG
TAE	Tris-Acetate-EDTA
TA	Teichoic acid
TES buffer	Tris- EDTA- Sodium buffer
Tris	Tris(hydroxymethyl)aminomethane
µg	Microgram
µM	Micromolar
V	Voltage
WTA	Wall teichoic acid
%	Percentage

Chapter 1: Introduction

1.1 General Introduction

Bacteria are primarily unicellular organisms, but some can be multicellular (Myxobacteria) that have adapted to live in almost every environment on Earth (Claessen *et al*., 2014). The basic structure of the bacteria cell consists of the outer layer (cell wall), which is a strong exoskeleton that can maintain its shape during growth and protect it from changes in environmental conditions (described in depth in Section 1.3). Beneath this cell wall, a phospholipid bilayer (cell membrane) acts to restrict the movement of molecules into the cell. This membrane also acts as a surface for the assembly of the PG, with the majority of the proteins involved being predominantly on the exterior face of the membrane or acting as transport systems for cytoplasmically synthesised precursors to the outside of the cell. Lastly, the space enclosed by the membrane is defined as the cytoplasm where the proteins are synthesized and genetic material is maintained (Hobot *et al*., 1984a; Silhavy *et al*., 2010a). Evolution has generated a multitude of variations to this basic structure. At a basic level, these can be discriminated between using staining techniques combined with microscopy, the best-known being the Gram stain. This provided a way to differentiate between two variations in the structure of the cell wall that exist and gave the definition of Gram-positive bacteria, which have a thick cell wall, and Gram-negative bacteria, where the cell wall is much thinner (Bartholomew & Mittwer, 1952).

In nature, bacteria have various shapes, from simple cocci and rods to more complicated spiral or appendage structures that are related to their function to adapt to different environments. Depending on their morphologies, bacteria are divided into five basic groups: rod-shaped (*Bacillus subtilis*), coccus (*Staphylococcus aureus*), appendaged (*Caulobacter crescentus*), spirillum (*Spirochetes/ Treponema pallidum*), and club-shaped rod (*Corynebacteria*/ *Corynebacterium glutamicum*) (Cabeen & Jacobs-Wagner, 2005) (Figure 1.1). Regardless of their shape differences, most of the bacteria production occurs through a process called binary fission where the single chromosome is replicated, and the copies segregate to opposite ends of the cell. The cell then enlarges and divides generally, resulting in two identical daughter cells. Under optimal conditions, some bacteria can grow and divide rapidly every 20 minutes or less. This growth indicates that the limiting factors for their multiplication are the synthesis and assembly of precursors (Adams & Errington, 2009).

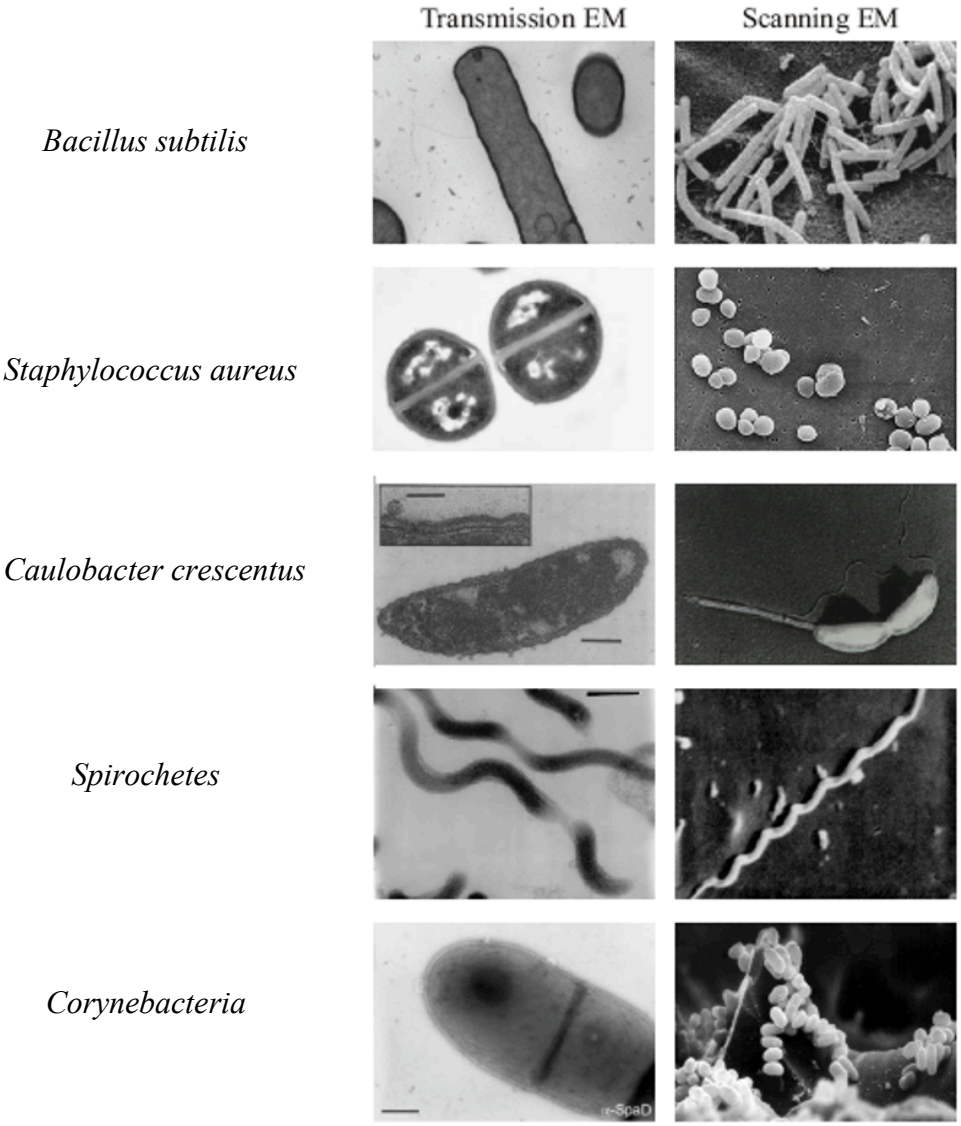

Figure 1. 1 Bacterial morphologies

Bacterial morphologies are divided into: rod-shaped (*Bacillus subtilis*), coccus (*Staphylococcus aureus*), and appendaged (*Caulobacter crescentus*), spirillum (*Spirochetes/ Treponema pallidum*), and club-shape rod (*Corynebacteria/ Corynebacterium glutamicum*). Figure adapted from presentation slides from R. Daniel.

1.2 Bacteria and research models

Bacteria have a multitude of potentially useful properties (e.g., biosynthesis of complex molecules that cannot be synthesised chemically) if they can be exploited. In this respect, there are two options: isolate the microorganism with the desired properties and try to manipulate it, probably through genetic changes to optimize the useful aspects and remove the unwanted. The alternative is to try to transfer the function of interest into an established model system. For this option, a comprehensive understanding of the biology of the model

bacterium is needed to ensure that processes are optimal. In this respect, research has primarily focused on two specific bacterial species. *Escherichia coli* is the best-characterised Gram-negative microorganism and has significance in both clinical research, as strains can be pathogenic, as well as microbiome research, as the organism is part of the natural gut flora (Hartl & Dykhuizen, 1984). In contrast, *Bacillus subtilis* has been established as the representative Gram-positive bacterium. The reasons for this are multifold, but primarily because it can be genetically manipulated easily, and the fact that it is able to change into a dormant state (sporulation) provided a simple model for understanding how cell differentiation could be regulated (J. Chen *et al*., 2015; Liu *et al*., 2017; van Dijl *et al*., 2001). The choice of these bacteria is essentially historical but seems to primarily be the result of the easy identification of methods to genetically manipulate the organisms, something that is often problematic in most other bacterial species, although as molecular biological methods have advanced, this limitation seems to be less of a problem. However, both model systems provide helpful insight into the key cellular processes that seem to be conserved in most free-living bacteria. They have also been adopted for industrial processes to permit the production of both biomolecules (e.g. vitamins or precursor metabolites that cannot be easily chemically synthesised) and enzymes and as such understanding basic cellular processes offers routes to the optimization of the fermentation process in several ways (Blount, 2015; Schallmey *et al*., 2004). Understanding cell envelope stability and turnover has applications in minimizing cell lysis during extended cultivation and being able to alter cell morphology potentially aids cell separation techniques. Both properties have importance for the application of bacterial systems in large-scale processes where the product may be in the culture media or retained in the biomass.

This project has focused on understanding cell wall metabolism in *B. subtilis* after synthesis, which is an aspect that has not been intensively studied. Additionally, since the cell wall is not enclosed by an outer membrane, the control and regulation of the enzymes involved is complicated by the fact that secreted enzymes are potentially lost to the environment unless there are mechanisms to retain them as they act to modify the wall. This, in turn, imposes a need for robust regulatory mechanisms for “active” enzymes that operate at a distance from the cell to ensure their activity does not compromise the integrity of the cell.

1.3 Bacterial cell wall structure

The bacterial cell wall is a complex and dynamic structure containing multiple layers and components. The cell wall is considered an essential structure that maintains the bacterial shape integrity and protects the cell against osmotic pressure. Bacteria can be taxonomically divided into two groups based on cell wall properties using a Gram stain (Bartholomew & Mittwer, 1952). The basic idea of the Gram stain is to define the bacteria depending on the retention of the stain in the cell wall. On this basis, a thick cell wall will retain the stain, which is called Gram-positive, while the bacteria that do not retain the stain are called Gram-negative. The cell envelope structure of Gram-negative bacteria has three distinct parts: the outer membrane (OM), which is the phospholipid bilayer, and the inner layer membrane, which is the cytoplasmic membrane (CM). Among the OM and CM, there exists a thin layer of peptidoglycan (approximately 15 nm) and a periplasmic space (Hobot *et al.*, 1984a). In contrast, Gram-positive bacteria contain the CM and a thick layer of peptidoglycan (approximately 30-100 nm), exposed to the extracellular environment (Hobot *et al*., 1984b; Rohde, 2019; Schleifer & Kandler, 1972; Sun *et al*., 2022).

Peptidoglycan (PG) is the common component found in both cell walls of Gram-negative and Gram-positive bacteria (Silhavy *et al*., 2010a). The chemical structure of PG in both is similar and is considered an essential structural component under normal conditions. PG is proposed to be a rigid and dynamic structure that is synthesized around the cell membrane and acts to maintain the stability and shape of the bacterial cell (Perkins, 2012; Rohde, 2019). In this study, the focus was primarily on the cell wall of the Gram-positive bacterium *Bacillus subtilis* (*B. subtilis*) as a model organism. *B. subtilis* is a rod-shaped bacteria with a thick layer of PG decorated with various other polymers. Throughout this study, peptidoglycan hydrolysis enzymes are the main focus.

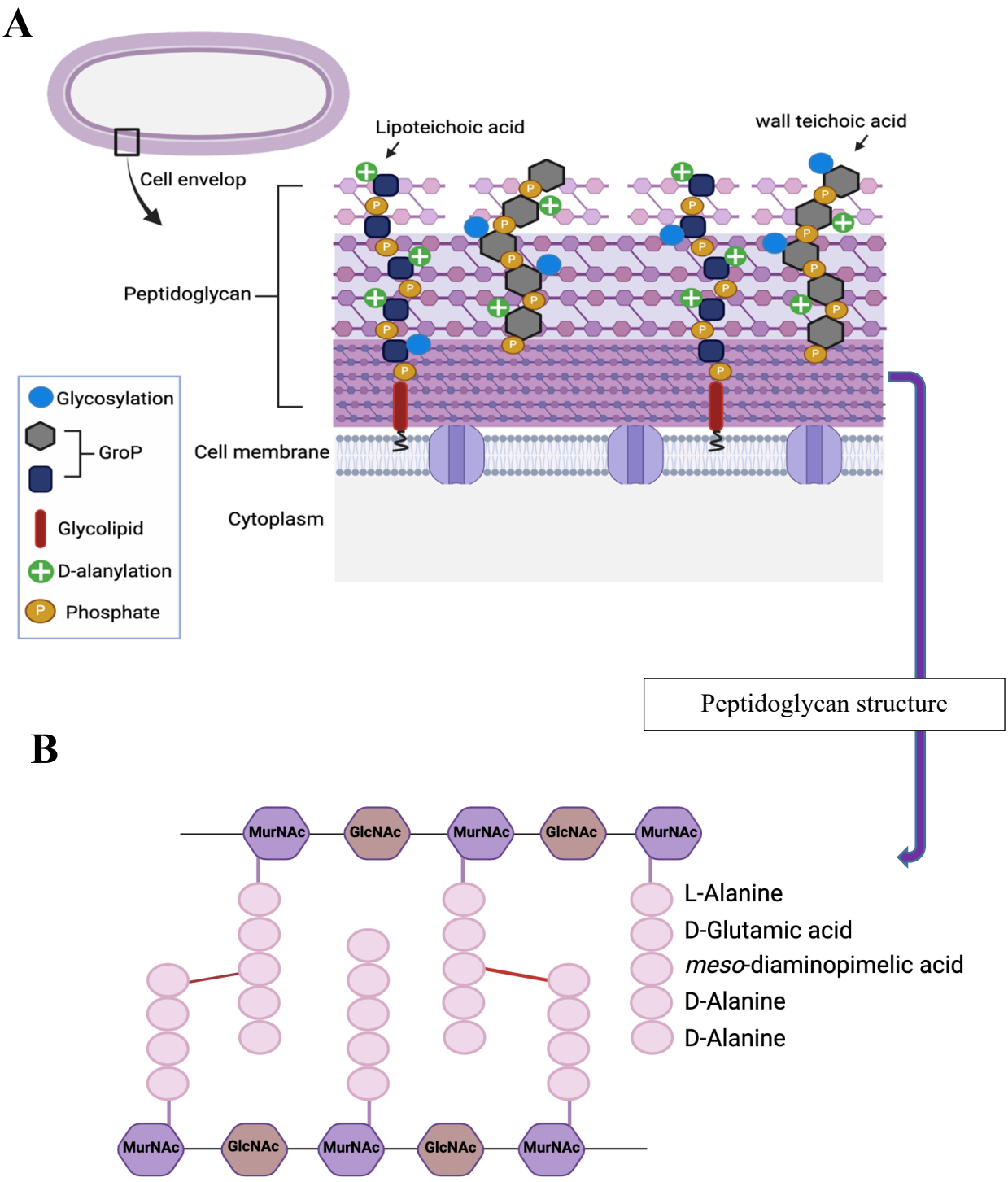

Figure 1.2 The general perception of the cell envelope structure in Gram-positive bacteria

(A)The diagram demonstrates the main components of the bacterial cell envelope, which are the cell wall (peptidoglycan, wall teichoic acid, and lipoteichoic acid) and cell membrane. (B) An illustration of the chemical structure of the PG. PG contains the glycan strand (Glc*N*Ac and Mur*N*Ac) and the stem peptides (L-alanine, D-glutamic acid, *meso*-diaminopimelic acid, D-alanine, and D-alanine, respectively). The stem peptide is linked to the glycan strand at Mur*N*Ac. The cross-linkage occurs at the *meso*-diaminopimelic acid in one chain to the D-alanine of the next chain. Image generated by BioRender.com.

1.4 Peptidoglycan structure

The main structure of the cell wall is the PG, a thick layer surrounding the cell membrane, as mentioned previously in Section 1.3. The PG is composed of glycan strands made up of polymers containing the alternating disaccharides N-acetylglucosamine (Glc*N*Ac) and N-acetylmuramic acid (Mur*N*Ac), which are joined by β-1,4 linkages. In glycan strands, the stem peptide attached to disaccharide by an amide bond between the lactyl group in Mur*N*Ac and the amino group in L-alanine. The stem peptides are made up of L-alanine (L-Ala), D-glutamic acid (D-Glu), *meso*-diaminopimelic acid (*m*DAP), D-alanine, and D-alanine (D-Ala), at positions 1 to 5, respectively (Figure 1.2B) (Archibald *et al*., 1993; Weidel *et al*., 1960; Weidel & Pelzer, 1964; Work, 1961). Variation does exist between species and generally occurs at the third position, which can be either *meso*-diaminopimelic acid or L-lysine. The *meso*-diaminopimelic acid is found in *Bacillus*, *Mycobacterium*, *Lactobacilli*, and Gram-negative bacteria, while L-lysine is present in other Gram-positive bacteria. In nascent PG, the cross-linking takes place between the *meso*-diaminopimelic acid at position three in one chain and the D-alanine at position four in the next chain, and this leads to the loss of the D-ala at position 5 (Figure 1.2B) (Schleifer & Kandler, 1972; Vollmer *et al*., 2008).

1.4.1 PG modifications (variation)

In mature PG, some modifications occur that alter the cell wall properties and protect the cells from lysozymes such as *N*-deacetylation , *O*-acetylation, and amidation. The *N*-deacetylation is modified by removing the N-acetyl group of the Glc*N*Ac to convert to glucosamine (Glc*N*). This modification is observed in the PG of *S. pneumoniae, Bacillus anthracis,* and *B. subtilis* (Davis & Weiser, 2011; N *et al*., 1982; Rajagopal & Walker, 2017). The *O*-acetylation occurs in the Mur*N*Ac residues at the C6 position and is found in many Gram-positive bacteria such as *B. subtilis, Bacillus cereus, Staphylococcus aureus, and Staphylococcus pneumonia* and Gram-negative bacteria such as *Neisseria gonorrhoeae, Neisseria meningitidi*s (Bera *et al*., 2005; Davis & Weiser, 2011; Laaberki *et al*., 2011; Mi *et al*., 2006; Rajagopal & Walker, 2017). The amidation is only found in Gram-positive bacteria, which amidate the carboxy group of the D-glutamic acid or *m*DAP at the second and third positions of the stem peptides, respectively. In *S. pneumoniae* and *S. aureus,* the D-glutamic acid is amidated to D-iso-glutamine by MurT/GatD amidotransferase complex (Figueiredo *et al*., 2012; Morlot *et al.*, 2018; Münch *et al*., 2012). In *B. subtilis*, the amidation occurs on the *m*DAP only by the action of the amidotransferase AsnB. AsnB is predicted to be a cytoplasmic protein, which suggests that the *m*DAP amidation occurs on PG

precursors inside the cell. It has been shown that cells lacking the gene encoding AsnB lead to cell deformation and eventually lysis without excess Mg, revealing the critical role of the *m*DAP amidation in cell wall homeostasis. Furthermore, the absence of the amidated *m*DAP causes deregulation of PG hydrolysis (Dajkovic *et al*., 2017). (Described in depth in Chapter 5).

1.4.2 Biosynthesis pathway of peptidoglycan

The biosynthesis of glycan polymers of the PG occurs in three distinct stages, starting in the cytoplasm through the assembly of simple precursors and then in the cell membrane, where the lipid attaches to the PG precursors to enable transport to the outer surface. The final stage takes place at the cell membrane surface to polymerize the PG mesh. The pathway of PG biosynthesis is well-conserved in most bacteria (Figure 1.3) (Scheffers & Pinho, 2005; Typas *et al*., 2012). The first step in PG synthesis is performed after forming Uridine diphosphate N-acetylglucosamine (UDP-Glc*N*Ac) from fructose-6-phosphate by a series of enzymes: GlmS, GlmM, and GlmU. The UDP-Mur*N*Ac is then formed from UDP-Glc*N*Ac by catalytic activity of MurA and MurB enzymes. The stem peptides (pentapeptides) are attached to UDP-Mur*N*Ac by a set of enzymes: MurC, MurD, MurE, and MurF, which act sequentially. The UDP-MurNAc-pentapeptides are then transferred to the cell membrane to be coupled to bactoprenol (lipid carrier) by MraY to produce lipid-I. Next, the MurG enzyme binds the UDP-Glc*N*Ac to lipid I to form lipid II, the PG precursor (Figure1.3). The flippase enzyme MurJ flip the PG precursor (lipid II) across the cell membrane. The final steps of PG assembly occur on the cell surface, where the PG precursor is polymerised into glycan strands by transglycosylation and where cross-linking of stem peptides occurs by transpeptidation; these enzymes are catalysed by RodA and penicillin-binding proteins (PBPs), respectively. Once the PG assembly is accomplished, the lipid carrier (bactoprenol) is recycled to the cytoplasm to be used again for the next PG subunit (Koch & Doyle, 1985; Scheffers & Pinho, 2005; Takahashi *et al*., 2016). The length of the glycan strands varies between species but does not correlate with the thickness of the PG layer, as the Gram-positive bacteria with a thick cell wall with either long (*B. subtilis*) or short (*S. aureus*) (Wang *et al*.,2008).

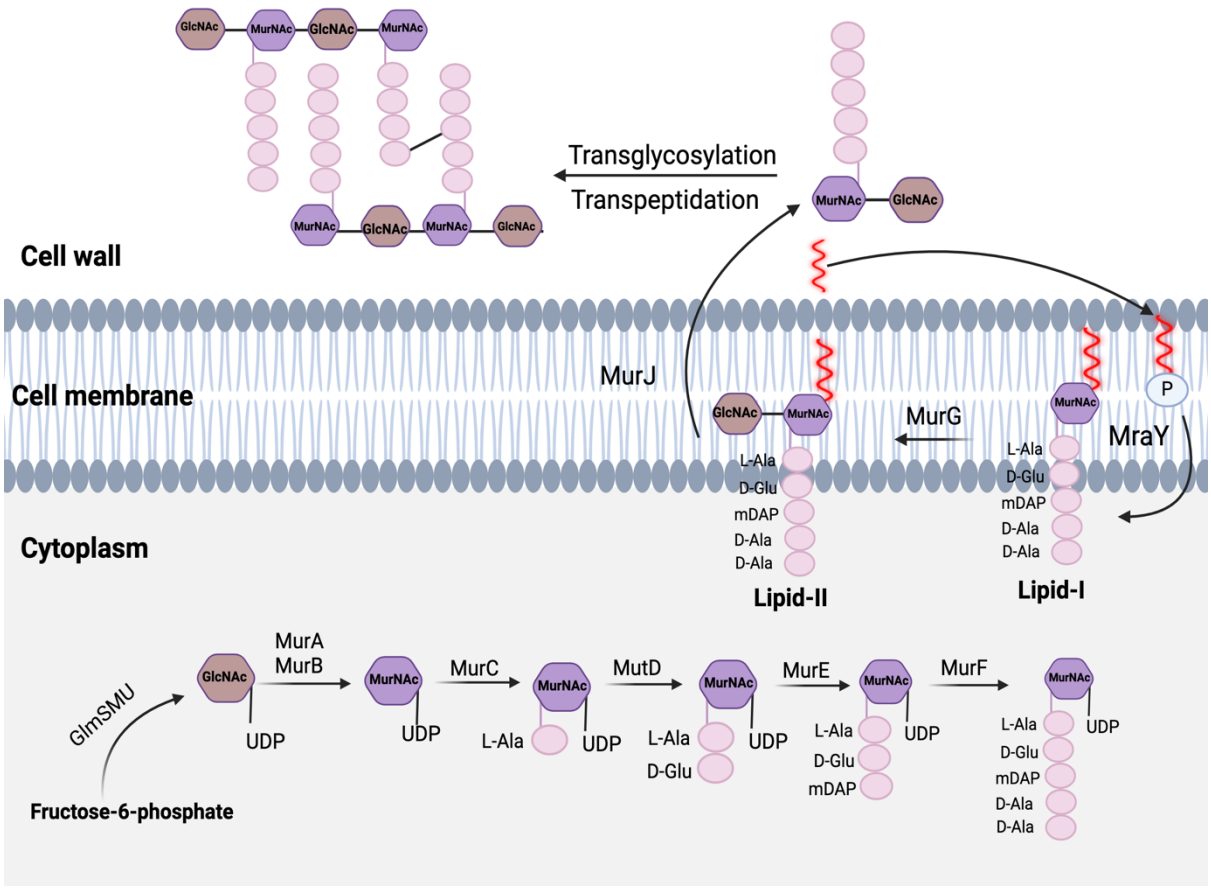

Figure 1.3 Peptidoglycan biosynthesis pathway

The scheme demonstrates the initial steps of PG synthesis in Gram-positive bacteria. The biosynthesis starts in the cytoplasm where the UDP-Mur*N*Ac and the stem peptides are synthesize. These are then translocated to the cell membrane to bind to the bactoprenol to produce lipid-I. Following binding to Glc*N*Ac to generate PG precursors (lipid-ll), these PG precursors then flip across the cell membrane into the cell wall to assemble the PG by transglycosylation and transpeptidation reaction. Image generated by BioRender.com.

1.4.3 Polymers associated with the peptidoglycan in Gram-positive bacteria

Intimately associated with the PG, there are a set of anionic polymers, collectively called teichoic acids (TAs) that can either be attached to the PG or the cell membrane and are proposed to project through the mesh-like structure of the PG (Rohde, 2019). There are two major types of TAs: wall teichoic acid (WTA), which covalently attached to the PG, and lipoteichoic acid (LTA), which anchored to the cell membrane via glycolipid (Figure 1.2A) (S. Brown *et al*., 2013; Percy & Gründling, 2014a; Swoboda *et al*., 2010). In addition, there may be other sugar polymers that are can be linked to the cell wall or simple on the surface of the cell resulting in a capsule or slime like layer. The additional polymers are absent in model strains of *B. subtilis* and are only partially studied. Interestingly the mechanism of attachment to the PG seems to be shared with the wall associated teichoic acids (Candela & Fouet, 2006).

The wall teichoic acid is a polymer chain of glycerol (GroP)- or ribitol (RboP)-phosphate residues that are covalently linked to peptidoglycan at Mur*N*Ac via a phosphodiester bond (Figure 1.2A). The poly RboP can be found in the WTA of *S. aureus* and *B. subtilis* (W23), while the poly GroP is found in *Lactococcus lactis* and *B. subtilis* (168) (S. Brown *et al*., 2013; Han *et al*., 2023). The GroP and RboP seems to be functionally interchangeable (Lazarevic et al., 2002) (exchanging the genes for GroP WTA with those for RboP WTA synthesis does not seem to have physiological consequences (K. Divine, unpublished)). Under phosphate-limited conditions, some strains of *B. subtilis* produce teichuronic acids that substitute for the wall teichoic acid and have a similar biosynthetic process but utilise uronic acid rather than phophoglycerol as the polymer subunits (S. Brown *et al*., 2013; Neuhaus & Baddiley, 2003; Rajagopal & Walker, 2017; Swoboda *et al*., 2010).

The WTA biosynthesis starts in the cytoplasm, and the enzymes involved are named Tag for teichoic acid glycerol. First, UDP-Glc*N*Ac is transferred to undecaprenyl phosphate by glycosyltransferase TagO. TagO is a reversible enzyme considered the first catalytic enzyme in WTA synthesis (Soldo *et al*., 2002). After that, an *N*-acetylmannosaminyl transferase (TagA) attaches a ManNAc to Glc*N*Ac to from β-linked disaccharide linkage unit. The glycerophosphate transferase TagB will then transfer a single phosphoglycerol from CDP-glycerol to be attached to ManNAc on the disaccharide linkage unit. Around 35 or more of the glycerol phosphate units were then attached to the disaccharide linkage unit to polymerize the chain of WTA by TagF. Once the WTA is assembled inside the cell and prior to export, the cytoplasmic glycosyltransferase TagE modifies the main chain of the WTA with glycose residues from UDP-glucose (WTA glycosylation). The WTA polymers are then translocated through the cell membrane by two-component ABC transporters TagG and TagH. Under phosphate-limited conditions, some strains of *B. subtilis* produce teichuronic acids that substitute for the wall teichoic acid and have a similar biosynthetic process but utilise uronic acid rather than phophoglycerol as the polymer subunits (S. Brown *et al*., 2013; Neuhaus & Baddiley, 2003; Rajagopal & Walker, 2017; Swoboda *et al*., 2010).

Lipoteichoic acid (LTA) is a polyglycerol-phosphate (PGP) chain that is anchored to the cell membrane via glycolipid and probably extends into the PG layers. The main structure of the LTA is composed of glyucolipid anchors to the cell membrane, and the chain consists of repeating units of polyglycerol phosphate (GroP) (Figure 1.1A) (Percy & Gründling, 2014b). The synthesis pathway for the LTA is completely different from WTA. The glycolipid anchor, diglucosyl diacylglycerol (Glc_2-DAG), is synthesized in the cytoplasm by

the UgtP enzyme, transferred two glucose molecules moieties from UDP-Glc to diacylglycerol (DAG) and is flipped through the cell membrane to the cell surface by enzymes called LtaA (Candela & Fouet, 2006; Lazarevic *et al*., 2005). The polyglycerol-phosphate is then synthesized by LTA synthase enzymes on the outside of the membrane using DAG. In *S. aureus,* LtaS is the only enzyme that responsible for creating the GroP chain (Grϋndling & Schneewind, 2007). In contrast, the situation is more complex in *B. subtilis,* which has three enzymes: LtaS, YqgS, and YfnI, that seem to be functionally interchangeable (Wörmann *et al*., 2011). However, LtaS is considered one of the most important enzymes for the LTA chain. The LTA can be modified with sugars, but the enzymes involved in LTA glycosylation have not been fully identified (Schirner, Marles-Wright, *et al*., 2009).

The backbone of both TAs (WTA and LTA) can also be modified by the addition of D-alanine esters after passing through the cell membrane. This D-alanylation seems to occur first on the LTA and then it is transferred to WTA. This process is mediated by the activity of four enzymes encoded by the *dltACBD* operon. As the linked D-alanine carries a positive charge, the cell surface charge can be modulated by D-alanylation (Reichmann *et al*., 2013; Wecke *et al*., 1997).

1.4.3.1 Teichoic acid role in cell wall

Both teichoic acid polymers are involved in critical functions in the cell wall, although it seems that they may be partially functionally redundant, in that Schirner *et al*., 2009 reported that *B. subtilis* requires at least one functional TA synthesis system (WTA or LTA) to survive, as the strains generated defective for both were unculturable. This suggests that these polymers have redundant functions and are essential for cell growth. The absence of TAs has been shown to have a pleomorphic effect on cell morphology (Schirner, Marles-Wright, *et al*., 2009). A previous study demonstrated that in both *B. subtilis* and *L. monocytogenes,* cells become spherical, and grow slowly when teichoic acid synthesis is blocked (*tagO* mutants) (Boylan *et al*., 1972; Eugster & Loessner, 2012). Defects in LTA synthesis (*ltaS*) show species-dependent effects. In *S. aureus*, the strain lacking *ltaS* increased in size and showed an irregular form at the division septa (Grϋndling & Schneewind, 2007). In *L. monocytogenes,* cells lacking *ltaS* showed defects in division septum formation and become temperature sensitive (Webb *et al*., 2009). In *B. subtilis*, the deletion of *ltaS* resulted in a filamentous phenotype suggesting defective cell division caused by deranged localisation

of FtsZ, one of the critical steps in the cell division process (Schirner, Marles-Wright, *et al*., 2009). In addition, the D-alanylation of both LTA and WTA seems to play a critical role in regulating the autolytic enzymes activity in the cell wall. In *B. subtilis,* the activity of autolytic enzymes has been found to be significantly increased in strains that lacked D-alanine ester modification on TAs, presumably resulting in elevated negative charge in and on the cell envelope. (Wecke *et al*., 1997).

1.4.4 PG dynamics

In order for bacterial cells to grow and divide, the PG formations occur from inside to outside the cell, meaning a new layer is synthesized near the cell membrane. This layer keeps pushing out and stretching until it reaches the outer surface of the cell wall in order to enlarge cells and ultimately becomes degraded (Figure 1.4) (Koch & Doyle, 1985). Insertion of a new layer is carried out by the action of synthesis enzymes known as glycosyltransferases and transpeptidases. These enzymes polymerize the glycan strand and form the cross-linkage, respectively (as previously described in Section 1.4.2) (Scheffers & Pinho, 2005). The old outer layer in the cell wall is degraded by distinct sets of enzymes referred to autolytic enzymes, which cleave the bond within the PG (described in depth Section 1.5) (Blackman *et al*., 1998; Smith *et al*., 2000). To ensure growth, the balance between the synthesis and hydrolysis enzymes is required to avoid cell lysis (Blackman *et al*., 1998; Takahashi *et al*., 2016).

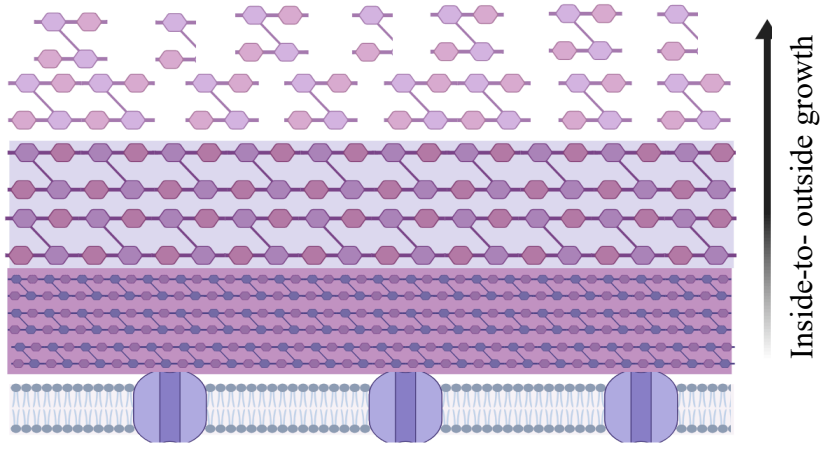

Figure 1.4 Peptidoglycan dynamic

The diagram illustrates the mechanism of how the PG enlarges. A new layer of PG inserted into the cell wall, where the older layer starts to stretch, and then the cell wall becomes elongated. The stretching layers keep pushing to the outer surface until it become amenable to degradation. Image generated by BioRender.com.

1.5 Autolytic enzymes characterizations

The *B. subtilis* genome encodes potential around 42 genes that are considered to be autolytic enzymes, and their functions are not clearly defined (Wilson *et al*., 2023). The autolytic enzymes expressed during vegetative growth exhibit redundancy and are required for growth. However, the most essential enzymes that were found to be synthetic lethality are LytE and CwlO (described in depth later in this chapter) (Bisicchia *et al*., 2007; Smith *et al*., 2000).

1.5.1 Autolytic enzymes specificities

The hydrolytic function is provided by a set of autolytic enzymes that digest the cell wall at different sites in the molecular structure of PG. The autolytic enzymes can be classified into three basic categories depending on their cleaving sites: sugar hydrolases (muramidase and glucosaminidase), amidases, and peptidases (Figure 1.5) (Smith *et al*., 2000; Vollmer *et al*., 2008).

Sugar hydrolases cleave the bond at the glycan strand and are divided into two main groups, muramidase and glucosaminidase. The muramidase family cleaves the glycosidic bond within the glycan strand between the Mur*N*Ac and Glc*N*Ac. There are two types of muramidase: lysozyme and lytic transglucosylase. The lysozyme hydrolyses the bond between the sugars and produces a free reducing end in the glycan strand, while the lytic transglucosylases cleave the bond to produce 1,6-anhydro ring at the Mur*N*Ac residue, leading to the insertion of a new glycan strand (Höltje, 1996; Vollmer, Joris *et al*., 2008). The glucosaminidase cleaves the glycosidic bond between Glc*N*Ac and Mur*N*Ac (Karamanos, 1997). Two glucosaminidase enzymes are known in *B. subtilis*, LytD and LytG, are part of the glycosyl hydrolase family 73 (GH73). LytD, a 90 kDa protein, is considered one of the major autolytic enzymes in vegetative growth that has a role in cell motility, separation, cell lysis, and cell wall turnover (Margot *et al*., 1994a; Rashid *et al*., 1993). LytG, a 31 kDa protein, is produced during vegetative growth and is involved in cell motility and cell division (Horsburgh, Atrih, Williamson, *et al*., 2003).

Amidases degrade the amide bond between the glycan strands (Mur*N*Ac) and the stem peptides (L-alanine) (Herbold & Glaser, 1975). In *B. subtilis*, three genes annotated as amidases in the genome are LytC, YrvJ, and YocH (Vollmer *et al*., 2008). LytC (52 kDa) is one of the major autolytic enzymes expressed in vegetative growth. This enzyme is encoded by the *lytC* gene and is the last gene of the *lytABC* operon. Characterisation of the roles of

these three proteins indicates that LytA is a membrane- associated lipoprotein, facilitates the translocation of LytC across the membrane upon the specific binding interaction between LytA and LytC. LytB is the modifier protein that increases the activity of the amidase (Duchêne *et al*., 2019; Herbold & Glaser, 1975; Lazarevic *et al*., 1992). The specific roles of YrvJ and YocH remain unclear.

Peptidases are the most prominent family of enzymes that cleave the peptide bonds within the amino acids in the stem peptides of the PG. Depending on their specificity, peptidases are divided into two main groups: carboxypeptidases and endopeptidases. The carboxypeptidases cleave the bond at the C-terminal of the stem peptides. The endopeptidase enzyme breaks the peptide bond within the stem peptides or in the cross-linked stem peptide (Vollmer *et al*., 2008).

The carboxypeptidases are further subdivided into DD-carboxypeptidase and LD-carboxypeptidase. The DD-Carboxypeptidase is present in vegetative growth that converts the pentapeptide into tetrapeptide by cleaving the bond between the two D-alanine residues (4^{th} and 5^{th} positions in the stem peptide chains) (Vollmer *et al*., 2008). The major DD-carboxypeptidase in *B. subtilis* is PBP5 (DacA), and a mutant of *dacA* leads to an increase in the amount of free pentapeptides side chains in the cell wall (Atrih *et al*., 1999a). The LD-carboxypeptidase breaks the amide bond between *meso*-diaminopimelic acid and D-alanine (3^{rd} position and 4^{th} position in the stem peptides, respectively). In *B. subtilis*, LD-carboxypeptidase A (LdcB) was shown to convert stem peptides from tetra- to tripeptides (Hoyland *et al*., 2014).

In a similar way, the endopeptidases are subdivided into three groups: DD-endopeptidase, DL-endopeptidase, and LD-endopeptidase. The DD-endopeptidase cleaves the cross-bridge linkage that links the D-alanine (4^{th} position) in one stem peptide and the *m*DAP (3^{rd} position) in the neighbouring chain. The LD-endopeptidase hydrolyses the L-alanine (1^{st} position) and D-glutamic acid (2^{nd} position) in the stem peptide (Vollmer *et al*., 2008). In *B. subtilis*, CwlK and LytH are identified as LD-endopeptidases involved in cell wall turnover and endospore cortex maturation, respectively (Fukushima *et al*., 2007; Horsburgh, Atrih, & Foster, 2003). The third group is the DL-endopeptidases, which break the link between D-glutamic acid (2^{nd} position) and *m*DAP (3^{rd} position) in the stem peptide. In *B. subtilis*, seven genes encode DL-endopeptidases in the C-terminal region of the proteins and generally have a distinct N-terminal domain that is unique to each gene: *lytE*, *lytF, cwlO,*

cwlS, cwlT, pgdS, and *ykfC*. Of these genes, *lytE*, *lytF*, *cwlO*, and *cwlS* are expressed during vegetative growth and play significant roles in cell morphology and growth (Fukushima *et al*., 2006, 2008; Margot *et al*., 1999a; Ohnishi *et al*., 1999; Xu *et al*., 2010; Yamaguchi *et al*., 2004).

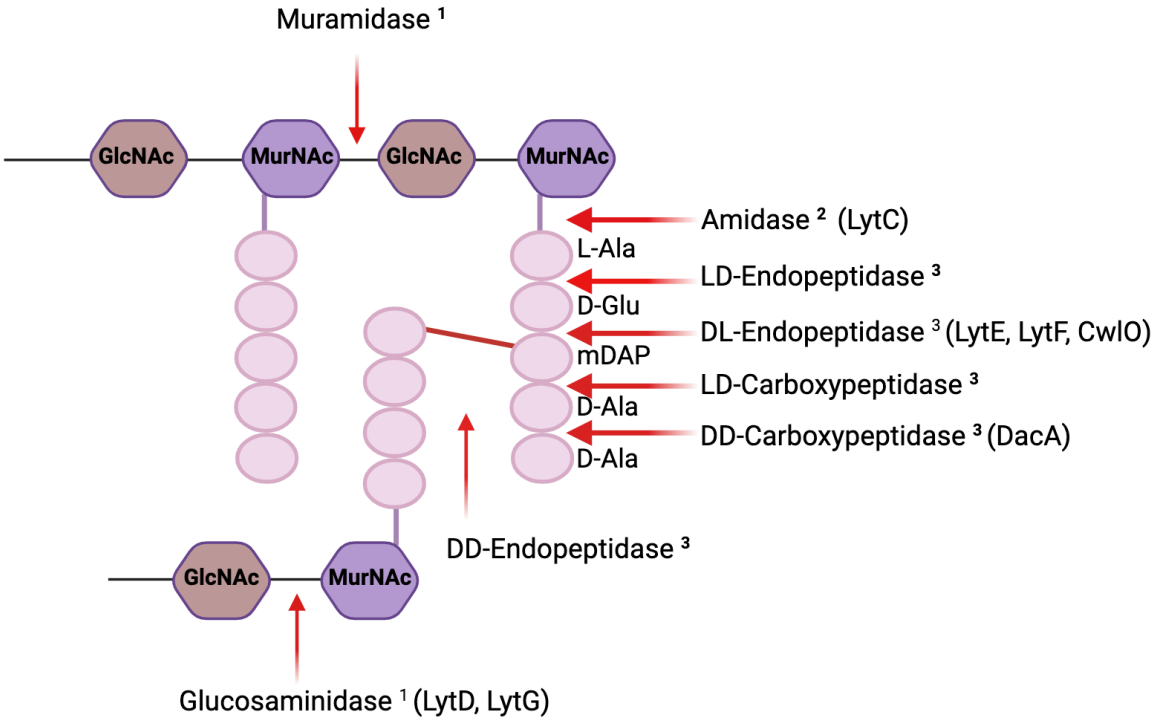

Figure 1.5 Autolytic enzymes classification

In *B. subtilis*, approximately 42 hydrolysis enzymes are divided into four different groups depending on their cleavage site. (1) Sugar hydrolases cleave the glycosidic bond in the glycan strands and are divided into muramidase and glucosaminidase. (2) Amidases cleave the peptide bond between the Mur*N*Ac and L-alanine residue at in the stem peptide. Lastly, (3) Peptidases, which are divided into endopeptidases and carboxypeptidases, break down the bonds within the stem peptide (LD-endopeptidase, DL-/ and DD- carboxypeptidase) and the cross-linkage (DD-endopeptidase). Image generated by BioRender.com.

1.5.2 Domain structure of the autolytic enzymes

The hydrolysis proteins are secreted across the cell membrane and could attach to either the cell membrane, the PG, or the TAs. The structure of autolytic proteins proposed to be retained in the cell wall generally consists of two domains: N-terminal and C-terminal. The N-terminal region of the protein contains a signal peptidase that was cleaved after secreted and a repeated motifs called a carbohydrate-binding (CBD) or cell wall-binding domain (CWBD) (Smith *et al*., 2000). The CBD is a non-catalytic domain that noncovalent attaches to the cell envelope. This is thought to help the autolytic enzymes to be retained in the cell wall and localise the catalytic domain (described previously in Section 1.5.1) (Visweswaran

et al., 2014; Voigt *et al*., 2009). The CBD is divided into seven categories: cysteine and histidine-dependent amidohydrolase/peptidases domain (CHAP), GW domain, SH3 domain, PlyPSA CBD, FtsN-peptidoglycan-binding domain, choline-binding domain, and LysM domain (Vollmer, Joris, *et al*., 2008). In this study, the focus is on the four types of cell wall binding domains present in the autolytic enzymes in *B. subtilis*, which play a major role in cell morphology and division rather than the recycling of material: SH3 domain, GW domain, LysM domain, and choline-binding domain.

i. SH3 Domain

Src homology 3 (SH3) is a small domain consisting of almost 60 amino acids anchoring to the PG. This domain has been found in the glucosaminidase enzyme (LytD) in *B. subtilis*, but the specific functional localisation of LytD in the cell wall remains unclear, other than it is secreted into the cell envelope (Margot *et al*., 1994). Similar motifs are known to be present in higher organisms and are proposed to function in protein-protein interactions. The SH3 domain contains a binding surface that recognizes the proline-rich sequence found in other proteins (Visweswaran *et al*., 2014; Vollmer *et al*., 2008; Whisstock & Lesk, 1999).

ii. GW Domain

The GW Domain is a repeated domain of 80 amino acids with a conserved dipeptide Glycine (G) - Tryptophan (W) that has defined the name of this domain (Vollmer *et al*., 2008). It has a variable number of the repeated sequences with the probability that the higher repeated number, the stronger its attachment to the cell wall polyanions. The GW domain is also involved in interaction with the host cells. In *L. monocytogenes*, Ami, an amidases enzyme, has GW domains, while in *B. subtilis*, the GW domain is found in the glucosaminidase enzyme LytG. (Horsburgh, Atrih, Williamson, *et al*., 2003; Milohanic *et al*., 2001).

iii. LysM

There are more than 4000 proteins (Pfam PF01476) that contain the LysM domain, which is a sequence of 44 to 65 amino acids that is often present in partial or perfect repeats (Bateman & Bycroft, 2000; Buist *et al*., 2008). Kj *et al*., 1986 described the first LysM motif in the lysozyme of *Bacillus* phage φ29 and was defined as 44 repeated amino acids in the C-terminal region. A similar sequence was found in the peptidoglycan hydrolases of *Enterococcus faecalis*. In some proteins where multiple LysM repeats are present, they are separated by spacing sequences containing serine (Ser), aspartic acid (Asp), and threonine

(Thr). The LysM motif can be detected at either the N- or C-terminus of the protein (Buist *et al*., 2008). The structure of the LysM takes the form of two α-helices and antiparallel β-sheets (Bateman & Bycroft, 2000). Most proteins that contain the LysM domain are involved in PG hydrolase enzymes. However there is no correlation with the presence of a LysM domain, tand catalytic specificity (Buist *et al.*, 2008). The efficiency of binding LysM to the cell wall seems to be influenced by the isoelectric points (IP) of the LysM amino acid sequence, which can range from 4 to 12, and multiple repeats of LysM can have different IP. The DL-endopeptidases of *Lactobacillus Plantarum*, LytA, and LytB show how the IP of LysM affects the enzyme binding efficiency to the PG. LytA contains one LysM domain, and its IP is basic (8.34), while LytB comprises two LysM domains, and its IP ranges between 5.43 and 5.18. In the PG, the inner layers (new layers) are potentially more acidic than the outer layers due to structural components, especially the cytoplasmic membrane and anionic polymers (e.g., TAs) (Jolliffe *et al*., 1981; Walter *et al*., 2020). This resulted in LytA being more active in the outer layer, where hydrolases act to permit elongation. On the other hand, LytB is active close to the cell membrane, which is involved in cell division (Duchêne *et al*., 2019).

In *B. subtilis,* the DL-endopeptidase LytE, LytF, and CwlS consist of the three, five, and four repeated sequences of LysM, respectively, at the N-terminal region (Fukushima *et al*., 2006; Margot *et al*., 1998, 1999a). Previous studies have observed that LytE, LytF, and CwlS subcellular localisation depend on the N-terminus (Hashimoto *et al*., 2012). LytE localised at the lateral cell wall, septa, and poles, while LytF and CwlS localised at the poles and cell septa (Hashimoto *et al*., 2012; Yamamoto *et al*., 2003a).

iv. Choline-binding domains

Two distinct types of choline binding domains have been identified; the first, known as the cell wall binding domain of Type 1 (CWBD1), is a sequence of approximately 20 amino acids repeated in five to ten times. The CWBD1 recognizes the choline residue present in the cell wall (Vollmer *et al*., 2008). In *S. pneumoniae*, LytA is an autolytic enzyme containing the N-acetylmuramoyl L-alanine amidase at the N-terminus and the Choline binding domain localised at its C-terminus. It has been proposed that LytA binds to the choline residue on the TAs (Desvaux *et al*., 2006; Fernández-Tornero *et al*., 2002).

The second type denoted as CWBD2, contains repeated sequences of around 100 amino acids. These repeats are responsible for binding the protein to the cell wall. The CWBD2 domain can be located in the N- or C-terminal region of the protein (Kuroda &

Sekiguchi, 1991). In *B. subtilis*, the amidase enzyme LytC contains three repeated sequences at its N-terminal region that serve as a cell wall binding domain. Additionally, LytC was localised at the entire cell wall (Yamamoto *et al*., 2003a). The autolysin Cwp66 protein from *Clostridium difficile* contains a repeated sequence with homology to LytC (Waligora *et al*., 2001).

1.5.3 Autolytic enzymes regulation in vegetative growth

The expression of autolytic enzymes is highly regulated, presumably preventing cell lysis; this is demonstrated by the fact that a large number of sigma factors (σ) act to modulate the expression of many autolytic enzyme in response to altering conditions (Helmann, 2016). To initiate the transcription of the gene, a combination of sigma factor is associated with core RNA polymerase that consists of two alpha (α) subunits, one beta (β) subunit, one beta prime (β') subunit, and one omega (ω) subunit to form the Holoenzyme. The sigma factor serves as a guide to enable the holoenzyme to recognize specific binding sequence in the promoter region of the gene (Figure 1.6) (Iyer & Aravind, 2012). The main sigma factor in *B. subtilis* is SigA (σ^A), which plays a critical role in cell survival and is a housekeeping enzyme. An alternative sigma factor SigI (σ^I) regulates gene expression under heat stress (Gruber and Gross, 2003; Zuber *et al.*, 2001). Furthermore, the extracytoplasmic function (σ^{ECF}) sigma factors are involved in various processes such as envelope stress, change in pressure, and osmolality. In *B. subtilis,* there are four of the σ^{ECF} involved in cell envelope stress SigM (σ^M), SigV (σ^V), SigW (σ^W), and SigZ (σ^Z) (Souza *et al*., 2014).

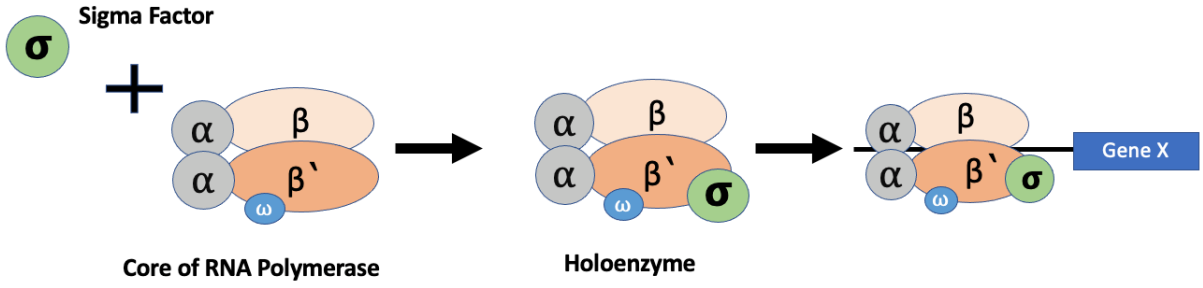

Figure 1. 6 Gene expression by sigma factor

The diagram illustrates the initial transcription of the gene. The sigma factor (green circle), along with the core RNA polymers, forms a complex known as the holoenzyme. The holoenzyme then binds to the promoter located upstream of gene.

During growth, the cells elongate, and then a division septum is made to separate the cells into two identical daughter cells. There are two main proteins that organize the elongation and division of the cell, MreB and FtsZ. The rod shape of the cells is governed by

MreB, while FtsZ governs the cell division. These two proteins interact directly or indirectly with the hydrolytic enzymes (Bisson Filho *et al*., 2017; Chastanet & Carballido-Lopez, 2012). The MreB is a cytoskeleton protein, a dynamic filament located under the cytoplasmic membrane. It was found that the MreB is essential for the rod shape of both Gram-positive bacteria (*B. subtilis*) and Gram-negative bacteria (*Rhodobacter sphaeroides* and *Caulobacter crescentus)*, and deletion of *mreB* resulted in lost cell shape (Carballido-López *et al*., 2006; Figge *et al.*, 2004; Jones *et al*., 2001). *B. subtilis* has three MreB isoforms named MreB, MreBH, and Mbl, and they have a role in cell shape determination. It has been reported that MreB controls the cell width and strain lacking *mreB* cells become thicker, while deletion of *mbI* causes cells to become slightly shorter. (Chastanet & Carballido-Lopez, 2012; Formstone & Errington, 2005a; Kawai *et al*., 2009). Deletion of MreBH results in mild cell shape defects, and it has shown that the localisation of LytE at the lateral cell wall requires interaction with MreBH. In the *mreBH* mutant, LytE was only found to localise at poles and septa (Carballido-López *et al*., 2006; Chastanet & Carballido-Lopez, 2012).

1.5.4 Autolytic enzyme secretion

In bacteria, proteins are transported from the cytoplasm into the culture by a process called the secretion system (Voigt *et al*., 2009). Bacterial cells can export a large number of proteins that carry out their normal biological functions either in the cell envelope or on the outside surface of the cell. There are three pathways of protein secreted: Secretory protein translocation (Sec), Twin-arginine transport (Tat), and ATP-binding cassette (ABC transporters). The main pathway is Sec, which transports unfolded proteins across the membrane. In contrast to the Sec pathway, the Tat pathway translocates folded proteins with their cofactors (van Dijl et al., 2001). The autolytic enzymes in *B. subtilis* are supposed to be transported via the sec pathway as they contain a signal peptide at N-terminus of the protein to direct the protein into an appropriate transport system. These proteins are then secreted through the cell membrane, and the signal peptide is cleaved off thus releasing the protein into the cell wall (Green & Mecsas, 2016; van Dijl *et al*., 2001; Voigt *et al*., 2009). However, the role of the Tat export system is complex, and its substrates poorly defined for *B. subtilis* (Barnett et al., 2009). It is possible that it also has a role in exporting this set of enzymes as indicated by the fact that a GFP-LytE fusion was functionally exported (Carballido-López et al., 2006)

The hydrolase enzymes are synthesized in the cytosol of the cells and secreted across the cell membrane. Previous studies revealed that the substrate of an ATP-binding cassette (ABC) transporter was found to regulate the activity of some autolytic enzymes. In *E. coli,* the FtsEX complex has been found to regulate the activity of the amidase enzymes AmiA and AmiB after interacting with EnvC (Yang *et al*., 2011). FtsEX is part of an ATP-binding cassette (ABC) transporter and has a role in cell division. FtsE has an ATPase activity, while the FtsX is a transmembrane protein (Schmidt *et al*., 2004; Yang *et al*., 2011). In *S. pneumoniae*, the FtsEX has been found to interact with hydrolysis enzyme PcsB (Sham *et al.*, 2011). The DL-endopeptidase CwlO in *B. subtilis* requires the ABC transporter FtsEX for activation. Recent research has identified SweD and SweC as co-factors that require FtsEX to regulate cell wall elongation (Brunet *et al*., 2019a).

1.5.5 Autolytic Enzyme stability

In *B. subtilis*, proteases are one set of proteins known to be retained in the cell wall and affect the autolytic enzymes. Eight extracellular proteases are identified as AprE, Bpr, Epr, Mpr, NprB, NprE, Vpr, and WprA; none of which are essential for cell growth (Harwood & Kikuchi, 2022). AprE and NprE are considered the most abundant extracellular proteases; a double mutant of *aprE* and *nprE* reduces the overall protease activity by 95% (Kawamura & Doi, 1984). The WprA and EpR (cell wall-associated protease and minor extracellular protease, respectively) have been shown to play a role in the stability of LytE and LytF. In double a mutant of *wprA* and *epr,* LytE and LytF accumulate in the cell wall extract. This suggests that extracellular proteases affect the stability of LytE and LytF in the cell wall. In contrast, LytC stability is unaffected by these proteases (Yamamoto *et al*., 2003).

The anionic cell wall polymers (TAs) also affected the stability and localisation of autolytic enzymes at the cell wall. In *B. subtilis*, experimental data suggest that WTA is necessary to bind LytC tightly to the cell wall. It was found that LytC weakly binds to the cell wall in a strain lacking WTA (Yamamoto *et al*., 2003b). Moreover, Yamamoto *et al* ., 2008 demonstrated that the WTA affects the localisation of LytF. LytF is localised at the septa and poles, while in a mutant of *tagO* or *tagB*, LytF- 6xFLAG was found to be significantly localised at the septa, poles, and lateral cell wall. This suggests a potential role of WTA in modulating the localisation of autolytic enzymes, however it is not clear if the modification of the protein to permit localisation altered its stability or localisation. Interestingly, the deletion of *ltaS* increased the length of the LTA, which was subsequently found to modulate

the activity of LytE. (Kasahara *et al*., 2016b). However, it is unclear how the activity of autolytic enzymes is regulated, and the altered localisation and activity caused by loss of LTA and WTA have not been fully studied.

1.5.6 Major autolytic enzymes in *B. subtilis*

The autolytic enzymes play key roles in modifying the cell envelope, essential for normal cell growth and division, and have biochemical activities that must be tightly regulated both in terms of where and when they are active. The role of PG hydrolysis in the cell wall has been studied intensively. They have been involved in cell division, elongation, motility, and cell wall rigidity. This study focused on the most important autolysins for the cell wall; the DL-endopeptidases LytE, LytF, CwlO, the amidase (LytC), and the glucosaminidase (LytD).

LytE is a 37 kDa protein controlled by three sigma factors: σ^A, σ^H, and σ^I (under stress) and has been observed to be localised at cell septa, poles, and lateral cell wall (Huang *et al*., 2013; Ishikawa *et al*., 1998a; Margot *et al*., 1998). LytF is a 51 kDa protein transcribed by σ^D RNA polymerase during the late exponential growth phase and found to be predominantly localised at cell poles and septum (Margot *et al*., 1999a; Ohnishi *et al*., 1999). The CwlO is 50 kDa and is controlled by σ^A (Domínguez-Cuevas *et al*., 2013a; Yang *et al*., 2012). The DL-endopeptidase LytE and CwlO are functionally redundant and play a critical role in cell growth. Both are localised at the lateral cell wall, and the strain lacking both *lytE* and *cwlO* genes is lethal (Bisicchia *et al*., 2007). The synthetic lethality of the double mutant *lytE cwlO* is caused by the lack of DL-endopeptidase activity at the cylindrical part, which is necessary for cell viability (Dominguez-Cuevas *et al*., 2013). LytE and CwlO have the same catalytic domain but seem to have distinct functions; a mutant of *lytE* leads to thinner and longer cells, while a mutant of *cwlO* was wider and slightly bent compared to the wild type (Margot *et al*., 1998; Yamaguchi *et al*., 2004). The other difference is that LytE is released into the culture medium, while the fate of CwlO is unclear. CwlO is composed of two coiled-coil domains in its N-terminus that activate in the side wall at the inner layer of PG (Dominguez-Cuevas *et al*., 2013; Meisner *et al*., 2013). It was suggested that the synthetic lethality of double mutant *lytE cwlO* is caused by the lack of activity of the DL-endopeptidase in the cylindrical part, which is necessary for cell viability. As mentioned before, LytE, LytF, CwlS, and CwlO have the same catalytic domains in their C-terminus, but the overexpression of *lytF* or *cwlS*, in *lytE*

cwlO double mutant does not suppress the synthetic lethality (Hashimoto *et al*., 2018; Hashimoto *et al*., 2012).

Several autolysins have been shown to play a role in the bacterial cell separation. In *S. aureus,* deletion of the *atl* gene, which encodes a bifunctional protein with both amidase and glucosaminidase enzymatic activities, resulted in the formation of cell clusters (Milohanic *et al*., 2001). Additionally, the cell hydrolysis enzyme AcmA in *Lactococcus lactis* is involved in cell separation (Buist *et al*., 1995). In *B. subtilis*, the hydrolysis enzymes LytE and LytF were found to be involved in cell separation. Research has demonstrated that the cells of the *lytE* mutant are longer than those of the wild type. In the case of *lytF* disruption, the cells exhibited longer chain compared to those of the *lytE* deletion. Additionally, a *lytE* and *lytF* double mutant resulted in the formation of extra-long chains (filaments) (Ishikawa *et al*., 1998a; Ohnishi *et al*., 1999).

LytC and LytD are considered the major hydrolysis enzymes during vegetative growth. Transcription of *lytC* is mediated by two sigma factors: σ^A and σ^D, with the latter responsible for 70-90% of *lytC* transcription (Kuroda & Sekiguchi, 1993; Lazarevic *et al*., 1992). The domain structure of LytC contains three tandem repeated sequences of the cell wall binding domains in the N-terminal region, while the C-terminal contains the catalytic domain (amidase) (Kuroda & Sekiguchi, 1991). The expression of LytD is controlled by σ^D (Margot *et al*., 1994; Chen *et al*., 2009). According to Blackman *et al*., 1998, the study found the overlapping role of LytC and LytD. LytC plays a role in cell wall turnover along with LytD. A single mutant of *lytC* decreased the rate of cell wall turnover; however, a double mutant of *lytC lytD* led to a significant decrease in the rate of cell wall turnover compared to the single mutant.

Earlier research found that autolytic enzymes play a role in cell swarming on soft agar, as some of autolytic mutations result in long chains of cell, which might impact swarming (Blackman et al., 1998; R. Chen et al., 2009). Chen *et al*., 2009 reported that LytF, LytC and LytD are under the control of σ^D, a sigma factor that transcribes genes involved in swarming motility. Cells lacking σ^D grow as long chain and are impaired in motility, similar to null mutants of *lytF lytC lytD*. However, a single mutant of *lytF, lytC*, or *lytD* did not affect the swarming motility. This might be because the cell length in the deletion mutants of *lytF lytC lytD* increased, and the cells are joined together, which might experience challenges in moving in different directions (Blackman *et al*., 1998; Margot *et al.*, 1999a). Additionally,

Blackman *et al*., 1998 suggested that LytC can completely compensate for the loss of *lytD*, but LytD is only able to partially compensate for the absence of *lytC* in cell wall turnover and motility.

1.6 Hypothesis and aim

The mechanisms by which cell wall degrading enzymes are localised correctly in the cell wall and how their activity is modulated are poorly understood. A significant number of these secreted proteins serve key roles in modifying the cell envelope, are essential for normal cell growth and division, and have biochemical activities that must be tightly regulated both in terms of where and when they are active. The current hypothesis is based on the idea that these enzymes are targeted to specific locations or that their activity is restricted to specific zones of the cell wall either by interaction with other proteins or by differences in the local state of the cell wall (either through chemical composition or physical state). The project was devised to develop methods to characterise the secretion and sub-cellular localisations of key enzymes acting in cell wall degradation/modification for viable growth. The primary aim of the project was to determine if the specific domain (e.g., carbohydrate-binding domain (CBD)) of the proteins interacts with the cell envelope and how this modulates localisation and/or activity in a way that is coordinated with cell growth.

As a starting point for the project, we will look at how the composition of the cell envelope influences the secretion, localisation, and activity of secreted proteins (LytE, LytC, LytF, LytD). For this, we will exploit the availability of a number of specific mutations that result in characterised changes in the cell wall composition (modification/synthesis of the PG).

As a second line of investigation, we will focus on two specific autolytic proteins, LytE and LytC, and characterise the functional importance of the proposed carbohydrate-binding domains of the protein. Both LytC and LytE have a cell wall binding domain in their N-terminal portion. We want to determine the binding specificity of these binding domains in relation to both known components of the cell envelope and understand if these carbohydrate binding domains (CBDs) have a role in the localisation of the enzyme and/or its biochemical activity. In parallel with this work, strains will be constructed encoding hybrid versions of the DL-endopeptidase LytE, LytF, and CwlO since they seem to have structures consistent with a localising domain attached to the catalytic portion of the protein. In so doing it may be possible to show that the catalytic domain is interchangeable.

Lastly, preliminary work was done on the possibility that cell wall modification may act in some way to modulate the action of autolytic enzymes. This is based on the observation that AsnB is essential and has a function in the cell wall. The essentiality of the AsnB seems to be related to the environmental conditions– specifically extracellular divalent metals (magnesium particularly), which are a common suppressor of cell wall synthesis and degradation defects.

Importance of the research

Understanding the mechanisms by which the autolytic proteins are both localised and regulated represents an initial step toward developing ways to interfere with their normal function. By gaining insight into these mechanisms, researcher can development a novel antibiotic. Additionally, studying the biochemical role of the autolytic enzymes in combination with how their localised and/or activity is modulated will provide a way to extend our comprehension of the dynamics of bacterial cell wall structure and how it is coordinated. This knowledge will improve our understanding of how cells maintain their shape and integrity during growth. An understanding of which might have application in biotechnological processes where cell lysis is a problem

Chapter 2: Methods and Materials

2.1 General bacterial growth conditions

For strain and plasmid constructions, nutrient agar (NA) and Penassay broth (Antibiotic media No.3 (Oxoid)) (PAB) plates were used with appropriate concentrations of antibiotics and inducer as described in Table 2.1. To determine the growth characteristics of a strain, cells were grown in Luria-Bertani broth (LB), Nutrient Broth (NB), PAB, or minimal media (described in Appendix 1-Buffer Components). Strains were incubated at 30°C overnight with shaking. The following morning, the cultures were diluted 1/10 and incubated at 37°C for 1 hour, then diluted back to OD_{600}~0.05 in fresh warm media with xylose (when required) or supplements (described in Table 2.1). Cultures that had grown overnight with an inducer were washed twice the next day without the inducer to assess the growth without induction.

The culture density was monitored by a spectrophotometer (Thermofisher Genesys 20) at 600 nm (OD_{600}). The optical density was measured every 20-30 minutes for 6-7 hours. To measure the OD, cuvettes filled with 1 ml of sterile media were used as blanks. For the samples, 1 ml of the culture or 10-fold dilutions in the same media, were used depending on the density of the culture. The time points were plotted on a graph to indicate bacterial growth stages.

Table 2.1 The final concentration of the antibiotics and inducers used in this study

Antibiotic/ Inducer	Stock	Final concentration
Ampicillin (bla/amp)	50 mg/ml	*E. coli* 100 µg/ ml
Chloramphenicol (cat)	10 mg/ml	*E. coli* 10 µg/ ml
		B. subtilis 5 µg/ ml
Spectinomycin (spec)	100 mg/ml	*E. coli* 50 µg/ ml
		B. subtilis 60 µg/ ml
Erythromycin (erm)	20 mg/ml	*E. coli* 120 µg/ ml
		B. subtilis 1 µg/ ml
Kanamycin (kan)	25 mg/ml	*E. coli* 25 µg/ ml
		B. subtilis 5 µg/ ml
Zeocin	100 mg/ml	*B. subtilis* 10 µg/ ml
Xylose	25%	0.5%
Isopropylthio-β- galactoside (IPTG)	1 M	1 mM
Magnesium sulphate ($MgSO_4$)	1 M	25 mM
Glucose (G)	40%	0.4%

2.2 Bacterial strains and plasmids constructed

Bacterial strains used in this study can be found in Table 2.2, where the strain name, genotype, and their sources are described. For gene deletions the following selection markers were used: *bla/amp*, *kan, spec*, *cat,* and *erm.* Plasmids used in this study are listed in Table 2.3.

Table 2.2 Strains used in this study

Strain	Genotype	Source
168CA	*trpC2*	Laboratory Collection
sAG1333	*trpC2 aprE::P_{pcn}-lacI-cat*	A Guyet
BSB1	Prototroph	(Nicolas *et al*., 2012)
AA001	*trpC2* Δ*lytC kan*	A Aljohani (unpublished)
AA002	*trpC2* Δ*lytD kan*	A Aljohani (unpublished)
AA003	*trpC2* Δ*lytE kan*	A Aljohani (unpublished)
AA004	*trpC2* Δ*lytF kan*	A Aljohani (unpublished)
AA006	*trpC2* Δ*cwlO kan*	A Aljohani (unpublished)
BKK14470	*trpC2* Δ*mreBH kan*	(Koo *et al.,* 2017)
PDC484	*trpC2* Δ*ftsEX neo spec*	(Domínguez-Cuevas *et al.,* 2013)
AG547	*trpC2* Δ*lytE cat*	A Guyet
AG609	*trpC2* Δ*ltaS cat*	A Guyet
BKK16470	*trpC2 ΔsigD kan*	(Koo *et al.*, 2017)
BKK07260	*trpC2* Δ*yfnI kan*	(Koo *et al.*, 2017)
BKK13450	*trpC2* Δ*sigI kan*	(Koo *et al.*, 2017)
BKK09520	*trpC2* Δ*sigM kan*	(Koo *et al.*, 2017)
BKK08425	*trpC2*Δ*mprF kan*	(Koo *et al.*, 2017)
BRB08	*trpC2 ΔnprB, ΔaprE, Δepr, Δbpr, ΔnprE, Δmpr, Δvpr, ΔwprA*	(Pohl *et al*., 2013)
RE101	*trpC2* Δ*ponA spec*	(Emami *et al*., 2017)
FU340	*trpC2* Δ*asnB neo*	(Yoshida, KI *et al.*,1999)

sAM001	*trpC2 amyE::*P_{xyl}*-lytE-linker-Halo spec*	This study
sAM002	*trpC2 amyE::*P_{xyl}*-*N_{lytE}*-linker-Halo spec*	This study
sAM003	*trpC2 amyE::*P_{xyl}*-lytC-linker-Halo spec*	This study
sAM004	*trpC2 amyE::*P_{xyl}-N_{lytC}*-linker-Halo spec*	This study
sAM005	*trpC2 aprE::*P*pcn-lacI cat* pAM034 *(*P_{spac} *spA erm)*	This study
sAM006	*trpC2 aprE::*P*pcn-lacI cat* pAM035 (P_{spac} *spA'erm)*	This study
sAM007	*trpC2 aprE::*P*pcn-lacI cat* pAM036 (P_{spac} N_{lytE}*- spA erm)*	This study
sAM008	*trpC2 aprE::*P*pcn-lacI cat* pAM037 (P_{spac} N_{lytE}*- spA' erm)*	This study
sAM009	*trpC2 aprE::*P*pcn-lacI cat* pAM038 (P_{spac} N_{lytC}*- spA erm)*	This study
sAM010	*trpC2 aprE::*P*pcn-lacI cat* pAM039 (P_{spac} N_{lytC}*-spA'erm)*	This study
sAM011	*trpC2* Δ*lytE cat amyE::*$P_{hyspank}$ –N_{lytE}- C_{cwlO} *spec*	This study
sAM012	*trpC2* Δ*lytF kan amyE::*$P_{hyspank}$ –N_{lytF}- C_{cwlO} *spec*	This study
sAM013	*trpC2* Δ*lytE cat* Δ*lytF kan amyE::*$P_{hyspank}$ N_{lytE}- C_{cwlO} *spec*	This study
sAM014	*trpC2* Δ*lytF kan* Δ*lytE cat amyE::*$P_{hyspank}$ –N_{lytF}-C_{cwlO} *spec*	This study
sAM015	*trpC2* Δ*yfnI* kan Δ*ltaS spec*	This study
sAM016	*trpC2* Δ*yfnI kan* Δ*ltaS spec* P_{spac} N_{lytE}*- spA erm*	This study
sAM016	*trpC2* Δ*yfnI kan* Δ*ltaS spec* P_{spac} N_{lytC} *spA erm*	This study
sAM017	*trpC2* Δ*lytE kan amyE'* P_{xyl}*-lytE-linker-Halo spec*	This study
sAM018	*trpC2* Δ*lytE kan amyE::*P_{xyl}*-*N_{lytE}*-linker-Halo spec*	This study
sAM019	*trpC2* Δ*lytC kan amyE::* P_{xyl}*-lytC-linker-Halo spec*	This study
sAM020	*trpC2* Δ*lytC kan amyE::* P_{xyl}*-*N_{lytC}*-linker-Halo spec*	This study
sAM021	*trpC2 amyE::*$P_{hyspank}$*-LytE spec*	This study
sAM022	*trpC2 amyE::*$P_{hyspank}$*-LytE(C247S) spec*	This study
sAM023	*trpC2 ΔnprB, ΔaprE, Δepr, Δbpr, ΔnprE, Δmpr, Δvpr, ΔwprA, ΔlytE cat*	This study
sAM024	*trpC2 ΔnprB, ΔaprE, Δepr, Δbpr, ΔnprE, Δmpr, Δvpr, ΔwprA, ΔcwlO kan*	This study
sAM025	*trpC2 ΔnprB, ΔaprE, Δepr, Δbpr, ΔnprE, Δmpr, Δvpr, ΔwprA, ΔlytE cat, ΔlytF spec*	This study

Table 2.3 Plasmids used in this study

Plasmid	Genotype	Function/ Host	Source
pAG-P08	*oriLS20 oriBR322* P_{spac}*-gfp alp7AR erm bla*	Self-replicating plasmid/ *B. subtilis -E. coli*	A Guyet
pDR111	*oriBR322 bla amyE::*$P_{hyspank}$*-lacI spec amyE*	*amyE* integration construct /*E. coli*	D. Rudner, (unpublished data)
pRD96	*bla cat* P_{xyl}	Xylose inducible promoter	(Daniel *et al.*, 1998)
pAK12	*amyE'* P_{xyl}*-linker-halo- spec amp*	Halo-tag/ DH5α	(Kondorosi *et al.,* 1982)
pET-28a (+)	*lacI T7 promoter, lacI operator RBS 6X His Tag T7 thrombin 6X His Tag T7 thrombin::kan*	6His Tag (N-terminal and C-terminal).	Laboratory Collection
pAM019 (H-LytE)	pET-28a (+) *6X His Tag-lytE kan*	Bl21 (DE3)	This work
pAM020 (H-CBD_{lytE})	pET-28a (+) *6X His Tag-*CBD_{lytE} *kan*	Bl21 (DE3)	This work
pAM021 (LytE-H)	pET-28a (+) *lytE -6X His Tag kan*	Bl21 (DE3)	This work
pAM022 (CBD_{lytE}-H)	pET-28a (+) CBD_{lytE}*-6X His Tag kan*	Bl21 (DE3)	This work
pAM023 (H-LytC)	pET-28a (+) *6X His Tag-lytC kan*	Bl21 (DE3)	This work
pAM024 (H-CBD_{lytC})	pET-28a (+) *6X His Tag-*CBD_{lytC} *kan*	Bl21 (DE3)	This work
pAM025 (LytC-H)	pET-28a (+) *lytC-6X His Tag kan*	Bl21 (DE3)	This work
pAM026 (CBD_{lytC}-H)	pET-28a (+) CBD_{lytC} *-6X His Tag kan*	Bl21 (DE3)	This work
pAM027 (H-LytD)	pET-28a (+) *6X His Tag-lytD kan*	Bl21 (DE3)	This work
pAM028 (H-LytF)	pET-28a (+) *6X His Tag-lytF kan*	Bl21 (DE3)	This work
pAM029 (CwlO-H)	pET-28a (+) *cwlO-6X His Tag kan*	Bl21 (DE3)	This work
pAM030	pAK12 *amyE::*P_{xyl}*-lytE-Halo spec amyE*	DH5α	This work
pAM031	pAK 12 *amyE::*P_{xyl}- N_{lytE}*-Halo spec amyE*	DH5α	This work
pAM032	pAK 12 *amyE'* P_{xyl}*-lytC-Halo spec amyE*	DH5α	This work
pAM033	pAK 12 *amyE'* P_{xyl}-N_{lytC}*-Halo spec amyE*	DH5α	This work
pAM034	*oriLS20 oriBR322* P_{spac}*-spA alp7AR erm bla*	DH5α	This work

pAM035	*oriLS20 oriBR322* P_{spac}-*spA' alp7AR erm bla*	DH5α	This work
pAM036	*oriLS20 oriBR322* P_{spac}-N_{lytE}- *spA alp7AR erm bla*	DH5α	This work
pAM037	*oriLS20 oriBR322* P_{spac}-N_{lytE}- *spA' alp7AR erm bla*	DH5α	This work
pAM038	*oriLS20 oriBR322* P_{spac}-N_{lytC}- *spA alp7AR erm bla*	DH5α	This work
pAM039	*oriLS20 oriBR322* P_{spac}-N_{lytC}- *spA'- alp7AR erm bla*	DH5α	This work
pAM040	*oriBR322 bla amyE::*$P_{hyspank}$*-lytE-lacI spec amyE*	DH5α	This work
pAM041	*oriBR322 bla amyE::*$P_{hyspank}$*-lytF-lacI spec amyE*	DH5α	This work
pAM042	*oriBR322 bla amyE::*$P_{hyspank}$*-cwlO-lacI spec amyE*	DH5α	This work
pAM043	*oriBR322 bla amyE::*$P_{hyspank}$-N_{lytE}-*linker-* C_{cwlO}-*lacI spec amyE*	DH5α	This work
pAM044	*oriBR322 bla amyE::*$P_{hyspank}$- N_{lytF}-*linker-* C_{cwlO}-*lacI spec amyE*	DH5α	This work
pAM045	*oriBR322 bla amyE::*$P_{hyspank}$- *lytE(C247S)-lacI spec amyE*	DH5α	This work

2.3 General Method

2.3.1 Genomic DNA Extraction

To allow the rapid transformation of genetic markers from one *B. subtilis* strain into another strain, the quick DNA extraction method developed by Ward and Zahler (1973) was used. A heavy inoculum from a fresh plate was grown in 5 ml LB or PAB media with an appropriate antibiotic and inducer if needed. Culture was incubated for 3-4 hours at 37°C with shaking, then centrifuged at 13,000 x g for 2 minutes. The pellet was resuspended in 1 ml of 1X saline sodium citrate (SSC) (Appendix 1-Buffer components) and 200 µg/ml lysozyme. The resuspension was then incubated at 37°C for 20 minutes, followed by adding 500 µl of 4 M NaCl. The resulting solution was filtered through a 0.45 µm filter and stored at -20°C.

To prepare pure genomic DNA from *B. subtilis* to use as a template in PCR, the Wizard® Genomic DNA Purification Kit (Promega) was used. The strain was grown in 5 ml of LB or PAB media with an appropriate antibiotic and inducer, if required. The culture was

then incubated for 3 hours at 37°C with shaking. Afterward, 2 ml of the culture was centrifuged at 13,000 x g. The resulting pellet was gently resuspended in 60 µl EDTA (50 mM) and 6 µl lysozyme (10 mg/ml) and incubated for 20-30 minutes at 37°C. Following incubation, 600 µl of Nuclei Lysis Solution (Promega) was added to the mixture and incubated for 5 minutes at 80°C, and then cooled on ice for 2 minutes. 200 µl of protein precipitation solution (Promega) was then added and mixed by vortexing for 10 seconds, and centrifuged for 9 minutes at 13,000 x g. The supernatant was transferred to a sterile Eppendorf tube containing 600 µl of isopropanol and then mixed and centrifuged for 3 minutes at 13,000 x g. The supernatant was discarded, and the pellet was washed with 600 µl of 70 % ethanol. The mixture was then centrifuged for 3 minutes at 13,000 x g and the ethanol was carefully removed. The pellet was allowed to dry in the air for 10 minutes before adding 100 µl of nuclease-free water, after which the gDNA was stored at -20 °C.

2.3.2 Plasmid DNA extraction

The Qiagen Miniprep Kit was used to extract plasmid from *E. coli*, following the manufacture's protocol. A single colony was inoculated in 10 ml of LB media with an appropriate antibiotic and grown overnight at 30°C, with shaking. The next day, 5 ml of the bacteria culture was centrifuged at 13,000 x g for 3 minutes, the supernatant was discarded, and the pellet was treated as described in Figure 2.1. The plasmid DNA was eluted in 30 µl of nuclease-free water and stored at -20°C.

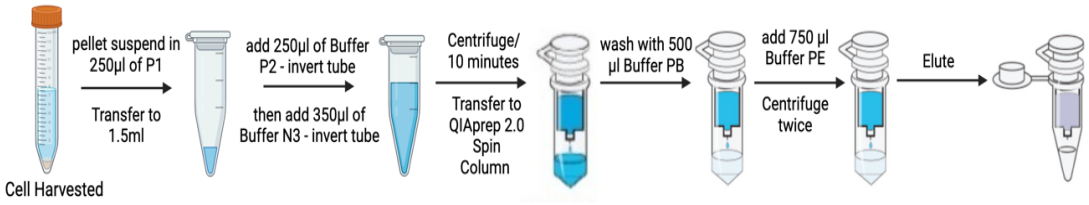

Figure 2.1 Diagram describes the process of the Qiagen Miniprep kit

The image demonstrates the process of the extract the plasmid according to Qiagen Miniprep Kit Image great by BioRender.com.

2.3.3 Oligonucleotides design

Oligonucleotides used in this study were designed using Snapgene software and synthesized by Eurogentec (Kaneka Corporation). Polymerase Chain Reaction primers should be 18-25 nucleotides and have a 40-60 % GC content. The stock solution (100 µM) of the primer was diluted in nuclease-free water to obtain either a 10 µM working solution for PCR or a 30 µM solution, which was used for sequencing and stored at -20°C. The Oligonucleotides used in this study are listed in Appendix 2.

2.3.4 Polymerase Chain Reaction (PCR)

Q5® High-Fidelity DNA Polymerase (NEB) was used according to the manufacturer's protocol to permit amplification of specific segments of DNA. The master mix of the PCR reaction in a total volume of 50 µl consisted of 10 µl of 5X Q5 Reaction Buffer, 4 µl of (10 mM) dNTPs, 2.5 µl of 10 µM forward Primer, 2.5 µl of (10 µM) reverse Primer, 1-2 µl of template DNA, 1 µl of Q5® High-Fidelity DNA Polymerase, and nuclease-free water to make 50 µl. To improve pipetting accuracy, the stock of the master mix was generally made for multiple PCR reactions. The PCR thermocycle used in the study is described in Table 2.4.

Table 2.4 The thermocycling protocol used with Q5® High-Fidelity DNA Polymerase in PCR reactions

Heated Lid Temperature 100°C		
Step	Temperature	Time
Denaturation	90°C	30 seconds
25-30 cycle Each cycle consisting of		
Denaturation	98°C	30 seconds
Annealing	55-62°C	30 seconds
Extension	72°C	30 seconds/kilobase (kb)
End Cycle		
Final Extension	72°C	2 minutes
Store at 8°C		

To confirm the correct construction of the plasmid in *E. coli*, GoTaq® G2 DNA Polymerase (Promega) was used for colony PCR. The PCR reaction consisted of 10 µl GoTaq buffer (5X), 1µl dNTPs (10 mM), 1µl forward primer (10 µM), 1µl reverse primer (10 µM), 0,25 µl GoTaq polymerase, 4 µl MgCl2 (25 mM), and 32.75 µl nuclease-free water. A single colony was directly taken from a fresh transformation plate using a toothpick and

resuspended in a PCR reaction mixture. The mixture was then cycled in a PCR machine as described in Table 2.5.

Table 2.5 The thermocycling protocol for colony PCR

Heated Lid Temperature 100°C		
Steps	Temperature	Time
Denaturation	95°C	2 minutes
30-35 Cycle Each cycle containing of		
Denaturation	98°C	30 seconds
Annealing	55-62°C	30 seconds
Extension	72°C	1 minutes/kilobase (kb)
End Cycle		
Final Extension	72°C	5 minutes
Store at 8°C		

2.3.5 Agarose Gel electrophoresis

Agarose gel electrophoresis was used to assess the size of DNA fragments after PCR reactions (Section 2.4.4). The agarose gel was prepared by dissolving 0.5% agarose powder in 50 ml of 1X TAE buffer (described in Appendix 1-Buffer components). The mixture was heated to dissolve the agarose and allowed to cool down before adding Nancy-520 (Sigma) at a final concentration of 0.12 µg/ml. Once the gel was set, it was placed in the electrophoresis tank filled with 1X TAE buffer. Samples were loaded after being mixed with gel loading dye (described in Appendix 1-Buffer components), and the gel was electrophoresed at 120 Volts (V) until the marker migrated to the required distance. The DNA bands were examined by using a UV transilluminator. In order to estimate the fragment sizes, a 1 kb ladder was loaded simultaneously with the samples to serve as a size standard.

2.3.6 PCR purification

QIAquick PCR Purification Kit was utilised to clean up the DNA fragments following PCR reaction or restriction digests. Before starting, a pH indicator was added to the binding buffer PB to ensure that the optimal pH for DNA binding (pH ≤ 7.5) was maintained. The five volumes of Buffer PB were added directly to the 1 volume of PCR reaction or digestion mixture. If the mixture changed to orange or violet colour, indicating a high pH. 10 µl of 3 M sodium acetate was added. The mixture was then applied to a QIAquick spin column and centrifuged at 13,000 x g for 1 minute. The flow-through was discarded, and the resin was washed with 700 µl of Buffer PE then centrifuged at 13,000 x g for 1 minute

(repeated twice/discard flow-through). The 30 µl of nuclease-free water was added to the QIAquick column to elute the DNA and centrifuged into a clean Eppendorf tube. The DNA was stored at -20°C.

2.4 Cloning

2.4.1 Restriction Digestion

The restriction enzymes were used to digest either the plasmid DNA or the PCR fragments with a corresponding restriction enzyme site for cloning purposes. Gently mixed 1 µg of DNA, 1 µl of restriction enzyme, 2 µl of 10x NEBuffer™, and nuclease-free water were added to the final volume of 20 µl. The mixture was then incubated at 37°C for 1 to 3 hours, after which the reactions were inactivated by heat treatment or purified using PCR purification protocol (described previously in Section 2.4.6). The restriction enzymes used in this study are listed in Table 2.6.

Table 2.6 Restriction Enzymes used in this study

Enzyme	NEBuffer™	Inactivation Method Used
*Dpn*I	rCutSmart	80°C
*Kpn*I-HF	rCutSmart	PCR purification
*EcoR*I-HF	rCutSmart	65°C
*Xba*I	rCutSmart	65°C
*BglI*I	r3.1	PCR purification
*Nco*l-HF	rCutSmart	80°C
*Hind*III-HF	rCutSmart	80°C

2.4.2 DNA Assembly

The cloning method predominantly used in this study to construct plasmids was NEBuilder HiFi DNA Assembly. The DNA fragments (insert) and plasmid (vector) were amplified with homologous ends (15-25 bp) using a PCR reaction (described previously in Section 2.4.6). The amplified vector was then treated with *Dpn*I (NEB) and incubated at 37°C for 1 hour to cleave methylated sites and prevent contamination. Both the insert and vector were then purified using PCR purification. Once the insert and vector had been purified, the NEBuilder HiFi master mix consisted of a ratio 1:2 (vector: insert), nuclease-free water was added to the final volume of 5 µl, and 5 µl of NEBuilder HiFi DNA Assembly

Master Mix. The mixture was incubated at 50°C with shaking for 60 minutes and then transformed into 50 µl of *E. coli*.

2.5 Transformations

2.5.1 *E. coli* Transformation

The recombinant DNA was transformed into *E. coli* (DH5α or BL21(DE3)) depending on the application. Competent cells were prepared by the method described by Hanahan *et al.*, 1991 and stored at -80°C. For transformation, the competent cells were thawed on ice, and then 50 µl of the competent cells were mixed with 10 µl of ligated fragment or 1µl of the extracted plasmid. The mixture was incubated on ice for 30 minutes, followed by heat-shocked at 42°C for 2 minutes, and then returned the mixture to the ice for 2 minutes. Three volumes of the LB media were added to the mixture and incubated at 37°C for 1 hour. To isolate the transformed cells, 100 µl of the mixture was spread onto a nutrient agar plate containing an appropriate antibiotic, and then incubated overnight at 37°C.

2.5.2 *B. subtilis* Transformation

B. subtilis transformation was performed as described in Anagnostopoulos and Spizizen (1961) and updated by Hamoen *et al*. (2002). Briefly, a strain to be transformed was grown on a fresh plate, after which a small inoculum was grown in 10 ml of competence medium (Appendix 1-Media composition) overnight at 37°C. The next day, the culture was diluted 1/10 into a fresh pre-warm competence medium and incubated at 37°C for three hours. An equal volume of the pre-warm starvation media (Appendix 1-Media composition) was then added to the culture and incubated for 2 hours at 37°C. DNA (5 µl of chromosomal DNA or 10-15 µl of plasmid DNA) was added to 300 µl of the starved culture and incubated for 1 hour at 37°C. Transformants were selected by spreading 100 µl of the cells onto a nutrient agar plate with an appropriate antibiotic and incubated overnight at 37°C.

2.6 Sequencing

2.6.1 PCR Sequencing

DNA fragments or plasmids were confirmed by Sanger sequencing at the MRC PPU unit at Dundee University (www.dnaseq.co.uk). Samples and primers were prepared according to the protocol provided.

2.6.2 Genomic DNA Sequencing

DNA sequencing was performed in this study to analyse the whole genome of the suppressor mutation (see Section 5.2.4). The GenElute^{TM} Bacterial Genomic DNA Kit was used according to the protocol designed for Gram-positive bacteria to prepare genomic DNA. The genomic DNA concentration was measured by nanodrop, and gel electrophoresis was employed to verify the quality of the genomic DNA, which was then sent to Novagen. The data was then analysed using CLC Genomics, and the *B. subtilis* genome (AL009136) was used as a reference.

2.7 Plasmid and strain constructions

All plasmids and strains used in this study are listed in Table 2.2 and 2.3

2.7.1 Xylose-inducible gene expression control

To construct a strain with an artificially induced native gene by altering the expression of a gene (e.g., *asnB*), the native promoter was removed and replaced it with a conditional promoter (e.g., P_{xyl}) using T4 DNA Ligase (NEB). Initially, the purified plasmid (pRD96) was digested with two different restriction enzymes. The gene of interest was then amplified by PCR using primers containing recognition sites for the restriction enzymes that digest the plasmid. The amplified gene fragment (with blunt ends) was ligated into a corresponding site in the digested plasmid using a T4 DNA ligase following the protocol provided (at a ratio of 1:3 vector to insert). The ligation reaction was then incubated overnight at 16°C. To inactivate the reaction, the mixture was heated at 65°C for 10 minutes, followed by transformation into the competent wild-type strain (described in Section 2.6.2).

2.7.2 Autolytic enzymes overexpression construct

To express and purify the autolytic enzymes LytE, LytC, LytD, LytF, and CwlO, plasmid pET-28 was used. The pET-28 plasmid carries a 6X-Histidine tag (6X-His-tag) at either the C-terminus or the N-terminus, a thrombin cleavage site, and a T7 promoter. The autolytic genes coding sequences were amplified by PCR, lacking the trans-membrane sequence and the signal peptide, and inserted into the plasmid in such a way that the codons corresponding to a 6X-His-tag was introduced to either the N- or C-termini of the encoded protein. The resulting plasmids were transformed into *E. coli* (DH5α) as a way to maintain the plasmid stable. Once the constructed plasmid was verified, it was transformed to BL21 (DE3) for high level expression of the cloned genes.

Four plasmid constructs were created for LytE and its carbohydrate-binding domain (CBD); the full-length of *lytE* and the first part of an extracellular domain containing the CBD were fused to 6X-His-tag at either the C-terminus or the N-terminus. To achieve this, the majority of *lytE* and CBD_{lytE} were amplified with primers oAM001/oAM002 and oAM003/oAM004, respectively, using *B. subtilis* 168CA DNA as a template. The pET-28a (+) was linearized using primers oAM005/oAM006 and oAM007/0AM008. The fragments of DNA were then ligated into the corresponding sites of the pET-28a (+) plasmid using the HiFi master mix method (described previously in Section 2.5.2). These generated plasmids are known as pAM019 (H-LytE) and pAM020 (H-CBD_{LytE}), which were tagged with 6X-His-tag at the N-terminal region of the gene.

For the 6X-His-tag fusion at the C-terminal region of LytE and CBD_{LytE}, different sets of primers were used. *lytE* and CBD_{lytE} were amplified using oAM009/oAM010 and oAM011/oAM012, respectively. The pET-28a (+) plasmid was linearized with PCR using two separate sets of primers, oAM013/oAM014 and oAM015/oAM016. The generated DNA fragments were then cloned into pET-28a (+) using the HiFi master mix method. The resulting plasmids containing either LytE or CBD_{LytE} fused with 6X-His-tag at the C-terminus are pAM021 (LytE-H) and pAM022 (CBD_{LytE}-H), respectively.

The other autolytic enzymes LytC, CBD_{LytC}, LytD, LytF, and CwlO were fused with 6X-His-tag plasmid in the same way with different sets of primers given in Table 2.7. All constructed plasmids were confirmed by PCR and sequencing.

Table 2.7 Primers used and plasmid names for the LytC, CBD_{LytC}, LytD, LytF, and CwlO fusion to 6X-His-tag (N-terminus or C-terminus).

N-terminal Fusion			
Genes	Oligos pairs (168CA)	Oligos for pET-28a	Plasmid named
lytC	oAM017/oAM018	oAM021/oAM022	pAM023 (H-LytC)
CBD_{lytC}	oAM019/oAM020	oAM023/oAM024	pAM024 (H-CBD_{LytC})
lytD	oAM033/oAM034	oAM035/oAM036	pAM027 (H-LytD)
lytF	oAM37/oAM38	oAM039/oAM040	pAM028 (H-LytF).
C-terminal Fusion			
Genes	Oligos pairs (168CA)	Oligos for pET-28a	Plasmid named
lytC	oAM025/oAM026	oAM029/oAM030	pAM025 (LytC-H)
CBD_{lytC}	oAM027/oAM028	oAM031/oAM032	pAM026 (CBD_{LytC}-H)
cwlO	oAM041/oAM042	oAM043 /oAM044	pAM029 (CwlO-H)

2.7.3 Plasmid encoded Halo-tag fusion

To investigate the expression and localisation of the autolytic enzymes LytE and LytC, plasmid pAK12 was used to fuse a Halo-tag at the C-terminal region of the protein. For LytE or its N-terminal region (N_{LytE}), the pAK12 plasmid containing a Halo-tag fusion was amplified using two sets of primers: oAM045/oAM046 and oAM045/oAM047. The full-length *lytE* (1002 bp) and N_{lytE} (588 bp) were amplified using primers oAM048/oAM049 and oAM048/oAM050, respectively, with *B. subtilis* 168 DNA as a template. Similarly, for LytC constructed fusion, plasmid pAK12 was linearized by oAM051/oAM052 and oAM051/oAM053. The full-length *lytC* (1488 bp) was amplified with oAM054/ oAM055, while oAM054/oAM056 was used to amplify N_{lytC} (954 bp), *B. subtilis* 168CA DNA was used as a template. The fragments were inserted between the P_{xyl} promoter and the Halo-tag using the HiFi master mix (described in Section 2.2.2), and then transformed into *E. coli* (strain DH5α) (described in Section 2.6.1) using an ampicillin resistance. The plasmids generated were known as pAM030, pAM031, pAM032, and pAM033, which the Halo-tag fused to the C-terminus of LytE, N_{LytE}, LytC, N_{LytC}, respectively. These plasmids were then transformed into 168CA (Section 2.6.2) to obtain strains sAM001 (LytE-Halo), sAM002 (N_{LytE}-Halo), sAM003 (LytC-Halo), and sAM004 (N_{LytC}-Halo) using spectinomycin as a selective marker. The constructions were confirmed by PCR and sequencing using primers to amplify the region from the P_{xyl} (oAM098) to the middle of the Halo-tag (oAM099) (Figure 2.2).

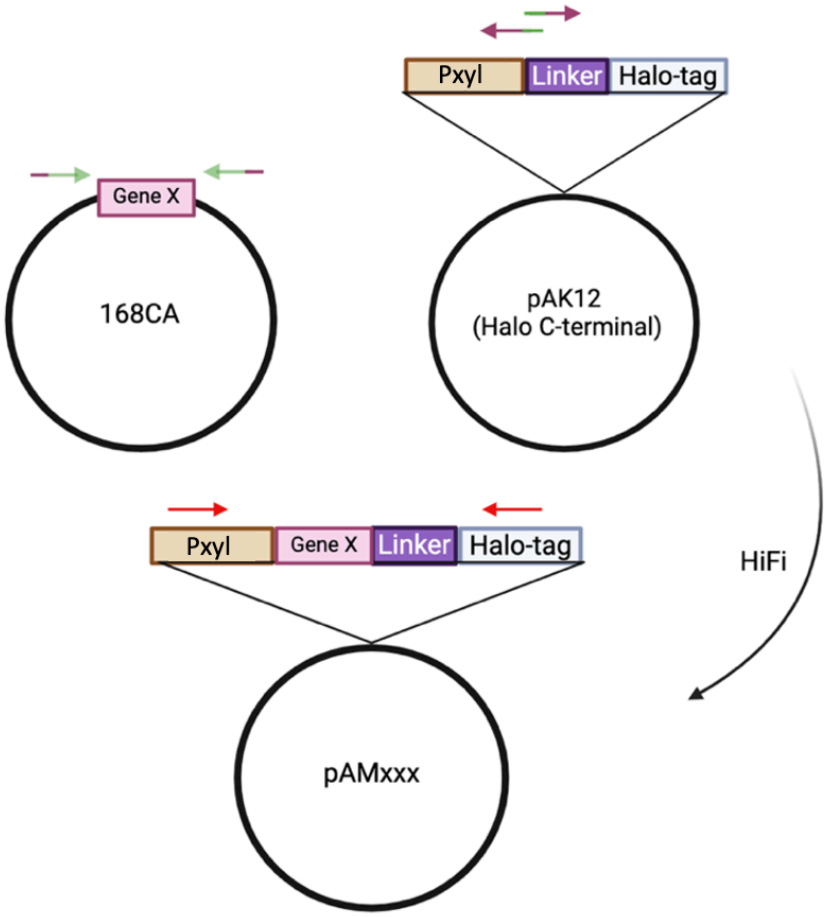

Figure 2.2 Diagram demonstrates the HiFi assembly for Halo-tag construct fusion

The gene of interest and the plasmid (vector) were amplified using a primer with homologous arms (green and purple). The amplification products were incubated with the HiFi master mix for 1 hour, shaking at 50°C, then transformed to *E. coli* to generate the pAMxx plasmid. Image created with BioRender.com.

2.7.4 Construction of chimeric proteins with Protein A (SpA) fusion

2.7.4.1 Construction of SpA expression constructs

Protein A (SpA) fragments with different domain structures were prepared by PCR using *S. aureus* DNA as a template. Full-length *spA* was amplified with oAM057 and oAM058, while the *spA* lacking the LysM and LPXTG domains (*spA*') was amplified using oAM057 and oAM059. A self-replicating plasmid pAG-P08 was used as a vector and linearized with PCR using oAM060/oAM061 primers to insert the SpA and SpA', respectively, followed by digested with *DpnI*. The amplified fragments and the linearized plasmids were cloned using the HiFi DNA assembly master mix method and then transformed into *E. coli* (strain DH5α) for expression, utilising ampicillin resistance as a selective marker. The resulting plasmids pAM034 and pAM035 were then transformed into *B. subtilis* 168*lacI* (sAG1333) to generate strain sAM005 (SpA) and sAM006 (SpA') to evaluate their expression in *B. subtilis*.

2.7.4.2 Construction of autolysin- SpA hybrid proteins

The N-terminal fragments of *lytE* and *lytC* (N_{lytE} and N_{lytC}) were amplified and cloned into pAM034 and pAM035. The N_{lytE} (497 bp) was amplified with the following primer pairs oAM062/oAM063 and oAM066/oAM067, using *B. subtilis* 168CA DNA as the template. The pAM034 and pAM035 were linearized using oAM064/oAM065 and oAM071/oAM072, respectively. Likewise, the N_{lytC} (867 bp) was amplified using the primers oAM073/oAM074 and oAM077/oAM078 and *B. subtilis* 168CA DNA was used as the template. The pAM034 and pAM035 were amplified using oAM075/oAM076 and oAM079/ oAM080, respectively. The fragments were then ligated into the appropriate recognition sites using the HiFi master mix method and transformed into *E. coli* (strain DH5α), with ampicillin resistance as a selective marker. This resulted in the plasmids pAM036, pAM038, in which the N-terminus of LytE and LytC were fused to the spA, respectively. Additionally, the plasmids pAM037 and pAM039 were constructed, which the N-terminus of LytE and LytC fused to spA', respectively. All plasmids were then transformed into *B. subtilis* 168*lacI* (sAG1333) to generate the strains sAM007 (N_{LytE}-SpA), sAM008 (N_{LytE}-SpA'), sAM009 (N_{LytC}-SpA), and sAM010 (N_{LytC}-SpA').

2.7.5 Hybrid genes construction

Hybrid genes were constructed by substituting the C-terminal region of either the *lytE* or *lytF* coding sequence with the C-terminal region of the *cwlO* coding sequence under the control of the inducible promoter P_{hyspac} contained in the pDR111 plasmid. To accomplish this, the full-length *lytE*, *lytF*, and *cwlO* genes were amplified with primers where a *Hind*II restriction site was introduced (primer named indicated in Table 2.8). The pDR111 plasmid was digested with *Hind*III. The PCR products were then ligated with the digested pDR111 plasmid using the HiFi DNA assembly master mix method. The ligated DNAs were then introduced into *E. coli* (strain DH5α) selected for ampicillin resistance to generate the plasmids pAM040, pAM041 and pAM042, which contained the full-length sequences of LytE, LytF, and CwlO, respectively, under the control of the P_{hyspac} promoter. The domain-swapped was then performed using pAM040 and pAM041 plasmids, in which the C-terminus of either LytE or LytF was replaced with the C-terminal of CwlO (C_{cwlO}) leading to create pAM043 ($N_{LytE}C_{cwlO}$) and pAM044 ($N_{LytF}C_{cwlO}$) plasmids. The resulting plasmids were then transformed into a strain lacking either *lytE* (AG547) to generate the sAM011 strain ($N_{LytE}C_{cwlO}$) or a strain lacking *lytF* (AA004) to generate the sAM012 strain ($N_{LytF}C_{cwlO}$).

Table 2.8 describes the template and the names of the oligonucleotides that were used to construct plasmids containing either full-length or swapped domains.

Table 2.8 Templates and oligonucleotides (oligos) used to generate the inducible *lytE*, *lytF*, and *cwlO* and hybrid genes constructs

Template	Oligos	Fragment/ Generate
168CA	oAM081/oAM082	*lytE*
168CA	oAM083/oAM084	*lytF*
168CA	oAM085/oAM086	*cwlO*
168CA	oAM087/oAM086	C_{cwlO}
pAM040	oAM088 /oAM089	Linearized Plasmid
pAM041	oAM090/oAM091	Linearized Plasmid

2.7.6 Construct point mutation in LytE

Site-directed mutagenesis was performed using the Q5 Site-Directed Mutagenesis Kit to replace the cysteine residue (C247- TGC) with the serine residue (AGC) in pAM040 plasmid (the full length of *lytE* under the control of the P_{hyspac} promoter. The pAM040 was amplified using oAM095 (forward primer), which contained the sequence required for the amino acid and flanked by 10 bp of complementary nucleotides. oAM096 primer was used as the reverse primer. The forward and reverse primers were designed as a back-to-back pair (Figure 2.3). 1 µl of the amplified product was mixed with 5 µl of KLD Reaction Buffer (2X), 1 µl KLD Enzyme Mix (10X), and 3 µl Nuclease-free Water. The mixture was incubated at room temperature for 5 minutes, and then 5 µl of the reaction mixture was transformed into *E. coli* (strain DH5α) to result in pAM045 plasmid. The resulting plasmid was then extracted and transformed into a strain lacking *lytE* (AG547) to generate the sAM022 strain.

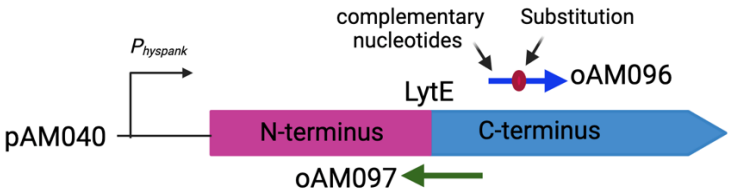

Figure 2.3 Diagram illustrates the primers that used in the Site-directed mutagenesis

The pAM040 (full length of *lytE* under the control of the P_{hyspac} was amplified with the forward primer (blue) contain the amino acid change and the reverse primer (green).

2.8 Protein Analysis

2.8.1 Sodium dodecyl sulphate-polyacrylamide gel electrophoresis (SDS-PAGE) analyses

Sodium Dodecyl Sulphate-Polyacrylamide Gel Electrophoresis (SDS-PAGE) is used to analyse and separate proteins depending on their molecular weight. To prepare the samples for SDS-PAGE, strains were grown until they reached the required growth phase, and then samples were collected and centrifuged at 13,000 x g for 3 minutes. The resulting pellet was suspended in 200 µl of the SDS-loading buffer (described in Appemdix1-Buffer components), sonicated for 30 seconds, and heated at 80°C for 10 minutes. The samples were then loaded on a NuPAGE 4-12% Bis-Tris midi protein gel (Invitrogen), and a Prestained Protein Ladder (Abcam) was used as a marker. The loading of each sample was adjusted to have the same amount of the total cell protein loaded in each lane (relative to OD_{600}). The gel was then run at 180 V in a tank filled with 1X of either NuPAGETM MES SDS Running Buffer or NuPAGETM MOPS SDS Running Buffer (Invitrogen). Once the run was completed, the gel was carefully removed from the cassette and stained with InstantBlue® Coomassie protein stain (Abcam) to visualize the proteins. Stained gels were scanned using an Epson scanner or subjected to a Western blot analysis (described in Section 2.5.2).

2.8.2 Western blot Analysis

To detect and quantify specific protein of interest in a sample, semi-dry Western blot analysis was performed using the Biorad Trans-Blot Turbo equipment. Proteins were separated on SDS-PAGE (described previously in 2.8.1) and then transferred onto an Amersham Hybond 0.45 µm PVDF membrane. Prior to transfer, the sandwich layers were prepared, which are 8 pieces of paper towel, each cut to the same size as the gel, and soaked in transfer buffer (described in Appendix 1-Buffer components). The membrane after being activated in methanol for 1 minute was placed on top of the sandwich layer, followed by the SDS-PAGE gel. Finally, 8 pieces of paper towel soaked in transfer buffer were placed on the gel. The Biorad Trans-Blot Turbo was run at 5 Volts for 30 minutes. Once the transfer was completed, the membrane was incubated in a blocking buffer (described in Appendix 1-Buffer components), with gentle shaking for 1 hour at room temperature. The blocking buffer was then poured off, and the primary antibody diluted in the blocking buffer was added and incubated at 4°C overnight, with gentle shaking. The following day, the membrane was washed four times with PBS-T (described in Appendix 1 -Buffer components) for 5 minutes each

and then incubated with the secondary antibody diluted in the blocking buffer for 1 hour at room temperature. The primary and secondary antibodies used in this study are described in Table 2.9. For Western blot detection, the membrane was incubated with ECL plus following the manufacturer's instructions (Thermo Scientific™ Pierce Fast Western blot Kit). A Luminescent image analysis (imageQuant LAS 4000 mini, GE Healthcare) was used to visualize the protein bands using an appropriate exposure time, which was determined empirically for each blot. Generally, this was between 30 seconds and 5 minutes, depending on the strength of the signal.

Table 2.9 The table describes the primary and secondary antibodies used in this study

Primary Antibody	Secondary Antibody	Molecular Weight of detected Protein
Anti-Penta-His antibodies 1/2000	Anti-mouse Peroxidase 1/10,000	NA*
Protein A antibody 1/2500	Anti-rabbit Peroxidase 1/10,000	42 kDa
PBP2B Antibody 1/10,000	Anti-rabbit Peroxidase 1/10,000	79 kDa
FtsZ Antibody 1/10,000	Anti-rabbit Peroxidase 1/10,000	40 kDa
LytE-Antisera 1/5000	Anti-rabbit Peroxidase 1/10,000	37 kDa
LytC-Antisera 1/2000	Anti-rabbit Peroxidase 1/10,000	52 kDa
LytF-Antisera 1/2000	Anti-rabbit Peroxidase 1/10,000	51 kDa
LytD-Antisera 1/5000	Anti-rabbit Peroxidase 1/10,000	95 kDa

NA* size depends on the protein fusion.

2.8.3 Secretion of recombinant proteins

To assess whether the recombinant protein interacted with the cell wall or was released into the extracellular space, the strain was grown in LB media at 30°C overnight. The next day, the culture was diluted to OD_{600} of 0,05 in 50 ml LB media and incubated at 37°C until it reached the mid-exponential phase then 10 ml of the culture was centrifuged. The resulting pellet was suspended in 2 ml of Protoplasting Buffer (described in Appendix 1-Buffer components) and incubated for 30 minutes at 37°C. After cells were protoplasted, proteinase

K was added to the protoplast at varying concentrations (0.2, 0.1, 0.05, and 0.025 mg/ml), and samples were collected at 5 and 10 minutes and then incubated for 5 minutes after the addition of Tween. The collected Samples were then centrifuged for 5 minutes at 13,000 x g, and the resulting cell pellets were suspended in an SDS-loading buffer. After resolving the proteins on a 4-16% gel, Western blot analysis was done using PBP2B and FtsZ antibodies, which were used as a control for extracellular and cytosolic proteins, respectively.

2.8.4 Overexpression of 6X-His-tag recombinant protein

The recombinant plasmid with 6X-His-tag fusion was expressed in *E. coli* (strain BL21-DE3), where the T7 RNA polymerase is present under the control of an inducible promoter (P_{spac}). The BL21 strains containing different plasmids containing autolytic gene fusions were grown in LB media supplemented with kanamycin at 37°C until reaching an optical density OD_{600} of 0.5. At this point, 1 mM IPTG was added, after which samples were collected every 30 minutes, and the density was measured. to the culture, and genes expression were monitored by measuring the optical density and collecting a 1 ml sample of the cultures every 30 minutes. The collected samples were centrifuged at 13,300 x g for 4 minutes, and the pellets were suspended in 200 µl of SDS-loading buffer. The samples were then sonicated and analysed via SDS-PAGE as described in Section 2.5.1.

2.8.5 Protein Solubilization

Protein solubilization was performed to check whether the protein of interest was in the soluble form (supernatant) or present in the insoluble fraction (pellet). Plasmids with 6X-His-tag fusion were grown until reaching an OD_{600} of 0.5 and then induced with 1 mM IPTG for 30 minutes to 3 hours. A culture of 1 ml was harvested by centrifugation at 13,300 x g for 4 minutes. The resulting pellets were suspended in Buffer Solution 1 (BS-1) (described in Appendix 1-Buffer components) and then sonicated. The mixture was then centrifugated for 5 minutes at 9000 rpm, and the supernatant was transferred to a clean tube while the pellet was suspended in 2 ml of BS-1. 20 µl of either the pellet or the supernatant was mixed with 60 µl of SDS-loading buffer to determine the solubility. Samples were then resolved in SDS-PAGE gel, followed by staining with Coomassie to determine the predominant location of the protein of interest.

2.8.6 Purification of 6X-His-tag fusion protein

The soluble proteins were overexpressed on a large scale of cultures (200 ml) incubated at 30°C and then induced with IPTG (1 mM) for suitable periods (up to 3 hours) to obtain the maximum protein production and avoid inclusion body formation. The cells were harvested by centrifugation at 9000 rpm for 5 minutes. Cell pellets were resuspended in BS-1 (described in Appendix 1-Buffer components) and sonicated to break down the cells, as judged by the optical density and microscopy. The samples were then clarified by centrifugation at 9000 rpm for 5 minutes, and the resulting supernatant was mixed with 1 ml of HisPur™ Cobalt Agarose. The mixture was incubated for 1 hour with rotation at 4°C, then centrifuged for 2 minutes at 500 rpm. Following the centrifugation, 20 µl of the supernatant was collected to mix with 60 µl of SDS-loading buffer as a control for binding. The resin was then washed with five resin-bed volumes of Wash Buffer 1 (described in Appendix 1-Buffer components). The resin was incubated with rotation for 5 minutes, then centrifuged for 2 minutes at 500 rpm, which was repeated 3 to 4 times. The samples were then eluted from the resin with 2 ml of Elution Buffer 1 (described in Appendix 1-Buffer components) with increasing concentrations of imidazole (5 mM, 10 mM, 25 mM, 50 mM, 100 mM, 150 mM, 200 mM, 250 mM, and 500 mM) and centrifuged for 2 minutes at 500 rpm. The supernatants from the wash and elution steps were then analysed by SDS-PAGE to assess protein purification.

2.8.6.1 Inclusion body purification

Where the expressed protein was insoluble, the cells were harvested after being induced with 1 mM IPTG for up to 3 hours at 9000 rpm for 5 minutes, and the pellets were resuspended in phosphate buffer saline (PBS) and Lysozyme. The suspension was incubated at room temperature for 20 minutes. The sample was then sonicated and centrifuged at 3000 rpm for 4 minutes. The resulting pellets were suspended in PBS with 8 M urea, rotated for 30 minutes at room temperature, and then centrifugated at 9000 rpm for 10 minutes. The supernatant containing the solubilized protein was collected and mixed with 200 µl of Chelating Sepharose Fast Flow, followed by incubation with rotation for 1 hour at room temperature and then centrifuged for 2 minutes at 500 rpm. After centrifugation, 20 µl of the supernatant was collected to mix with 60 µl of SDS-loading buffer, and the rest was discarded. The agarose beads were then washed with five-column volumes of Wash Buffer 1 (described in Appendix 1-Buffer components), rotated for 5 minutes, then centrifuged for 2 minutes at 500 rpm (washed steps repeated 3 to 4 times). The final wash was performed with

Wash Buffer 2 containing 5 mM of imidazole. After that, the samples were eluted from the beads with 2 ml of either Elution Buffer 2 (100 mM imidazole) or Elution Buffer 3 (50 mM EDTA), then centrifuged for 2 minutes at 500 rpm. The supernatants of the washing and elution steps were analysed by SDS-PAGE to assess protein purification.

2.8.6.2 Acetone Precipitation Protein

To remove detergents, urea, imidazole, EDTA, and other chemicals from eluted protein samples, four times the sample volume of ice-cold acetone was added and incubated at -20°C overnight. The following day, samples were centrifuged at 4°C for 10 minutes at 15,000 rpm. The supernatant was then removed by pipetting without disrupting the pellets, while the pellets were left at room temperature in open tubes to dry, allowing the acetone to evaporate. Once dried, the pellets were suspended in 200 µl of PBS. Proteins were then sent to Eurogentec to raise antisera after measuring the concentration and purity on the nanodrop spectrophotometer and SDS-PAGE, respectively. This resulted in the generation of 200 µl samples supplied for each injection (Table 3.1).

2.9 Pull down method for Protein A fusions

2.9.1 Generation of affinity resin

The GlycoLink Micro Immobilization Kit was used to immobilize the antibodies and attach anti-Protein A and LytC-antisera to resin beads. For this, the Protein A- antibody was dissolved in 1 ml GlycoLink coupling buffer at 10 mg/ml. Whereas the LytC-antisera protein concentration was measured using nanodrop, and the pH was checked to ensure it was pH<6 then the material was diluted three-fold in 1 ml of GlycoLink coupling buffer (this step named solution 1 for either Protein A- antibody or LytC-antisera). To the solution 1, 2.1 mg of sodium meta-periodate was added, and the mixture was incubated for 30 minutes in the dark (step 2). During the incubation, the desalting column was equilibrated by removing the top and bottom caps and placing the column in a 15 ml collection tube, and centrifugation at 1000 rpm for 2 minutes, this process used to remove the storage solution. The column was then washed with 2.5 mL of GlycoLink coupling buffer and centrifuged at 1000 rpm for 2 minutes to remove the buffer (this step was repeated twice). The column was then placed in a new collection tube, and the samples from step 2 were slowly poured into the centre of the compacted resin bead. The column was centrifuged at 1000 rpm for 2 minutes, the eluted material was collected in a 15 ml tube, and then the column was discarded (step 3). In a 1.5 ml Eppendorf tube, 18 µl of aniline was added to 1 ml of Glycolink coupling buffer, then

vortexed for 10 seconds until the aniline was dissolved, and subsequently added to step 3 to obtain a 0.1 M aniline (solution 2).

To prepare the resin, the UltraLink Hydrazide resin bottle was mixed by end-over-end rotation, and then 2 ml of the resin was placed in a 5 ml spin column. The column was then placed in a 50 ml tube and centrifuged 1000 rpm for 2 minutes to remove the storage buffer (used swing-out centrifuge). Washed the column with 3 ml of GlycoLink coupling buffer and centrifuged 1000 rpm for 2 minutes (this step was repeated once). After completing the washing steps, replaced the bottom cap and added mixture from Step 3 to the column. The mixture was mixed by rocking or end-over-end mixing at room temperature for 3 hours. Following the incubation, the top and bottom caps were removed, and the column was placed in a new 50 ml tube and centrifuged at 1000 rpm for 2 minutes to collect the non-bound protein. The column was washed twice with 2 ml of GlycoLink coupling buffer, centrifuged for 2 minutes at 1000 rpm, and then twice with 2 ml of Wash Buffer 1, followed by centrifugation at 1000 rpm for 2 minutes. Finally, the column was washed twice with 3 ml of degassed PBS buffer (pH 7-8) and centrifuged at 1000 rpm for 2 minutes. The bottom cap was then replaced, and 2 ml of degassed PBS buffer (pH 7-8) was added, and then placed the top cap. The resin beads to which antibodies of the LytC-antisera or protein A antibody had bound were stored upright at 4ºC. Immediately before use the resin beads, 700 µl of the antibody resin was centrifuged for 2 minutes at 1000 rpm. The resin was washed twice with Tris-NaCl-sucrose buffer, followed by centrifugation at 1000 rpm for 1 minute.

2.9.2 Pull-down assay

The antibody resin prepared in (2.6.1) was used for the pull-down assay. The strains with protein A fusions were grown overnight at 30ºC in an LB media with an appropriate antibiotic. The next day, the cultures were diluted 1/10 in a fresh media and incubated for 2 hours at 37°C. The culture was then diluted with fresh pre-warmed media to an optical density of OD_{600}~ 0.05 and incubated at 37°C until they reached an OD_{600} of 0.5. IPGT (to 1 mM) was added to the cultures to induce full expression, and the cultures were incubated for 30 minutes. At suitable time points, 10 ml of the culture was harvested via centrifugation at 9000 rpm for 4 minutes, and the supernatant was discarded. The pellet was suspended in 2 ml of Protoplasting buffer containing proteinase inhibitor (described in Appendix 1-Buffer components) and incubated for 30 minutes to lyse the cells (cell lysis was verified by

microscopy). The lysate cells were then centrifuged at 13,000 x g for 3 minutes, and the supernatant was transferred to a clean 10 ml tube.

One millilitre of the supernatant was then added to the antibody resin (prepared in Section 2.6.1) and mixed by rotation at 4ºC for 1 hour. After 1 hour of incubation, the suspension was centrifuged for 1 minute at 1000 x g, and the resin was washed with Tris-NaCl-sucrose buffer three times. The bound material was then eluted from the resin twice using 200 µl of 0.1-0.2 M glycine-HCL at pH 2.5. The eluted samples were then analysed by SDS-PAGE and processed for mass spectrometry analysis.

2.10 Preparation of cultures for Mass Spectrometry Analysis (MS)

Strains were grown overnight in 10 ml of LB media at 30°C. The following day, the cultures were diluted in 20 ml of minimal media (described in Appendix 1-Media composition) until they reached the exponential phase, then diluted back to an OD_{600} ~ 0.05 in 100 ml of minimal media. The cultures were grown at 37°C until they reached an OD_{600}~ 0.6, at which point they were divided into two 50 ml samples. One was used to prepare a "total cell material" sample, while the other was to be treated with 1.5 M lithium chloride (LiCl) to extract wall bound proteins. Both were centrifuged 4 minutes at 9000 rpm, and the cell pellets were frozen in liquid nitrogen. The culture media from these samples was also processed by the addition of cold 100% Trichloroacetic acid (TCA) to give a final concentration of 10% TCA and held at 4°C overnight to precipitate secreted proteins.

The cell pellets were processed in two different ways. One was kept as a total protein sample, whereas the other pellet was allowed to defrost and suspended in 10 ml of 1.5 M LiCl containing 1 tablet of mini protease inhibitor EDTA-free and incubated on ice for 10 minutes. After incubation, the samples were centrifuged for 8 minutes at full speed at 4°C. The resulting pellet was then placed in liquid nitrogen and frozen, while the supernatant precipitated with TCA as described earlier at 4°C overnight. The next day, the TCA-treated samples were centrifuged for 15 minutes at 20,000 rpm at 4°C. The supernatants were poured off, and the pellets were washed twice with 1 ml of cold acetone. Finally, the precipitated material was allowed to dry for 20 minutes before being suspended in 200 µl of PBS. Samples were then sent to the mass spectrometry department for analysis.

2.11 Microscopy technique

2.11.1 Fluorescence microscopy

Strains were grown overnight in suitable media at 30°C with shaking. The following day, the culture was diluted back to OD_{600} of 0.05 and allowed to grow until reaching the exponential or stationary phase. To stain the cell membrane, 1 µl of FM5-95 dye (Molecular Probes 10 µg/ml) was mixed with 30 µl of the cell culture. To prepare the microscope slide, 600 µl of 1.2% agarose pads (0.24 g agarose heated in 20 ml water) were added to the slide, and then another slide was applied on top. Before using the slide for the microscope, the top slide was removed from the agarose pad followed by the addition of 1 µl of cell suspension onto the agarose pad. Samples were allowed to dry before being covered with a cover slip. The microscope images were acquired using a Nikon Plan Fluor 100× lens with phase contrast or epifluorescence illumination (excitation 560-440 nm and emission at 630-675) and collected by Metamorph® imaging software. The ImageJ, Fiji software was used to analyse the resulting microscopy images.

2.11.2 Immunostaining

To localise the native hydrolysis enzymes using their specific antisera, the wild type and the deletion strains were grown overnight in an LB media overnight at 30°C. The cultures were then diluted back into fresh and warm LB media to the OD_{600}-0.05 and incubated at 37°C for up to 2 hours. Cells were fixed by mixing them with an equal volume of 1% paraformaldehyde and holding the mixture on ice for 30 minutes were centrifuged, followed by resuspending he pellet in PBS (this wash step was repeated 3 times). Pellets were then resuspended in GTE buffer (Appendix 1-Buffer Components), and the buffer volume was adjusted according to the optical density to ensure an approximately equal number of cells in each sample. 20 µl of the cells suspended in GTE buffer were then spotted on a Multi-Spot Shandon 12 well microscope slide for 5 minutes, followed by aspiration of the solution and allowing the slide to dry. Once the slide was dry, 20 µl of 0.01% poly-L-lysine was applied to each spot for 2 minutes, after which the excess solution was removed and the slide allowed to dry. 10 mg/ml lysozyme (Sigma) was dissolved in GTE buffer and then used to treat cells for 1 minute. Culture spots were then washed in PBS and allowed to dry before blocking in 2% Bovine serum albumin (BSA) dissolved in PBS for 15 minutes. Once that was done, the primary antibody was applied and incubated overnight at 4°C. The primary antibodies used in the immunostaining were the LytE-antiserum, and LytC-antiserum, which were diluted 1/250 in PBS with 2% BSA. The following day, the cell spots were washed with

PBS (10 times), and the secondary antibody (anti-rabbit FITC (Sigma) was then applied after diluting 1/250 in PBS with 2% BSA and incubated in the dark for 1 hour. The cell spot was then washed with PBS (10 times) before adding 2 µl of VectaShield antifade mounting medium with 0.2 µg/ml DAPI to each spot then placed the coverslip and samples were ready for analysis under the microscope.

Chapter 3: Determining the relative abundance of specific autolytic enzymes in *B. subtilis*

3.1 Introduction

The autolytic enzymes LytE, LytF, CwlO, LytC, and LytD play a crucial role in maintaining cell shape, growth, and motility. LytE, LytF, and CwlO belong to the DL-endopeptidase family and play a significant role in cell morphology (Ishikawa *et al*., 1998b; Ohnishi *et al.*, 1999). Meanwhile, LytC and LytD (amidase and glycosaminidase, respectively) are considered to be the major autolytic enzymes involved in cell wall turnover and cell motility (Atrih *et al*., 1999a; C. T. Brown *et al*., 2011; R. Chen *et al*., 2009). Previous studies have determined that the loss of both *lytE* and *cwlO* results in cell death; however, individual mutations of these genes do not lead to lethality but do significantly alter cell morphology (Bisicchia *et al*., 2007). Thus, these two autolytic enzymes are presumed to have overlapping functions, some of which are critical for cell growth. The expression of the autolytic enzymes has been shown to be tightly regulated and can be altered by changes in environmental conditions or genetic mutations that result in affect cell wall composition (Kasahara *et al*., 2016a; Kiriyama *et al*., 2014a; Meisner *et al*., 2013; Salzberg *et al*., 2013).

Environmental conditions such as temperature, pH, oxygen level, and nutrient availability significantly influence the abundance of autolytic enzymes (Koo *et al.*, 2017). Furthermore, magnesium and glucose have been demonstrated to play a role in both the activity and expression of the autolytic enzymes. Previous studies have shown that magnesium plays a role in rescuing the viability and rod-shaped morphology in strains lacking *mreB* or *ponA*. inhibited PG autolysin (Chastanet & Carballido-Lopez, 2012; Kleppe *et al*., 1982). PonA is a penicillin-binding protein (bifunctional glucosyltransferase/ transpeptidase) that has a role in cell division and elongation (Claessen *et al*., 2008). The precise mechanism how the $MgSO_4$ rescue remines unclear; however, some theories suggest that $MgSO_4$ may modulate the activity or stability of cell wall enzymes. Glucose supplementation has been demonstrated to increases the abundance of the LTA synthases (LtaS and YfnI), which in turn enhances LTA production and leading to accumulate LytE levels. Furthermore, recent investigations has revealed that the transmembrane protein MprF (aminoacyl-phosphatidylglycerol synthase) contributes significantly to modulating the LTA biosynthesis (Guyet *et al*., 2023). However, how alteration in the cell wall composition affect the autolytic enzymes remains unclear. This chapter focused on analysing the abundance of the key autolytic enzymes (LytE, LytF, CwlO LytC, and LytD) in different mutant strains and culture conditions, suggesting that these conditions directly or indirectly affect cell wall turnover, which implies a change in autolytic

activity. The emphasis is placed on the sigma factors SigI, sigD, and SigM, (described earlier in Section 1.5.3), PonA and MprF.

Initially, the aims were to purify active autolytic enzymes and to characterise both their biochemical activity and how they interacted with the cell wall *in vitro*. However, the objectives of this work had to be redefined by the problems encountered in overexpressing the proteins of interest. The main consequence was that a more *in vivo* approach had to be employed. Despite this, polyclonal antisera specific for the autolytic enzymes LytE, LytC, LytF, and LytD were generated that were able to detect the autolytic enzyme of interest and allow us to identify changes in the relative abundance of the enzymes during growth by Western blot analysis.

3.2 Results

3.2.1 LytE overexpression and purification in *E. coli*

A set of plasmids based on pET-28a was constructed, encoding the complete or partial (carbohydrate-binding domain CBD/ LysM) coding sequence of *lytE* (all constructs were verified by DNA sequencing). The expression of these plasmids would result in the encoded protein being fused to a 6X-His-tag (H) at either the beginning or the end of the protein. This resulted in plasmids named H-LytE (pAM019), H-CBD_{LytE} (pAM020), LytE-H (pAM021), and CBD_{LytE}-H (pAM0022) (cloning described in Section 2.8.1). These plasmids were then transformed into *E. coli* (strain BL21-DE3) and grown to the mid-exponential phase. At this point, expression was induced by IPTG, and samples were collected every 30 minutes over two hours. The total cellular proteins of these samples were then extracted and loaded onto an SDS-PAGE gel, adjusting the amount loaded according to the optical density of the culture at the time of sampling to detect if the overexpression of a protein corresponding to the expected size was occurring. Upon staining the gel with Coomassie, proteins of the expected size of either LytE or CBD_{LytE} were observed to accumulate over time for the respective constructs, as indicated by the red arrows in Figure 3.1.

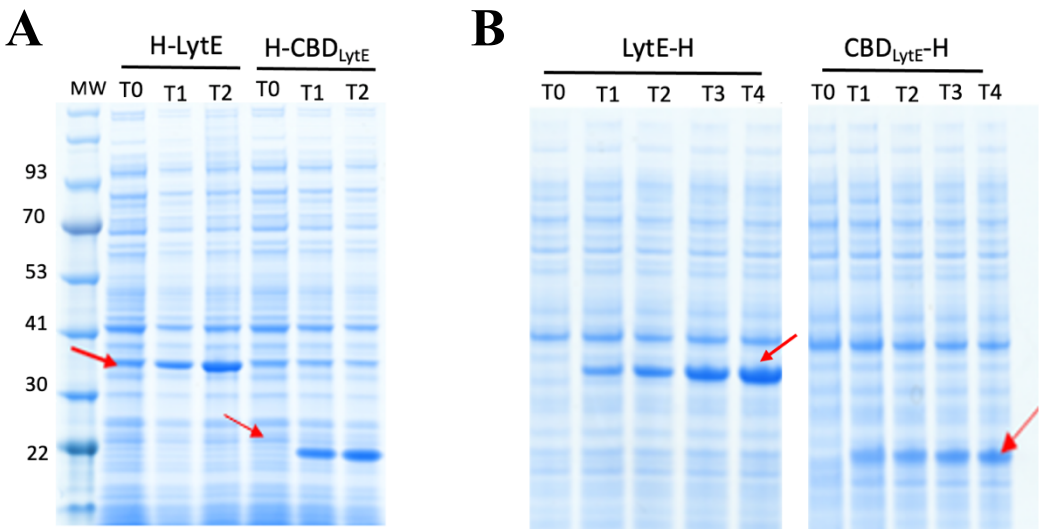

Figure 3.1 Overexpression of LytE and CBD_{LytE} fused to 6X-His-tag

The 6X-His-tag (H) fusion was introduced into both the N-terminus (A) and the C-terminus (B) of the full-length LytE and the CBD_{LytE} as well. Samples were collected before induction (T0) and at 30-minutes intervals after induction (T1, T2, T3, and T4). The collected samples were centrifuged, and then the pellets were suspended in an SDS-loading buffer. The molecular weight marker (kDa) is indicated by MW, and the red arrow indicates the predicated molecular weight of LytE (37 kDa), and CBD_{LytE} (22 kDa).

Having established that the genes can be overexpressed, the solubility of the overexpressed proteins was determined as described in the methods in Section 2.9.5. Briefly, BL21 transformants containing the plasmids (H-LytE, H-CBD_{LytE}, LytE-H, and CBD_{LytE}-H) were cultured in an LB media supplemented with kan selection until they reached the mid-exponential phase (OD_{600}~ 0.5), then induced with 1 mM IPTG for 2 hours. The cells were harvested by centrifugation, and the cell pellets were suspended in Buffer solution 1 (BS-1) (described in Appendix 1-Buffer components) and then broken by sonication. The resulting pellets and supernatants were then analysed using SDS-PAGE. The SDS-PAGE gels were then stained with Coomassie and indicated that both LytE and CBD_{LytE} fused to the 6X-His-tag at the N-terminal or C-terminal regions were present in the pellet when overexpressed (Figure 3.2A and B). Suggesting that they were either insoluble or had aggregating as an inclusion body. Visualization of the cells after induction under microscopy showed small spherical-shaped refractile particles suggesting inclusion body formation.

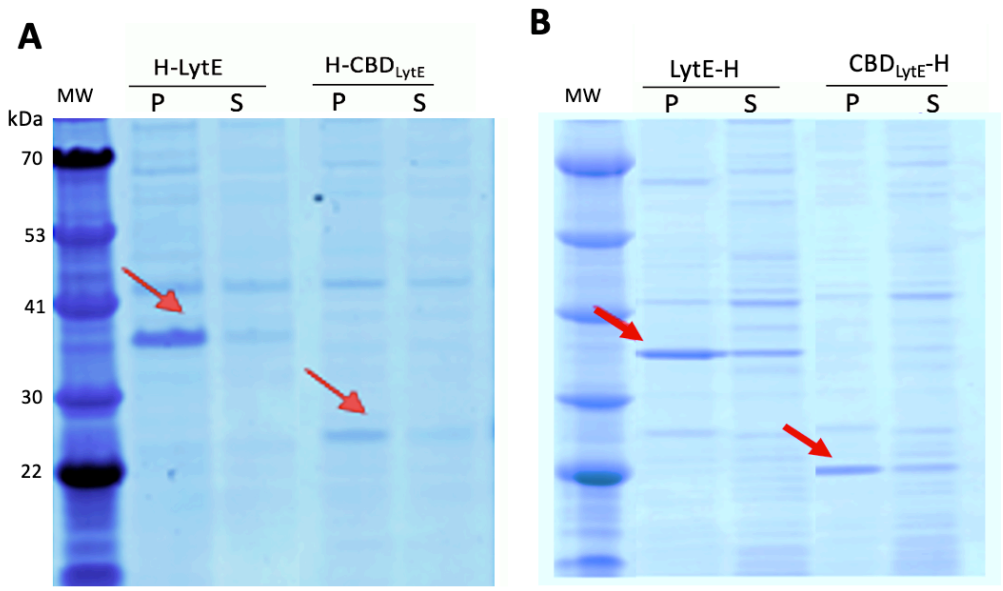

Figure 3.2 Analysis of the solubilisation of LytE and CBD_{LytE} fused to a 6X-His-tag by SDS-PAGE

Samples were harvested after 2 hours of overexpression. The cell pellets were suspended in Buffer Solution 1 (BS-1), which contains 50 mM Tris (pH 8), 300 mM NaCl, and 10 mM imidazole, and then centrifuged at 13,300 x g for 4 minutes. The samples were then analysed by SDS-PAGE. (A) 6X-His-tag was fused to the N-terminus and (B) 6X-His-tag was fused to the C-terminus of either LytE or CBD_{LytE}. The molecular weight marker (kDa) is indicated by MW, and the red arrow indicates the expected size of LytE and CBD_{LytE}. (P) represents the pellet, and (S) represents the supernatant.

One way to address the insolubility of LytE and CBD_{LytE} was to manipulate the buffer condition used for extraction combined with lower levels of expression. This approach aimed to determine if it was possible to obtain soluble protein by varying salt concentrations and pH. Since both fusion constructs exhibited similar solubilisation conditions, the focus was placed on the 6X-His-tags fused to the C-terminal region due to a small amount of LytE presented in the supernatant. The LytE-H and CBD_{LytE}-H were grown and collected samples after two hours of induction and suspended the cell pellet in different buffers with varying pH (5 to 8) (BS-2, BS-3, BS-4, and BS-5) (described in Appendix 1- Buffer components). The sample solubility was assessed by SDS-PAGE and revealed that LytE and CBD_{LytE} remained predominantly insoluble, as the major band corresponding to LytE and CBD_{LytE} was presented in the pellet under all conditions used (Figure 3.3).

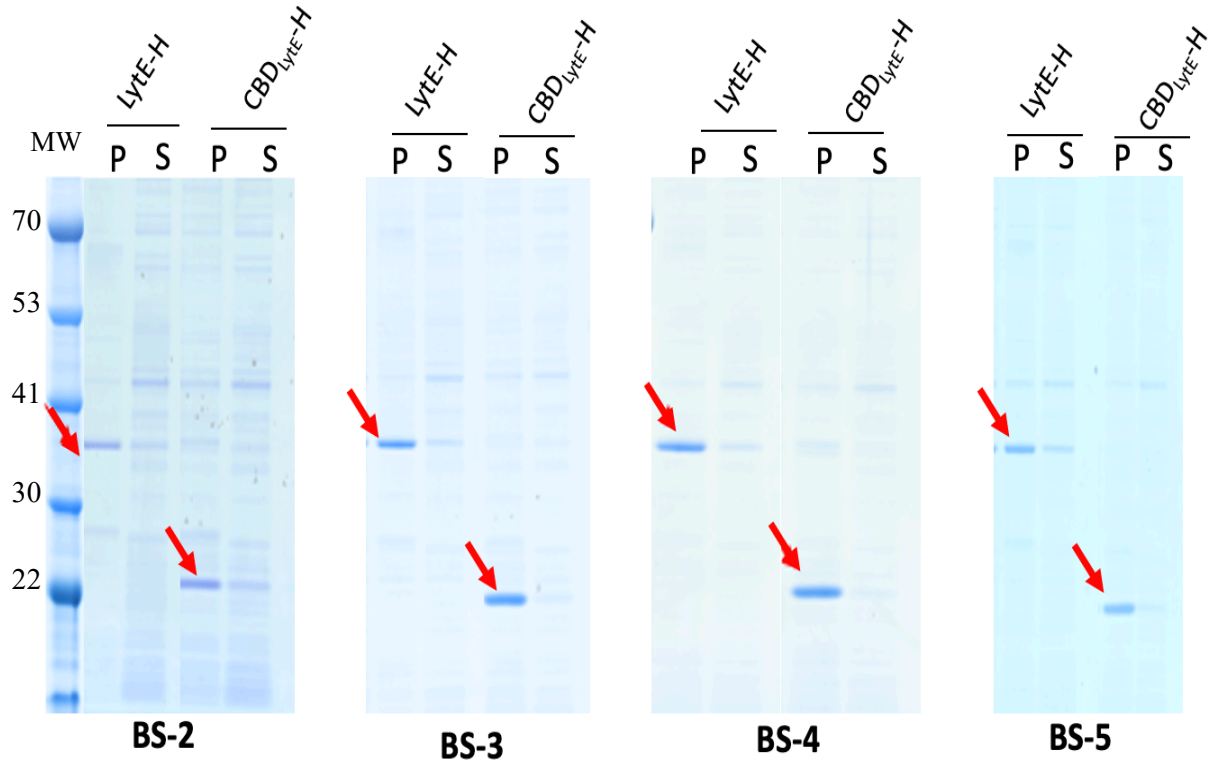

Figure 3.3 Assessing the solubilisation of LytE and CBD_{LytE} fused to 6X-His-tag at the C-terminal region using different buffer solutions by SDS-PAGE

Samples collected 2 hours after induction were treated with one of the following buffers: Buffer Solution 2 (BS-2), Buffer Solution 3 (BS-3), Buffer Solution 4 (BS-4), or Buffer Solution 5 (BS-5), as described in Appendix 1-Buffer Components. The molecular weight marker (kDa) is indicated by MW, and the red arrow indicates the expected size of LytE and the CBD_{LytE}. (P) represents the pellet, and (S) represents the supernatant.

Using different pH and salt concentrations, no solubilisation of LytE and CBD_{LytE} was observed. Thus, it was assumed that inclusion bodies were formed in cells during the expression period. To avoid this, the induction conditions were adjusted, and direct purification of the soluble protein was attempted using an affinity resin. Here, LytE-H was overexpressed at 30°C for 3 hours. The cell pellet was suspended in BS-1 and sonicated to release the overexpressed proteins, followed by centrifugation to remove insoluble material. The resulting supernatant was then mixed with 1 ml of HisPur™ Cobalt Agarose beads with rotation for 1 hour at 4°C. After washing the beads four times with Wash Buffer 1, proteins were eluted by Elution Buffer 1 with varying concentrations of imidazole (5 mM, 10 mM, 25 mM, 50 mM, 100 mM, 150 mM, and 200 mM) and running in SDS-PAGE (described in Appendix 1- Buffer components). By staining the gel with Coomassie stain, it was found that under these induction conditions, approximately 50 % of the expressed protein was in the supernatant, indicating solubility (annotated with red arrows Figure 3.4A, second lane). The series of washing steps removed all unspecific bands. During the elution step, the sample was

successfully eluted from the bead at an imidazole concentration between 25-100 mM, and 50 mM was the highest protein elution (Figure 3.4A). All elution samples were then collected and concentrated using Amicon® Ultra 15 mL centrifugal filter. Thus, purification was possible for the full-length LytE protein to yield a reasonably pure sample, but the final concentration of the purified protein was low to do the biochemical activity (Figure 3.4B).

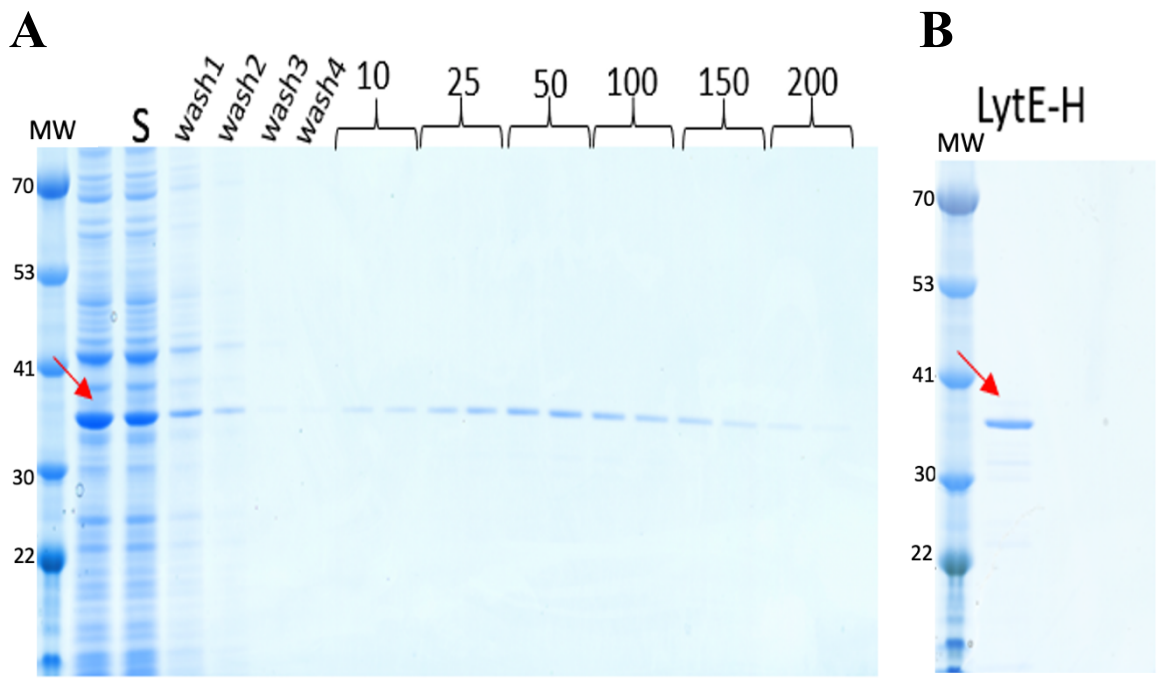

Figure 3.4 LytE-H purification at 30°C

SDS-PAGE analysis was performed on purified LytE-H. (A) LytE-H was overexpressed at 30°C for 3 hours (first unannotated lane) then suspended in BS-1(indicated as S). The supernatant (S) was mixed with HisPur™ Cobalt Agarose. The mixture was washed four times with Wash Buffer 1 (Wash 1, Wash 2, Wash 3, and Wash 4). Elution was performed using Elution Buffer 1 with different imidazole concentrations ranging from 10 to 200 (indicated by the numbers above the lanes (mM)). (B) All the elution samples were collected using centrifugal filtration (Amicon® Ultra 15 mL) to concentrate the purified LytE-H. The molecular weight marker (kDa) is indicated by MW, and the red arrow indicates the expected size of LytE.

As the priority at this stage in the project was to obtain sufficient material to allow antibodies to be raised, the purification of the protein was exploited from the inclusion bodies. Strain with a transformed plasmid (LytE-H) was grown in LB media with kan antibiotic until reaching OD_{600}~0.5, then added IPTG and incubated at 37°C for 4 hours. The culture was then harvested, and the pellet was suspended in PBS and lysozyme. It was incubated for 20 minutes at 37°C, then sonicated and centrifuged. The resulting pellet was treated with 8 M of urea in PBS to denature the protein and incubated for 30 minutes at room temperature (Figure 3.5A and B (S lane)). The sample was then centrifuged, and the soluble

materials were mixed with Chelating Sepharose Fast Flow and incubated with rotation for 1 hour at room temperature (described in Section 2.9.6.1). The beads were washed series with Wash Buffer 1 and then eluted twice with either Elution Buffer 2 (containing 100 mM imidazole) (Figure 3.5A) or Elution Buffer 3 (containing 50 mM EDTA) (Figure 3.5B) (Appendix 1-Buffer components). The eluted samples were then precipitated with cold acetone for overnight (described in Section 2.9.6.2). Upon analysis of SDS-PAGE, LytE-H was found to be present in the soluble fraction (present in the supernatant (Figure 3.5A and B). The imidazole or EDTA elution seemed to give a similar level of eluted LytE-H, but there were other bands detected in the participating samples (A1 and A2). Western blot analysis was performed using an anti-Penta-His antibody to assess the purification of LytE-H, A1 detects one band, while A2 presents two bands, which could be caused by loading or denaturation artifacts or post-translational modification of the protein (Figure 3.5B).

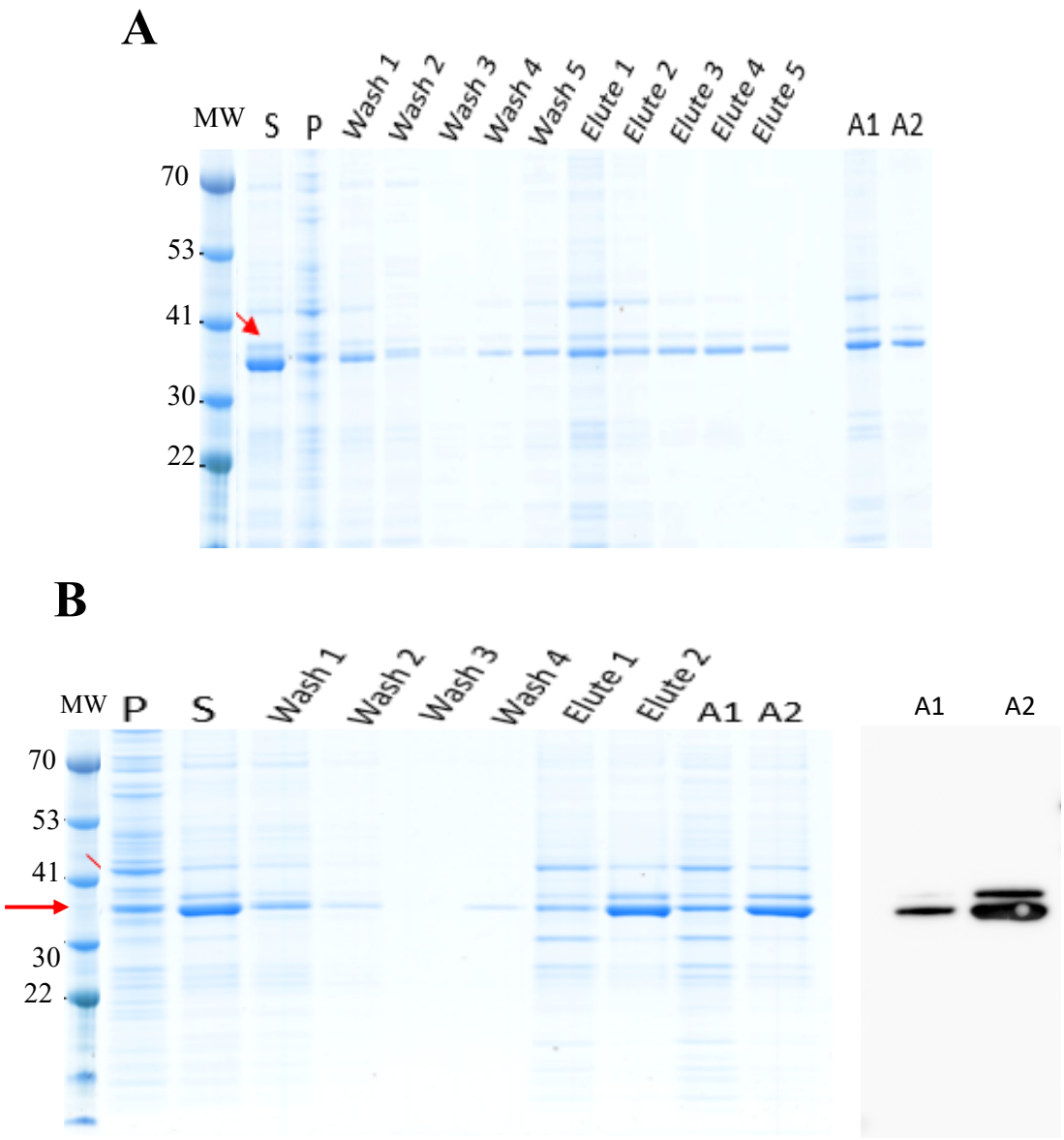

Figure 3.5 LytE-H purified from inclusion bodies using 8M urea

LytE-H was induced for 4 hours at 37°C, and then the cell pellets were suspended in PBP with 8 M of urea. (A) The sample was washed three times with Wash Buffer 1 (Wash 1, Wash 2, and Wash 3). The fourth and fifth washes were performed with Wash Buffer 2, which included 5 mM Imidazole (Wash 4 and Wash 5). LytE-H was eluted five times with Elution Buffer 2 containing 100 mM Imidazole (Elute 1, Elute 2, Elute 3, Elute 4, and Elute 5). The Elute 1, Elute 2, and Elute 3 were pooled precipitated with acetone (A1) and Elute 4 and Elute 5 were collected and precipitated with acetone (A2). (B) The sample was washed three times with Wash Buffer 1 (Wash 1, Wash 2, and Wash 3). The fourth wash was performed with Wash Buffer 2, which included 5 mM imidazole. LytE-H was eluted twice with Elution Buffer 2 (Elute 1 and Elute 2) containing 50 mM EDTA. The eluted samples were then precipitated with acetone (A1 and A2). The Western blot image shows the precipitated samples A1 and A2 detected by Anti-Penta-His antibodies. The molecular weight marker (kDa) is indicated by MW, and the red arrow indicates the expected molecular weight of LytE (37 kDa).

3.2.2 LytC overexpression and purification in *E. coli*

In order to purify LytC and the carbohydrate-binding domain (CBD_{LytC}) of LytC, 6X-His-tag fusion constructs were generated at the N- /C-terminal regions as described in method in Section 2.8.1. The resulting plasmids were pAM023 (H-LytC), pAM024 (H-CBD_{LytC}), pAM025 (LytC-H), and pAM026 (CBD_{LytC}-H) construct without the transmembrane and signal peptide regions. To check the protein overexpression, the H-LytC, H-CBD_{LytC}, LytC-H, and CBD_{LytC}-H were grown in LB media with kan resistance until they reached OD_{600}~0.5, and then the IPTG was added for induction. Samples were collected before and at 30-minute intervals after induction. The total cells were then separated in SDS-PAGE, and it was revealed that all constructed fusions were overexpressed over time after being induced with IPTG (Figure 3.6A and B). The stained gels determined an increased intensity of the bands after induction compared with the samples before (T0). After verifying the overexpression, the solubilisation of the LytC and CBD_{LytC} fused with 6X-His-tag at either the N- or C-terminal regions was evaluated using BS-1. By analysing the SDS-PAGE gel, it was found that most of LytC and CBD_{LytC} were present in the pellet fraction, which indicated they were insoluble (Figure 3.7A and B).

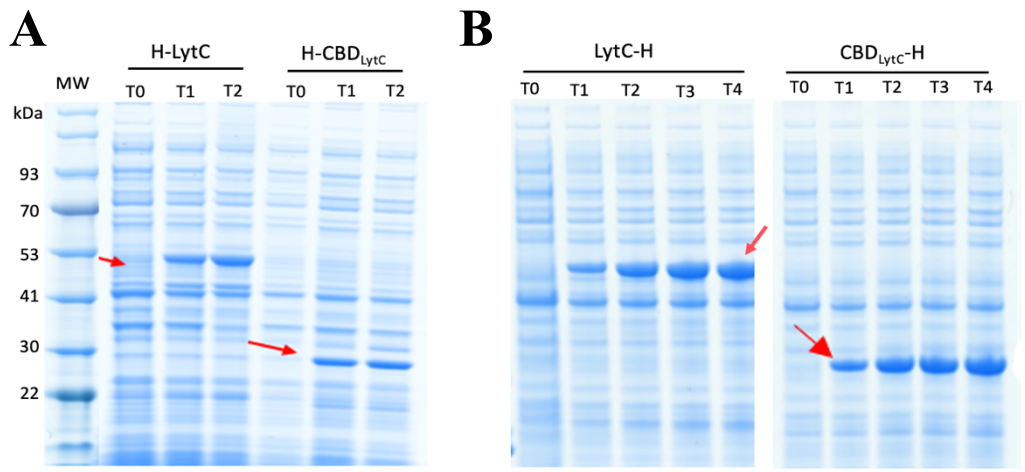

Figure 3.6 Overexpression of the LytC and CBD_{LytC} fused to 6X-His-tag at the N-terminus (A) and the C-terminus (B)

Plasmids were grown in LB media at 37°C until they reached OD_{600}~0.5, then samples were collected before induction (T0). 1 mM IPTG was then added, and samples were collected at 30-minute intervals (T1, T2, T3, and T4). The collected samples were centrifuged, and the cell pellet were suspended in 200 µl of SDS-loading buffer for SDS-PAGE analysis. The SDS-PAGE gel was stained with Coomassie to visualize the protein overexpression. The red arrow indicates the bands corresponding to LytC and CBD_{LytC}. The molecular weight marker (kDa) is indicated by MW, and the red arrow indicates the predicated molecular weight of LytC is 52 kDa, while 33 kDa for CBD_{LytC}.

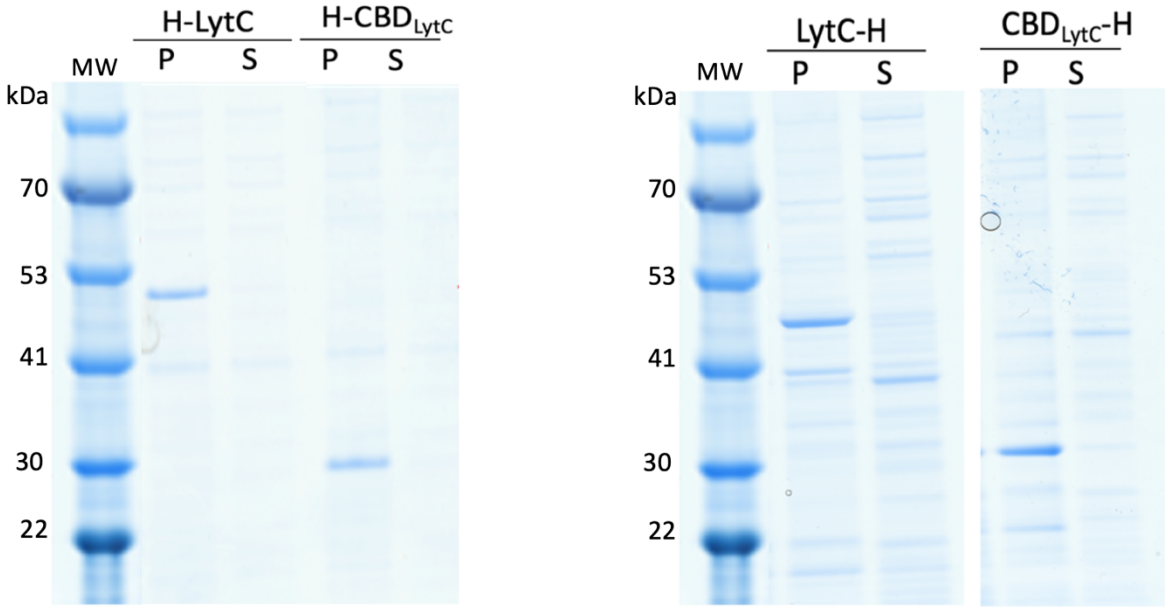

Figure 3.7 The solubilisation analysis of H-LytC, H-CBD_{LytC}, LytC-H, and CBD_{LytC}-H by SDS-PAGE

Samples were harvested after being induced with IPTG for two hours at 37°C. The cell pellets were suspended with Buffer Solution 1(BS-1). The molecular weight marker (kDa) is indicated by MW, and the red arrow indicates the expected size of LytC and the CBD_{LytC}. (P) represents the pellet, and (S) represents the supernatant.

Since both the N-terminal and C-terminal 6X-His-tags fusion constructs were expressed sufficiently to produce a reasonable yield of protein, the C-terminal fusion was chosen for the entire study. The purification of LytC-H and CBD_{LytC}-H was performed using different buffer conditions (BS-2, BS-3, BS-4, and BS-5) with varying pH levels from 6 to 8 in an attempt to improve their solubility (described in Appendix 1-Buffer components). However, SDS-PAGE analysis indicated that the fusion constructs LytC-H and CBD_{LytC}-H were present in the pellet material and remained insoluble (Figure 3.8).

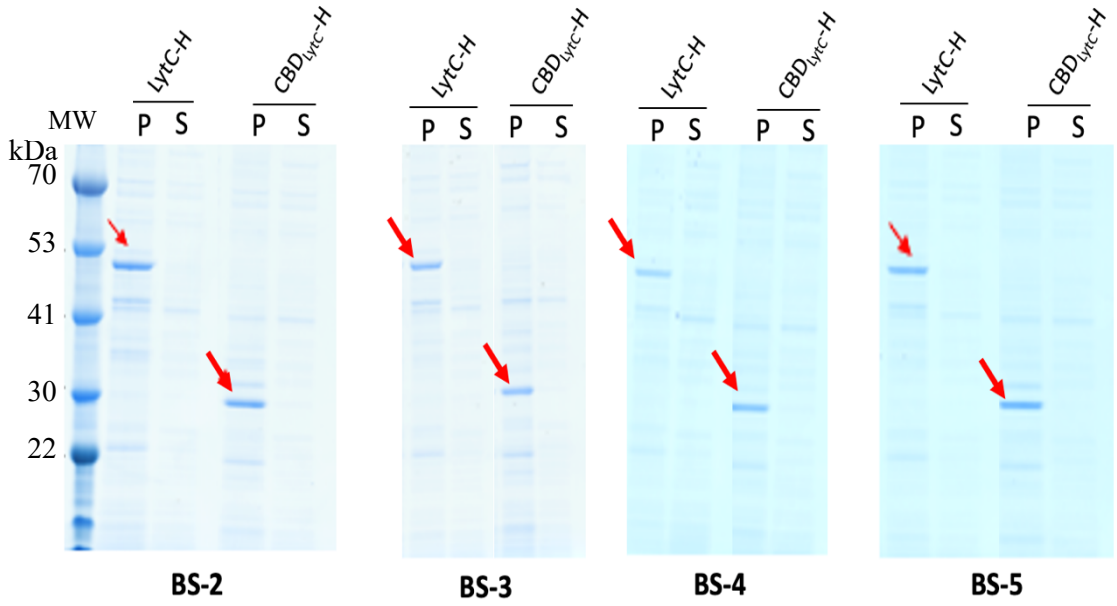

Figure 3.8 The solubilisation of LytC-H and CBD_{LytC}-H analysed using SDS-PAGE

Samples collected 2 hours after induction were treated with one of the following buffers: Buffer Solution 2 (BS-2), Buffer Solution 3 (BS-3), Buffer Solution 4 (BS-4), or Buffer Solution 5 (BS-5), as described in Appendix 1-Buffer Components. The (P) represents the pellet, and (S) represents the supernatant. The molecular weight marker (kDa) is indicated by MW, and the red arrow indicates the predicted molecular weight of the LytC and CBD_{LytC}.

Despite altering the buffer condition, LytC and CBD_{LytC} fused to 6X-His-tag remained insoluble. In an attempt to resolve this problem, LytC-H was expressed at 30°C for two hours to reduce the rate at which it was produced and avoid the inclusion body formation. Following the method described in Chapter 2-Section 2.9.6, a sample of LytC-H was collected and suspended in BS-1, and then mixed with HisPur Cobalt Superflow Agarose Beads. The beads were washed three times with Washing Buffer 1 then eluted twice with different imidazole concentrations, starting from 10 mM, 25 mM, 50 mM,100 mM, 150 mM, and 200 mM, respectively. Upon analysing the samples using SDS-PAGE, LytC was found to have disappeared on elution step (Figure 3.9). Thus, although the presence of the 6X-His-tag fusion in all constructs was confirmed by sequencing, the SDS-PAGE gel indicated that LytC-H did not bind to the beads. This step was also performed with the N-terminal fused protein, and the same result was obtained.

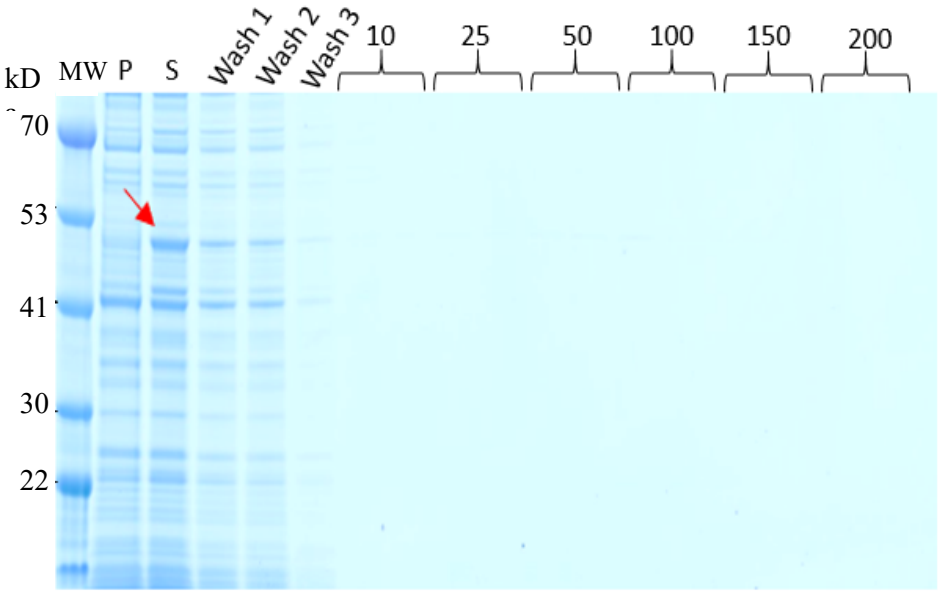

Figure 3.9 LytC-H Purification at 30°C

The strain was grown at 30°C, induced for 2 hours with IPTG, and then suspended the cell pellet in BS-1. After mixing the superannuant with HisPur Cobalt Superflow Agarose, the beads were washed three times with Wash Buffer 1 (Wash 1, Wash 2, and Wash 3). The sample was then eluted using Elution Buffer 1 with different imidazole concentrations ranging from 10 to 200 (indicated by the numbers above the lanes (mM)). The molecular weight marker (kDa) is indicated by MW, and the red arrow indicates the expected size of LytC. (P) represents the pellet, and (S) represents the supernatant.

To understand the reason why LytC-H did not bind to nickel agarose beads, Western blot analysis was used to detect the 6X-His-tag fusion at both the N- and C- terminal regions of the full-length LytC using Anti-Penta-His antibody (Figure 3.10A and B). The samples were grown in LB media supplemented with kan selection at 30°C and 37°C. Once the cultures reached OD_{600}~0.5, it was induced with 1 mM IPTG. Samples were then collected at 30-minute intervals and subjected to SDS-PAGE and Western blot analysis. The antibody successfully detected bands at the position corresponding to the appropriate molecular weight, indicating that the fusion protein was constructed correctly in both fusions (C-terminal and N-terminal regions). However, both constructed fusions observed degradation in LytC over time. The degradation was reduced at 30°C and observed to be more significant in the N-terminal fusion than the C-terminal fusion. This degradation could potentially affect the binding of the 6X-His-tag fusion to Cobalt agarose beads (Figure3.10 A and B).

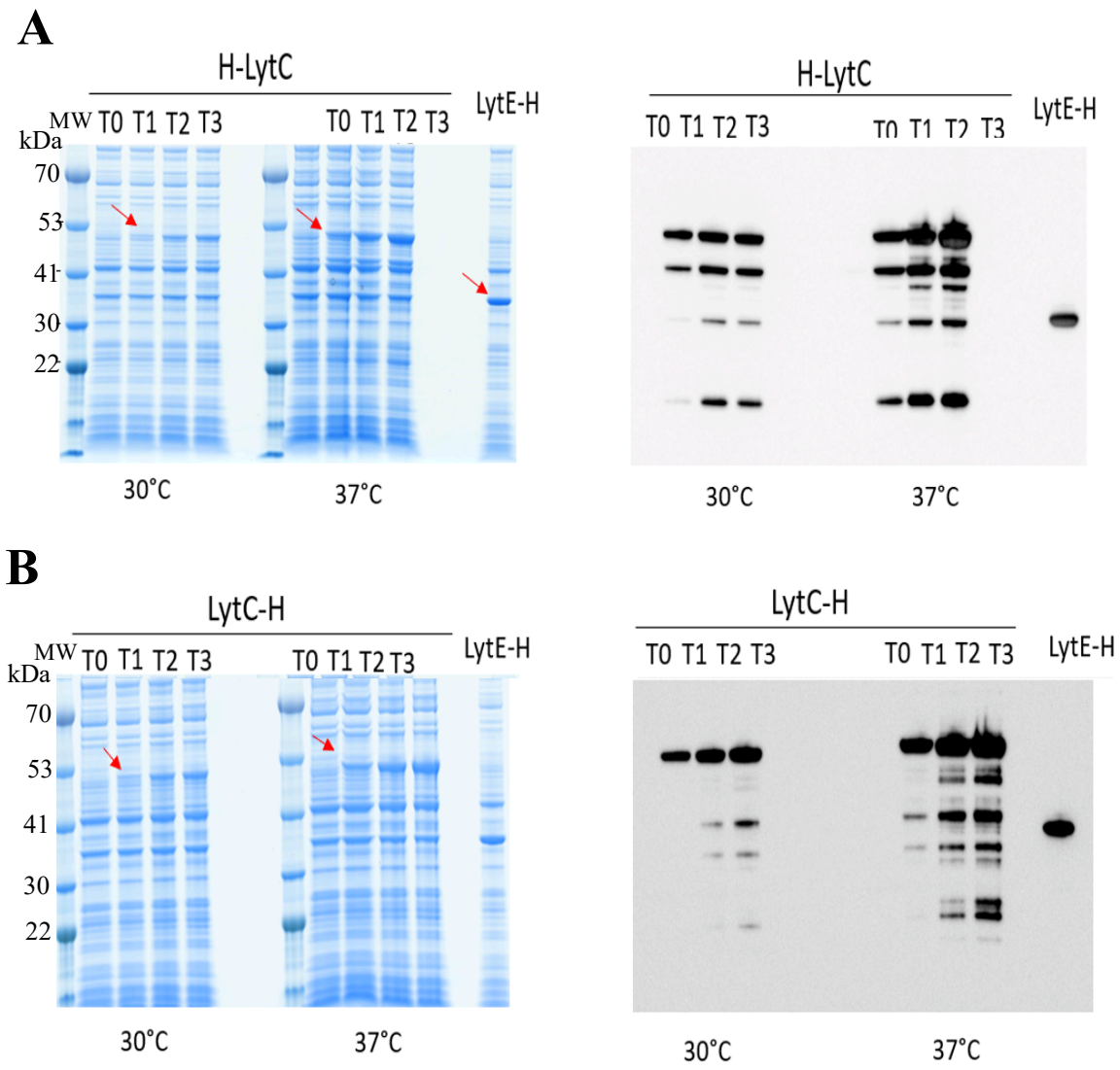

Figure 3.10 SDS-PAGE and Western blot analysis of the 6X-His-tag fused to the N- and C-terminal fusions of LytC

H-LytC (A) and LytC-H (B) were grown in LB media with kan resistance at 30°C and 37°C. The samples were collected before induction (T0). At OD_{600} of 0.5, IPTG was added, and samples were collected at 30-minute intervals (T1, T2, T3, and T4) after induction. The samples were then subjected to SDS-PAGE analysis to be stained with Coomassie, and Western blot analysis was performed using Anti-Penta-His Antibody. LytE-H was used as a control. The molecular weight marker (kDa) is indicated by MW, and the red arrow indicates the predicated molecular weight of either LytC or LytE.

As a quick solution to the degradation problem of the LytC fusion constructs specifically for antibody production, LytC-H purification was done by extracting it from inclusion bodies under denaturing conditions, following the same procedure as previously done with LytE purification (described in method Section 2.9.6.1). Upon analysis of the samples by SDS-PAGE, LytC-H was found to be solubilised with 8 M urea and eluted five times with Elution Buffer 2 containing 100 mM imidazole (Figure 3.11). The eluted samples

were then precipitated with acetone and separated on SDS-PAGE as A1 and A2. A1 and A2 provide a good yield of LytC, allowing the protein to be used to generate antisera despite the presence of lower molecular weight. Although from the previous Western blot analysis (Figure 3.10B, right panel) it is most probable that there are fragments of the protein generated by degradation during expression.

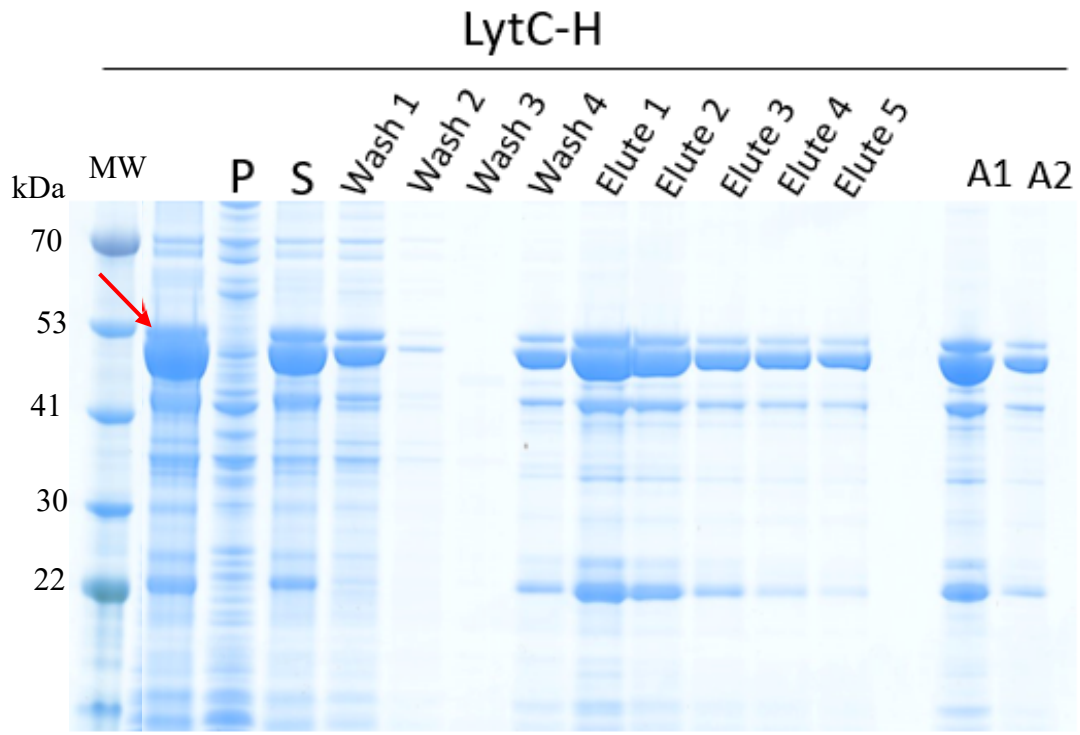

Figure 3.11 LytC-H purified from inclusion bodies using 8M urea

LytC-H was induced for 4 hours with IPTG at 37°C. Cells were harvested, and the pellet was suspended in PBP with 8 M of urea and then washed three times with Wash Buffer 1 (Wash 1, Wash 2, and Wash 3). The fourth wash was performed with Wash Buffer 2, which included 5 mM imidazole (Wash 4). LytC-H was eluted five times with Elution Buffer 3, which contained 100 mM Imidazole (Elute 1, Elute 2, Elute 3, Elute 4, and Elute 5). Elutes 1 and 2 were collected and precipitated with acetone (A1). Elutes 3, 4, and 5 were collected and precipitated with acetone (A2). The molecular weight marker (kDa) is indicated by MW, and the red arrow indicates the expected size of LytC. (P) represents the pellet, and (S) represents the supernatant.

3.2.3 LytF and LytD overexpression and purification in *E. coli*

To generate an antiserum for LytF and LytD (51 kDa and 90 kDa, respectively), a 6X-His-tag fused to the N-terminal of either LytF or LytD (pAM028 (H-LytF) and pAM027 (H-LytD) (plasmid constructed described in method Section 2.8.1). The H-LytF and H-LytD were grown in LB media with kan antibiotic until reaching the mid-exponential phase before being induced with 1 mM IPTG for 3 hours at 37°C. A considerable amount of soluble LytF and LytD were produced and then mixed with HisPur Cobalt Superflow Agarose (described in method Section 2.9.6) (Figure 3.12A and B (S lane)). The proteins were then washed four times with Wash Buffer 1 and eluted with Elution Buffer 2 containing 100 mM imidazole (Figure 3.12A and B). During the washing steps, a significant amount of LytF and LytD were observed to be washed out of the column, resulting in a decrease in the protein yield. This loss might be due to overloading the samples onto the beads, which leads to prevent a strong binding between the proteins and the beads. The first two elution samples, 1 and 2, were collected and precipitated with acetone (A1), while the last three or four elution samples were collected and precipitated with acetone (A2) (Figure 3.12A and B (label A1 and A2). Despite the loss of LytF and LytD during the washing steps, the two collected elution samples provided sufficient material to permit antisera to be raised.

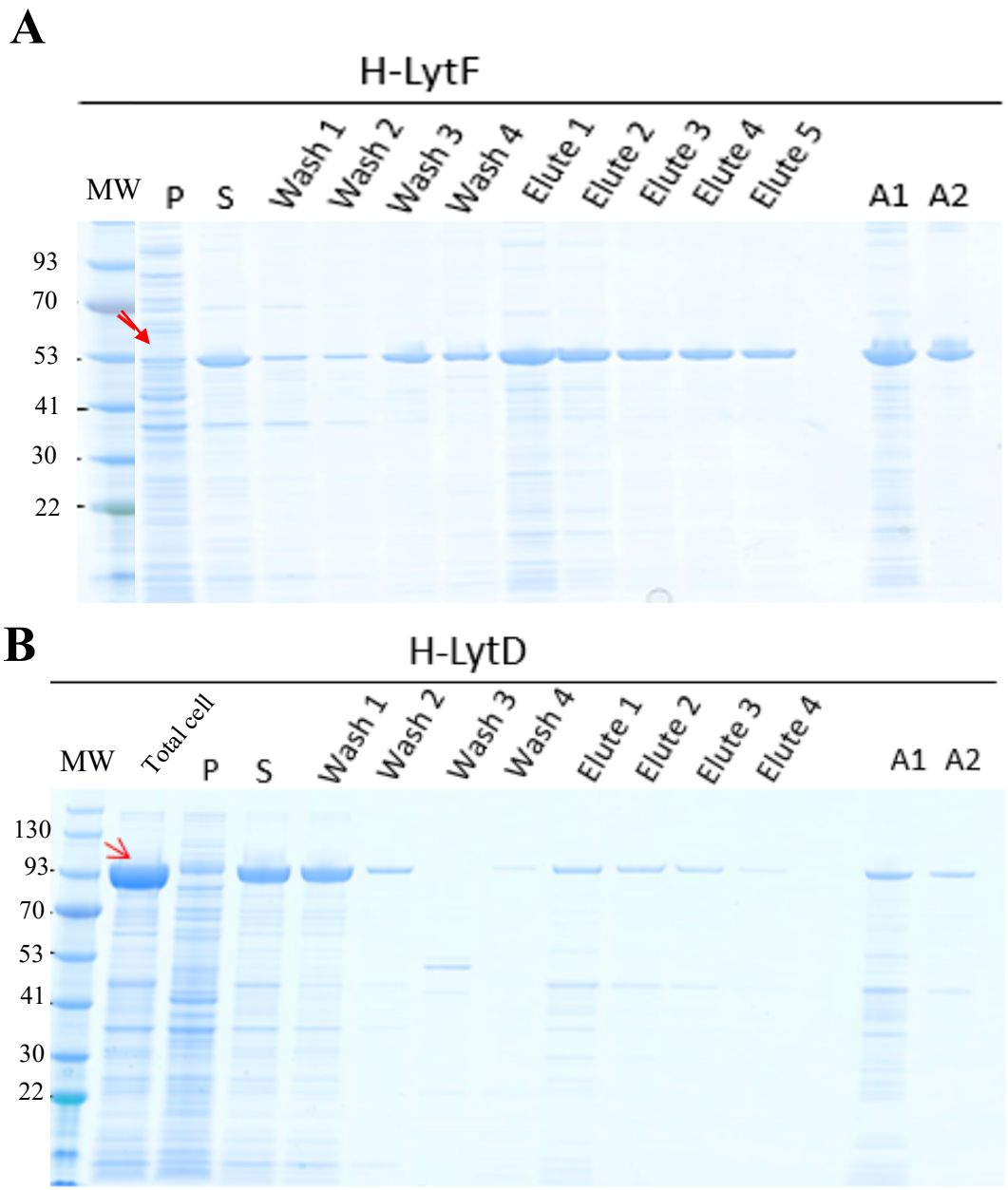

Figure 3.12 The purification of LytF and LytD fused with 6X-His-tag at the N-terminus

Samples were grown in LB media with kan resistance until reaching the mid-exponential phase and then induced with IPTG for 3 hours at 37°C. After harvesting, the supernatants were combined with HisPur Cobalt Superflow Agarose. The agaroses were then washed four times with Wash Buffer 1 (Wash 1, Wash 2, Wash 3, and Wash 4). The proteins were eluted four to five times using Elution Buffer 1. The last two lines (A1 and A2) represent the collected elution samples of H-LytF and H-LytD, which were subsequently concentrated using acetone precipitation. The molecular weight marker (kDa) is indicated by MW, and the red arrow indicates the expected size of LytF (51kDa) and LytD (95 kDa). (P) represents the pellet, and (S) represents the supernatant.

3.2.4 CwlO overexpression and purification in *E. coli*

To obtain CwlO as an antigen, the 6x-His-tag fusion construct was made at the C-terminal region of the gene (pAM029 (CwlO-H)) as it was a workable construct and did not need to construct fusion at the N-terminal region (plasmid constructed described in method Section 2.8.1). The overexpression of CwlO-H was monitored at 30-minute intervals for 1 hour after induction at 37°C. Samples of the induced cells were analysed in SDS-PAGE to assess the expression level (Figure 3.13A). The results demonstrated that the strain with the expression construct showed a band corresponding to the molecular weight of CwlO (50 kDa) that increased over time. CwlO-H purification was then done after 3 hours of induction at 37°C. The sample was then suspended in BS-1 (described in Appendix 1-Buffer components), sonicated, and the broken cells were centrifuged. The resulting pellet and supernatant were then analysed in SDS-PAGE, which found the CwlO in the supernatant fractions (soluble protein) (Figure 3.14B). The supernatant was then collected and mixed with HisPur™ Cobalt Agarose (described in method Section 2.9.6). The mixture was washed four times with Wash Buffer 1 and 2, then eluted five times from the beads using Elution Buffer 1 containing 100 mM Imidazole. Samples were then running in SDS-PAGE, and it was observed that the majority of CwlO-H was eluted in the first elution step. The eluted samples 1 and 2 were collected and precipitated with acetone (A1), while eluted samples 3, 4, and 5 were collected and precipitated with acetone named (A2) (Figure 3.14). The precipitated samples, as shown in Figure 3.14 are suitable for generating antisera against CwlO.

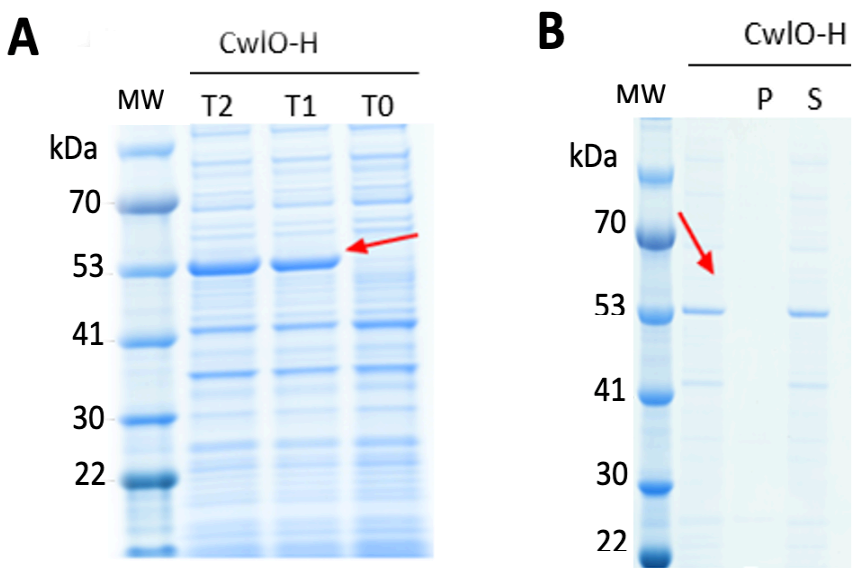

Figure 3.13 CwlO-H overexpression and solubilisation

(A) CwlO-H was grown in LB media with kan resistance, and samples were collected at 30 minutes (T1) and 1 hour (T2) after induction. (B) CwlO-H was induced for 2 hours at 37°C and then suspended with Buffer Solution 1 (BS-1). The molecular weight marker (kDa) is indicated by MW, and the red arrow indicates the expected size of CwlO (50 kDa). (P) represents the pellet, and (S) represents the supernatant. The first unannotated lane in (B) represents the samples taken after induction.

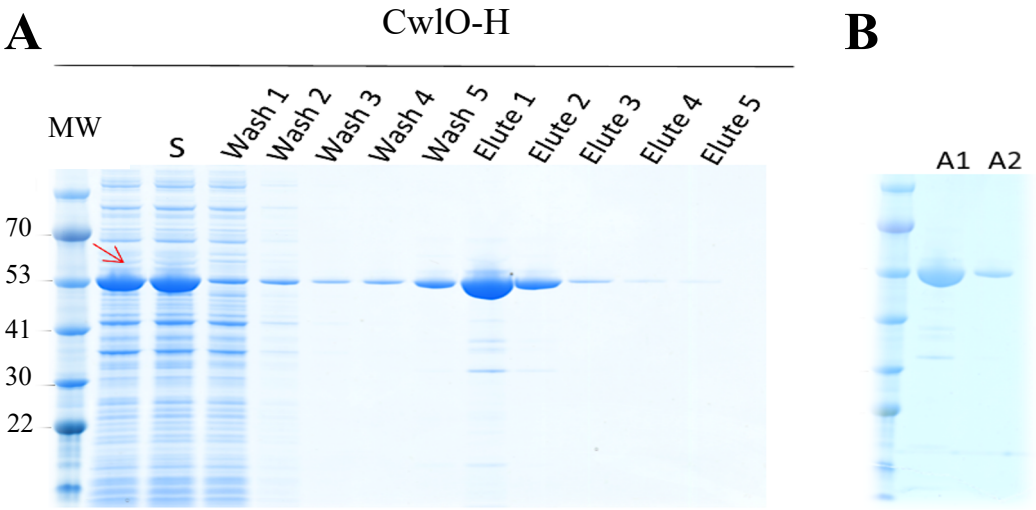

Figure 3.14 CwlO-H purification

The sample was grown in LB media with kan resistance until it reached the mid-exponential phase, and then induced with IPTG for 3 hours. After harvested, the supernatants were combined with HisPur Cobalt Superflow Agarose. Some protein loss occurred during the washing steps using Wash Buffer 1(Wash 1, Wash 2, Wash3) and Wash Buffer 2 (Wash 4). Elution Buffer 1 was used to elute the sample five times. (B) A1 represents the collected elution samples 1 and 2, while A2 represents the collected elution samples 3,4, and 5 after concentrated using acetone precipitation. The red arrow indicates the molecular wight of CwlO (50 kDa). (MW) represents the molecular weight marker (kDa), (P) represents the pellet fraction, and (S) represents the supernatant fraction.

3.2.5 Protein samples preparation for antisera

All purified protein samples used to generate antisera were concentrated using acetone precipitation (described in method Section 2.9.6.2). Samples of the precipitated material were then subjected to SDS-PAGE to evaluate the purification of the target proteins and to provide an estimate of the amount obtained after acetone precipitation. The concentration of the purified proteins was also measured using a nano-drop (mg/ml), as shown in Table 3.1. These samples were then sent to Eurogentec for use in the 28-day speedy immunisation protocol for rabbits.

Table 3.1 The concentration of the purified proteins was estimated using Nano-drop

Name	Construct	Figure reference	A1 (mg/ml)	A2 (mg/ml)
LytE	LytE-H	Figure 3.5	0.65	1.48
LytC	LytC-H	Figure 3.11	0.62	0.56
LytF	H-LytF	Figure 3.12A	4.24	7.70
LytD	H-LytD	Figure 3.12B	0.32	0.21
CwlO	CwlO-H	Figure 3.14B	0.3	0.2

3.2.6 Determination the antisera specificity

Once the antisera of the full-length LytE, LytC, LytF, LytD, and CwlO were generated, two antisera were raised using separate rabbits for each of these autolytic enzymes. The aim was then to determine the specificity of the antisera using total protein from the wild type 168CA and the deletion strains for the corresponding gene. The strains were grown in LB media until they reached the mid-exponential phase, and then 1 ml of the culture was collected by centrifugation and processed to allow total cellular material to be separated by SDS-PAGE in duplicate gels. One gel stain with Coomassie served as a loading control to ensure that an equal amount of the samples had been loaded, while the other gel was used for Western blot analysis using a range of dilutions to provide an indication of specificity for the target protein which should be detected in the wild type of sample, but not in the deletion mutant.

3.2.6.1 LytE antisera specificity

To assess the LytE-antisera, in addition to the 168CA and Δ*lytE*, a strain lacking *cwlO* was used as previously reported that deletion of *cwlO* leads to an increase in the level of *lytE* expression (Bisicchia *et al*., 2007; Dobihal *et al*., 2019). In Western blot analysis, different concentrations of the first LytE-antiserum (SY0733) were used in 1/2000, 1/5000, and 1/10,000 dilutions. A band corresponding to the expected size of LytE (37 kDa) was detected in 168CA, and it was more intense in the Δ*cwlO* strain as expected. This band was not observed in the Δ*lytE* strain, as shown in Figure 3.15A. However, two bands with higher molecular weights than expected for LytE were detected in 168CA, Δ*lytE*, and Δ*cwlO*, which could potentially detect other hydrolytic enzymes (e.g., LytF) that contain a similar sequence at the N-terminus (LysM motif).

Since the first antiserum (SY0733) detected unspecific bands across all strains, the second LytE- antiserum (SY0734) was used to assess its specificity. Using the same protein samples for the Western blot, it was found that the antiserum SY0734 exhibited a higher strength of signal and specificity (Figure 3.15B). However, SY0734 did seem to cross-react with one nonspecific band across all strains, although it was significantly weaker in intensity compared to the first antiserum (SY0733) (Figure 3.15B). In 168CA, a band corresponding to LytE was observed, and the intensity of the band was more abundant in Δ*cwlO*.

In conclusion, The LytE-antiserum (SY0733) observed a good detection of LytE, but there was a problem with seeing significant unspecific bands. In contrast, the SY0734 antisera exhibited a higher specificity. The LytE-antiserum (SY0734) was considered an appropriate antiserum for the entire study and was used at a dilution of 1/5000, as demonstrated by its ability to detect the LytE accurately.

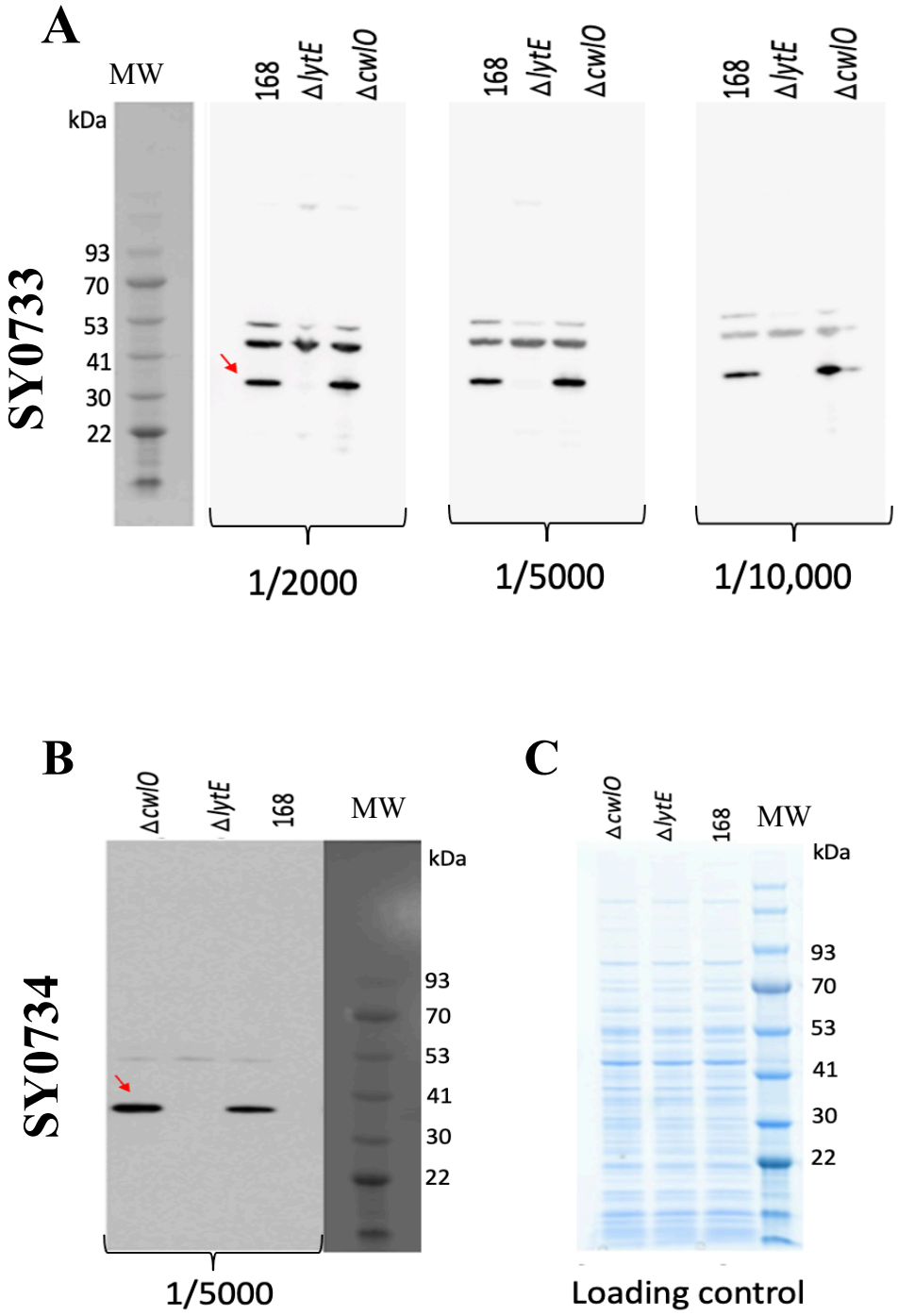

Figure 3.15 Specificity of the LytE-antisera SY0733 and SY0733

168CA, Δ*lytE*, and Δ*cwlO* strains were grown until they reached an OD_{600} of 0.5, at which point the cells were centrifuged resuspended in SDS-loading buffer. (A) and (B) Western blot analysis was performed for the SY0733 and SY0734 antisera, respectively. (C) SDS-PAGE was used as a loading control. The molecular weight marker (kDa) is indicated by MW, and the red arrow indicates the predicated molecular weight of the native LytE (37 kDa).

3.2.6.2 LytC antisera specificity

In order to examine the LytC-antisera, 168CA and *lytC* mutant strains were used. Using the same methods as described earlier (Section 3.2.6), the first LytC- antiserum (SY0735) detected numerous bands in both strains, indicating that it was not specifically detecting LytC (Figure 3.16A). On the other hand, the second LytC- antiserum (SY0736) exhibited higher specificity and successfully detected a band at the expected size of LytC (52 kDa), with no significant signal in *lytC* deletion strain (Figure 3.16B). The reliable LytC-antiserum (SY0736) was used throughout the entire study, and it was determined that a dilution of 1/2000 was suitable for reliably detecting the LytC protein (Figure 3.16B).

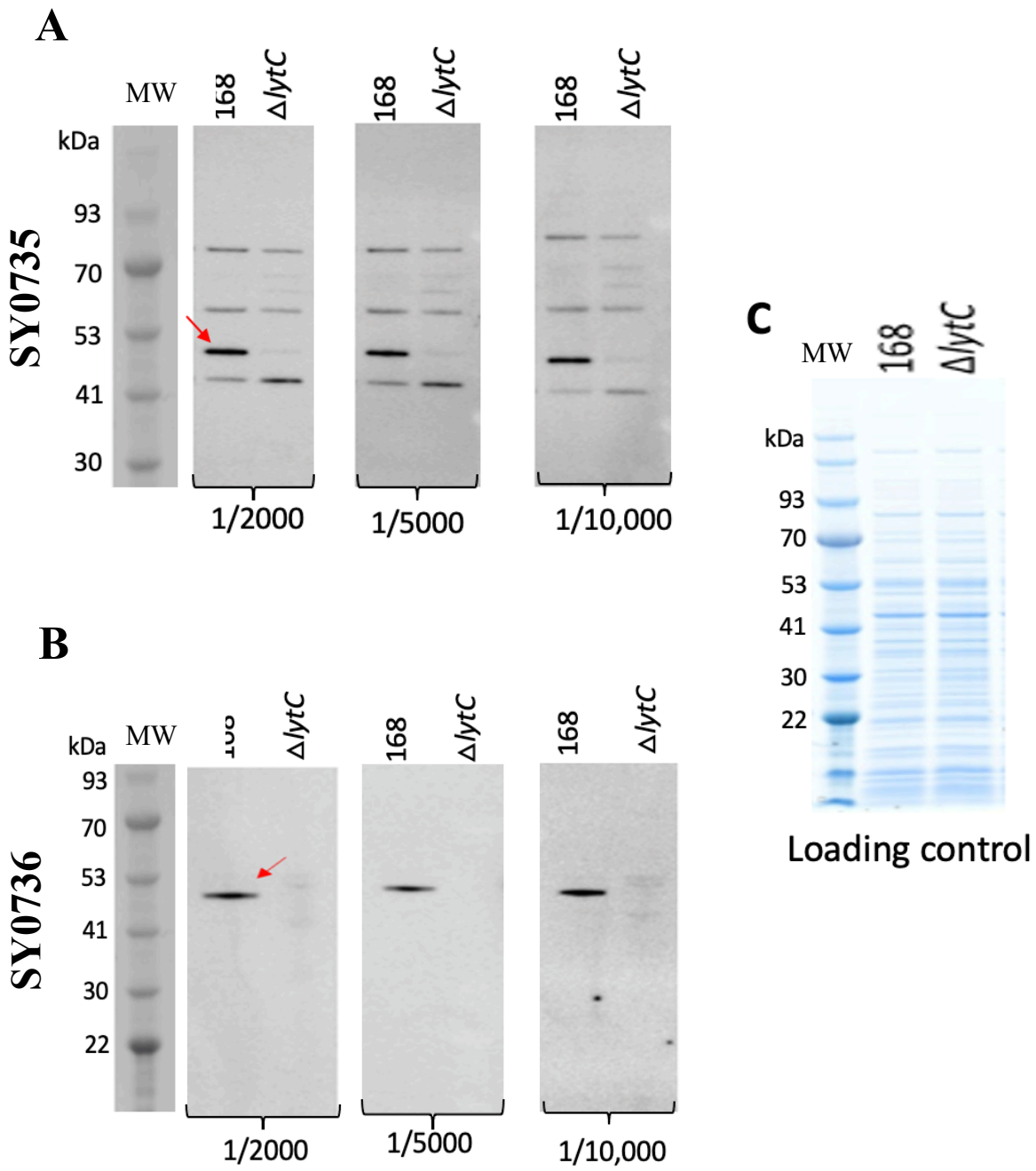

Figure 3.16 Specificity of the LytC-antisera SY0735 and SY0736

168CA, Δ*lytC* strains were grown until they reached an OD_{600} of 0.5, at which point the cells were centrifuged resuspended in SDS-loading buffer. (A) and (B) Western blot analysis was performed for the SY0735 and SY0736 antisera, respectively. (C) SDS-PAGE was used as a loading control. The molecular weight marker (kDa) is indicated by MW, and the red arrow indicates the predicated molecular weight of the native LytC (52 kDa).

3.2.6.3 LytF antisera specificity

LytF-antisera specificities were evaluated in 168CA and *lytF* mutant strains. According to Western blot analysis, both LytF antisera (SY0739 and SY0740) successfully detected LytF at the corresponding size (51 kDa) (Figure 3.17). However, both antisera detected unspecific bands in 168CA and the strain lacking *lytF*. In the case of SY0739, these unspecific bands were weaker (1/2000), while with SY0740, cross-reacting bands were detected in the 168CA, only one of which was present (at a lower level) in the deletion mutant. Overall, the LytF- antiserum (SY0739) was considered to have good detection of LytF, showing a strong band at the expected molecular weight and a suitable working concentration for this antiserum (1/2000).

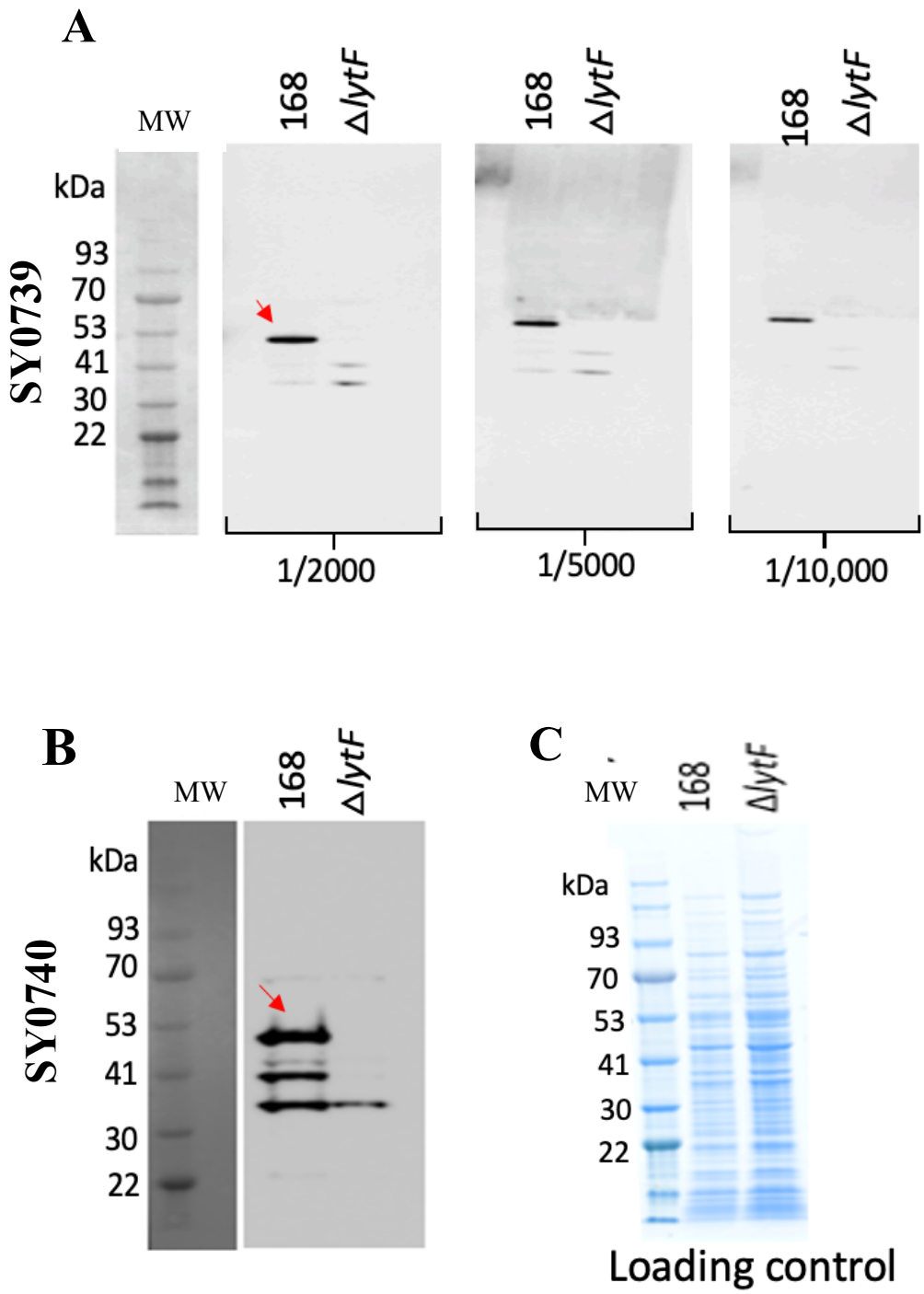

Figure 3.17 Specificity of the LytF-antisera SY039 and SY040

168CA, Δ*lytF* strains were grown until they reached an OD_{600} of 0.5, at which point the cells were centrifuged resuspended in SDS-loading buffer. Western blot analysis was performed for the SY0739 antiserum at different concentration (A) and SY0740 antiserum at a 1/5000 (B). (C) SDS-PAGE was used as a loading control. The molecular weight marker (kDa) is indicated by MW, and the red arrow indicates the predicated molecular weight of the native LytF (51kDa).

3.2.6.4 LytD antisera specificity

For LytD, the SY0737 and SY0738 antisera were generated, and their specificities were evaluated in 168CA and mutant *lytD* strains. The first antiserum SY0737 did not detect any band in the 168CA and *lytD* mutant strains (data not shown). The second antiserum (SY0738) successfully detected the expected size of LytD (95 kDa), and no band was observed in strains lacking *lytD* (Figure 3.18). Since only one antiserum worked effectively, it was used throughout the rest of the study using a dilution of 1/5000, where it reliably detected a signal corresponding to LytD (Figure 3.18).

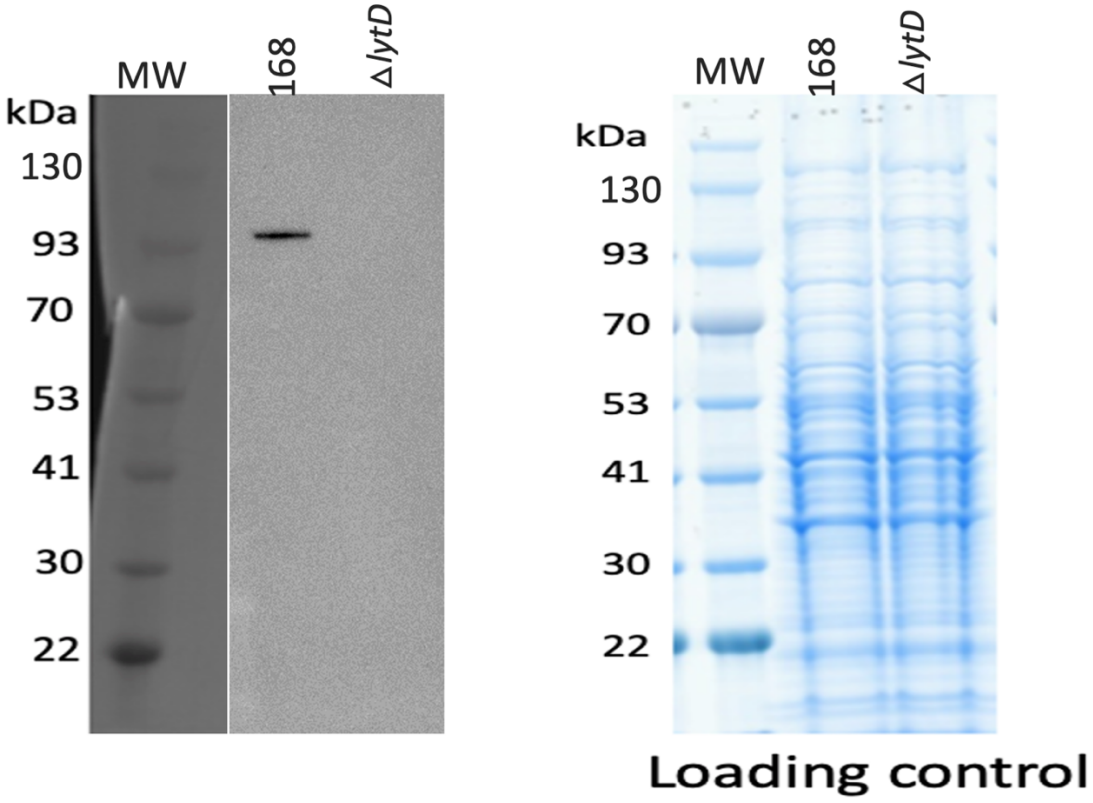

Figure 3.18 Specificity of the LytD-antiserum SY0738

168CA, Δ*lytD* strains were grown until they reached an OD_{600} of 0.5, at which point the cells were centrifuged resuspended in SDS-loading buffer. The sample was run in two gels: one was used for Western blot analysis (left panel), while the other was stained with Coomassie (right panel). The molecular weight marker (kDa) is indicated by MW, the predicated molecular weight of the native LytD (95 kDa).

3.2.6.5 CwlO antisera specificity

The CwlO antisera, SY0858 and SY0859 were problematic. The antisera expected to be specific to CwlO was evaluated in wild type (168CA), and the Δ*cwlO* and Δ*lytE* strains. It was expected that the deletion of *lytE* might result in an increased level of *cwlO*. Both antisera SY0858 and SY0859 identified multiple bands across all strains (Figure 3.19A and B). A band was observed in 168CA at the corresponding size of CwlO (50 kDa) in SY0858 and SY0859, but it was weak and not detected in the Δ*lytE*. Thus, it seemed unlikely to correspond to CwlO (Figure 3.19A and B). Several attempts were made with both antisera using modified conditions, including overnight incubation for the primary antibody, using BSA as a blocking agent, and trying various dilutions, but none of these approaches successfully detected the native CwlO. Thus, it was concluded that these antisera were unsuitable for further work, and this aspect of the project had to be approached in a different way.

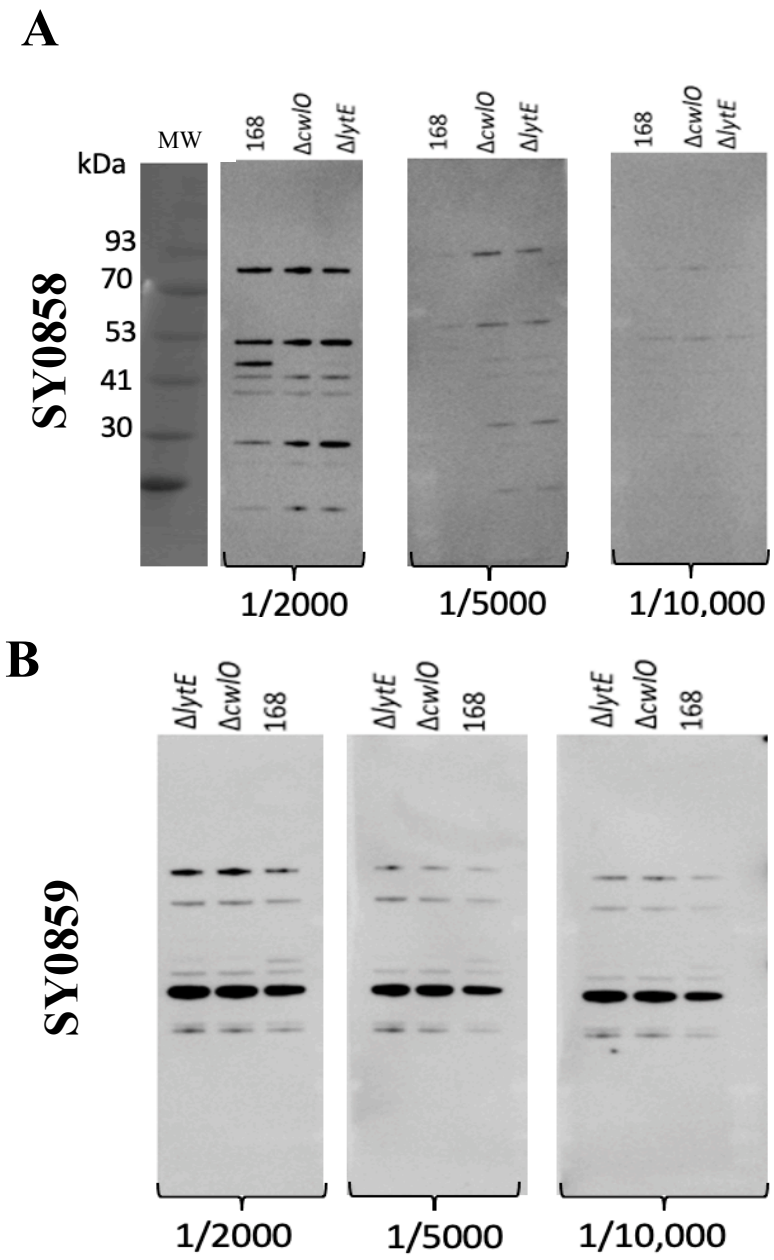

Figure 3.19 Specificity of the CwlO-antisera SY0858 and SY0859

(A)SY0858 and (B)SY0859 antisera were analysed by Western blot on the 168CA wild-type strain, and the *ΔlytE* and *ΔcwlO* in different concentrations. Strains were grown until they reached an OD_{600} of 0.5, at which point the cells were centrifuged resuspended in SDS-loading buffer. The molecular weight marker (kDa) is indicated by MW. The expected size of CwlO is 50 kDa.

3.2.7 Autolytic enzyme abundance in strains with altered cell wall composition or synthesis

The antiserum for the autolytic enzymes provides a valuable tool to gain insight into how these enzymes respond to different growth media and genetic backgrounds. The *lytE, lytC, lytF*, and *lytD* genes were evaluated in 168CA, Δ*sigI*, Δ*sigD*, Δ*sigM*, Δ*ponA*, and Δ*mprF* strains since these strains modulate either cell morphology or expression level of the autolytic enzymes . The growth characteristics of these strains were also examined in different media (NB or NB supplemented with 25 mM $MgSO_4$ or 0.4 % Glucose), as $MgSO_4$ and glucose play a role in gene expression (described in section 3.1) (Carballido-López *et al*., 2006; Dajkovic *et al*., 2017b; Guyet *et al*., 2023; Kawai *et al*., 2009). The growth was monitored by measuring the OD_{600} at 30-minute intervals over three hours. Growth curves were then plotted based on the OD_{600} measurements (Figure 3.20). The NB media exhibited a similar growth pattern across all strains, except in the *ponA* deficient strain, which showed a slower growth rate (Figure 3.20A). This observation was consistent with previous studies that showed the absence of *ponA* impacts cell growth and morphology where the cell is slightly longer unless media supplemented with $MgSO_4$ (Kawai *et al*., 2009; Kleppe *et al*., 1982; Popham & Setlow, 1996). The addition of 25 mM $MgSO_4$ to the culture media enhanced the growth rate in all strains, even in strain lacking *ponA* (Figure 3.20B). Introducing 0.4% glucose to the culture media resulted in increased the growth rate across strains, and the strains entered the stationary phase earlier than the other culture media (Figure 3.20C).

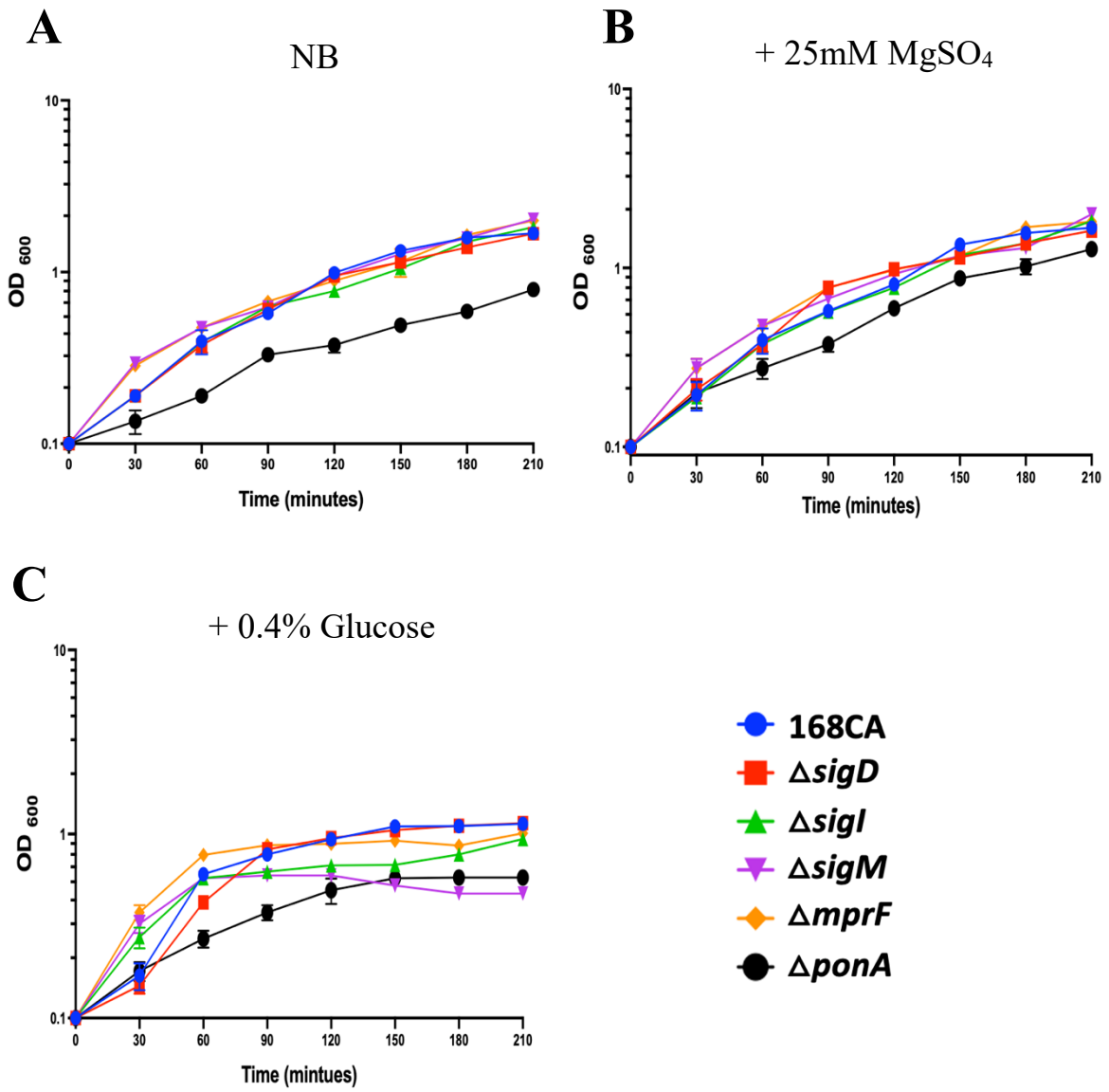

Figure 3.20 Growth characteristics of wild type and mutant strains in various media

The growth of the 168CA, Δ*sigD*, Δ*sigI,* Δ*sigM*, Δ*mprF,* and Δ*ponA* strains in NB medium (A), NB supplement with either 25 mM $MgSO_4$ (B) or 0.4% Glucose (C) over 3.5 hours. The OD_{600} was measured every 30 minutes. Growth curves were generated from two independent experiments and plotted on a logarithmic base 10 scale. Standard deviation is represented by error bars (n=2). The blue line is 168CA, the red line is Δ*sigD*, the green line is Δ*sigI*, the purple line is Δ*sigM*, the orange line is Δ*mprF,* and the black line is Δ*ponA*.

Following the analysis of the growth characteristics of the 168CA, Δ*sigD*, Δ*sigI*, Δ*sigM*, Δ*mprF*, and Δ*ponA* strains in different media conditions, the abundance of the LytE, LytF, LytC, and LytD was subsequently evaluated using Western blot analysis with specific antiserum. In order to perform the Western blot analysis, samples were collected at 60 minutes (exponential phase) from 168CA, Δ*sigD*, Δ*sigI*, Δ*sigM*, Δ*mprF*, and Δ*ponA* grown in NB media and NB supplemented with either $MgSO_4$ or glucose. The collected samples were

then suspended in an SDS-loading buffer for analysis. PBP2B and FtsZ antibodies were used as loading controls to verify that the amount of the proteins was loaded equally.

3.2.7.1 LytE

A LytE- antiserum was generated as previously described to evaluate the abundance of LytE under different conditions (growth media /genetic backgrounds). The blot in Figure 3.21A indicated that the LytE abundance was significantly changed by several mutations in combination with supplementation of the media with $MgSO_4$ or glucose. To obtain a numerical value for the change in LytE abundance, the LytE signal on the blot (Figure 3.21A) was measured using ImageJ, Fiji software, and the quantification was normalised relative to the signal obtained for PBP2B (used as loading control) (Figure 3.21B). The chart in Figure 3.21B displays the ratio of the LytE signal relative to PBP2B, while the number above each chart demonstrates the fold change in relation to the value obtained for the wild type (this analytic protocol was also used for other autolytic enzymes).

In the wild type (168CA), the abundance of LytE did not change significantly under the different conditions. On the other hand, the abundance of LytE was dramatically different in the sigma factor deletion strains (Figure 3.21A and B). In a strain lacking *sigD*, the level of LytE was increased 1.5-fold compared to the wild type in the NB medium, and 1.3-fold when the media was supplemented with glucose. While in NB supplemented with the $MgSO_4$, the abundance of LytE was similar to the that of 168CA in NB media. However, across all media, LytE was virtually absent in a strain lacking *sigI,* which is consistent with previous findings showing SigI-dependent lytE expression (Huang *et al*., 2013). The deletion of *sigM,* which has a role in maintaining the integrity of the cell wall, resulted in a significant reduction in LytE level (Figure 3.21B,Thackray & Moir, 2003). Interestingly, there was slightly change in the LytE abundance in the Δ*mprF* background, even when grown in the supplemented media. However, most notably, in Δ*ponA* background, the abundance of LytE was found to dramatically increase by around 7.5-fold in NB media and 8.8-fold in NB supplemented with glucose. In contrast, in the presence of $MgSO_4$, the LytE abundance was significantly decreased (about 1.5-fold) (Figure 3.21B).

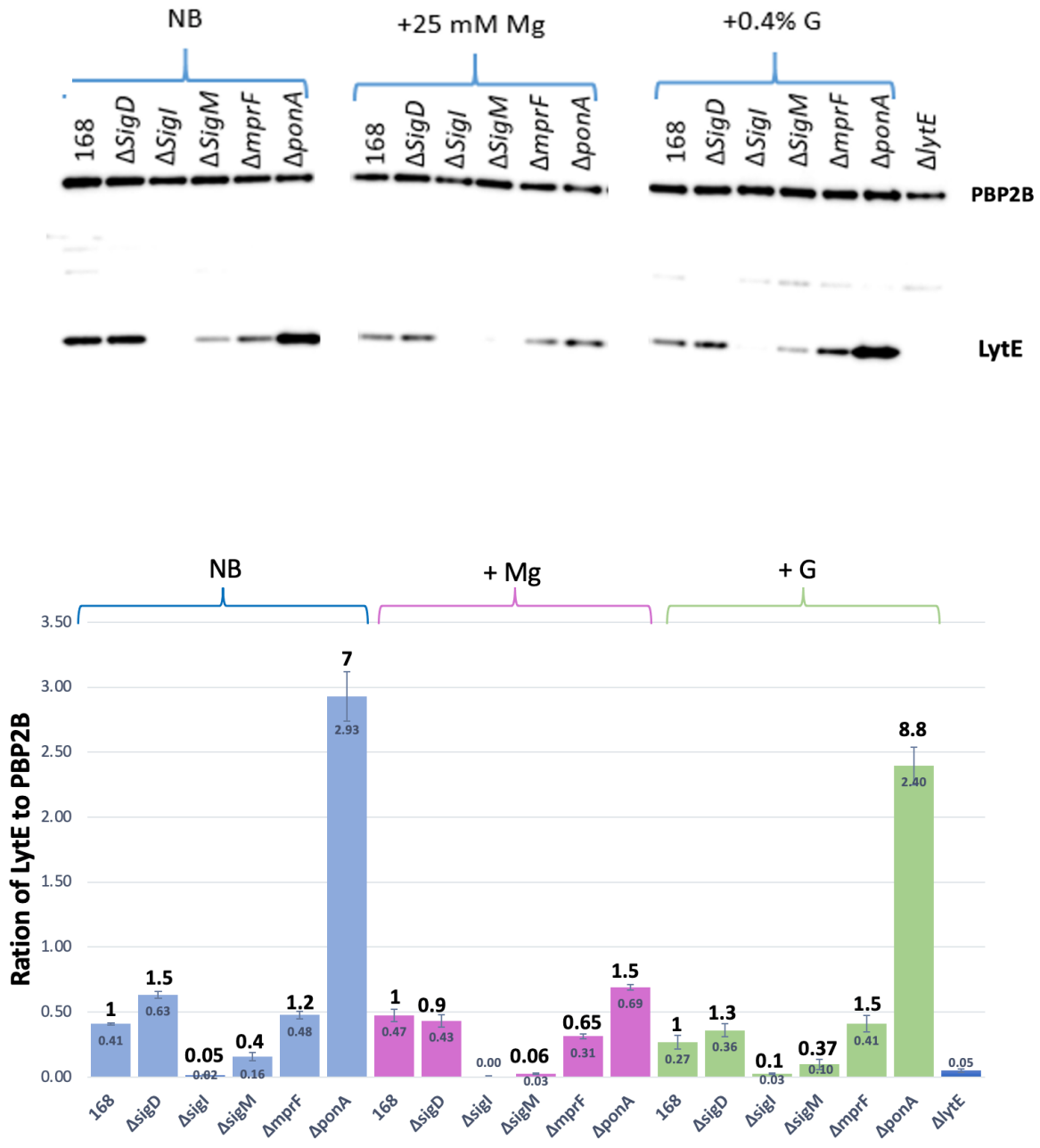

Figure 3.21 Western blot analysis to assess the level of LytE under various conditions

168CA, Δ*sigI,* Δ*sigD,* Δ*sigM,* Δ*mprF,* and Δ*ponA* were grown in NB and NB supplement with either 25 mM $MgSO_4$ (pink-Mg) or 0.4 % glucose (green-G) until they reached the mid-exponential phase. 1 ml of the samples was collected and suspended in an SDS-loading buffer. To ensure that the loading of total cellular material was comparable between samples, the detection of PBP2B was used. This also served as a reference standard to quantify the signals. The mutant *lytE* strain was used as a negative control. (A) Western blot analysis used LytE-antiserum combined with PB2B antibody (1/5000 and 1/10,000 dilutions, respectively). (B) The signals were quantified as a ratio of LytE to PBP2B antibody. The bold black number above the chart indicates the fold difference compared to the wild type (168CA). Standard deviation is represented by error bars (n=3).

3.2.7.2 LytF

The abundance of the native LytF was also evaluated among different strains and media conditions using LytF-antisera by following the same process used to examine the abundance of LytE (Section 3.3.1). Based on the Western blot analysis shown in Figure 3.22 A and B, the abundance of LytF in the168CA (wild type) was reduced in the presence of $MgSO_4$, while significantly increasing in media containing glucose compared to the level in the NB medium. In sigma factor deletion strains, LytF was found to be barely detected in a strain lacking *sigD,* consistent with the previous reports that *lytF* expression was dependent on the sigma factor D _. On the other hand, LytF was markedly elevated in either Δ*sigI* or Δ*sigM* deletion strains in NB media or NB supplemented with $MgSO_4$. The observed elevation of LytF level might represent a compensation for the LytE function, as shown in Figure 3.21B. In the *mprF* deletion strain, the abundance of LytF was similar to the 168CA in NB media. However, the LytF abundance in the Δ*mprF* was increased (1.8-fold) when media was supplemented with $MgSO_4$, while the addition of glucose led to a slightly decreased LytF level. Lastly, in the strain lacking *ponA,* LytF abundance remained reduced across different media. A degradation product was observed in NB alone and in the presence of glucose in *ponA* deletion strain that was not detected in the other samples, even with a long exposure (Figure 3.22B).

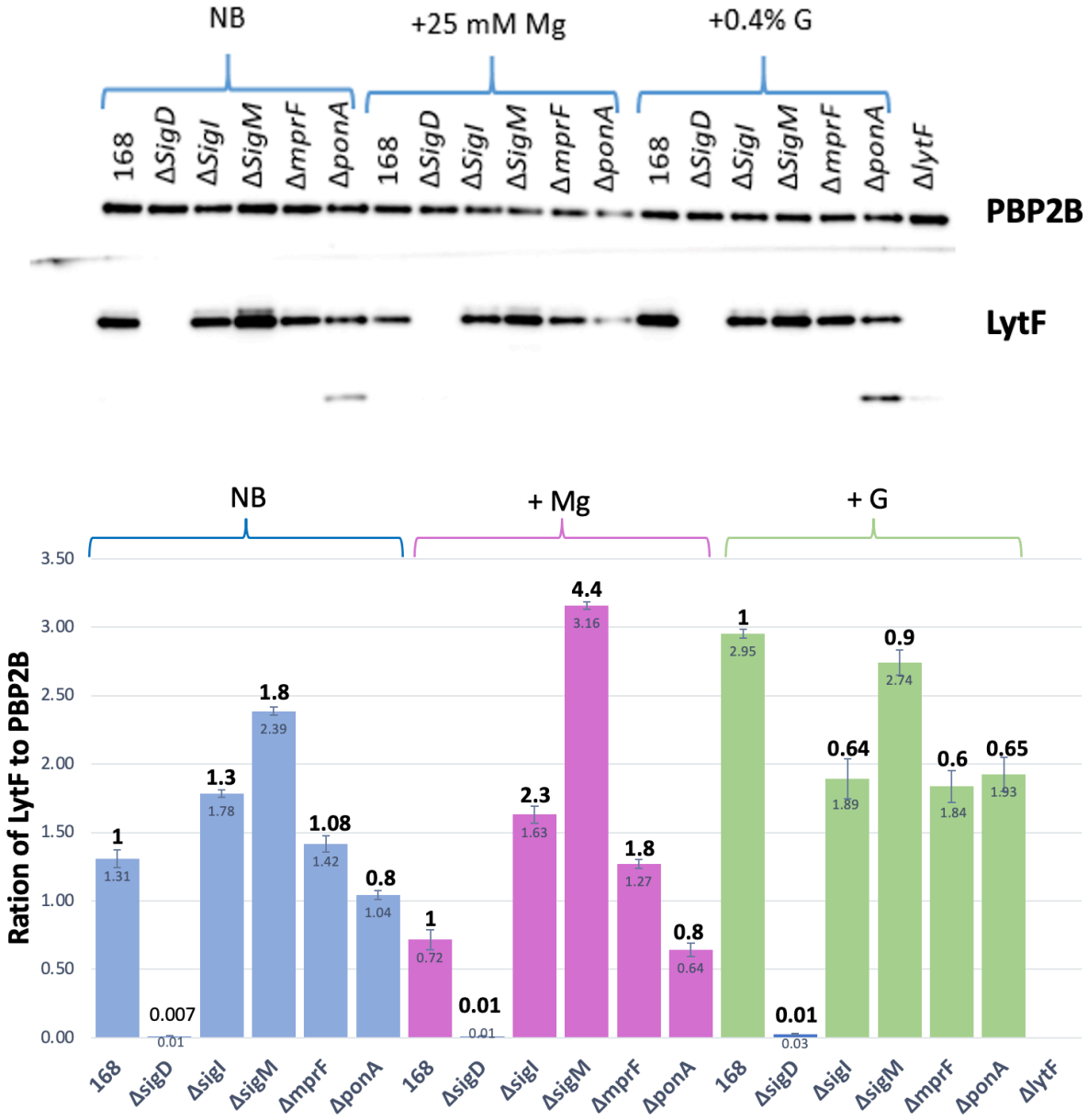

Figure 3.22 Western blot analysis to assess the level of LytF under various conditions

168CA, Δ*sigI,* Δ*sigD,* Δ*sigM,* Δ*mprF,* and Δ*ponA* were grown in NB (blue) and NB supplemented with either 25 mM $MgSO_4$ (pink-Mg) or 0.4 % glucose (green-G) until they reached the mid-exponential phase. 1 ml of the samples was collected and suspended in an SDS-loading buffer. To ensure that the loading of total cellular material was comparable between samples, the detection of PBP2B was used. This also served as a reference standard to quantify the signals. The mutant *lytF* strain was used as a negative control. (A) Western blot analysis used LytF-antiserum combined with PB2B antibody (1/2000 and 1/10,000 dilutions, respectively). (B) The signals were quantified as a ratio of LytF to PBP2B antibody. The bold black number above the chart indicates the fold difference compared to the wild type (168CA). Standard deviation is represented by error bars (n=3).

3.2.7.3 LytC

This study also examined the abundance of LytC, which is considered one of the major autolytic enzymes in vegetative growth, using LytC-antiserum (SY0736) (antisera generation described in Sections 3.2.1.2 and 3.2.2). The abundance of native LytC in the wild type was increased in media containing $MgSO_4$ or glucose compared to the NB media alone. In the sigma factor deletion strains, the level of LytC was found to be almost absent in Δ*sigD*. This observation was consistent with previous reports, demonstrating that the SigD controls the expression of *lytC* (Blackman *et al*., 1998). The reduction in the LytC abundance was also observed in Δ*sigI,* Δ*sigM,* Δ*mprF,* and Δ*ponA* backgrounds, across different media conditions, suggesting that these genetic factors contribute to control the expression or stability of LytC (Figure 3.23A and B).

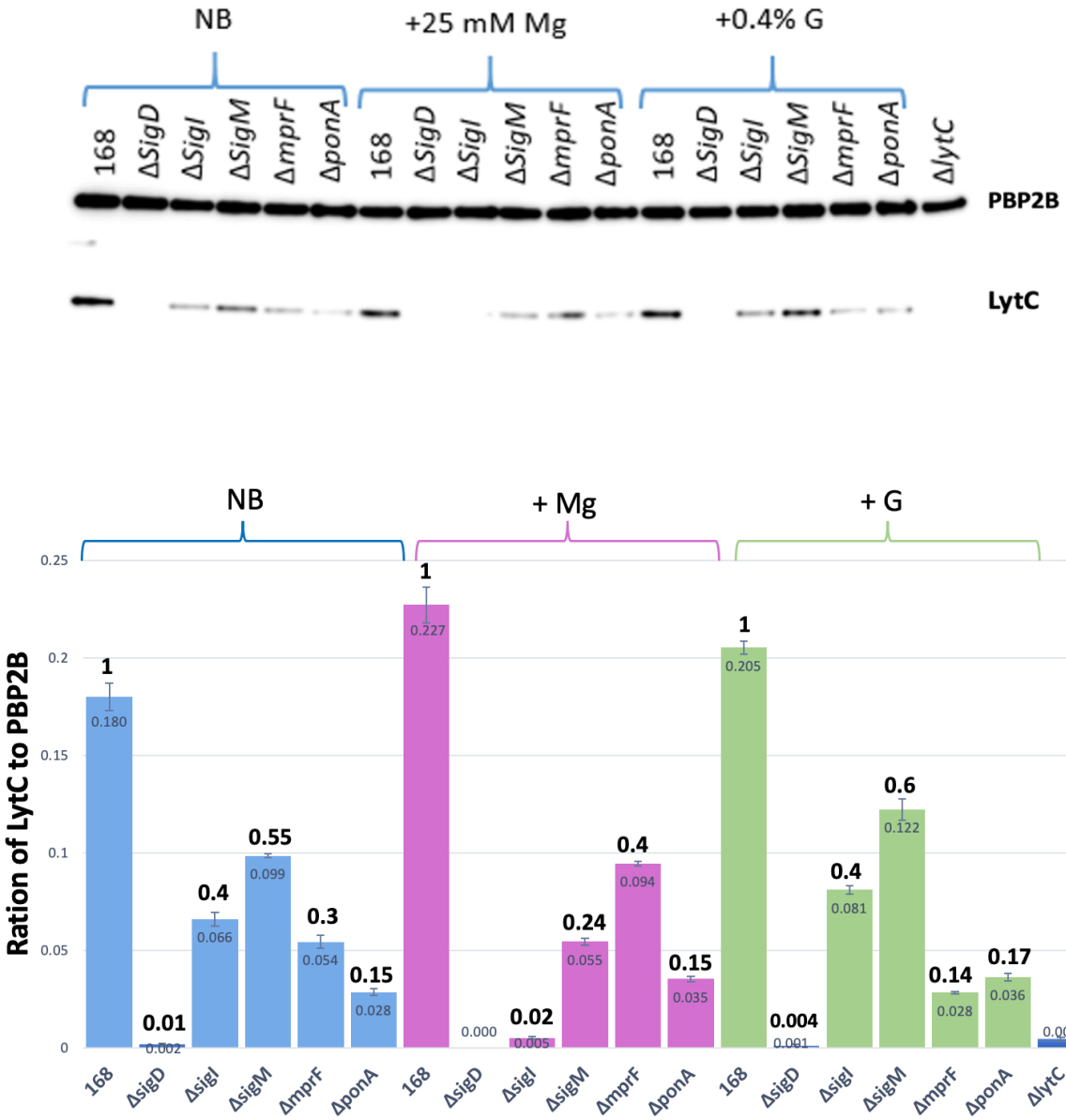

Figure 3.23 Western blot analysis to assess the level of LytC under various conditions

168CA, Δ*sigI,* Δ*sigD,* Δ*sigM,* Δ*mprF,* and Δ*ponA* were grown in NB (blue) and NB supplemented with either 25 mM $MgSO_4$ (pink-Mg) or 0.4 % glucose (green-G) until they reached the mid-exponential phase. 1 ml of the samples was collected and suspended in an SDS-loading buffer. To ensure that the loading of total cellular material was comparable between samples, the detection of PBP2B was used. This also served as a reference standard to quantify the signals. The mutant *lytC* strain was used as a negative control. (A) Western blot analysis used LytC-antiserum combined with PB2B antibody (1/2000 and 1/10,000 dilutions, respectively). (B) The signals were quantified as a ratio of LytC to PBP2B antibody. The bold black number above the chart indicates the fold difference compared to the wild type (168CA). Standard deviation is represented by error bars (n=3).

3.2.7.4 LytD

LytD, known as one of the major autolytic enzymes in vegetative growth, was assessed across different genetic backgrounds and media using LytD-antiserum (SY0738) (described earlier in Sections 3.2.1.3 and 3.2.4). According to the published work by Margot *et al.,* 1999, LytD is under the control of SigD. Consistent with this, this study observed that the LytD was not detected in strain lacking *sigD,* as demonstrated by Western blot analysis (Figure 3.24A and B).

In NB media or NB supplemented with glucose, the abundance of LytD was observed to be increased across the genetic backgrounds Δ*sigI,* Δ*sigM,* and Δ*ponA* from 1-fold to 2.5-fold. In contrast, the abundance of LytD was extremely reduced in the presence of $MgSO_4$. In strain lacking *mprF,* the level of LytD was reduced when the media contained either $MgSO_4$ or glucose. These findings align with earlier work by Dajkovic *et al*., 2017, which indicated that $MgSO_4$ inhibited the activity of various hydrolytic enzymes as occurred with LytE, LytF, and LytC.

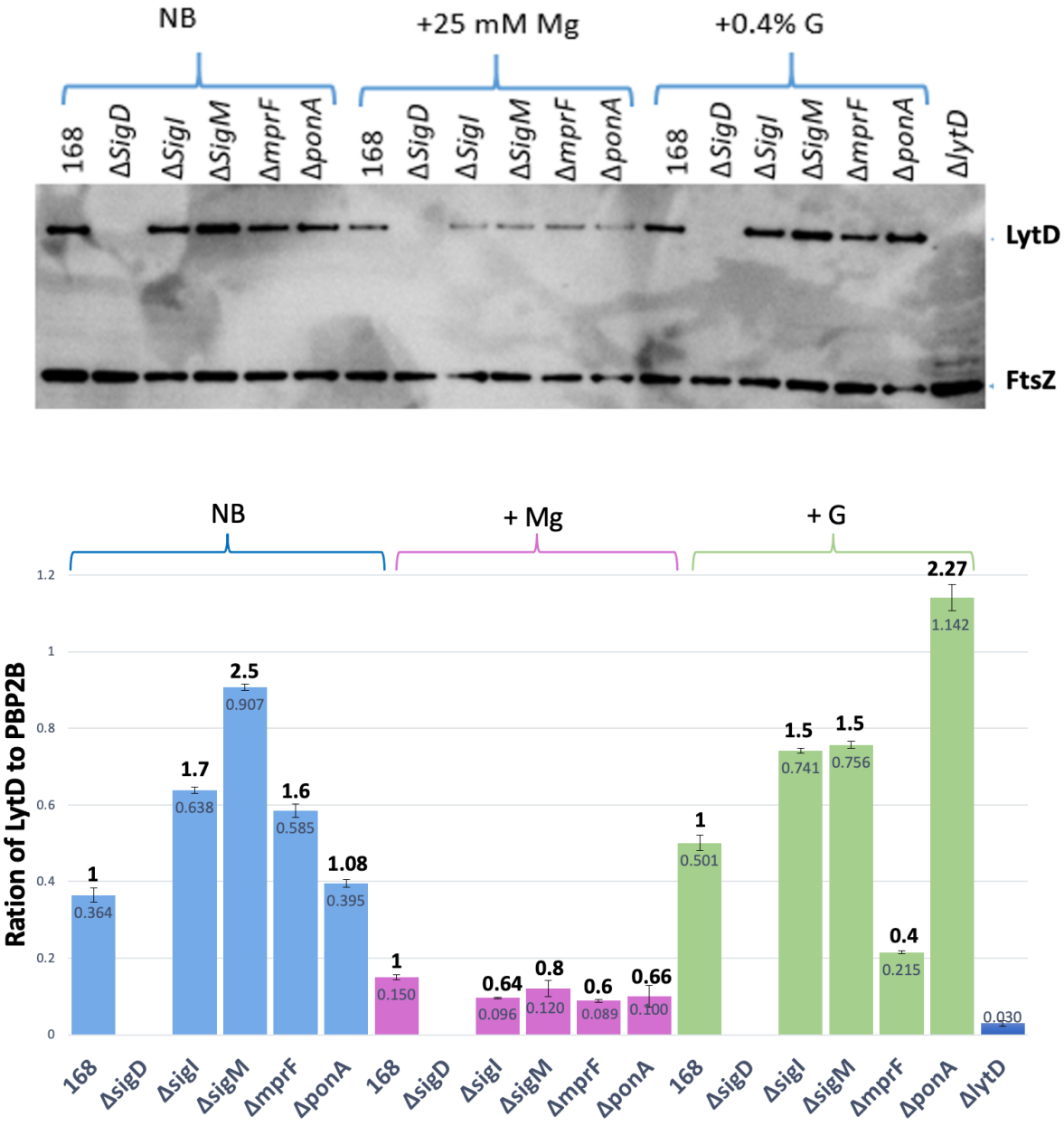

Figure 3.24 Western blot analysis to assess the level of LytD under various conditions

168CA, Δ*sigI,* Δ*sigD,* Δ*sigM,* Δ*mprF,* and Δ*ponA* were grown in NB (blue) and NB supplemented with either 25 mM $MgSO_4$ (pink-Mg) or 0.4 % glucose (green-G) until they reached the mid-exponential phase. 1 ml of the samples was collected and suspended in an SDS-loading buffer. To ensure that the loading of total cellular material was comparable between samples, the detection of FtsZ was used. This also served as a reference standard to quantify the signals. The mutant *lytD* strain was used as a negative control. (A) Western blot analysis used LytD- antiserum combined with FtsZ antibody (1/5000 and 1/10,000 dilutions, respectively). (B) The signals were quantified as a ratio of LytD to FtsZ antibody. The bold black number above the chart indicates the fold difference compared to the wild type (168CA). Standard deviation is represented by error bars (n=3).

3.8 Proteomic analysis of the autolysins

Mass spectrometry analysis was used to examine the stability and anchoring of hydrolytic enzymes on the cell wall surface. To achieve this, the cell wall surface of *B. subtilis* was disrupted using 1.5 M of lithium chloride (LiCl). The downside of the mass spectrometry was that it examined the population rather than the individual cells. The hypothesis here was that if the autolysin is secreted and anchored to the cell wall and gradually degraded then released to the culture medium, the majority of this protein would be expected to be in the cell wall (LiCl extract). The intensity of the LytE, LytF, CwlO, LytC, and LytD was normalised in the different genetic backgrounds that considers as cell wall-associated genes (Δ*cwlO*, Δ*ponA*, Δ*ltaS* (long LTA), or Δ*mprF*) and compared them to the wild-type strain 168CA as shown in Figure 3.25. The hydrolytic enzymes intensity in 168CA indicate as 1 at the graph in Figure 3.25. Strains were grown in a minimal media (described in Appendix 1- Media composition) until they reached OD_{600} of 0.7. The samples were then collected, and either used the culture supernatant (CS) or treated the pellet with 1.5 M LiCl (LS) then sent for mass spectrometry analysis (described in method in Section 2.11).

After normalising the signal intensity for the hydrolytic enzymes, it was evident that samples from the strain lacking the DL- endopeptidase *cwlO* had an increased the level of LytE in the culture supernatant rather than anchored to the cell wall. On the contrary, the Δ*cwlO* background negatively impacted the intensity of LytF in both culture supernatants and LiCl extraction, where the signal was reduced. A similar effect was also observed for LytE and LytF in the *ponA* deletion strain. Deletion of *lytE* resulted in elevated levels of LytF relative to 168CA, with this increase predominantly observed in the culture supernatant (Figure 3.25B). The strain lacking *ltaS* resulted in cells with elongated LTA chain, and the abundance of LytE was shown to be significantly increased, as previously published by Kasahara *et al*., 2016b. Recent work from Guyet *et al*., 2023 demonstrated that the level of the LytE increased in the absence of *ltaS* and in Figure 3.25 indicated that the intensity of LytE in the Δ*ltaS* was more abundant in the culture supernatant. Whereas there was no obvious change in the LytF quantity in the strain lacking *ltaS*. MprF has also been indicated to play a role in the regulation of LTA synthesis, specifically the polymer length(Guyet *et al*., 2023). This study has exhibited that LytE and LytF are anchored to the cell wall in absence of *mprF* and present in low quantities within the culture supernatant (Figure 3.25A and B).

Interestingly, the abundance of the DL-endopeptidase CwlO was not as expected by this analysis. It was proposed that CwlO level would be higher in in the strain lacking *lytE* (Figure 3.25C). However, as indicated by the mass spectrometry analysis (Figure 3.25C), the level of CwlO was reduced in the *lytE* background. Additionally, the CwlO abundance appeared to remain consistent across the other different genetic backgrounds examined (Δ*ponA*, Δ*ltaS*, and Δ*mprF)* (Figure 3.25C). The mass spectrometry analysis of the amidase enzyme, LytC, did not reveal any obvious change in the LytC intensity across different backgrounds except in (Δ*ponA*) (Figure 3.25D), indicating that manipulating the LTA at the cell wall did not have a significant effect on the abundance of CwlO and LytC. By comparison, the glycosamides, LytD, was consistently high in the lithium extract (LS) across all mutation backgrounds and probably indicates that the LytD is associated with the cell wall and significantly increased with altered the cell wall compositions (Figure 3.25E).

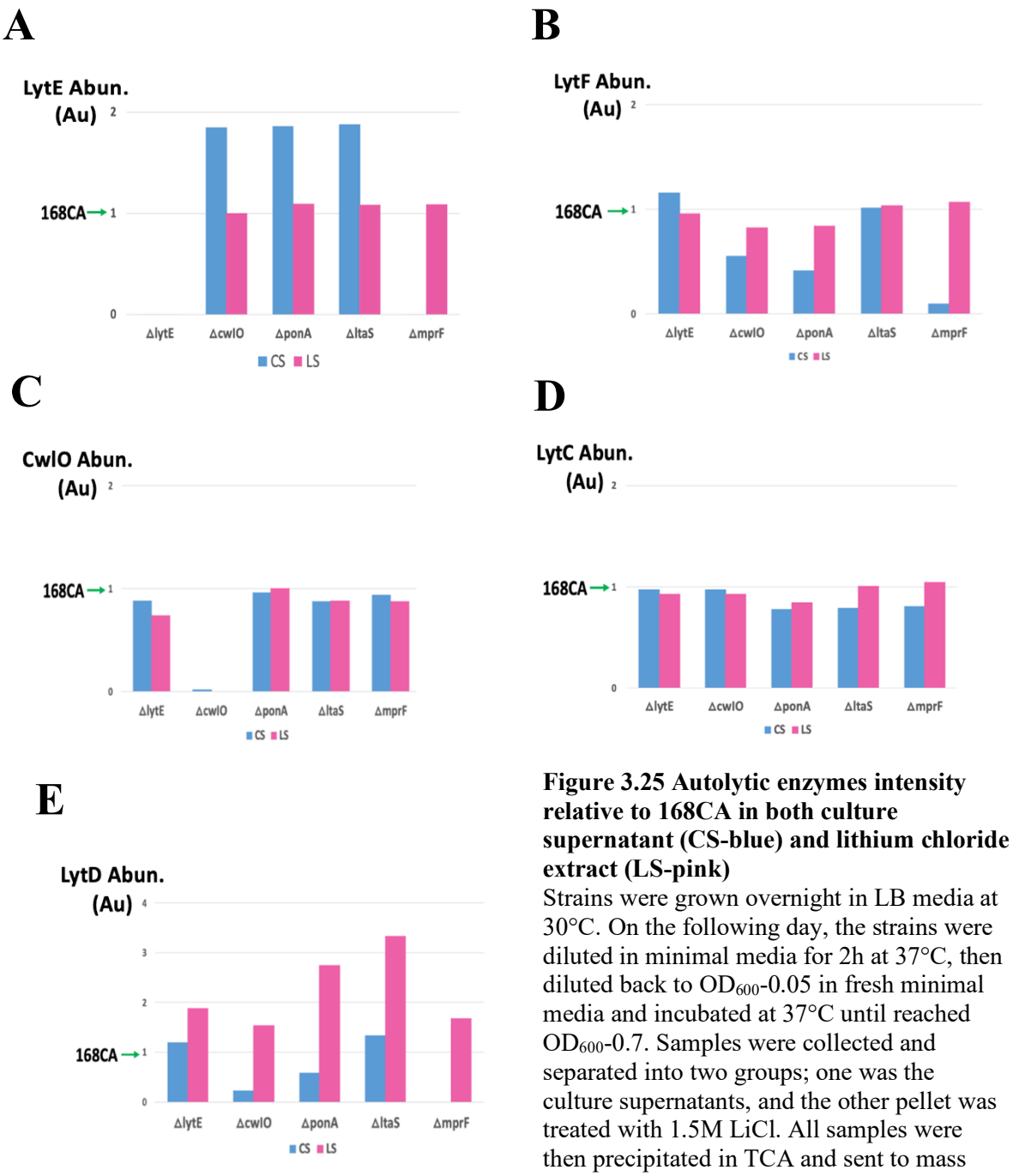

Figure 3.25 Autolytic enzymes intensity relative to 168CA in both culture supernatant (CS-blue) and lithium chloride extract (LS-pink)
Strains were grown overnight in LB media at 30°C. On the following day, the strains were diluted in minimal media for 2h at 37°C, then diluted back to OD_{600}-0.05 in fresh minimal media and incubated at 37°C until reached OD_{600}-0.7. Samples were collected and separated into two groups; one was the culture supernatants, and the other pellet was treated with 1.5M LiCl. All samples were then precipitated in TCA and sent to mass spectrometry for analysis. This experiment was conduct once.

3.3 Discussion

The activity of the autolytic enzymes plays a role in constructing and remodelling the PG layer. In this chapter, we found that the abundance of the autolytic enzymes changes, either through expression or stability, to allow the cells to adapt to changes in growth. This adaptability is perhaps expected as a mechanism to maintain the cell wall rigidity but permit changes in the rate of cell expansion (a function restricted by the cell wall). Nutrient Broth (NB) is considered a rich media that provides the necessary nutrients to support the relatively rapid growth of *B. subtilis,* primarily in the form of amino acids and was used as the standard growth medium to look at the abundance of the key autolytic enzymes (LytE, LytF, LytC, and LytD) by their specific antiserum. This then provided the possibility of altering the composition of the media by adding supplements such as $MgSO_4$ and glucose, which have been suggested to play a critical role in modifying autolytic activity (Dajkovic *et al*., 2017; Guyet *et al*., 2023; Wilson *et al*., 2023), and determine if this was due to alterations in the autolytic enzymes were altered in expression or stability.

Both $MgSO_4$ and glucose seem to have opposing effects on aspects of cell wall hydrolysis in *B. subtilis*. Importantly early research found that increased extracellular $MgSO_4$ stabilised sporulation mutants and later it was found to suppress the lethality of a variety of deletion mutations and restore the cell shape, but it is unclear how this suppression of phenotype works (Chastanet & Carballido-Lopez, 2012; Claessen et al., 2008; Mandelstam & Waites, 1968; Murray *et al*., 1998; Schirner, Marles-Wright, *et al*., 2009). The work presented in this chapter has extended our understanding of these observations. The deletion of *ponA* in Figure 3.20 showed slow growth unless the media is supplemented with $MgSO_4$, which consistent with Murray T *et al*., 1998. Additionally, the data presented in Figures 3.21 and 3.24 indicate that the presence of $MgSO_4$ negatively affected the abundance of LytE and LytD (DL-endopeptidase and glycosidase, respectively). This finding is consistent with recent studies published during my PhD study, which proposed that the hydrolysis enzymes were inhibited by excess $MgSO_4$ (Tesson *et al*., 2022; Wilson *et al*., 2023). This reinforces the idea that the expression of the autolytic enzymes may be modulated, or the stability of these enzymes may be altered by elevated $MgSO_4$. Both of these processes would be expected to result in reduced levels of the proteins being detected in the cells and consequently difficult to differentiate between. In contrast, glucose is considered a “good” carbon source and as such promotes the growth of the cell by enhancing the metabolic capability of the cell (Figure 3.20). It has also been shown that the growth on glucose has an

impact on cell wall integrity, resulting in the activation of at least SigM, a transcription factor activated by cell wall stress and presumed to play a role in maintaining PG integrity. Thus, the end result is a potentially complex set of transcriptional changes in addition to metabolic changes. However, this may simply be a response to an enhanced growth rate in Figure 3.20, causing a transient stress to be perceived (Ogura & Asai, 2016). Recently published work has shown that glucose increases the expression of *ltaS* in strain lacking all class A penicillin binding proteins (Δ4) and exacerbates the phenotype of some strains defective in cell wall synthesis (Guyet *et al*., 2023). In this study, the addition of glucose to a culture of the wild type strain increased the level of LytF, LytC, and LytD (Sections 3.3.2, 3.3.3, and 3.3.4), and that seems to fit with the idea that the activity of the autolytic enzymes is influenced by the increased carbon source, however it does not rule out the possibility that altered enzyme kinetics, through a change in the conformation of the peptidoglycan or by enzymes sub-cellular localisation is altered as well. These would be more difficult to characterise, but a change in the abundance of the enzymes might not be expected if they were the main mechanisms acting.

B. subtilis has at least 40 PG hydrolysis with presumably redundant functions, in that null mutation for most are phenotype less and multiple deletions can be combined without significant effects (Wilson *et al*., 2023). This sort of genetic approach has shown that only LytE or CwlO are necessary for viability, but with altered cell morphology. Recently found that LytE and LytF are potentially partially redundant to each other (Wilson *et al*., 2023 & A. Aljohani, thesis (unpuplished)). This can be demonstrated by the fact that combining the *dacA* mutation with *lytE* or *lytF* resulted in reduced cell viability, whereas the triple mutant *dacA lytE lytF* was conditionally lethal. Interestingly, this triple mutant strain was dependent upon high levels of $MgSO_4$ in the culture medium (A. Aljohani, thesis (unpublished)). In this study, deleting specific sigma factors such as *sigI* and *sigM* was found to change the abundance of specific hydrolytic enzymes, consistent with Tseng *et al*., 2011and Dobihal *et al*., 2019, who indicated that the expression of *lytE* was mediated by SigI. In this work, using LytE-antiserum, LytE was essentially absent in strain lacking *sigI* under various conditions and significantly reduce in the deletion of *sigM* (Figure 3.21). In contrast to LytE, LytF (the other DL-endopeptidase) was increased in strains with the deletion of *sigI* or *sigM* in either NB or NB supplemented with $MgSO_4$ or glucose. This is a hint that transcription regulation can be modulated and that increasing LytF abundance can compensate for the absence of LytE in either the *sigI* or *sigM* backgrounds.

Cell wall modifications are important for the control of the PG hydrolases. The modification of the TAs by the D-alanytion thought to reduce the activity of the PG hydrolases (Neuhaus & Baddiley, 2003). Recently shown that the MprF and PonA play a role in altering the length of the LTA, and the presence of glucose in the culture media impacts the LTA synthesis (Guyet *et al*., 2023). Additionally, it has been shown that in strain lacking *ltaS* (increase in the length of the LTA), the level of LytE increased (Kasahara *et al.*, 2016). In the present study, we tried to examine the accumulation of major autolytic enzymes on the cell wall in *ltaS*, *mprF*, and *ponA* backgrounds by mass spectrometry analysis. From the analysis it was found that the absence of these cell envelope components significantly impacts LytE level within the cell. Furthermore, the deletion of *mprF* resulted in enhanced levels of the LytF, LytC, and LytD detected in the cell wall-associated proteins. These results strongly suggest that modifying the composition of the PG can significantly impact the accumulation of enzymes involved in PG hydrolysis.

Antisera were raised against LytE, LytC, LytF, and LytD expressed as full-length proteins, were also expected to permit the subcellular localisation of the target proteins within whole cells by combination with fluorescently labeled secondary antibodies. However, this approach did not generate useful data as the antibodies only gave weak and diffuse signals observed in the wild-type and null mutant strains (data not shown). This suggested that the antisera bound non-specifically to the cell wall and did not recognize the specific proteins in the native state after light fixation. This might be explained by differences in the conformation of antigens in the different detection methods. The Western blot samples denatured the protein through SDS-PAGE, resulting in the epitopes becoming linear and exposing epitopes that were recognized by antibodies in the serum. Whereas, for immunolocalisation, the conformation of the protein is expected to be retained in the folded state to a greater degree, so the “recognized” epitopes may not be exposed (Figure 3.26).

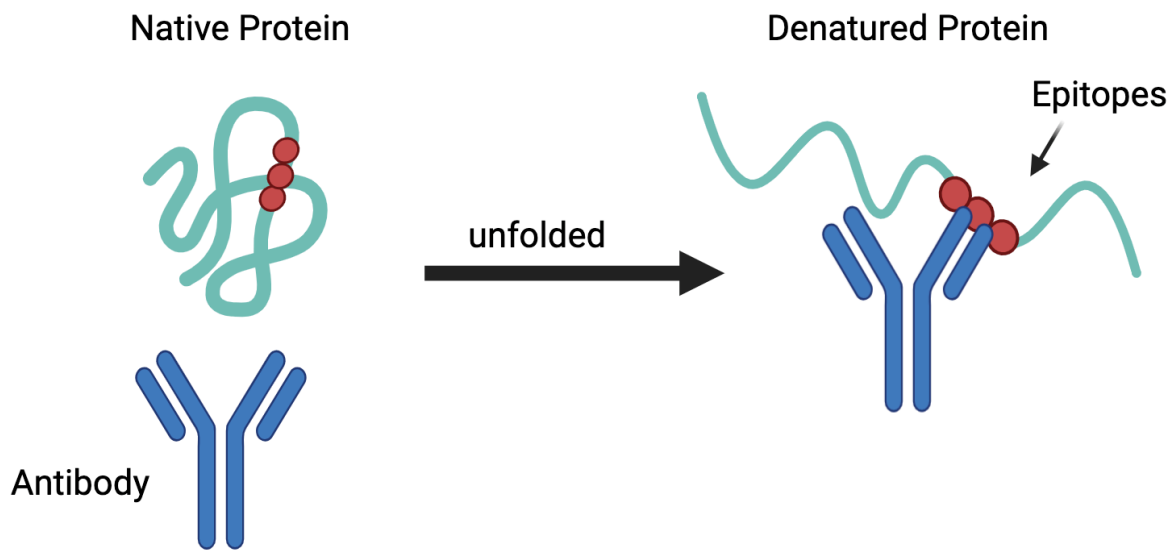

Figure 3.26 Differences in protein conformation

In the case of the native protein (left side), the epitopes are hidden inside the structure and are not recognized by the antibody. In contrast, upon denaturation (right side), the epitope become exposed, allowing for antibody to bind.

Chapter 4: LytC and LytE Carbohydrate-Binding Domain Analysis and Chimeric Gene Characterisation

4.1 Introduction

The DL-endopeptidases enzymes LytE, LytF, and CwlO play a critical role in cell morphology and separation, while the amidase enzyme LytC is involved in cell motility (Domínguez-Cuevas *et al*., 2013a; Ishikawa *et al*., 1998b; Kuroda & Sekiguchi, 1991; Ohnishi *et al*., 1999). Understanding their function in the cell wall is the key to gain an insight into how cell wall metabolism is modulated. This chapter is focused on characterising the functional importance of the proposed carbohydrate-binding domains (CBD) encoded in the N-terminal region of the genes. As a starting point, the aim was to understand the function of the cell wall binding domains of LytE and LytC (DL-endopeptidases and amidase, respectively) to identify what these proteins interact within the cell envelope. In parallel, chimeric genes were constructed by swapping the catalytic domain and binding domain of the autolysin to determine if the biochemical activity of the C-terminal domain was important for the localisation/binding domain.

4.1.1 Analysis of the functionality of the affinity tags

An affinity tag is a short sequence of amino acids fused to a target protein to facilitate the characterization of protein. Several affinity tags can be used in protein fusions, such as the Hexahistidine tag (6X-His-tag used in Chapter 3), a green fluorescent protein (GFP), a FLAG tag, a Halo-tag, and protein A. The coding sequences of these affinity tags can be fused to the target gene, resulting in the tag being located at either the N- or C-terminal end of the target protein. The GFP and Flag tags have been used previously to determine the localisation and the expression of the autolytic enzymes (Carballido-López *et al*., 2006; Domínguez-Cuevas *et al*., 2013a; Hashimoto *et al*., 2012; Kiriyama *et al*., 2014a; Meisner *et al*., 2013; Salzberg *et al*., 2013; Yamamoto *et al*., 2003a). In this study, the Halo-tag and protein A were used. The Halo-Tag is a self-labeling protein derived from haloalkane dehalogenase enzyme (DhaA) from *Rhodococcus rhodochrous*. The Halo-tag reacts covalently to a fluorescent ligand that is a substrate mimic of the natural substrate, allowing the specific labeling of the tagged protein. The fluorescent ligands then enable tracking of the protein localisation and identification of protein-protein interactions (Georgyi V Loos, 2008). It has also been demonstrated that the tag can be secreted without loss of function, unlike GFP, which normally becomes unfolded or cannot adapt its fluorescent configuration once secreted. However, in this work (described in Section 4.2), this tag proved to be problematic, and so an alternate option was devised.

A second approach used in this work to determine protein characteristics was to create a fusion with protein A from *S. aureus*. Protein A (SpA) can be described as having essentially three major domains (Figure 4.2): an export domain at the N-terminus consisting of a signal sequence (transmembrane segment) that is cleaved by signal peptidase (S), a repeat sequence of IgG binding domains and finally a region involved in cell wall association (LysM) and PG linkage (LPXTG). The IgG binding domains have the ability to bind the FC region of immunoglobulins (IgG). The LPXTG serves as a sorting signal motif (O'Halloran *et al.*, 2015). Thus, Fusion SpA with cell wall binding domains of the autolytic proteins in B. *subtilis* potentially provided a way to "pull down" the protein and determine what it may interact with (methods are described in section 2.6.2).

4.1.2 Domain structure of the proteins

AlphaFold provides prediction of the three-dimensional (3D) structure of proteins, and a database of these structures has been generated (Marks *et al*., 2012). Using this data, Table 4.1 was generated for the predicted structures of the LytC, LytE, LytF, and CwlO, along with a linear representation of the amino acid sequence colour coded for the domains represented in the structural prediction (adapted from AlphaFold DBP). These predictions provided a good way to define the domains of the proteins in a visual way linked to the linear sequence of amino acids encoded by the genes. The first 24, 25, 25, and 30 amino acids (aa) of LytC, LytE, LytF, and CwlO, respectively, are identified as signal peptides, as shown in Table 4.1 panels A, B, C, and D (red colour). Most secreted proteins contain a signal peptide that is cleaved off after passing through the cell membrane (von Heijne, 1986). In the AlphaFold structure, the N-terminal region contains the carbohydrate-binding domain (CBD), and the C-terminus carries the catalytic activity. Of the known enzymes, LytC is considered to be a major autolytic enzyme belonging to the amidase family. The localisation of LytC was found to be in the entire cell wall, and this seems to be determined by the N-terminal domain, which consists of three repeated sequences of the CBD (Table 4.1 panel A). No obvious morphological change is observed in the *lytC* single mutant, indicating that LytC does not play a key role in cell growth or separation, but the swarming motility of the cell was reduced (Kuroda & Sekiguchi, 1991; Yamamoto *et al*., 2003a). In contrast to LytC, the AlphaFold structures of LytE and LytF exhibited that the N- and C-terminal domains were less tightly packed, with the domains are separated by potentially flexible linkers (Table 4.1 panel B and C). In the N-terminal region of LytE and LytF, there are three and five repeat sequences, respectively, each containing 44 amino acids, which are referred to as LysM.

Besides the similarities in their N-terminal domains, the C-terminus of both LytE and LytF have a protein sequence/structure that belongs to the NlpC/P60 family. The CwlO protein also has a catalytic domain that is very similar to that of LytE and LytF, but its N-terminal portion of the protein structure is entirely different (Table 4.1 panel D) (Bisicchia *et al*., 2007; Ishikawa *et al*., 1998b; Margot *et al.*, 1999a; Yamaguchi *et al*., 2004). It was found that LytE and CwlO play a critical role in cell growth. The double mutant of *lytE* and *cwlO* was synthetic lethality presumably because of the loss of DL-endopeptidase activity in the lateral cell wall (Bisicchia *et al*., 2007; Hashimoto *et al*., 2012). LytE was observed to be localised at the poles, cell septa, and along the sidewall, while CwlO was near the cell membrane on the sidewall. LytF, by contrast, was found to be localised at the cell septa and poles (Hashimoto *et al*., 2012). A previous study revealed that the localisation of LytE, LytF, and CwlO is controlled by their N-terminal region (Hashimoto *et al*., 2012; Yamamoto *et al*., 2003a). A strain where each of these genes was individually deleted had characteristic phenotypes; cells in the *cwlO* mutant were shorter and wider, *lytE* mutant cells were longer and slightly thinner, while the *lytF* mutant formed chains (Domínguez-Cuevas *et al*., 2013a; Ohnishi *et al.*, 1999).

Table 4.1 AlphaFold predicated structure and the amino acid sequence of LytC, LytE, LytF and CwlO

The AlphaFold LytC (Q02114), LytE (P54421), LytF(O07532), and CwlO (P40767) were adapted from Uniprot. Colours change depending on the region; red colour represents the signal peptide/ transmembrane, pink colour represents the CBD of LytC, yellow colour indicates the amidase family, purple colour represents the LysM domain, blue colour represents the DL-endopeptidase, and green colour represents the CBD of CwlO. The colour of the AlphaFold changed from PyMOL.

Name/ AlphaFold predict	Amino acid sequences
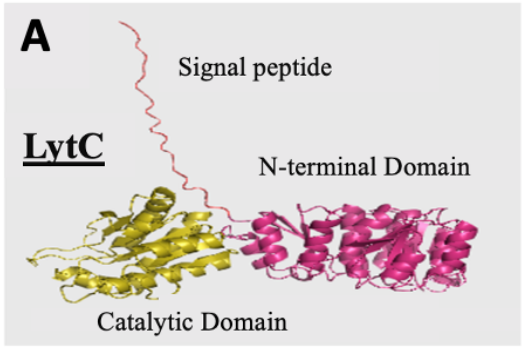	1 20 40 56 MRSYIKVLTMCFLGLILFVPTALADNSVKRVGGSNRYGTAVQISKQMYSTASTAVI 57 76 96 112 VGGSSYADAISAAPLAYQKNAPLLYTNSDKLSYETKTRLKEMQTKNVIIVGGTPAV 113 133 153 168 SSNTANQIKSLGISIKRIAGSNRYDTAARVAKAMGATSKAVILNGFLYADAPAVIP 169 189 209 224 YAAKNGYPILFTNKTSINSATTSVIKDKGISSTVVVGGTGSISNTVYNKLPSPTRI 225 245 256 280 SGSNRYELAANIVQKLNLSTSTVYVSNGFSYPDSIAGATLAAKKKQSLILTNGENL 281 301 321 336 STGARKIIGSKNMSNFMIIGNTPAVSTKVANQLKNPVVGETIFIDPGHGDQDSGAI 337 357 377 392 GNGLLEKEVNLDIAKRVNTKLNASGALPVLSRSNDTFYSLQERVNKAASAQADLFL 393 412 432 448 SIHANANDSSSPNGSETYYDTTYQAANSKRLAEQIQPKLAANLGTRDRGVKTAAFY 449 469 490 VIKYSKMPSVLVETAFITNASDASKLKQAVYKDKAAQAIHDGTVSYYR
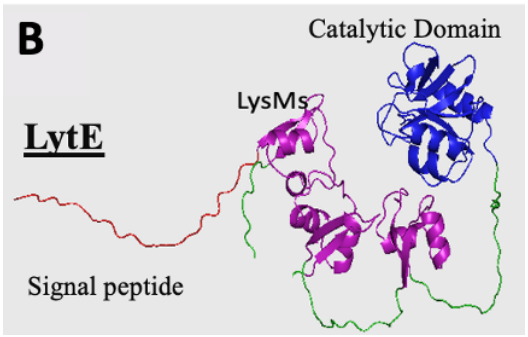	1 20 40 56 MKKQIITATTAVVLGSTLFAGAASAQSIKVKKGDTLWDLSRKYDTTISKIKSENHL 57 76 96 112 RSDIIYVGQTLSINGKSTSSKSSSSSSSSTYKVKSGDSLWKISKKYGMTINELKK 113 132 152 168 LNGLKSDLLRVGQVLKLKGSTSSSSSSSKVSSSSTSTYKVKSGDSLSKIASKYGT 169 188 208 224 TVSKLKSLNGLKSDVIYVNQVLKVKGTSTSSSKPASSSSSSSSKTSSTSLNVSKLV 225 245 265 280 SDAKALVGTPYKWGGTTTSGFDCSGFIWYVLNKQTSVGRTSTAGYWSSMKSIASPS 281 301 321 335 VGDFVFFTTYKSGPSHMGIYIGNNSFIHAGSDGVQISSLNNSYWKPRYLGAKRF
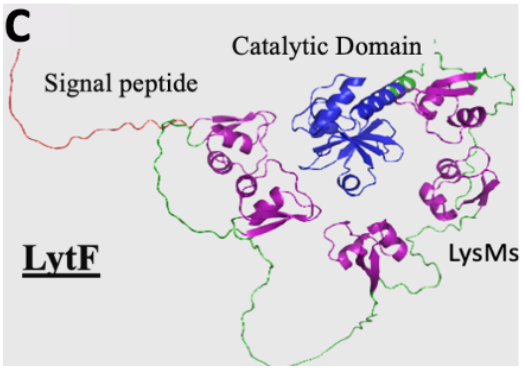	1 20 40 56 MKKKLAAGLTASAIVGTTLVVTPAEAATIKVKSGDSLWKLAQTYNTSVAALTSANH 57 77 97 112 LSTTVLSIGQTLTIPGSKSSTSSSTSSSTTKKSGSSVYTVKSGDSLWLIANEFKMT 113 133 153 168 VQELKKLNGLSSDLIRAGQKLKVSGTVSSSSSSSKKSNSNKSSSSSSKSSSNKSSS 169 189 209 224 SSSSTGTYKVQLGDSLWKIANKVNMSIAELKVLNNLKSDTIYVNQVLKTKSSGSDT 225 245 265 280 SSKDNSSKSNQTSATTKYTVKSGDSLWKIANNYNLTVQQIRNINNLKSDVLYVGQV 281 301 321 336 LKLTGKASSGSSSSSSSSSNASSGTTTTYTVKSGDSLWVIAQKFNVTAQQIREKNN 337 357 377 392 LKTDVLQVGQKLVISGKASSSSSSGSSNTTSSTSAKINTMISAAKAQLGVPYRWGG 393 413 433 448 TTPSGFDCSGFIYYVLNKVTSVSRLTAAGYWNTMKSVSQPAVGDFVFFSTYKAGPS 449 496 489 HVGIYLGNGEFINANDSGVVISNMNNSYWKQRYLGAKRYF
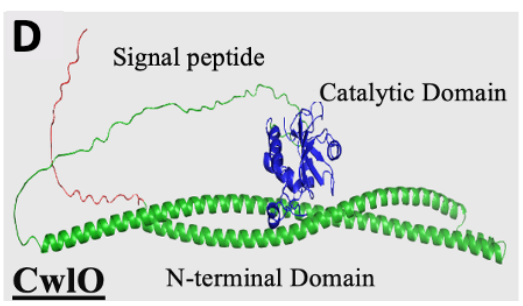	1 20 40 56 MRKSLITLGLASVIGTSSFLIPFTSKTASAETLDEKKQKIESKQSEVASSIEAKEK 57 77 97 112 ELTELQENQSKIEKELKDINDKALDTSNKIEDKKEENDKTKEEIKKLKKEIKETEA 113 133 153 168 RIEKRNEILKKRVRSLQESGGSQGYIDVLLGSTSFGDFISRATAVSSIVDADKDLI 169 189 209 224 KQQEQDKAKLEDSEADLNDKLKEVQAALAKLETMQKDLDKQLNEKDKLFDEAKASQ 225 245 265 280 KKTAKAISELKSEASELANQKANTEAEQARIKKEQEAAAALIKKQEEAQKASDETQ 281 301 321 336 TDDSQTATTESSKASSSDDSSDNSSDNSSNGSSNSSSNGSSSKKSSGSNSNSGGTV 337 357 377 392 ISNSGGIEGAISVGSSIVGQSPYKFGGGRTQSDINNRIFDCSSFVRWAYASAGVNL 393 412 432 448 GPVGGTTTDTLVGRGQAVSASEMKRGDLVFFDTYKTNGHVGIYLGNGTFLNDNTSH 449 471 GVSVDSMSNPYWKAAFKGVVRRVVQ

4.2 Result

4.2.1 *In Vivo* tagging of the enzymes

As an initial step toward being able to determine the localisation and interaction of the autolytic enzymes LytE and LytC, fusion construct strains sAM001, sAM002, sAM003, and sAM004 were created carrying *lytE*-Halo, N_{lytE}-Halo, *lytC*-Halo, and N_{lytC}-Halo fusion genes, respectively, under the control of a P_{xyl} promoter (Figure 4.1A) (cloning and construction described in method Section 2.8.2).

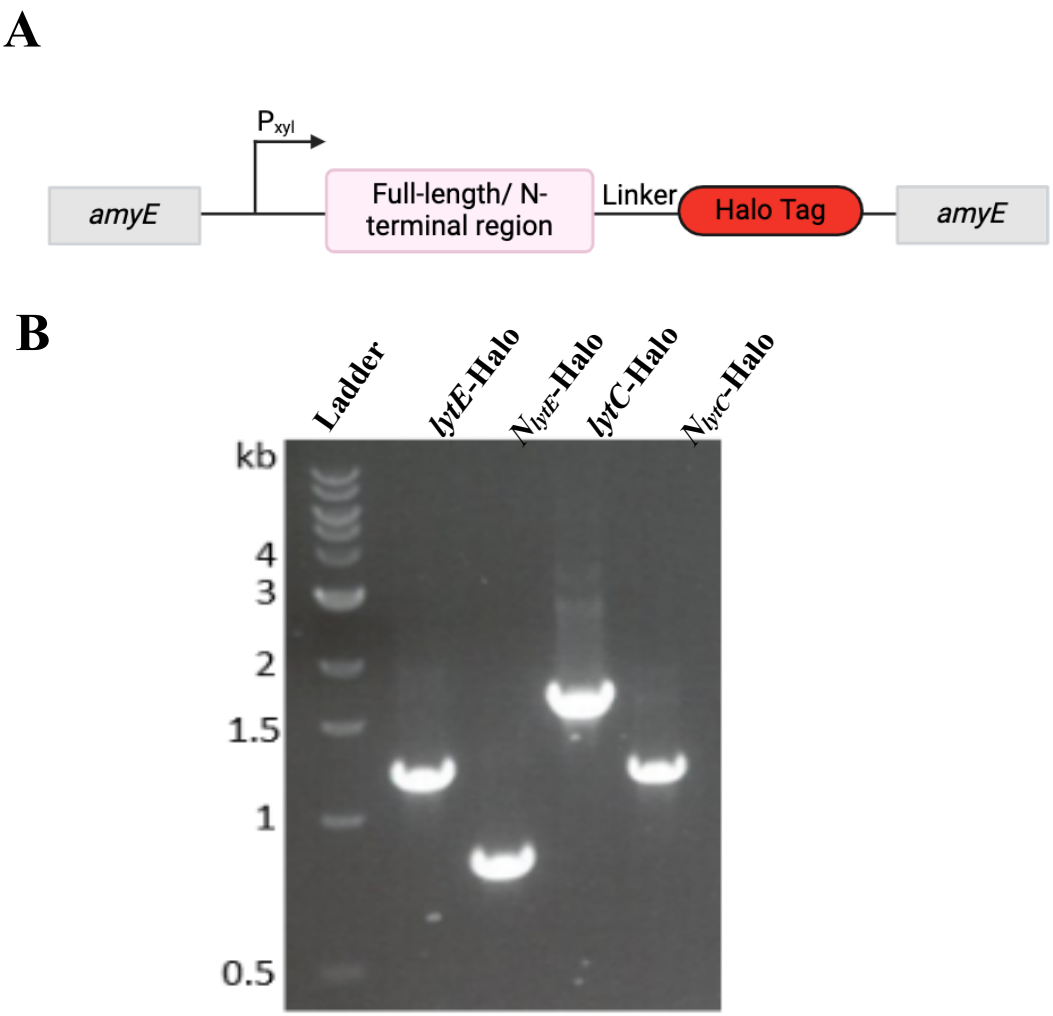

Figure 4.1 Halo-tag constructed

(A)Schematic diagram demonstrates the Halo-tag fusion constructed by HiFi DNA Assembly Cloning to generate *lytE*-Halo, N_{lytE}-Halo, *lytC*-Halo, and N_{lytC}-Halo. (B) Agarose gel electrophoresis of the PCR products using P_{xyl} (oAM098) as a forward primer and from the beginning of Halo-tag (oAM099) as a reverse primer to confirm the construct. The expected size of *lytE*-Halo (1204 bp), N_{lytE}-Halo (790 bp), *lytC*-Halo (1693 bp), and N_{lytC}-Halo (1170 bp).

Strains containing the Halo-tag construct were confirmed by PCR (Figure 4.1B) and sequencing to ensure the fusions were in frame. Then strains carrying the fusions (strain

sAM001, sAM002, sAM003, and sAM004 where the Halo-tag fused to the *lytE*, $N_{lytE,}$ *lytC,* and $N_{lytC,}$ respectively were grown in LB media until they reached an OD_{600} of 0.5. At this point, the cultures were induced to express the fusion by adding xylose (0.5% final concentration) and incubation continued. Samples of the culture were collected before and after induction by centrifugation, and the total cell protein was extracted in the SDS-loading buffer. The proteins in the samples were then resolved using SDS-PAGE in duplicate, with one gel being stained with Coomassie to visualize the protein bands (Figure 4.2A). This allowed an assessment of the overall amount of protein loaded on the gel, ensuring that any comparisons can be corrected for the amount of sample. The second gel was blotted onto a membrane to allow detection of specific proteins by Western blot analysis using an Anti-HaloTag® Monoclonal Antibody (Promega/Cat No.G9211). Here, the aim was to confirm the specificity of the antibody. To achieve this, a positive control sample was included, strain bGS28 (Bisson Filho *et al*., 2017), which encoded a C-terminal Halo-tag fusion with Pbp2B. This fusion construct was previously confirmed functional, but not used with this particular commercial antibody. The Halo-tag fusions were predicted to be of different molecular weights; the LytE-Halo fusion was estimated to be 70 kDa, N_{LytE}-Halo 53 kDa, LytC-Halo 85 kDa and N_{LytC}-Halo 66 kDa. On developing the Western blot (Figure. 4.2B) a strong band was detected, but it was present at the same molecular weight in all samples. No bands corresponding to the predicted molecular weights could be identified in any sample despite repeated Western blots altering the detection conditions (e.g., changing blocking buffer, antibody dilutions, and incubation times). Figure 4.2B is a representative example of what was obtained in all cases). This suggested that either the Anti-HaloTag® Monoclonal Antibody was not able to detect Halo-tag fusion in bacteria cells or that the fusion protein was not stable enough to be detected using the sampling conditions of the experiment. The fact that the positive control sample was not detected suggested an issue with the antibody.

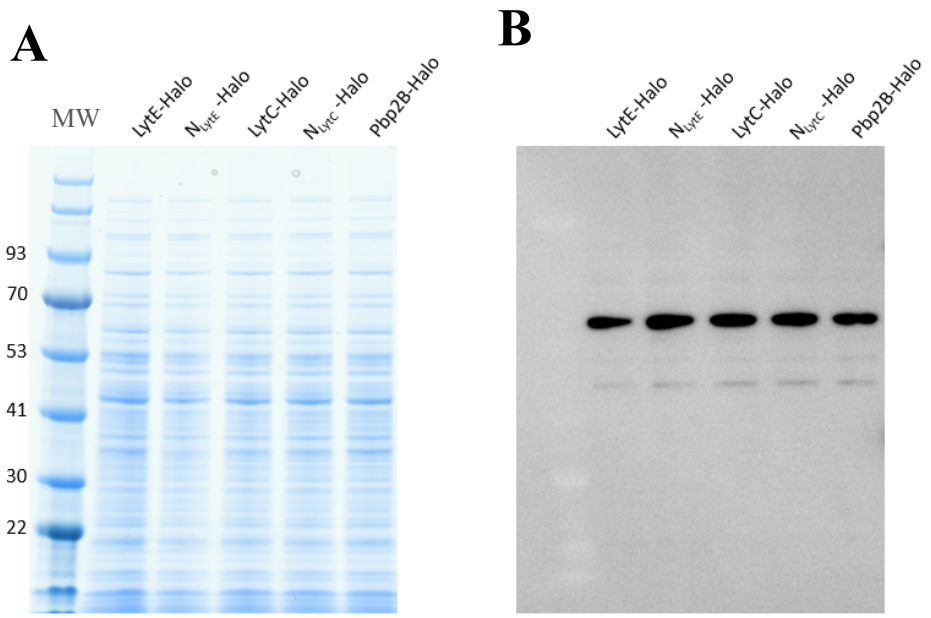

Figure 4.2 Analysis of the Halo-tag fusion using Anti-HaloTag® Monoclonal Antibody

Samples were collected after induction with xylose, and strain bGS28 (Pbp2b-Halo (*pbp2B::erm-Phyperspank-Halo-tag-15aa-pbp2B*) was induced with IPTG. (A) After running the sample in SDS-PAGE, the gel was stained with Coomassie as a loading control. (B) The expression of the Halo-tag fusions was examined by Western blot using Anti-HaloTag® Monoclonal Antibody. The molecular weight marker (kDa) is indicated by MW.

From the work described earlier (Chapter 3), polyclonal antisera for LytE and LytC had been raised, and these provided a potential way to check the stability of the constructed fusions. In this case, the wild strain (168CA) was used as a positive control for the antisera, while strains deleted for *lytE* or *lytC* served as a negative control. Thus, again it was expected that different sizes of bands would be detected for the Halo-tag fusion as they would have higher molecular weights than the native proteins (LytE-Halo (70 kDa), N_{LytE}-Halo (53 kDa) LytC-Halo (85 kDa), and N_{LytC}-Halo (66 kDa). However, no bands were detected at the expected sizes for the fusion proteins. The only proteins detected were identified as corresponding to the native LytE and LytC proteins (Figure 4.3). Having repeated the detection method with varied conditions with no positive detection of the Halo-tag fusions, it was concluded that the fusion proteins were either not expressed or not sufficiently stable enough to be detected.

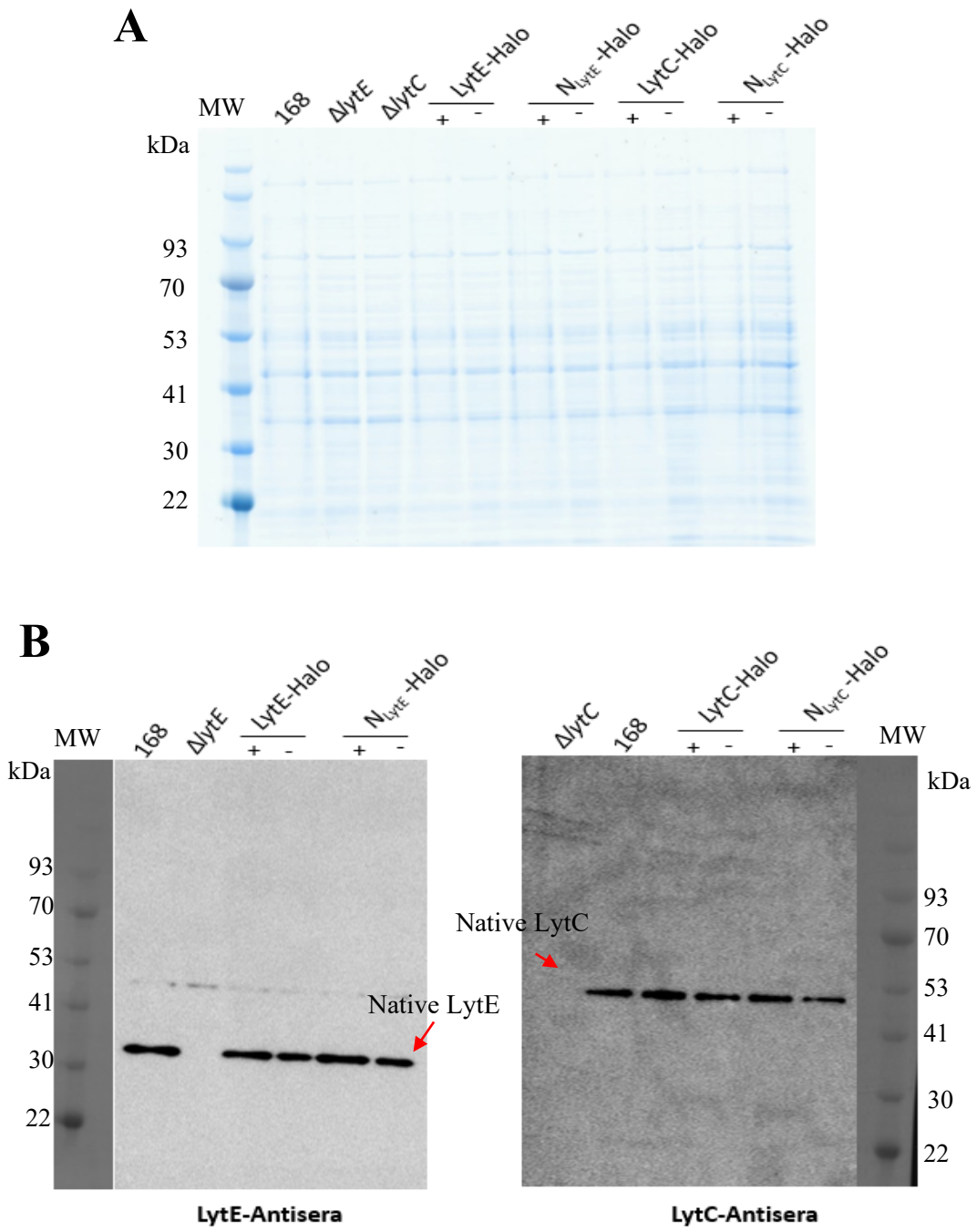

Figure 4.3 Analysis of the Halo-tag fusion using LytE-antiserum and LytC-antiserum

The figure displayed the expression of the full-length and the N-terminal of either LytE or LytC fused with the Halo-tag. Samples were treated as previously done with the samples in Figure 4.2 (A) demonstrates Coomassie of SDS-PAGE gel confirming uniform loading control of the samples. (B) Western blot analysis of the samples by utilising LytE-antiserum (left panel) or LytC-antiserum (right panel). As a positive control, 168CA was used, and as a negative control, either deletion of *lytE* or *lytC* was used. The molecular weight marker (kDa) is indicated by MW. The molecular weight of LytE-Halo (70 kDa), N_{LytE}-Halo (53 kDa) LytC-Halo (85 kDa), and N_{LytC}-Halo (66 kDa). The red arrows indicate the native size of LytE and LytC.

4.2.2 Protein interaction

Since the Halo-tag fusions were unstable, an alternate approach was devised to exploit the properties of Protein A (SpA) from *S. aureus* (described in Section 4.1.1). The aim was to exploit the IgG-binding domains of SpA as an easy to detect the autolytic proteins fused to SpA. Additionally, it provides a possible way to "pull down" the fusion protein and determine what it is associated within the cell wall.

Since SpA is a complex multi-domain protein, the initial work was set out to determine if the individual domains of SpA were stable and if the IgG-binding domains could be expressed without the other domains, thereby avoiding potential complications related to their functions. For this, two SpA constructs were generated in the shuttle plasmid pAG-P08 (cloning and construction described in method in Section 2.8.3.2) (Figure 4.4). In each case, a different segment of the *spA* coding sequence was inserted to replace the GFP coding sequence in the parent plasmid. The end result being the construction of synthetic genes encoding the full-length protein A (*spA*) and the one lacking the LysM and LPXTG domains (*spA'*) and under the control of the P_{spac} promoter as shown in Figure 4.4. The resulting plasmids were then transformed into the *B. subtilis* strain 168*lacI* (sAG1333) to generate sAM005 and sAM006 bearing the full-length *spA* and the truncated version of *spA'*, respectively, under P_{spac} promoter. The 168*lacI* background was used to permit induction of expression by adding IPTG. The resulting strains were grown in LB media until they reached the mid-exponential phase (OD_{600} of 0.5). IPTG was then added, and samples were collected 10, 15, and 30 minutes after induction. As previously done with Halo-tag constructs, the cells were pelleted and suspended in an SDS-loading buffer, lysed by sonication, and the proteins separated on SDS-PAGE. To determine if the genes were expressed, a protein A polyclonal antibody (Sigma) was utilised (Figure 4.5). A parallel gel provided a loading control, confirming that the samples were loaded with comparable amounts of total cell protein (Figure 4.5A). Western blot analysis was then carried out with the expectation that the full-length SpA would result in a band corresponding to 56 kDa, while the SpA' would yield a band at 44 kDa. The resulting blot (Figure 4.5B) was found to have the expected signal at the appropriate molecular weight. However, it was clear that the expression of the genes was not tightly controlled, something that was a little unexpected, with a clearly detectable signal at the start of the experiments prior to induction. This observation was unexpected as the pAG-P08 plasmid (Guyet, unpublished) had been extensively characterised in terms of GFP expression. Previous work (Guyet, unpublished) had shown no suggestion of expression form

similar plasmid constructions in the absence of IPTG provided it was maintained in the 168*lacI* background (sAG1333), but this was determined by fluorescence microscopy and so may not have been a sensitive to low level expression. However, uncontrolled expression was not a significant problem in this experimental work. A close inspection of the blot indicated that SpA samples presented with six bands that gradually reduced molecular weight. In contrast, the construct lacking the LysM and LPXTG motif was predominantly present as a single band. This was potentially consistent with the idea that the LysM and LPXTG might act to retain the exported protein into the cell wall, where it might then be degraded. This interpretation would also predict that there would be a lower abundance of the SpA' in the samples because it would be more likely to pass into the culture media and be lost from the cell sample. Here, visual inspection of the blot seemed to suggest that there was a lower amount of SpA' protein present in the samples compared to full-length SpA.

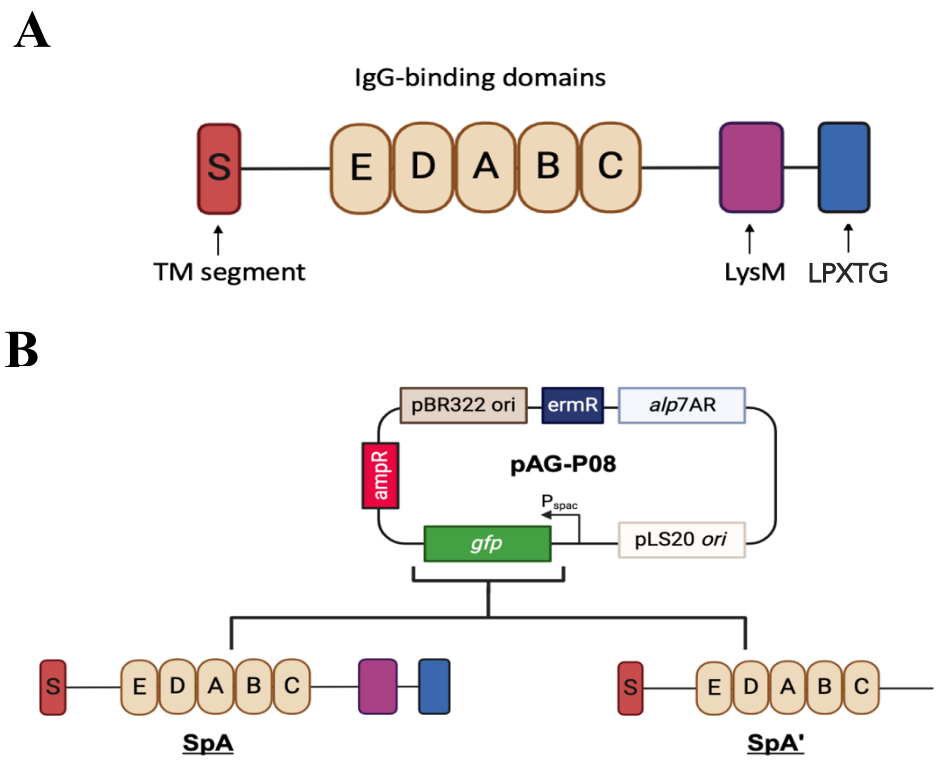

Figure 4.4 Generated constructs containing variants of Protein A (SpA)

(A) A diagram representing of the basic domain structure of protein A (SpA). At the N-terminal SpA contains of transmembrane segment signal sequence (S), followed by five IgG-binding domains (E-D-A-B-C). The C-terminal consists of LysM, which anchors to the cell wall and sorting region (LPXTG motif). (B) The SpA (full-length) and SpA' (lacking LysM and LPXTG motifs) replaced the *gfp* in the self-replicated plasmid pAG-P08 by using the HiFi DNA Assembly Cloning (described in method in Section 2.5.2).

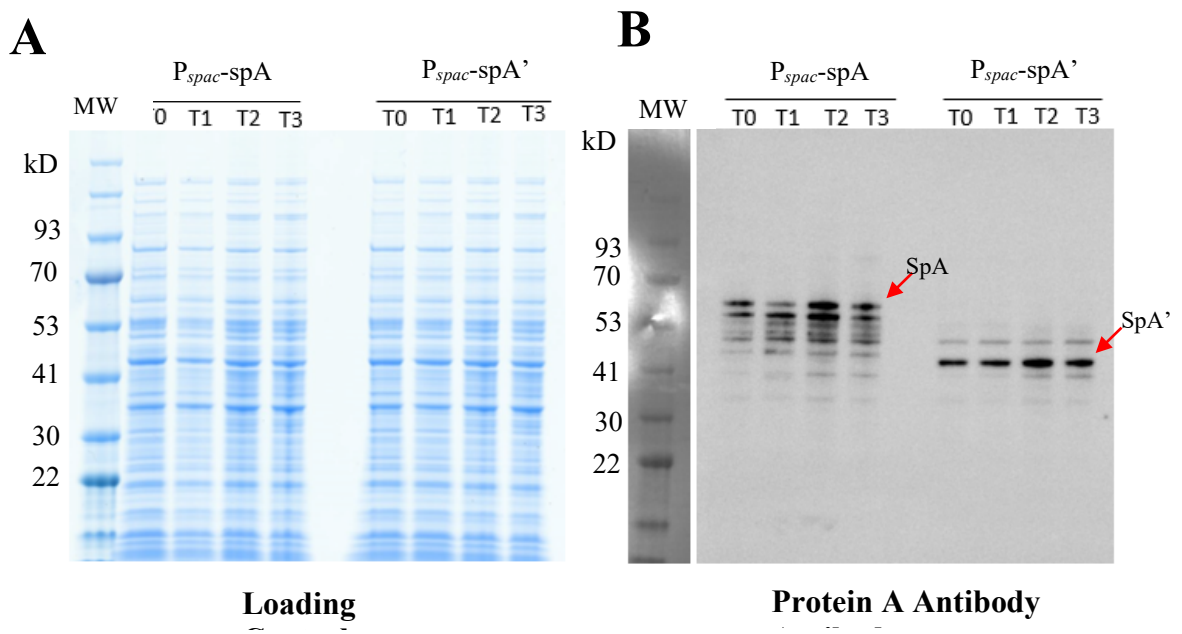

Figure 4.5 Analysis the expression of the protein A (SpA) constructs in *B. subtilis*

(A) Loading control of full-length Protein A (SpA) and the protein A lacking the LysM and LPXTG (SpA') constructs using Coomassie. (B) Western blot analysis was performed to assess the expression of SpA and SpA' at different time points after induced. T0 samples are collected before adding IPTG, while T1, T2, and T3 samples are collected after induction (10, 15, and 30 min, respectively (B). The molecular weight marker (kDa) is indicated by MW, and the red arrow indicates the predicated molecular weight of SpA (56 kDa) and SpA' (44 kDa).

Based on the results obtained with these pilot constructions (SpA and SpA'), the N-terminal region of either LytC or LytE was fused to the SpA and SpA'. As previously mentioned, LytC consists of signal peptide and the three repeated sequences considered to be CBD domains at the N-terminal region and the catalytic amidase domain at the C-terminal region. In comparison, the N-terminus of LytE is composed of a signal peptide followed by three repeated sequences of the LysM motif and a DL-endopeptidase domain at the C-terminal end of the protein (catalytic domain). The N-terminal portion of LytC or LytE fused to SpA and SpA' are highlighted with grey colour in Figure 4.6A and B. The constructed fusions N_{LytE}-SpA, N_{LytE}-SpA', N_{LytC}-SpA, and N_{LytC}-SpA' are illustrated in the diagram presented in Figure 4.6A and B. This approach aimed to assess whether these fusion proteins, once secreted, would be retained in the cell wall through the wall-binding domains of the autolytic proteins.

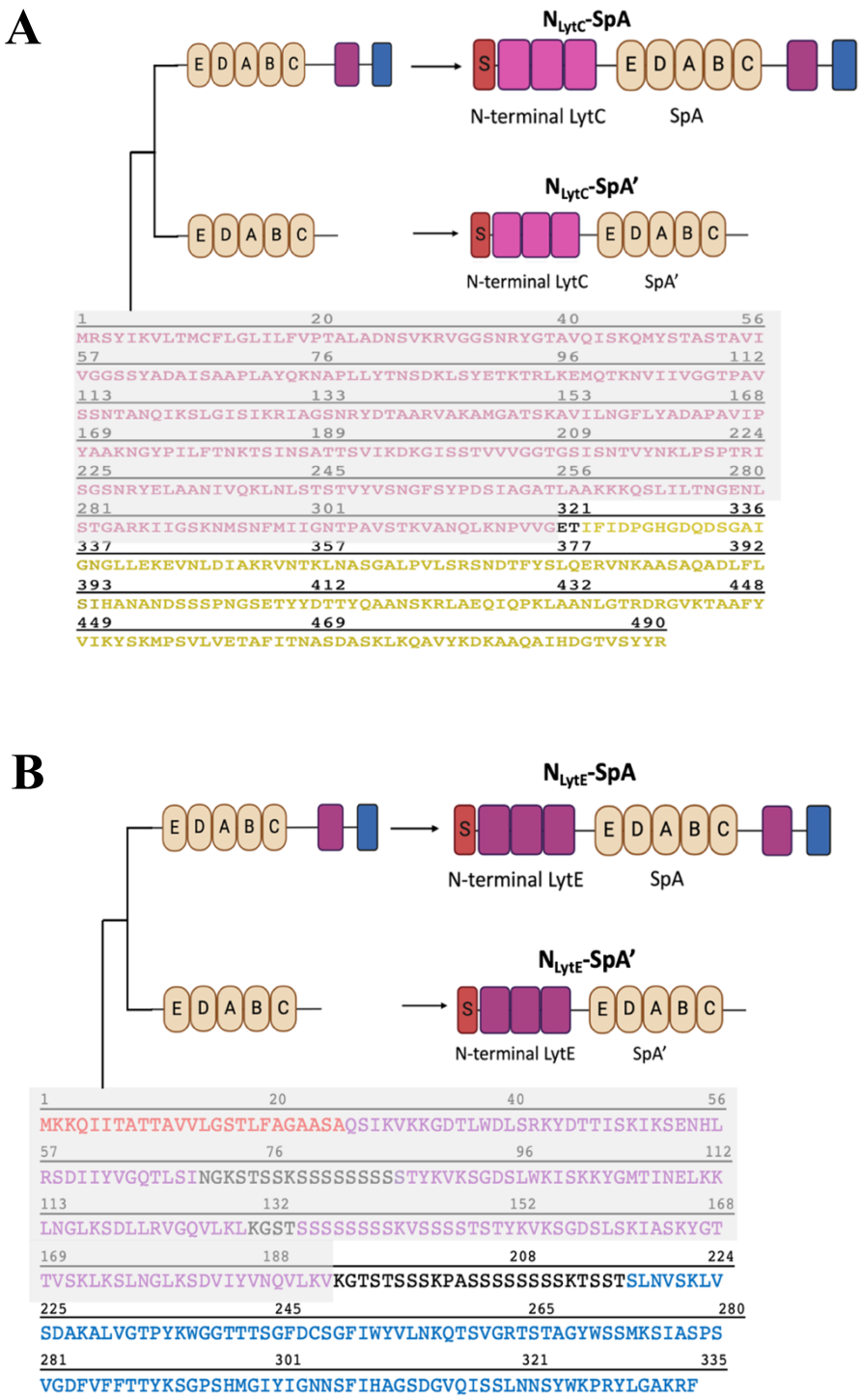

Figure 4.6 Diagram displays the fusion constructs of the N-terminal region of either LytC or LytE to SpA and SpA'

The amino acid sequence of the N-terminus of LytE and LytC is highlighted with grey colour, which was fused to the either the full-length SpA or the truncated one SpA' using HiFi DNA Assembly to generate N_{LytE}-SpA, N_{LytE}-SpA', N_{LytC}-SpA, and N_{LytC}-SpA'.

4.2.3 Characterisation of N_{LytC} fusion to protein A (SpA)

To determine if the N-terminal domain of LytC fused to SpA was expressed in *B. subtilis*, the strains N_{LytC}-SpA and N_{LytC}-SpA' (sAM009 and sAM010, respectively) were grown in LB media (in the presence of erythromycin to maintain the plasmid) until they reached an OD_{600} of 0.5. IPTG was then added to induce expression, and samples were collected 10, 15, and 30 minutes after induction. The cells were then harvested and lysed by sonication, and the proteins were separated on SDS-PAGE. The samples on SDS-PAGE were adjusted to standardise the amount of protein loaded (Figure 4.7A). Western blotting was then used to determine the relative abundance of the expressed protein fusions over time using antisera specific for either LytC or protein A (Figure 4.7B). LytC-antiserum detected the native LytC and the N-terminal region of LytC fused to SpA, with the identity of the fusion construct also being confirmed by Protein A antibody. This showed that the expression level of both constructs remained relatively constant throughout the induction period and that the expression fusion construct was leaky, as had been indicated by the preliminary experiments. Interestingly, the fusion of the N_{LytC} with SpA resulted in an apparently stabilized protein, as there was clearly less degradation compared to that seen for the SpA protein (Figure 4.6B). It was also observed that N_{LytC}-SpA fusion was present in two distinct bands; the first probably corresponded to the N_{LytC} fused to the full-length SpA (85.4 kDa), while the second was a lower molecular weight (78 kDa), similar in size to the N_{LytC} fused to the truncated SpA'. This potentially suggested that the LysM region in the full-length SpA construct fusion might be targeted by proteases in *B. subtilis*.

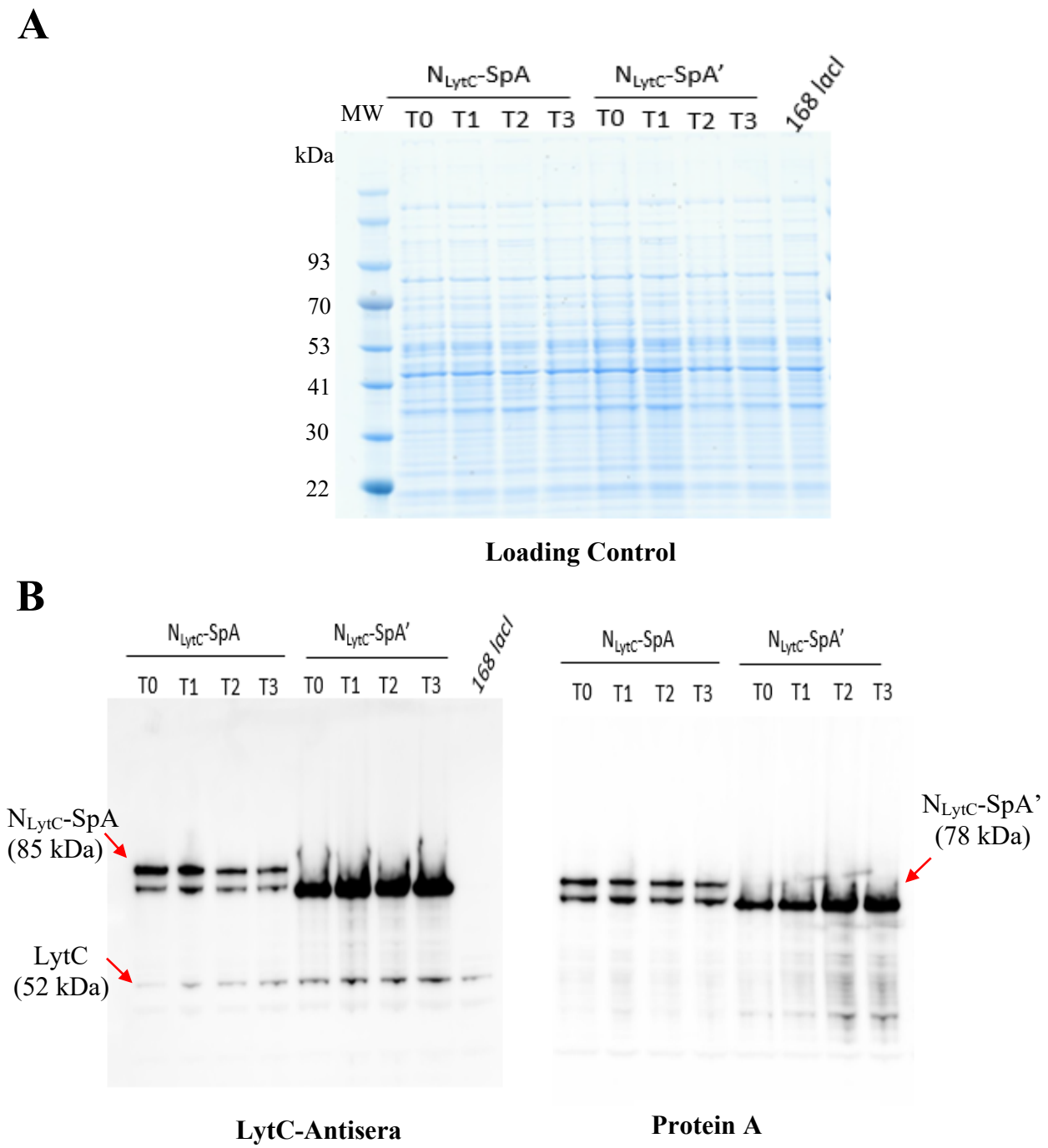

Figure 4.7 N_{LytC}-SpA and N_{LytC}-SpA' expression

(A) Image of the gel stained with Coomassie identically serving as a loading control for the N_{LytC}-SpA and N_{LytC}-SpA' samples. (B) Western blot examined the expression of N_{LytC}-SpA and N_{LytC}-SpA' using LytC antisera and protein A antibody over time. Samples were collected at different time points: T0 before adding IPTG, T1, T2, and T3 samples were collected after induction (10, 15, and 30 min, respectively). The molecular weight marker (kDa) is indicated by MW, and the red arrow indicates the predicated molecular weight of N_{LytC}-SpA (85 kDa), N_{LytC}-SpA' (78 kDa), and the native LytC (52 kDa).

Since the fusion constructs N_{LytC}-SpA and N_{LytC}-SpA' were expressed and easily detectable, the next goal was to determine whether the fusion proteins were secreted or remained bound to the cell wall. Therefore, the N_{LytC}-SpA and N_{LytC}-SpA' were grown in LB

media with erythromycin until they reached the mid-exponential phase. Samples were collected 40 minutes after induction with IPTG, and then the pellets were suspended in an isotonic buffer (Protoplasting Buffer- described in Appendix 1-Buffer components) containing lysozyme to degrade the cell wall but prevent lysis of the resulting protoplast. The resulting protoplast suspension was then gently centrifuged, and the supernatant and pellet were loaded onto SDS-PAGE in duplicate. One gel was stained with Coomassie to visualize the protein distribution between the pellet and supernatant fraction. Another gel was used for Western blot analysis using Protein A antibody (Figure 4.8A and B, respectively). From this test, it was observed that both N_{LytC}-SpA and N_{LytC}-SpA' were detected in almost equal proportions in both pellet fraction and supernatant fraction (Figure 4.8B). This suggested that some of the N_{LytC} (CBD) were present in either coupled to the cell membrane or trapped in the cytoplasm, while the remainder was released from the cell by the degradation of the cell wall.

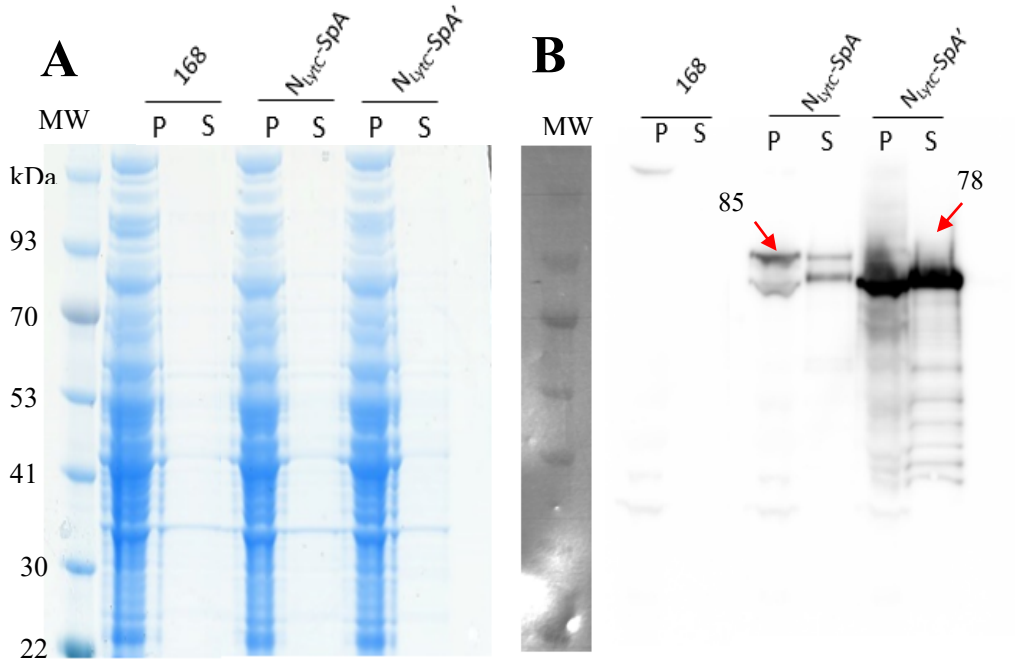

Figure 4.8 Examining the secretion of the fusion construct (N_{LytC}-SpA and N_{LytC}-SpA')

The N_{LytC}-SpA and N_{LytC}-SpA' samples were suspended in Protoplasting buffer to assess the secretion. A Coomassie stain was used to stain the gel (A) with the corresponding Western blot image (B) of the samples using Protein A antibody. Samples generated from a culture of strain 168*lacI* were used as a negative control. The molecular weight marker (kDa) is indicated by MW, and the red arrow indicates the expected size N_{LytC}-SpA and N_{LytC}-SpA'. (P) represents the pellet, and (S) represents the supernatant.

4.2.3.1 "Pull-down" identification of interacting proteins:

A pull-down assay is a technique used to study protein-protein interactions using antibodies to capture or pull down the target protein and potentially anything bound to it. In

the case of the $N_{LytC,}$ the pull-down assay specifically used the N_{LytC}-SpA' construct for two reasons. Firstly, the fusion protein N_{LytC}-SpA' was found to be more abundant than N_{LytC}-SpA. The second reason was that the full-length construct fusion N_{LytC}-SpA contains the LysM and LPXTG sequences from protein A. Therefore, it was possible that the LysM domain in the protein A can be recognized and interact with the *B. subtilis* cell wall, considering that many cell wall associated proteins in *B. subtilis* possess the LysM domain.

Following the method in Section 2.6.2, the initial step of the pull-down assay is to develop a way to capture the protein of interest onto some sort of separable material. In this case, agarose beads were the matrix of choice onto which either the protein A antibody or LytC-antiserum were coupled. The antibody-bound beads with the appropriately coupled antibodies were then incubated with the supernatant of N_{LytC}-SpA*'* and *ΔlytC* (as a negative control). During the incubation, the antibodies should selectively capture the N-terminal region of the LytC that was fused to protein A. The beads were washed twice and then eluted using glycine-HCl. The abundance of the eluted proteins was assessed using SDS-PAGE and Western blot analysis before sending the samples for mass spectrometry analysis. LytC-antiserum and Protein A antibody were utilised for the Western blot analysis, as shown in Figure 4.9A and B, respectively. For this analysis, the efficiency of the pull-down with both antisera was sufficient for mass spectrometry analysis using the beads and protein eluted from the beads (Figure 4.9A and B).

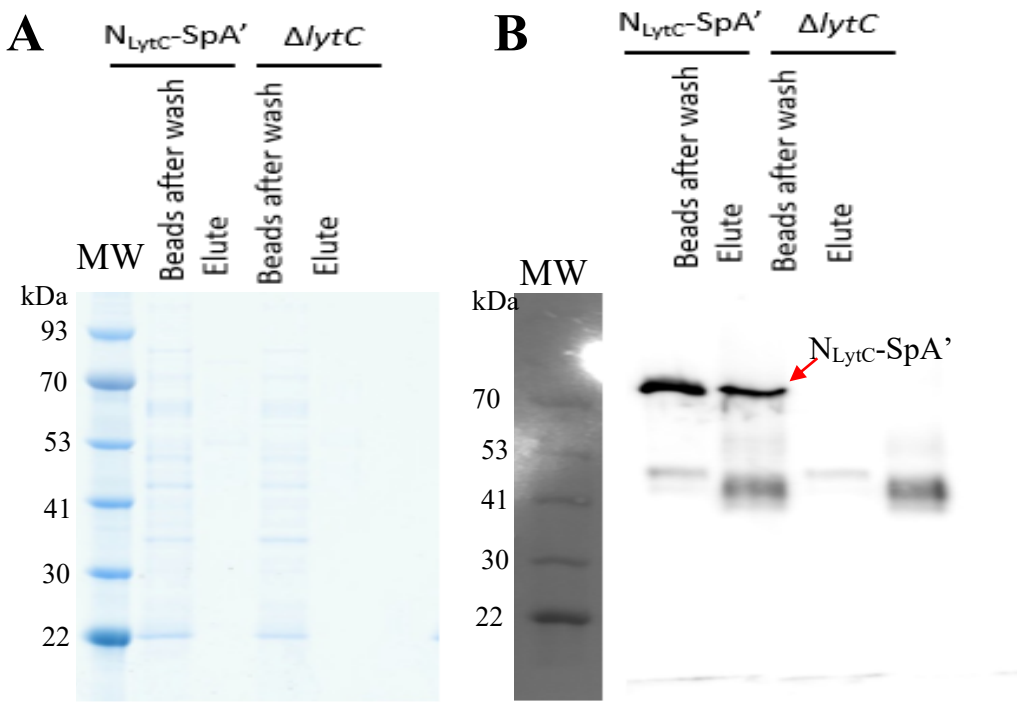

LytC antisera- bound beads/ LytC-Antisera detection

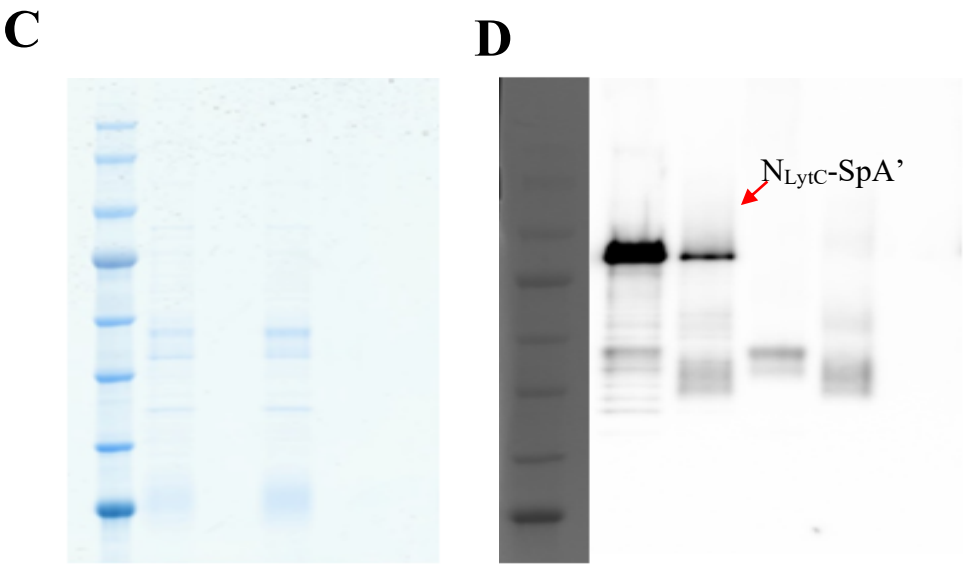

Protein A bound beads/ Protein A antibody detection

Figure 4.9 Pull-down assay using LytC-antisera- bound beads and protein A antibody- bound beads

Protein A antibody-bound beads and LytC-antisera -bound beads were incubated separately with the N_{LytC}-SpA' or Δ*lytC* samples for one hour at 4°C. After the incubation, the samples were washed with PBS. The samples were then eluted in glycine-HCl, and 20 µl of the eluted samples were taken and mixed with 20 µl SDS-loading buffer. (A and C) loading control. (B and D) Western blot analysis using LytC-antisera and protein A antibody, respectively. The molecular weight marker (kDa) is indicated by MW. The red arrow indicates the expected size of N_{LytC}-SpA'.

4.2.3.2 Mass spectrometry analysis

In order to identify proteins that interact with the N-terminal region of the LytC, several processing and analytical steps were undertaken by the mass spectrometry team to assess the differences between the pull-down samples (described in Appendix 2. Mass spectrometry analysis). The primary objective was to identify the protein that was present in N_{LytC}-SpA' strain and absent in the strain lacking *lytC*. Unfortunately, at the time this work was done, the facility of the mass spectrometry department was only able to operate peptide analysis, and consequently, all of the analytical work was specifically focused on potential protein-protein interactions described in Appendix 3.

The mass spec department analysed the samples using the Perseus software package (version 1.6.15.0, https://maxquant.net/perseus/). The abundance of LytC in all samples was determined to serve as a reference for identifying proteins that were present at a similar level to LytC but absent in the mutant strains using LytC-antiserum bound beads and protein A antibody bound beads (Anti-protein A and Anti-LytC, respectively) (Figure 4.10A). Among the samples, it was observed that LytC exhibited a high level in the N_{lytC}-*spA'* 168*lacI*, while the others showed lower levels. Subsequently, the focus shifted to identifying proteins that were present in high quality in the N_{lytC}-*spA'* 168*lacI* but were low or absent in the samples with mutant *lytC.* Three proteins, namely XkdG, XkdK, and XkdM, along with LytC, appeared to be present in high abundance (Figure 4.10B). The XkdG, XkdK, and XkdM are proteins encoded by the PBSX prophage, however their subcellular function and localization have yet to be fully elucidated (McDonnell *et al*., 1994; Wood *et al*., 1990).

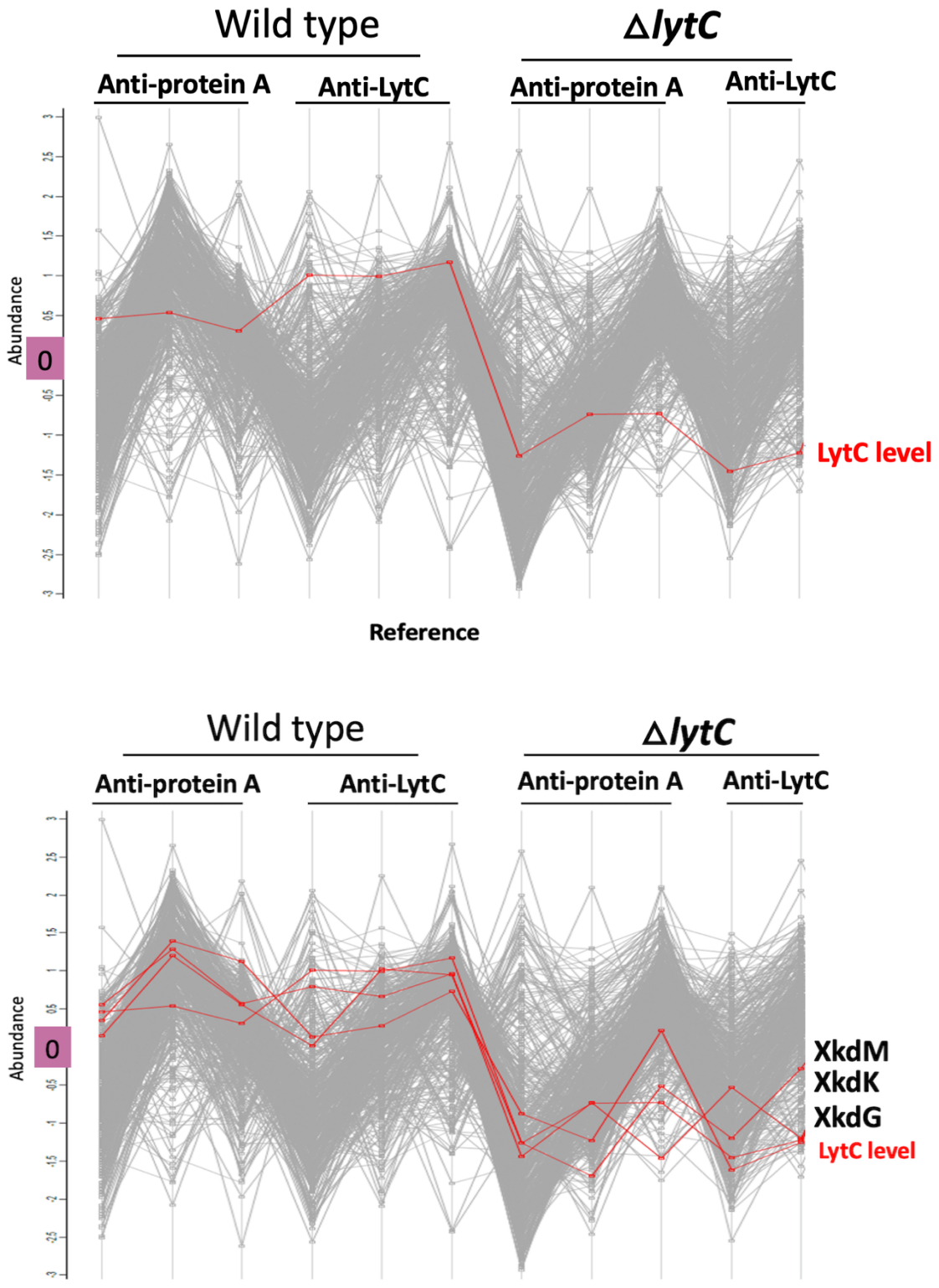

Figure 4.10 The mass spectrometry analysis to assess protein interaction

The Perseus software was used to determine the abundance of LytC fusion construction together with the protein that interacts with the LytC. (A) LytC abundance in the N_{LytC}-SpA*' 168lacI* and Δ*lytC* samples (three replicates) that were used as a reference. (B) XkdG, XkdK, and XkdM abundance were similar to the LytC.

4.2.4 Characterisation of N_{LytE} fusion to protein A (SpA)

For the N-terminus LytE (N_{LytE}), the transformations of the constructed plasmid containing the fusion with either SpA or SpA' (pAM036 and pAM037, respectively) into 168*lacI* (sAG1333) were repeated multiple times due to the plasmids integrating into the genome. After screening multiple transformants, a strain was isolated where the fusion constructs were correctly present in the *B. subtilis* strain. The expression of N_{LytE}-SpA and N_{LytE}-SpA' in 168*lacI* (sAM007 and sAM008, respectively) was assessed before and after induction by Western blot analysis with LytE-antiserum and Protein A antibody. The loading control was utilised to confirm that the samples loading was normalized and consistent (Figure 4.11A). Prior to induction, leaky expression of N_{LytE}-SpA and N_{LytE}-SpA' was observed with both antibodies (Figure 4.11B and C lane T0). However, for N_{LytE}-SpA the expression seems to be elevated 15 minutes after being induced with IPTG. The N_{LytE} fused to the full-length SpA resulted in a reduction in the degradation of SpA compared to Figure 4.5. This result indicates that the N-terminus LytE fusion to either the full-length protein A or protein A lacking the LysM and LPXTG can be expressed in *B. subtilis*. However, there is clear evidence that the protein is subject to specific proteolysis, resulting in a ~50 kDa fragment that is detected by the LytE-antiserum but not the protein A antibody. It was also evident that the gene fusions were expressed in the absence of IPTG, although induction did seem to result in a moderate increase in the level of expression for the N_{LytE}-SpA fusion. Nevertheless, the plasmid encoding N_{LytE}-SpA' was potentially integrating into the *lytE* gene, as indicated by the fact that the level of native LytE increased in the presence of IPTG. Transformation of the construction into a strain deleted of the *lytE* gene proved to be problematic as well. However, as the fusion proteins were being expressed, further analysis was done using this initial strain construct.

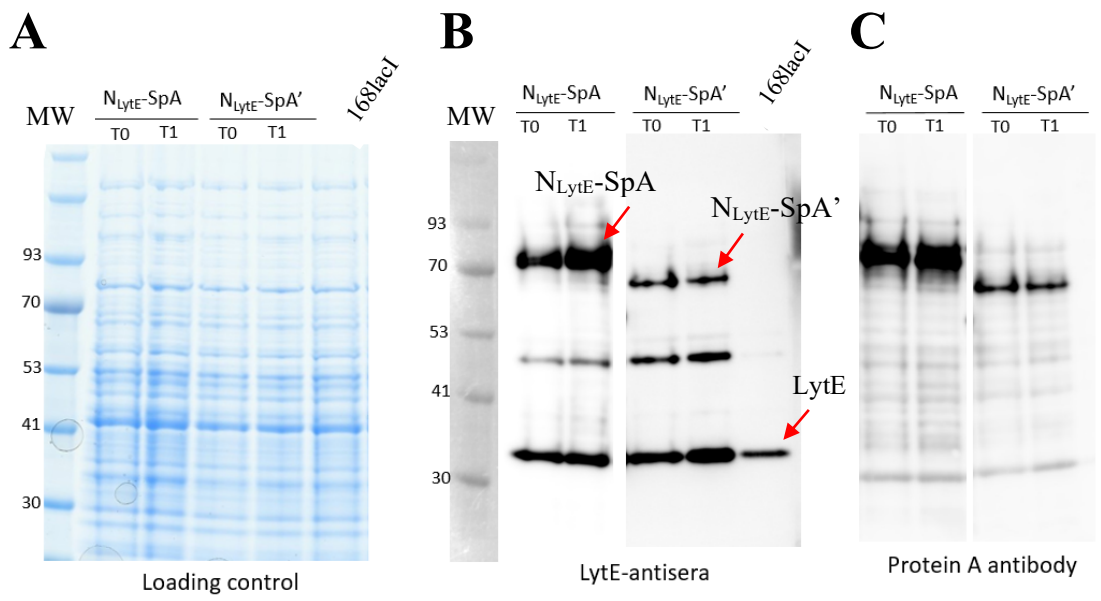

Figure 4.11 Analysis the expression of N_{LytE}-SpA and N_{LytE}-SpA'

Sample of N_{LytE}-SpA and N_{LytE}-SpA' were collected at two time points: before adding IPTG (T0),15 minutes after induction with IPTG (T1). (A) The loading control of N_{LytE}-SpA and N_{LytE}-SpA' using Coomassie. Western blot analysis was performed to assess the expression N_{LytE}-SpA and N_{LytE}-SpA' using protein A antibody (B) and LytE-antiserum (C). The 168*lcaI* was used as a control for LytE. The molecular weight marker (kDa) is indicated by MW, and the red arrow indicates the predicated molecular weight of N_{LytE}-SpA (76 kDa), N_{LytE}-SpA' (64 kDa), and the native LytE (37 kDa).

The next step was to assess whether the fusion proteins (N_{LytE}-SpA and N_{LytE}-SpA') were secreted into the culture media, associated with the cell wall, or trapped in the cytoplasm. Here, the methodology used for N_{LytC} fused to the SpA was also used for N_{LytE}-SpA and N_{LytE}-SpA'. Samples of cells expressing the fusions were treated with lysozyme in an isotonic buffer (Protoplasting Buffer- Appendix 1-Buffer components) to prevent cell lysis. The protoplasts and the supernatant were separated by SDS-PAGE in duplicated. One gel was stained with Coomassie, and the other was used for Western blot analysis using the Protein A antibody. The gel stained with Coomassie was conducted to visualize the pellet and supernatant fraction (Figure 4.12A). The Western blot analysis revealed that both fusion constructs were clearly present in the pellet fraction. However, in the case of N_{LytE}-SpA, a light band was observed in the supernatant (Figure 4.12B). This observation raised two questions: whether LytE interacts with the cell membrane or whether the C-terminal region is required for LytE secretion.

Since it was apparent that the N_{LytE} fusions were being retained on the cells, two possibilities existed either the LytE binding domain was causing the fusion protein to be retained on the cell surface, perhaps through an interaction with the membrane lipoteichoic acids (LTA) or the fusion proteins were poorly secreted and hence were inside the cells. To test the first possibility, a strain was constructed (strain sAM015) which was deleted for the main LTA synthases, *ltaS yfnI,* and so would not have LTA as previously published by (Guyet *et al*., 2023), and the N_{LytE}-SpA' expression plasmid was transformed into this background (as control the plasmid encoding the N_{LytC}-SpA' fusion was transformed into Δ*ltaS* Δ*yfnI*). Both strains, N_{LytE}-SpA' Δ*ltaS* Δ*yfnI* and N_{LytC}-SpA' Δ*ltaS* Δ*yfnI* were grown in LB media until they reached the mid-exponential phase. Cells were then harvested, and the cell wall removed, as previously described, and the samples centrifuged to gain the pellet and supernatant fractions. These samples were then separated on SDS-PAGE for Western blot analysis using the protein A antibody to determine the abundance of the protein. Analysis of the resulting blot (Figure 4.13A and B) showed that the N_{LytE}-SpA' again predominantly remained in the pellet fraction even in the absence of the LTA. Whereas the N_{LytC} construct previously analysed was present in both the pellet and supernatant fraction (Figure 4.13A and B).

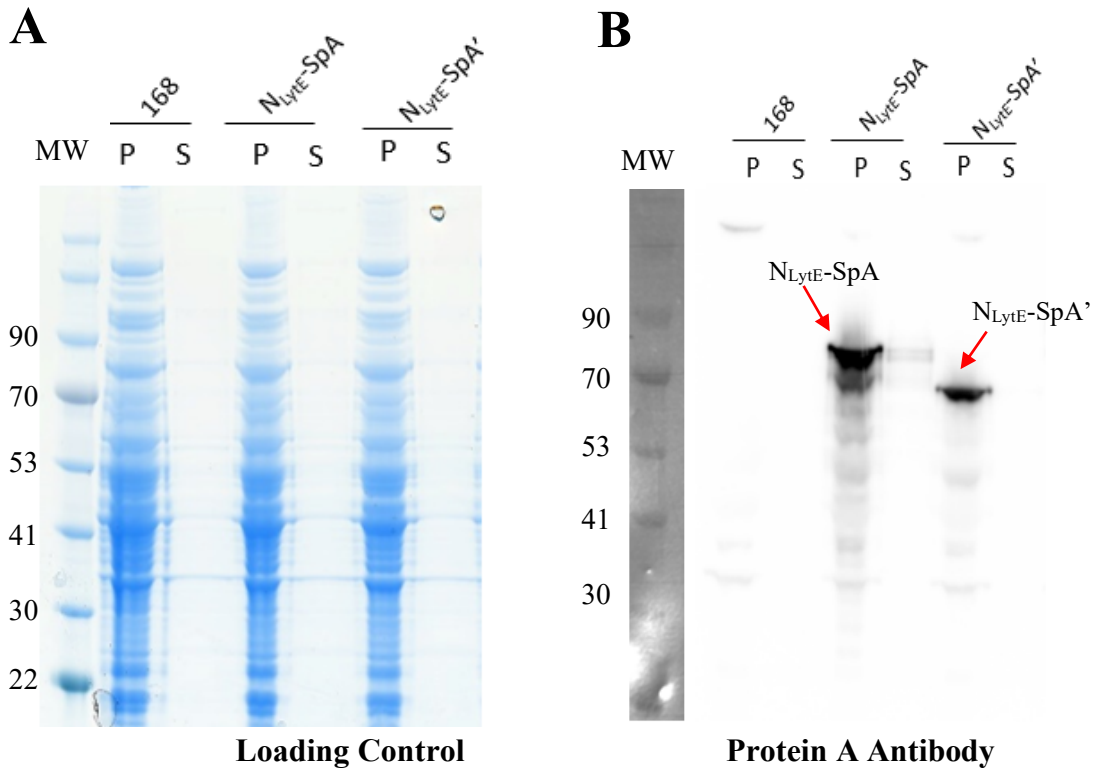

Figure 4.12 Examining the secretion of N_{LytE}-SpA and N_{LytE}-SpA'

Sample of N_{LytE}-SpA and N_{LytE}-SpA' were suspended in Protoplasting buffer to assess their secretion. (A) Coomassie staining was used as a loading control. (A) Western blot analysis using Protein A antibody. The molecular weight marker (kDa) is indicated by MW, and the red arrow indicates the expected size of N_{LytE}-SpA (76 kDa) and N_{LytE}-SpA' (64 kDa). (P) represents the pellet, and (S) represents the supernatant.

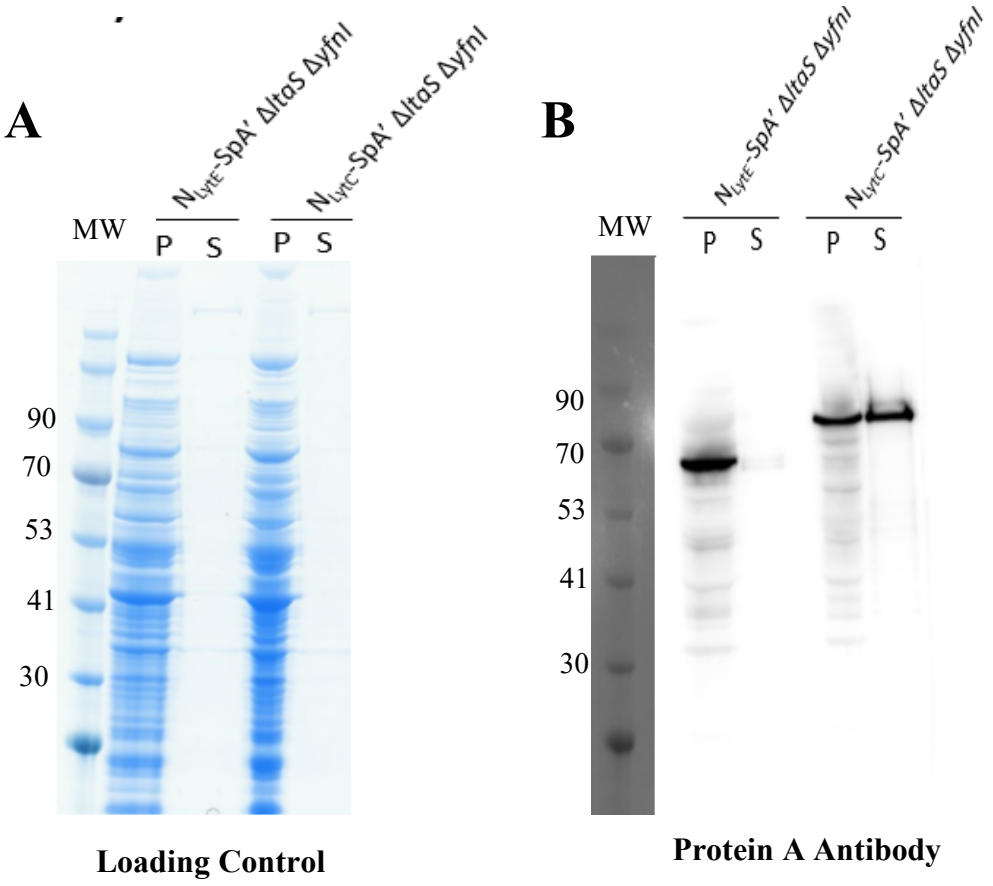

Figure 4.13 Analysis the secretion of the fusion construct N_{LytE}-SpA' in Δ*ltaS* Δ*yfnI* background

The samples of N_{LytE}-SpA' and N_{LytC}-SpA' in strain lacking Δ*ltaS* Δ*yfnI* were suspended in Protoplasting buffer to assess the secretion of LytE. Panel A shows an image of the stained gel to act as a loading control. Panel B shows the corresponding Western blot analysis of (A) using Protein A antibody. N_{LytC}-SpA' was using as a control. The molecular weight marker (kDa) is indicated by MW, (P) represents the pellet, and (S) represents the supernatant.

These results indicated that N_{LytE}-SpA*'* was not being secreted and remained in the cytosol. A simple protease resistance was done to test secretion of the fusion protein. The concept behind this is that proteinase resistance will be dependent upon the location of the protein relative to the cytoplasmic membrane. If the N_{LytE}-SpA' is secreted out of the cell it would be degraded by the proteinase K. On the other hand, if the N_{LytE}-SpA' is in the cytosol, it will be protected. For the test, the strain carrying the N_{LytE}-SpA*'* fusion in the 168*lacI* background (strain sAM008) was grown in LB media until reaching the mid-exponential phase, and then 1 mM IPTG was added to ensure expression, and the culture incubated for 40 minutes. The cells were then harvested and suspended in the Protoplasting buffer to degrade the cell wall and obtain the protoplasts. Proteinase K was then added to degrade the proteins outside of the cell. Different concentrations (0.2, 0,1, 0.05, and 0.02 mg/ml) of proteinase K were used because the excessive activity of proteinase K leads to destabilisation of the protoplasts. Tween was then added to one sample, and incubation continued for 5 minutes as a control where disruption of the protoplast would occur and confirm that the protein of interest can be degraded. Samples treated with proteinase K were incubated for 5 and 10 minutes prior to the SDS-loading buffer with protease inhibitor being added and the material sonicated, followed by the proteins being resolved using SDS-PAGE. One gel was stained with Coomassie to assess the general effect of the protease (Figure 4.14A). Another gel was used for Western blot analysis using antibodies against PBP2B and FtsZ. FtsZ is a cytosolic protein that should not be degraded and act as a control for the stability of the protoplasts in the experiment. In contrast, PBP2B, a membrane protein with its major domain outside the cell will be degraded. The results showed that the PBP2B was degraded in all proteinase K concentrations, whereas FtsZ was degraded at 0.1 mg/ml and 0.2 mg/ml. Under Tween conditions, it was clear that all proteins were significantly degraded, indicating that the protease addition had destabilised the protoplasts. The N_{LytE}-SpA*'* was not significantly degraded at any of the proteinase K concentrations except where tween was added, indicating that the constructed fusion was probably present in the cytosol or in some other way protected from the protease and detergent interferes with this protection (Figure 4.14B).

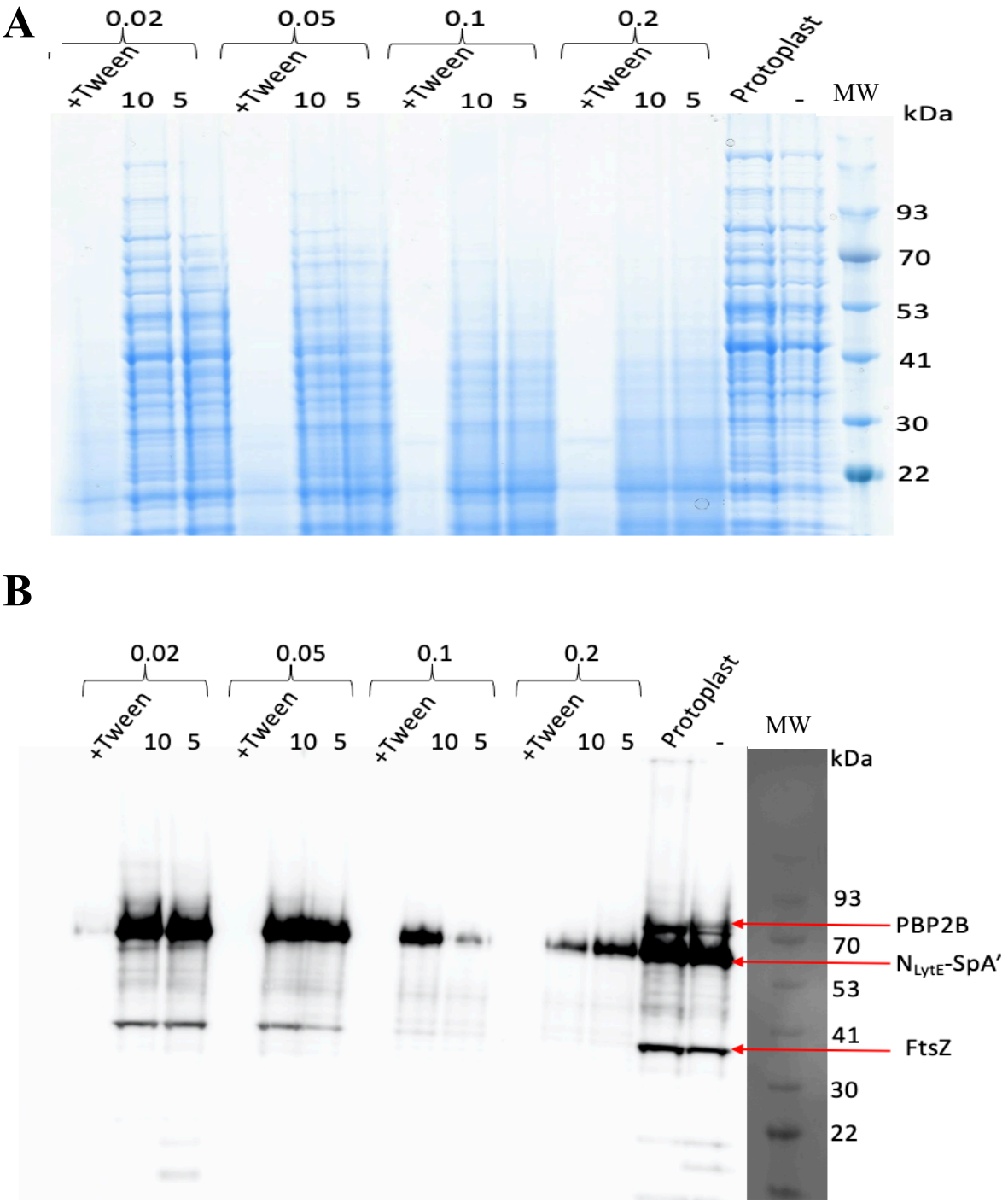

Figure 4.14 Assessing the secretion of N_{LytE}-SpA' using proteinase K

The N_{LytE}-SpA' protoplast was treated with different concentrations of proteinase K (0.2, 0.1, 0.05, and 0.02 mg/ml) for 5 to 10 minutes. Tween was then added for an additional 5 minutes. The treated samples were then resolved using SDS-PAGE for Coomassie staining (A), as well as Western blot analysis (B). The PBP2B and FtsZ antibodies were used (1/10,000, 1/10,000, and 1/2500, respectively). The (-) indicated the total cells before lysis, the protoplast lane indicated cells after lysis and being. The molecular weight marker (kDa) is indicated by MW.

4.2.5 Characterise the secretion of the native LytE

To further investigate the issues with the secretion of the N_{LytE} fusions, the properties of native LytE were characterised in comparison to a combination of overexpression of *lytE* (sAM021) and C-terminal truncations of the *lytE* (sAM022). For this, protoplast experiments were used, similar to those done for the tag fusions, and the relative abundance of LytE was assessed by Western blot using LytE-antiserum (Figure 4.15). In the wild type (168CA), the majority of LytE was found to be present in the supernatant on degradation of the cell wall and hence it seems to be exported efficiently (Figure 4.15A indicated by the red arrow). The 168CA sample was low due to the dilutions that occurred during the experiments. If the *lytE* was ectopically expressed under control of the IPTG-inducible promoter, it was found that LytE was mostly present in the pellet fraction and a light band appeared in the supernatant (Figure 4.15B). The truncated form of *lytE* was clearly observed in the pellet fraction (Figure 4.15C). This finding suggested that ectopically expressed LytE becomes trapped in the cell when artificially expressed. Although, it would also seem that the C-terminal domain of the protein may have a role in efficient secretion, as it does seem to accumulate in the protoplasts.

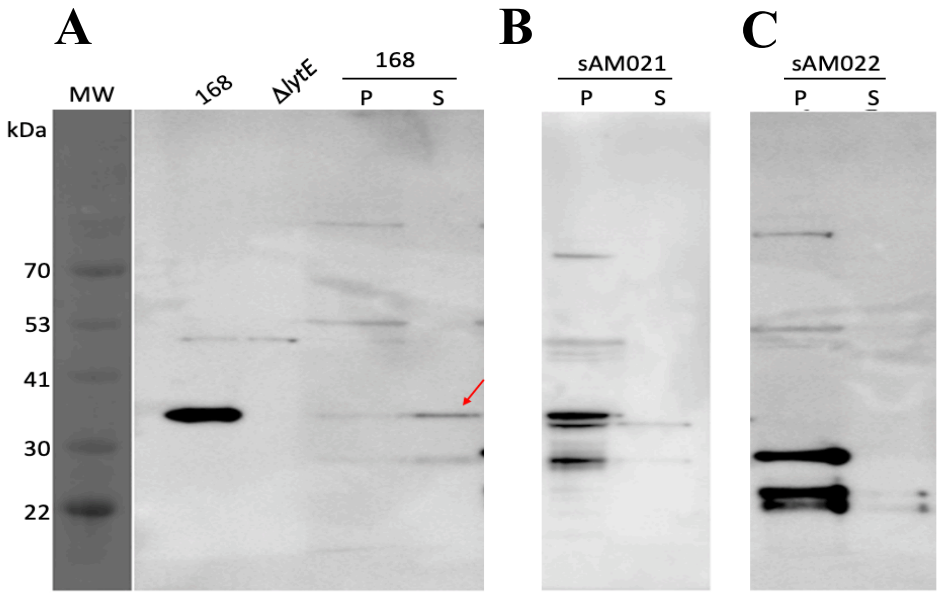

Figure 4.15 Assessing the secretion of native LytE and the truncated LytE'

The secretion of the LytE protein was assessed by Western blot analysis using LytE-antiserum in three strains: (A) Full-length native *lytE* in the 168CA, (B) inducible *lytE* in Δ*lytE* (sAM021), and (C) truncated *lytE'* (sAM022). The 168CA and Δ*lytE* were used as positive and negative controls, respectively. The molecular weight marker (kDa) is indicated by MW, and the red arrow indicates the majority of size LytE in supernatant in 168CA. (P) represents the pellet, and (S) represents the supernatant.

4.2.6 Chimeric genes characterisations

4.2.6.1 Comparison of the key autolysins by amino acid sequence alignment

In parallel with the above experiments, a second approach was used to determine if the LytE, LytF, and CwlO have identical catalytic activities and that the N-terminal regions provided their unique properties. As a starting point, the linear amino acid sequences of these proteins were aligned against each other using Clustal Omega (http://www.clustal.org). The alignment is shown in Figure 4.16, with the N-terminal transmembrane sequence, which would be cleaved on secretion indicated in red colour, and the LysM domains that are highlighted in pink.

In so doing, the C-terminal catalytic domains of the LytE, LytF, and CwlO clearly show significant similarity, as has previously been indicated by Kunst *et al*., 1997 and in Section 4.1.2, with them being assigned to the NlpC/P60 family in the Pfam database. By contrast, the N-terminal regions differ significantly. However, for the LytE and LytF the LysM domains are indicated as being common elements, but the number of repeats of this domain differs. One feature that did stand out from this comparison was the presence of stretches of poly-serine, which seemed to be a boundary between domains. As such, this appeared to provide a potential region where domain-swaps could be made. This would permit the construction of chimeric proteins that, in theory, should have minimal disruption of the domain structure. This also seems to be supported by the predicted 3D structure of these proteins generated by AlphaFold (Table 4.1). Constructing these chimeric proteins and determining if they are functionally capable to complement null mutations for any of the native autolytic proteins would be a simple test to show if the catalytic C-terminal domain are biochemically redundant. On the basis that CwlO is regulated by a complex interaction with the FtsEX protein, that mediates structural rearrangement of the protein to expose the active site (Brunet *et al*., 2019b; Meisner *et al*., 2013). Here, the focused was on using the catalytic domain of CwlO in the constructs as it has been shown that this domain alone is catalytically active in the absence of the N-terminal domain (Hashimoto *et al*., 2012).

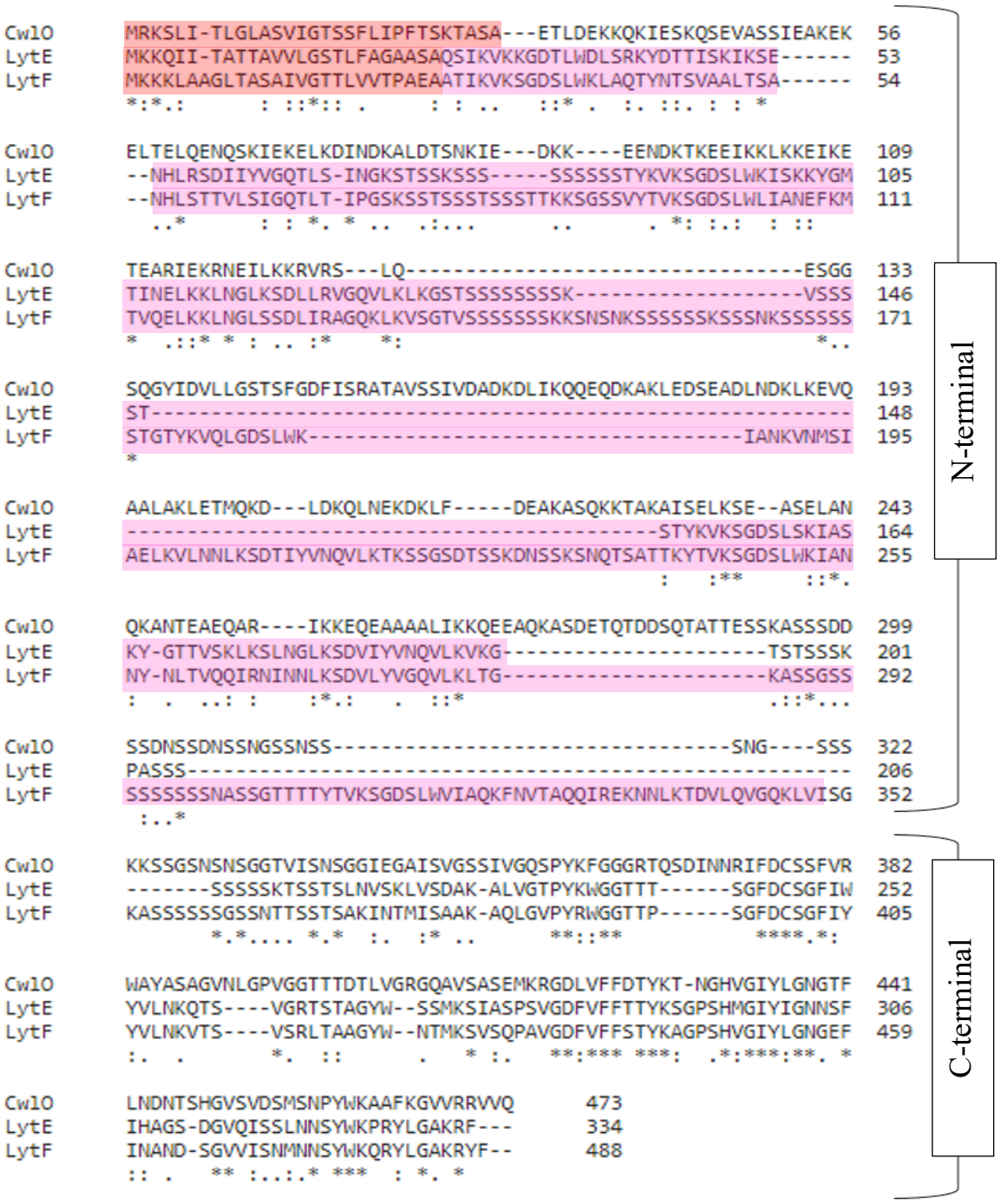

Figure 4.16 The sequence alignment of CwlO, LytE, and LytF

The alignment was generated by Clustal Omega. The * indicate the identical residues, : indicate the similar residues,. indicates different residues. The red highlighted indicates the signal sequence. The pink highlighted indicated the LysM domain.

4.2.6.2 Chimeric genes constructed

Using the alignment of LytE, LytF, and CwlO (Figure 4.16) as a guide, a set of chimeric coding genes was constructed by fusing the coding sequences for N-terminus (LysM repeats) of either LytE or LytF to the catalytic domain of the CwlO in a way that could be cloned into pDR111 vector. The chimeric genes were generated initially by constructing full-length *lytE* or *lytF* under the control of an IPTG promoter using a pDR111 plasmid (cloning described in method in Section 2.8.4). The C-terminal region of either LytE or LytF was then swapped for the C-terminal region of CwlO using PCR combined with the action of HiFi DNA Assembly. Consequently, $N_{lytE}C_{cwlO}$ and $N_{lytF}C_{cwlO}$ were placed under the control of an IPTG inducible promoter to give plasmids pAM043 and pAM044, respectively, and then transformed into the Δ*lytE*, Δ*lytE* Δ*lytF*, and Δ*cwlO* mutants (discussed later). PCR was initially used to confirm that the hybrid genes were at the expected size in different backgrounds (Figure 4.17), and sequencing analyses of the plasmids validated the accuracy of the construct.

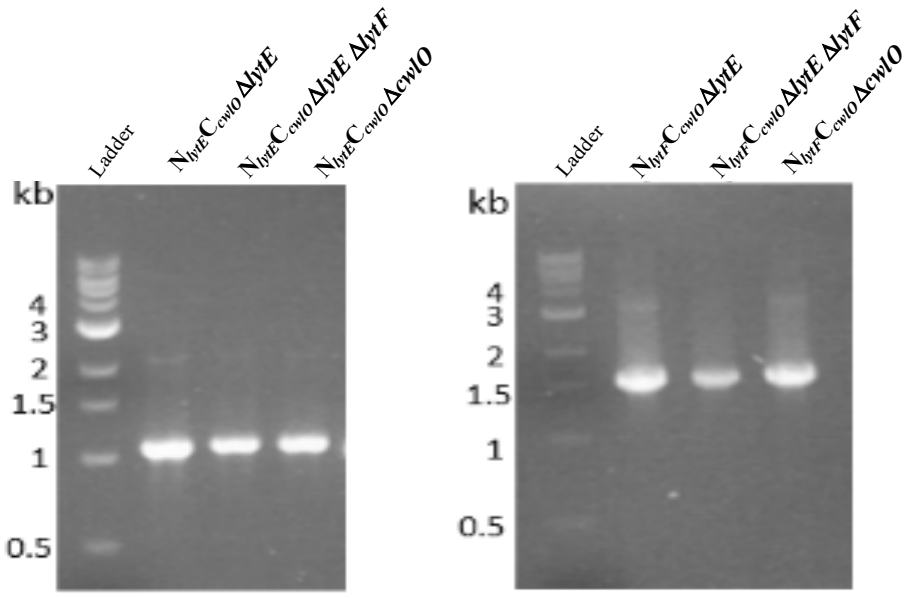

Figure 4.17 PCR analysis to confirm the hybrid genes constructs

The hybrid genes constructs were generated using HiFi DNA Assembly and confirmed by PCR in different genetic backgrounds. For the $N_{LytE}C_{CwlO}$ construct, LytE-F (oAM081) used as a forward primer and CwlO-R (oAM086) used as a reverse primer, while for the $N_{LytF}C_{cwlO}$, we used LytF-F (oAM083) as a forward primer and CwlO-R as a reverse primer. The expected size of $N_{lytE}C_{cwlO}$ is 1076 bp, and $N_{lytF}C_{cwlO}$ is 1535 bp.

4.2.6.3 Complementation of *lytE cwlO* double mutant by chimeric protein

As a quick way to assess whether the chimeric genes $N_{lytE}C_{cwlO}$ and $N_{lytF}C_{cwlO}$ were functional and could act as suppressors of synthetic lethality of double mutant *lytE cwlO*, the strain AG547 (Δ*lytE::cat)* was used, to introduce the hybrid genes $N_{lytE}C_{cwlO}$ or $N_{lytF}C_{cwlO}$. The Δ*cwlO::kan* mutant strain was then introduced into $N_{lytE}C_{cwlO}$ Δ*lytE* and $N_{lytF}C_{cwlO}$ Δl*ytE*, selecting for kanamycin resistance in the presence of IPTG (to allow expression of the chimeric gene). The flowchart diagram illustrates the expected consequences of generating a Δ*lytE* Δ*cwlO* strain with a chimeric construct that may or may not complement the lethal mutation combination (Figure 4.18B). Patching the transformants onto chloramphenicol and kanamycin plates supplemented with IPTG provided a way to check the markers present and determine viability. Separately, the inducible full-length *lytE* construct (sAM021) was tested and found to complement the double mutant as would be expected (data not shown), indicating that the construction had the potential to express the gene sufficiently. On doing the transformation for both constructions ($N_{lytE}C_{cwlO}$ Δ*lytE* Δ*cwlO* and $N_{lytF}C_{cwlO}$ Δ*lytE* Δ*cwlO*) only a small number of colonies were obtained. Upon verification, all colonies had lost chloramphenicol resistance (Δ*lytE::cat*) (Figure 4.18B). Based on this result, neither of the chimeric genes $N_{lytE}C_{cwlO}$ nor $N_{lytF}C_{cwlO}$ were able to suppress the lethality of the *lytE cwlO* double mutations, suggesting that they were either not expressed sufficiently or non-functional.

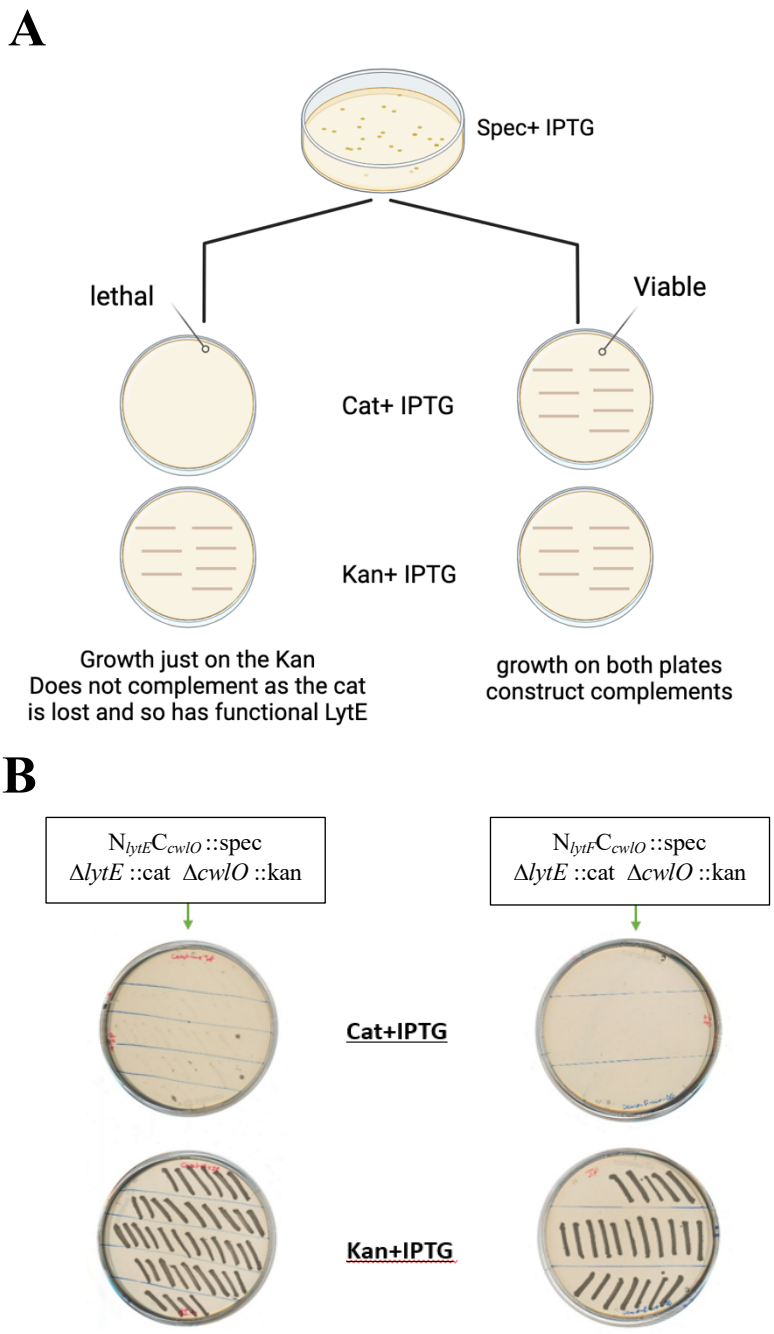

Figure 4.18 Chimeric genes role in suppressor the synthetic lethality

$N_{lytE}C_{cwlO}$ and $N_{lytF}C_{cwlO}$ were transformed individually into Δ*lytE* (cat), and then the Δ*cwlO* (kan) was introduced to check if the chimeric genes could suppress the synthetic lethality. (A) A flowchart indicating the expected transformation efficiency and phenotypes. The first row represents NA plate supplemented with chloramphenicol (cat) and 1 mM IPTG for the Δ*lytE*, and the second row represents NA plates with (kanamycin) kan and 1 mM IPTG for the Δ*cwlO* strain. (B) The resulting patches of $N_{lytE}C_{cwlO}$ Δ*lytE* Δ*cwlO* and $N_{lytF}C_{cwlO}$ Δ*lytE* Δ*cwlO*. Plates were then incubated at 37°C ON.

4.2.6.4 Cell morphology of strains expressing the chimeric proteins

RYO Ohnishi (1991) and Patricia Domínguez-Cuevas (2013) have previously reported that LytE, LytF, and CwlO obviously affected cell morphology and division. As mentioned earlier, single mutant *cwlO* cells appear shorter and wider, while the *lytE lytF* double mutant cells have a chained cell morphology. Therefore, it was hypothesised that the chimeric proteins might have partial activity, and so could potentially correct or reduce the phenotypic abnormalities. To test this hypothesis, the *cwlO* null mutation was introduced into strain express $N_{lytE}C_{cwlO}$ or $N_{lytF}C_{cwlO}$. For the double mutant Δ*lytE* Δ*lytF*, the *lytF* deletion was transformed into $N_{LytE}C_{cwlO}$ Δ*lytE* and $N_{LytF}C_{cwlO}$ Δ*lytE*. The resulting strains were then grown overnight in LB media with IPTG, and the following day, the cultures were diluted in fresh LB media in the presence and absence of the IPTG until they reached the mid-exponential phase (OD_{600} ~ 0.3). Cell morphology was then examined by fluorescence microscopy after staining the cell membrane with FM5-95. In the Δ*cwlO* background, the resulting cells of $N_{LytE}C_{cwlO}$ Δ*cwlO* or $N_{LytF}C_{cwlO}$ Δ*cwlO,* both in the presence and absence of induction, were exhibiting a slightly short and wide cell phenotype, essentially identical to that of a strain with just the *cwlO* mutation (Figure 4.19A). Similarly, there was no significant difference in cell morphology seen between the strains $N_{LytE}C_{cwlO}$ Δ*lytE* Δ*lytF*, and $N_{LytF}C_{cwlO}$ Δ*lytE* Δ*lytF* and the double mutant *lytE lytF*, with all three strains presenting as chained and slightly longer cells (Figure 4.19B). Thus, there was no significant evidence that the expression of the $N_{lytE}C_{cwlO}$ and $N_{lytF}C_{cwlO}$ chimeric genes had any effect on altering cell morphology.

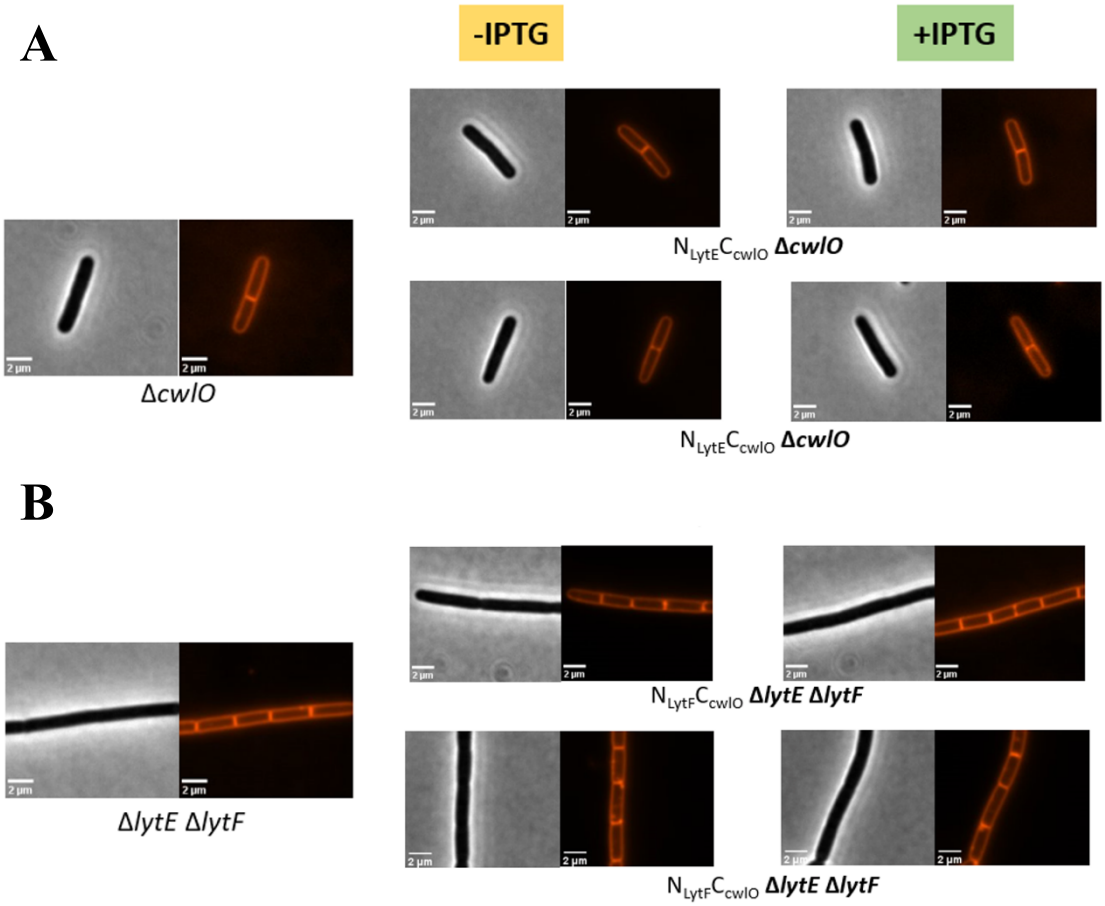

Figure 4.19 Hybrid genes morphology in Δ*lytE* Δ*lyF* and Δ*cwlO* backgrounds

The strains were grown in LB media with IPTG overnight. The follwing day, the strains were washed and diluted to an OD_{600} of 0.05 in LB media with/without IPTG until reaching an OD_{600} of 0.3. 30 µl of cells were mixed with 1µl of fluorescent dye (FM5-95) to stain the cell membrane. Fluorescent microscopy was used to capture images of the $N_{LytE}C_{cwlO}$ Δ*cwlO*, $N_{LytE}C_{cwlO}$ Δ*lytE* Δ*lytF* $N_{LytF}C_{cwlO}$ Δ*cwlO* and $N_{LytF}C_{cwlO}$ Δ*lytE* Δ*lytF* and compared to Δ*cwlO* and Δ*lytE* Δ*lytF*. A scale bar is 2 microns.

4.2.6.5 Chimeric genes expression in *lytE* or *lytF* backgrounds

The above results indicated that the chimeric genes were not enzymatically active in restoring the lethality of the double mutant *lytE cwlO* or phenotype defect of the Δ*cwlO* or Δ*lytE* Δ*lytF*, and a final check was performed to determine if the chimeric proteins were expressed. This was achieved using the antisera that were generated previously (Chapter 3). The predicted molecular weight of the chimeric construct and native proteins could potentially complicate the results. The molecular weight of LytE is 37 kDa, and the predicted molecular weight for $N_{LytE}C_{cwlO}$ was 36.8 kDa, while the LytF is 51 kDa, and $N_{LytF}C_{cwlO}$ was predicted to be 52 kDa.

Thus, strains were constructed in which either *lytE* or *lytF* were deleted and carried the chimeric proteins to permit Western blot analysis. This permitted the use of LytE or LytF

specific antisera without the potential complications of detecting the native protein and/or degradation products. The constructed strains $N_{LytE}C_{cwlO}$ Δ*lytE,* $N_{LytE}C_{cwlO}$ Δ*lytE* Δ*lytF,* $N_{LytF}C_{cwlO}$ Δ*lytF,* and $N_{LytF}C_{cwlO}$ Δ*lytE* Δ*lytF* were grown in LB media until they reached the exponential phase OD_{600} ~ 0.4. At this point, 1 mM of the IPTG was added to induce the chimeric gene constructs and incubation continued for 40 minutes prior to collecting samples. As controls, samples for strains 168CA, Δ*lytE,* Δ*lytF*, and Δ*lytE* Δ*lytF* were generated under the same conditions. From the Western blot analysis (Figure 4.20), it was observed that there were potential degradation products of the $N_{LytE}C_{cwlO}$ in both Δ*lytE* or Δ*lytE* Δ*lytF* backgrounds (Figure 4.20A and B). Whereas for $N_{LytF}C_{cwlO}$ Δl*ytF*, a band was detected after induction with IPTG, however, this band was around 70 kDa, which did not correspond to the expected size of the $N_{LytF}C_{cwlO}$. This observation occurred only after the induction of the hybrid genes but was also evident in the strain $N_{LytF}C_{cwlO}$ Δ*lytE*Δ*lytF*, suggesting that it was specific for the chimeric construction. These results indicate that the chimeric gene constructions were expressed, and at least $N_{LytE}C_{CwlO}$ was produced at the expected molecular weight. Hence, it had to be concluded that the catalytic domain of CwlO was not functional *in vivo* when fused with the N-terminal domains of the other autolytic genes.

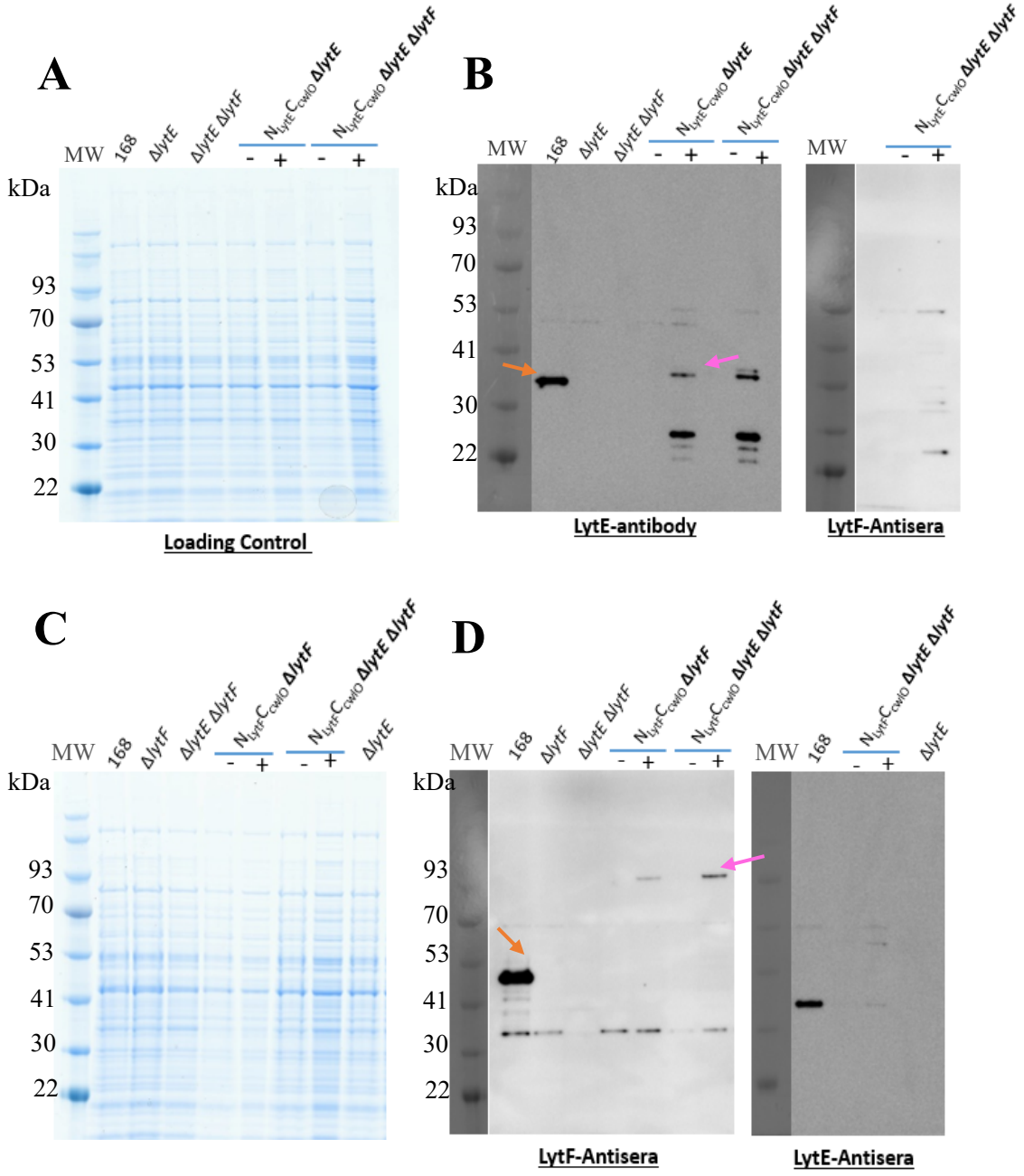

Figure 4.20 $N_{LytE}C_{cwlO}$ and $N_{LytF}C_{cwlO}$ expression in Δ*lytE* and Δ*lytE* Δ*lytF*

The strains were grown overnight in LB media at 30°C. Following the overnight culture, the cells were diluted to an OD_{600} of 0.05 in fresh LB media and incubated at 37°C until they reached the mid-exponential phase. 1 ml of the sample was harvested, and 1 mM of the IPTG was added to the culture for 40 minutes. (A and C) SDS-PAGE was stained with Coomassie and used a loading control. (B) Western blot analysis was carried out using LytE-antiserum to detect the $N_{LytE}C_{cwlO}$ in Δ*lytE* and Δ*lytE*Δ*lytF*. (D) The $N_{LytF}C_{cwlO}$ in Δ*lytF* and Δ*lytE* Δ*lytF* was detected using LytF-antiserum. The 168CA served as a positive control, while the mutant Δ*lytE*, Δ*lytF* and Δ*lytE* Δ*lytF* served as a negative control. MW represents the molecular weight. The molecular weight of native LytE is (37 kDa) and LytF is (51 kDa),. The molecular weight of $N_{LytE}C_{cwlO}$ is 36 kDa and the $N_{LytF}C_{cwlO}$ is 52 kDa. The orange arrow indicates the band detected by LytE-antiserum, while the pink arrow indicates the band that was detected by LytF-antiserum.

4.3 Discussion

In *B. subtilis*, the expression of the cell wall lytic enzymes LytC, LytE, LytF, and CwlO are required for normal growth and morphology. The AlphaFold predicted structure of these enzymes, as shown in Table 4.1 provides a way to visualize the structures in a manner that clearly demonstrates the variations in the domain structures and the similarity of the catalytic portions of the protein. The initial focus of this chapter was to determine the functional roles of the proposed carbohydrate-binding domains in relation to the function of enzymes. As a starting point, LytC and LytE were chosen as previous research had indicated that they clearly are involved in different processes and were expected to localise to different regions at the cell wall (R. Chen *et al*., 2009; Kasahara *et al*., 2016a; Uelze, 2022; Yamamoto *et al*., 2003a). This localisation was presumably mediated by the N-terminal portion of these proteins proposed to bind to the cell envelope in some way. Previously, an epitope-tagging method in which a 3xFLAG polypeptide was used to determine the localization of LytE and LytC (Yamamoto *et al*., 2003). Thus, in this study the primary objective was to determine if using synthetic tags fused to LytE and LytC would provide a way to determine both the subcellular localisation of the protein and what it was physically binding to. Initial work attempted to use the Halo-tag for this purpose, but although the genetic construct could be generated, no evidence of any expression was obtained (Figure 4.2). It is still very unclear what technical issue prevented the functional expression of these protein fusions, but as it was clearly not a viable approach, an alternate method using Protein A (SpA) from *S. aureus* was devised.

The SpA protein was suitable for the proposed analyses as it is a protein that is known to be secreted and has the ability to interact with antibodies in a way that permits the native protein (LytE and LytC) to be “pulled out” of complex mixtures relatively specifically. However, the properties of SpA protein were not ideal, the major problem being that the C-terminal portion of the protein has motifs that potentially mediate its association with the bacterial cell wall (O’Halloran *et al.*, 2015). The first is a well-characterised small sequence, often referred to as LPXTG recognized by the sortase system, and results in covalent attachment to the cell wall in *S. aureus*. The second is a single LysM motif, not dissimilar to those known to be present in two of the proteins in this study (LytE and LytF), although multiple LysM motifs are present in these *Bacillus* proteins (O'Halloran, Wynne, & Geoghegan, 2015; Becker, Frankel, Schneewind, & Missiakas, 2014). From this work, it was observed that the full-length SpA was subject to degradation, whereas the truncated SpA (SpA’) was more stable. The obvious conclusion here was that the stability of the SpA

protein was altered by removal of the C-terminus, and this provide an indication that the LysM and potentially the LPXTG motif contribute to cell wall association. Furthermore, the LysM and LPXTG motifs of SpA were retained in the cell wall of *B. subtilis* in a way that increased the probability of proteolytic degradation (Figure 4.5B). Based on these data, the analysis progressed in an attempt to determine what the CBD domain of LytC and LytE is bound to, as subcellular localization of these is mediated by their CBD domain (Yamamoto *et al*., 2003b).

From the analysis of the LytC-related constructs, it was clear that this fusion was expressed and remained in the cell wall of *B. subtilis*. Unfortunately, due to time and some degree the technical limitations of the mass spectrometry facility, it was only possible to look at proteomic data. The results indicate that LytC may be associated with a set of uncharacterised secreted bacteriophage proteins XkdG, XkdK, and XkdM. Since these were the most significant pull-down proteins, it is tempting to think that they may be localised to the poles of the cell, as the bacteriophage in *B. subtilis* has been found contact the cell at the polar region . These proteins might be indirectly pulled down with the LytC (CBD fusion), which known to be distributed throughout the entire cell wall (Jakutytė *et al*., 2011; Yamamoto *et al*., 2003a). However, further work is needed to validate this result, as relatively little has been done to study this aspect of bacteriophage biology (Wood *et al*., 1990).

In case of the LytE-SpA', unfortunately, issues were encountered in relation to the secretion of the fusion protein. Previous report demonstrate that the LytE found outside the cytoplasmic membrane (Margot *et al*., 1998). However, our data indicated that the LysM repeats of LytE are problematic in secretion and consequently seem to become trapped in the cytoplasm of the cell (or perhaps get "stuck" in the membrane) (Figure 4.12). Various attempts to diagnose these issues and resolve the secretion problem were not very successful. This problem seems to be exacerbated by increased expression, and the protein constructions were essentially uninformative. Other work was done to further analysis the secretion efficiency of LytE (Figure 4.15) showed that the C-terminus or catalytic domain of LytE seems to play a role in ensuring effective secretion of the protein.

Previous work by Hashimoto *et al*., 2012, which examined the N-terminal region of hydrolytic enzymes belonging to the DL-endopeptidases LytE, LytF, and CwlO, reported that the N-terminal region plays a critical role in determining their subcellular localisation. In

addition, they found that the synthetic lethality of distributed *lytE cwlO* is caused by the lack of activities of the DL-endopeptidases at the lateral cell wall. Another study by Uelze, 2022 found that the transcription level of *lytE* increased and could complement the loss of *cwlO*. Furthermore, expressing *lytF* in the *cwlO* locus was able to fulfill the requirement of the DL-endopeptidase for viability in double mutant *lytE cwlO,* although with defects in cell growth and morphology – supported by the recent identification of a partial functional redundancy between LytE and LytF when CwlO function is perturbed (A. Aljohani (PhD thesis)). Based on this data, the hypothesise was to investigate the synthetic lethality of the double mutant *lytE cwlO* further by substitute the N-terminus of CwlO with either the N-terminus of LytE or LytF. Despite the high sequence similarity of the catalytic domains of LytE, LytF, and CwlO indicated by alignment (Figure 4.17), the chimeric genes containing the C-terminus of the CwlO were insufficient to fulfill the requirements of the DL-endopeptidase activities at the lateral cell wall. Furthermore, LytE and CwlO have different mechanisms for activation. CwlO activity seems to be regulated by FtsEX, an ATP-binding cassette transporter. The mechanism by which CwlO associates with FtsEX is unknown, but it is important for CwlO to function effectively (Meisner *et al*., 2013). On the other hand, LytE export/localisation at the lateral cell wall is governed by MreBH (Carballido-López *et al*., 2006). The process of how these interactions turn on/off the endopeptidase activity of the enzymes and whether the activity is dependent on localisation or activated only under specific conditions or when certain changes occur is unclear. However, other work by Guyet *et al*., 2023 indicates that there is a significant role played by the teichoic acids in relation to LytE, a feature that was also indicated by Kasahara *et al*., 2016 when looking at the localisation of the autolytic enzymes.

Chapter 5: Role of AsnB in the Modulation of Autolytic Activity

5.1 Introduction

PG modifications are the mechanisms that alter cell wall properties to avoid degradation and bacterial lysis. The common modification that only occurs in Gram-positive bacteria is the amidation of the carboxyl group within the second (D-Glu) or third (*m*DAP) amino acid of the stem peptides. Research has shown that the amidation of peptidoglycan cross bridges in *Lactococcus lactis* was absent in the deletion of *asnB* (Veiga *et al*., 2009a). Later, the characterisation of the *asnB* gene of *B. subtilis* (BSB1 genetic background) indicated that the *asnB* had a role in the PG amidation of *m*DAP (Dajkovic *et al*., 2017). Interestingly *B. subtilis* cells lacking *asnB* have been observed to undergo lysis and need the presence of 25 mM of $MgSO_4$ to grow in the BSB1 background. Independent research in other Gram-positive bacteria, *L. plantarum* and *C. glutamicum* also identified genes homologous to *asnB*, *asnB1* and *ltsA*, respectively, were also affected in growth and cell morphology and were able to show that AsnB was required for *m*DAP amidation (Bernard *et al*., 2011; Levefaudes *et al*., 2015). The degree of the amidation is variable and culture condition-dependent, with clear evidence that high $MgSO_4$ results in a significant reduction of amidation in *B. subtilis*. Interestingly, the effect of elevated $MgSO_4$ concentrations in growth media also represses the lethality of several mutations that have direct or indirect effects on cell wall synthesis (Chastanet & Carballido-Lopez, 2012; Formstone & Errington, 2005b; Kawai *et al*., 2009; Sassine *et al*., 2020). The role of this modification remains poorly defined, although it is essential. In the absence of *asnB* in *B. subtilis,* the cell morphology changes, with cells becoming wider and shorter than the wild type (Dajkovic *et al*., 2017). This suggested that AsnB has a functional role in the cell wall. The Dajkovic *et al*., 2017 study reported that in the absence of amidated *m*DAP, the control of cell wall hydrolysis is disrupted. In light of the previously published results, additional characterisation of the system was initiated to examine the relationship between cell wall amidation and autolytic enzymes at the genetic level. The insights gained from this work are detailed in the following sections.

5.2 Result

5.2.1 Introduction of *asnB* null mutation into 168CA

To gain insight into the role of AsnB in cell wall metabolism, an attempt was made to backcross the previous mutant of *asnB* (FU340) (Yoshida *et al*., 1999) into the standard wild type used in the laboratory (168CA). FU340 exhibited remarkable stability when cultured in Difco Sporulation Medium (DSM) supplemented with asparagine (Yoshida *et al*., 1999). Initial attempts to do this simple transfer of an antibiotic resistance marker into the standard

wild type resulted in very inconsistent results ranging from nothing to heterogenous transformants that were generally difficult to culture. To try and resolve this problem, and because previously published work had used the BSB1 strain background, the transformation was carried out for both 168CA and BSB1 backgrounds, separately, using the same genomic DNA preparation from FU340. When the transformants were selected on NA plates supplemented with kanamycin for selection and $MgSO_4$, no transformant colonies were obtained. However, when PAB plates supplemented with kanamycin and 25 mM $MgSO_4$ were used, colonies were obtained, but they exhibited different sizes. This clearly suggested that the null mutation in *asnB* was causing significant growth defects in the transformed cells. Interestingly, there also seemed to be a significant difference in the transformability of the BSB1 and 168CA with the *asnB* allele (Figure 5.1A; left and right plates, respectively).

On streaking out the transformant colonies, it was observed that the small colonies did not grow either with or without $MgSO_4$. In contrast, the large colonies struggled to grow on a plate supplemented with 25 mM $MgSO_4$ (Figure 5.1B), resulting in thin smear-like growth that often appeared to have colonies growing up through the initial growth. However, it was apparent that the BSB1 derivatives were much more stable than those of 168CA. Thus, two conclusions could be drawn from these observations. Firstly, the BSB1 background is in some way genetically distinct from that of 168CA background . This seemed to imply that neither genetic background was suitable for phenotypic characterisation of the original knockout mutation as it was clear that suppressor-like mutations were being acquired, although none seemed to result in an easily culturable strain. Secondly, it was clear that *asnB* encodes an essential function in *B. subtilis* and that there was a requirement for both high $MgSO_4$ levels and apparently glucose in the culture media to permit any viable growth, consistent with results in Dajkovic *et al*., (2017).

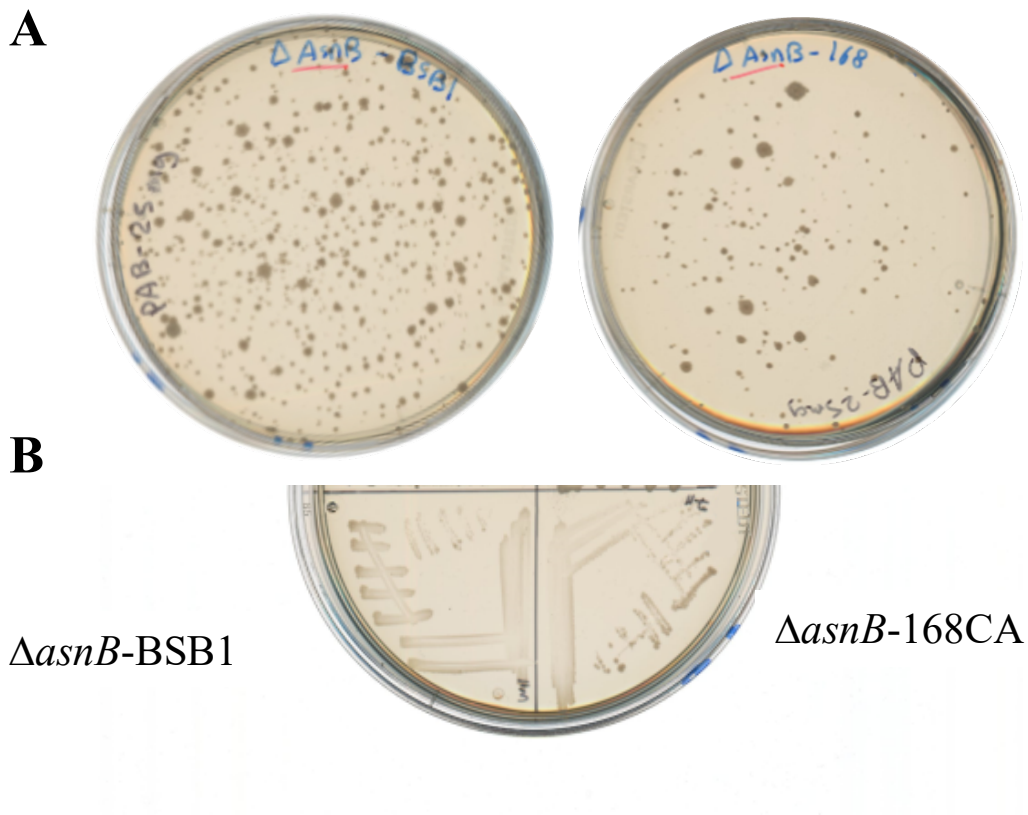

Figure 5.1 Backcross transformation of Δ *asnB* (FU340) into BSB1 and 168CA strains

(A)The PAB transformation plates were supplemented with kanamycin (5 µg/ ml) and 25 mM $MgSO_4$ and incubated overnight at 37°C. The resulting colonies on the plates exhibited a variation in size. (B) The large colonies were streaked into PAB supplemented with kanamycin (5 µg/ ml) and 25 mM $MgSO_4$, and it was observed that they struggled to grow. In contrast, the small colonies were not able to grow.

5.2.2 Construction of a strain with a conditional allele of *asnB*

The previous attempts that were made to transfer the mutant *asnB* (FU340) into the 168CA or BSB1 background were unsuccessful. An attempt was made to construct a condition allele strain of *asnB*, placing the expression of the *asnB* under the control of the P_{xyl} promoter, using the 168CA strain background. For this, an intermediate DNA construction was made by inserting the antibiotic resistance gene *cat* (chloramphenicol) and P_{xyl} promoter (from plasmid pRD96) immediately upstream of the *asnB* coding sequence such that the transcription of *asnB* would be xylose dependent. The assembly of the DNA fragments is indicated in Figure 5.2A. This DNA construct was then transformed into 168CA with selection for *cat* resistance on PAB plates containing xylose (0.5%). One of the resulting colonies was then isolated and designated as strain sAM202.

To confirm the genetic construction in the sAM202 strain (inducible *asnB*), PCR amplification was performed using the forward primer oAM092 and the reverse primer

oAM095 (Figure 5.2B). Following PCR of the genomic DNA of both the sAM202 strain along with the 168CA strain as a template, the amplification products were digested with the restriction enzymes *Nco*I and *Bgl*II, known to digest at the selective marker (*cat* resistance) and the P_{xyl} promoter, respectively. The digested fragments were separated by gel electrophoresis and compared with 168CA (Figure 5.2C). The *Nco*I digestion was expected to result in three bands of different sizes in the sAM202 strain, while the 168CA strain should show only two bands. On the other hand, the *Bgl*II digestion should produce two bands in the sAM202 strain, whereas the 168CA strain should exhibit only one band (Figure 5.2C). By comparison of the digested fragments of sAM202 to those of the 168CA strains, it was possible to show that the insertion of the P_{xyl} promoter had occurred in the correct location upstream of *asnB* leading to its expression being artificially controlled, correlating with the observed requirement for xylose (see next section).

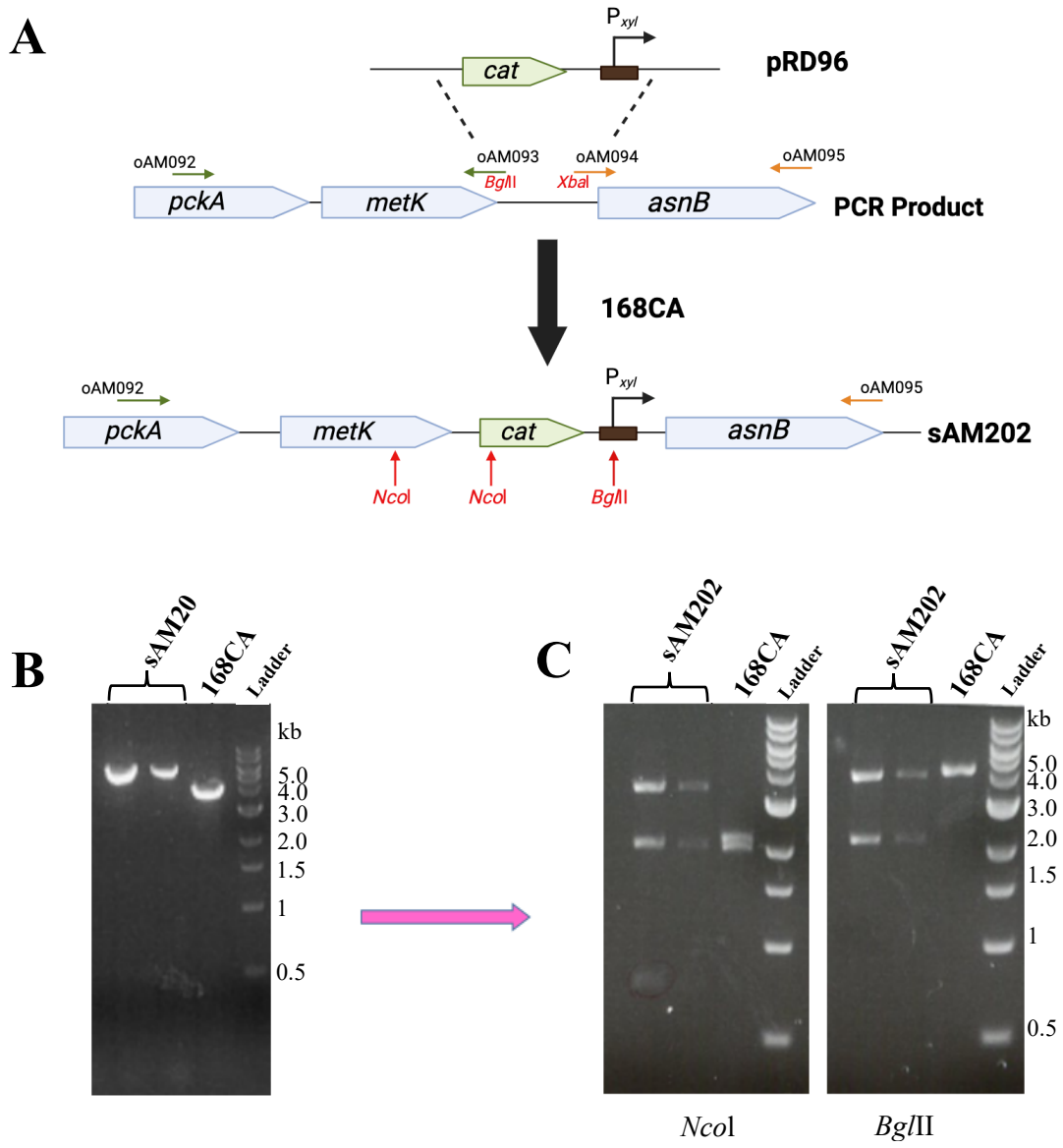

Figure 5.2 Construct a conditional allele of *asnB*

(A)A Diagram illustrates the digested fragments of pRD96 with *Bgl*II and *Xbal*, and the amplified fragments of asnB with accompanying primer binding site to construct an inducible *asnB* (sAM202). The green arrows indicate the amplified upstream region of the *asnB* consisting of recognition sites of *Bgl*II, while the orange arrows represent the amplified the *asnB* with *Xbal* recognition sites. The two resulting DNA fragments with blunt ends were then ligated with the digestion fragments of pRD96 using a T4 DNA ligase following manufacture protocol. The ligated DNA was then transformed into the native locos of *asnB* in 168CA using a PAB plate supplemented with 0.5% xylose and 5 µg/ ml chloramphenicol (B) A gel electrophoresis image demonstrates the PCR fragments obtained from the sAM202 and 168CA strains using oAM092 as a forward primer and oAM095 as a reverse primer. The predicted size of the PCR fragment of sAM202 was 4987 bp, while the size of the 168CA was 4120 bp. (C) The gel electrophoresis image shows the amplified fragments of sAM202 and 168CA after digestion with *Noc*l and *Bgl*ll restriction enzymes.

5.2.3 Growth characteristics of inducible *asnB* in *Bacillus subtilis*

As previously shown, the null mutant of *asnB* is conditionally lethal (Section 5.2.1; Dajkovic *et al*., 2017), but could be rescued by elevated $MgSO_4$ levels in the culture medium. The growth characteristics of the sAM202 strain, where expression of *asnB* was conditional on the presence of xylose, were examined in the PAB and NA plates supplemented with either xylose to induce *asnB* expression, 25 mM $MgSO_4$, or 0.4% glucose (G) and incubated overnight at 37°C (Figure 5.3). In the absence of xylose, the sAM202 exhibited little growth (other than a few colonies when the heavy inoculum was applied) on the PAB plate but showed normal growth on the NA plate. The strain grew well, as expected, in the presence of xylose and $MgSO_4$. However, in the PAB or NA plates supplemented with glucose, the sAM202 strain failed to grow. This observation suggests that the distinct concentrations of $MgSO_4$ and glucose present in PAB and NA media may influence growth. The NA media does not contain glucose, while PAB media is rich in glucose (1g/L). The $MgSO_4$ and glucose seem to have a role in *asnB* expression, making them required for optimal growth.

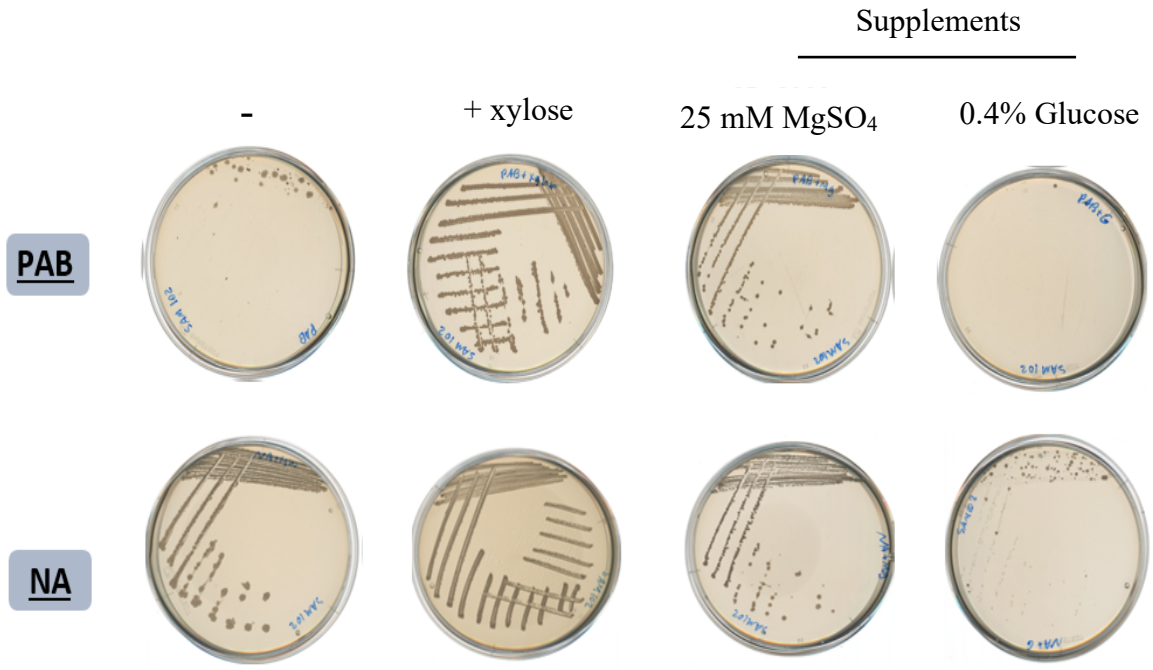

Figure 5.3 Conditional growth of the sAM202 on PAB and NA plates

The sAM202 strain was streaked onto PAB or NA plates, or PAB or NA plates supplemented with either 0.5% xylose, 25 mM $MgSO_4$, or 0.4% glucose.The plates were then incubated overnight at 37°C.

To determine if this effect could be reproduced in a liquid media where cultures grow more homogeneously and sampling is possible, the sAM202 strain was grown overnight in the PAB media supplemented with xylose. On the following day, the culture was diluted and incubated at 37°C for 1 hour, then washed and grown in liquid media with different supplementation: PAB only; PAB with either xylose, 25 mM $MgSO_4$ or 0.4% glucose; xylose with either 25 mM $MgSO_4$ or 0.4% glucose; and 25 mM $MgSO_4$ with 0.4% glucose. The sAM202 strain exhibited robust growth when PAB was supplemented with $MgSO_4$, as well as when induced with xylose in combination with $MgSO_4$. Additionally, strain displayed relatively normal growth when induced with xylose alone in the absence and presence of additional glucose. However, after 80 minutes, the sAM202 strain stopped growing in PAB alone, as well as in PAB supplemented with either glucose or both $MgSO_4$ and glucose, as determined by the fact that the OD did not increase and after long incubation in these conditions, the OD started to decrease indicating cell lysis. Altogether, these results reinforce the idea that glucose negatively impacts the growth of the sAM202, even in the presence of $MgSO_4$.

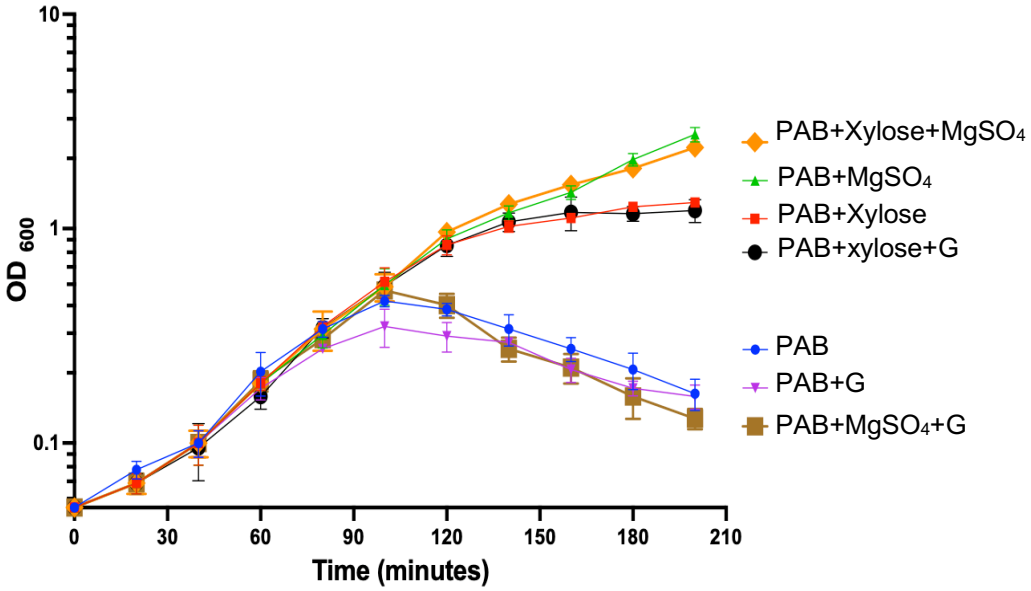

Figure 5.4 Conditional growth of the sAM202 strain in different media conditions (liquid media (PAB)

The sAM202 strain was grown overnight at 30°C in PAB media supplemented with xylose. The next day, the culture was washed with PAB media and then diluted back to an OD_{600}~ 0.05 into a fresh warm PAB media supplemented with different chemicals: PAB (blue), PAB+xylose (red), PAB+ $MgSO_4$ (green), PAB+G (purple), PAB+xylose+ $MgSO_4$ (orange), PAB+xylose+G (black), PAB+ $MgSO_4$+G (brown). The cultures were then incubated at 37°C, and the OD_{600} was measured every 20 minutes for 4 hours. The data was plotted on a Log 10, Standard deviation is represented by error bars (n=3).

5.2.4 Mapping of the suppressor mutations

In this study, the sAM202 strain exhibited a lethal phenotype in the absence of xylose or $MgSO_4$. As shown in (Figure 5.3) when sAM202 was plated on PAB medium, over time colonies appeared that were presumed to be spontaneous suppressor mutants. Subculturing these colonies was possible under the non-permissive conditions of the parent strain, permitting the reliable isolation of the strain on plates without xylose. Thus, it was assumed these strains contained mutations that somehow compensated for the loss of *asnB*.

Logically, three types of suppressor mutation were expected, the first being promoter mutations resulting in loss of repression, secondly, loss of function mutations in the repressor protein (XylR), and finally, mutations in genes that in some way bypassed the need for *asnB* completely. Eight independently isolated suppressor strains were used for further analysis. Their genomic DNA was then extracted to permit "back transformation" into the wild-type strain to permit differentiation between the possible mutation types. The flow chart in Figure 5.5 outlines the logic of the screening used. If the mutation was in the promoter of the conditional promoter of *asnB*, the transformation of the suppressor strains would result in all colonies obtained being xylose-independent. The analysis of the transformants obtained permitted the elimination of strains S2, S3, S5, and S6 as being uninteresting. On the other hand, if the transformants were xylose-dependent, then it would suggest that the suppression mutation was due to a mutation elsewhere in the genome and not linked to the *asnB* locus. Analysis of the transformants obtained with gDNA from strains S1, S4, S7, and S8 showed low-frequency xylose-independent colonies. Thus, whole genome analysis was employed to identify the mutation(s) in these suppressor strains (see Section 5.2.4.2).

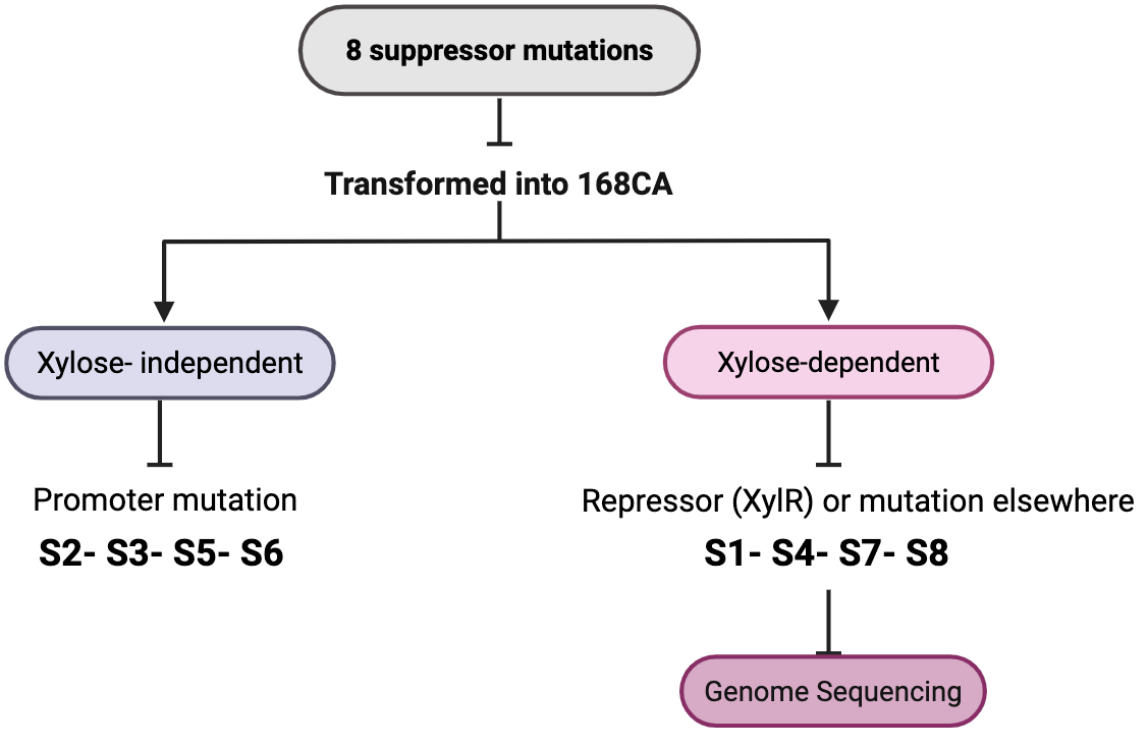

Figure 5.5 Flow chart described the mapping of the suppression mutations

Eight of the isolated suppressor mutations were back transformed into 168CA to determine the nature of the suppressor mutation. If the transformation resulted in a high frequency of xylose-independent colonies (left), the mutation was in the promoter mutation. If the transformation was low frequency xylose independent, it was probably a *xylR* repressor mutation or a true suppressor for *asnB* repression (right).

5.2.5 Phenotypic analysis of the suppressor mutations associated with repressed *asnB*

After mapping the suppressor mutations, the growth of the suppressor mutations that were clearly related to bypassing the need for AsnB function was characterised. As a starting point, the growth of the suppressor mutation in the absence and presence of xylose was compared with the parent "AsnB dependent" strain, sAM202. Figure 5.6A shows the growth profile of the suppressor strain S4 grown with and without xylose. The growth of S4 closely resembled the growth of sAM202 in the presence of xylose and did not exhibit the growth perturbation seen for sAM202 in the absence of xylose (shown in Figure 5.4).

In parallel with the growth analysis, the cell morphology of the *asnB* depletion and the suppressor mutations was assessed in the mid-exponential phase by fluorescence microscopy (Figure 5.6B) (samples prepared described in method Section 2.8.1). In the absence of xylose, the *asnB* deletion (sAM202) exhibited significant cell lysis, while in the suppressor mutation, there was no suggestion of any lysis, consistent with the growth curves.

This phenotype was also observed to be the same for the other suppressor mutations (S1, S7, and S8), suggesting that the suppressor mutation prevented cell lysis in some way.

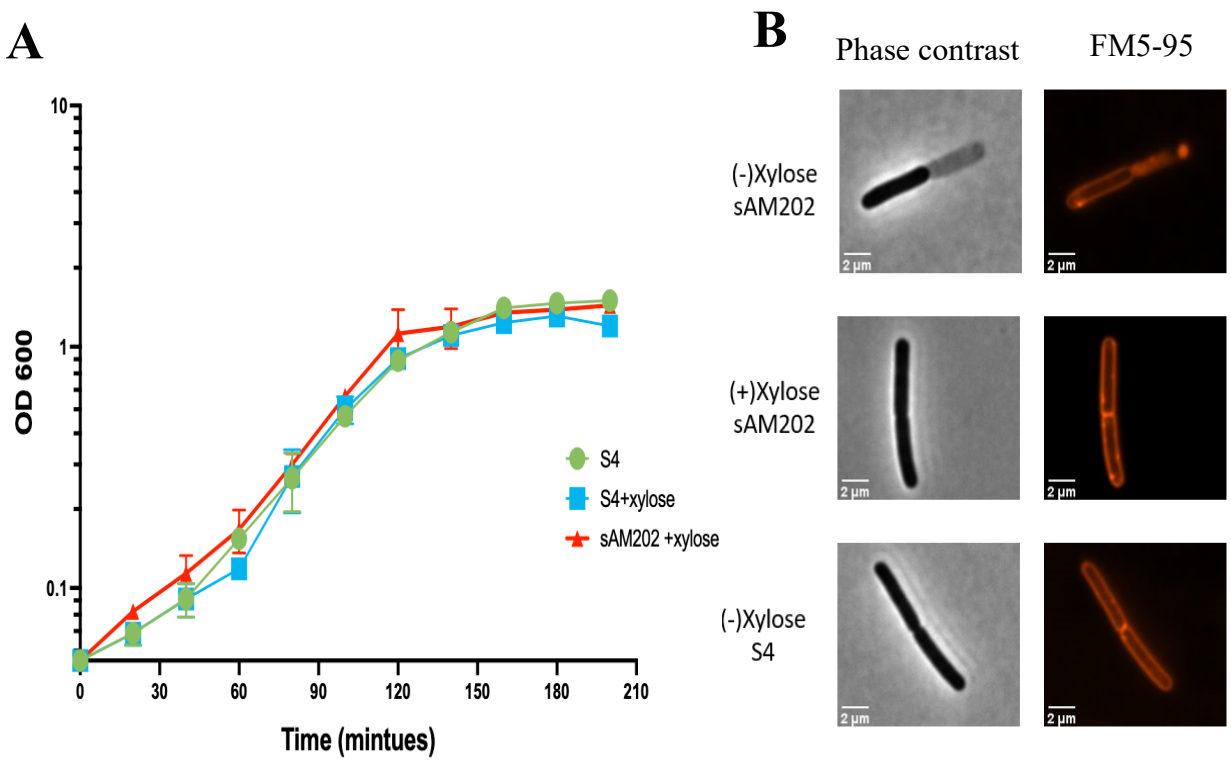

Figure 5.6 Characterise the suppressor mutation in PAB media

The sAM202 strain and the S4 (suppressor mutation) were grown overnight in PAB media supplemented with xylose and incubated at 30℃. The following day, the cultures were washed with PAB media and then diluted back to OD_{600}~ 0.05 in either PAB or PAB containing xylose. (A) the growth curve of the sAM202 and S4 strains was measured every 20 minutes for 3 hours and potted onto a Log 10 scale. Standard deviation is represented by error bars (n=3). (B) the cell morphology of the sAM202 and S4 strains in the mid-exponential phase. Phase contrast image (left panel) and FM5-95 membrane dye (right panel). Images were processed in ImageJ and the scale bar represents 2 microns.

5.2.6 Genome sequence analysis of the suppressor mutations

In order to identify the nature of the suppressor mutation(s) in the 4 strains selected to be tolerant of the *asnB* repression (Section 5.2.4), these original mutants were back transformed into 168CA as a way to ensure that they were true genetic changes and potentially to clean up the strains of irrelevant mutations. The genomic DNA was then extracted from each of the 4 strains (S1, S4, S7, and S8) selected along with the parent strain sAM202, and this material was sent for Illumina sequencing. The resulting sequence data was then processed in CLC software to permit comparison. For this, the genome sequence of the

parent strains was compared to that of the reference strain 168CA from the database (Reference no. AL009136). The same was done for each suppressor mutant, and then the list of variations was compared. This approach allowed us to eliminate the permitted mutations present in the parent background and identified the mutations that were potentially specific to the suppressor strain, these are listed in Table 5.1, along with the gene they are associated with and the consequences of the mutation.

Table 5.1 All variations found in the four isolated suppressor mutations

Strain	Nucleotide change	Gene	Protein function change
S1	266 (T>A) 265 (T>A)	*xylR*	Asn>Tyr Gln>Leu
S4	1891741 (C>T)	Between *xylR* and *xylA*	Not sure
	95 (T>C)	*ppsA*	silent
S7	Deletion from 1673 to 1677	*srfAB*	Stop codon
	1671 (AA)	*srfAB*	Stop codon
	1179 (T>C)	*ppsA*	Ile>Val
S8	1179 (T>C)	*ppsA*	Ile>Val
	176 (G>A)	*yknX*	Ala>Thr
	1671 (deletion AA)	*srfAB*	Stop codon

For the suppressor strain S1, mutations were found in the repressor of the P_{xyl} promoter (*xylR*), resulting in amino acids change at positions that would be expected to result in the dysfunction of the protein and hence result in the loss of P_{xyl} repression. This was one of the predicted outcomes at the onset of the suppressor mutation analysis.

Surprisingly, for suppressor S4, the only significant mutations that could be identified from the sequence data were located in the intergenic region between *xylR* and *xylA*. The consequences of this nucleotide change are unclear, but it is reasonable to predict that it might result in some alteration in the expression of the *xylR* gene, which then alters the repression of the P_{xyl} promoter. The only other mutation that could be identified in the sequence was a nucleotide change in the coding sequence of the *ppsA* gene. On analysis this would not result in a change in amino acid, though it could have implications for the translation efficiency of the protein. However, as this, the encoded protein of *ppsA* is not known to have any effect on bacterial growth, rather it is related to the production of an

antibacterial compound, thus it is difficult to see how this mutation would be directly related to the suppression of the essentiality of *asnB* expression.

In contrast, suppressor strains S7 and S8 share common mutations, none related to the *xyl* regulon. Of these, the *ppsA* gene is mutated, in this case conservative change of amino acid at position 1179 in the protein and a very convincing inactivation of the *srfAB* gene. The fact that this mutation is present in both strains with a mutation in *ppsA* is interesting, but this was only identified in the late stages of the project, and it has not been possible to validate that these are the direct cause of the reduced need for AsnB function in vegetative growth. To take this further, it would be necessary to introduce a defined mutation in *srfAB* and *ppsA* into the sAM202 background and see if that results in the strain being xylose independent. However, due to time constraints this experimental work was not possible.

5.2.7 Effect of conditional expression of *asnB* in strains lacking autolytic functions

Since the phenotype of the *asnB* mutant strains indicated a loss of cell wall integrity, consistent with Dajkovic *et al*., 2017, the role of AsnB may be to modify the peptidoglycan in a way that modulated autolytic activity. Thus, the loss of this modification may result in the overactivity of specific autolytic enzymes. As a way to directly test this idea, deletions of the two key autolytic enzymes, *cwlO* and *lytE*, were introduced into the sAM202 background along with null mutations in genes encoding for accessory proteins involved in autolytic activities (*ftsEX* and *mreBH*, involved in CwlO and LytE function, respectively). The resulting strains were then characterised for their ability to grow under conditions where the expression of *asnB* was limited` by sub-optimal levels of xylose in the culture medium.

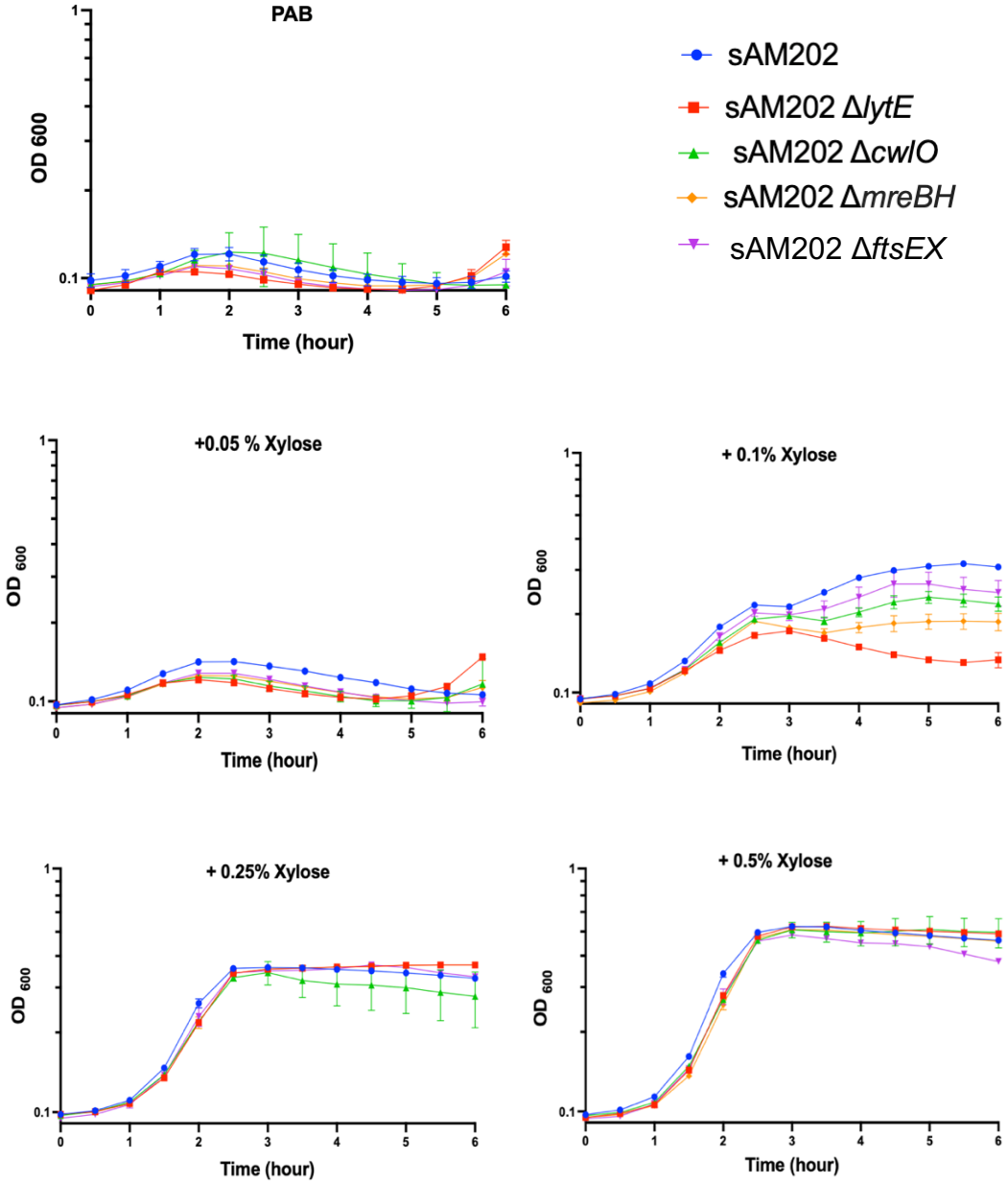

Figure 5. 7 Examined the amidation effect on the autolytic enzymes

The individual Δ*lytE* (red), Δ*cwlO* (green), Δ*mreBH* (orange), and Δ*ftsEX* (purple) was introduced into the sAM202 strain. Strains were grown overnight in PAB with xylose at 30°C. The following day, cultures were washed twice with PAB and then diluted in PAB containing different concentrations of xylose (0.05, 0.1, 0.25, and 0.5%). The cells were plated in a 96-well microtiter plate and then incubated at 37°C using Tecan. Standard deviation is represented by error bars (n=3). The optical density value was measured at OD_{600} and plotted on a Log 10 scale.

From the growth in (Figure 5.7), it was clear that the strain exhibited relatively normal growth of *asnB* expression and that required around 0.25% to 0.5% of xylose, regardless of the genetic background. The introduction of null mutations of the two autolytic

enzymes (*lytE*/*cwlO*) had no significant effect on the growth properties of the sAM202 strain (similarly for *ftsEX* and *mreBH*). These findings indicate that the lytic phenotype observed on depletion of *asnB* was unlikely to be caused by over-activity or miss-regulation of either LytE or CwlO. At the critical level of the expression (0.1% xylose), there was some variation in the strain expressed. In the inducible strain *asnB* lacking the *cwlO* or *ftsEX*, the strain was higher than the strain lacking either *lytE* or *mreBH*.

5.3 Discussion

In Gram-positive bacteria, amidation is one of the common modifications that occur in the second or the third position of the stem peptide (α-carboxyl of D-glutamic acid (D-glu) or ε-carboxyl group of the *meso*-diaminopimelic acid (*m*DAP), receptively) (Atrih *et al*., 1999a). The role of the amidated *m*DAP on the cell wall of *B. subtilis* remains unclear, but it has been shown that similar modifications are present in other bacteria. In the case of *S. aureus,* characterisation of the Penicillin-binding proteins (PBPs) involved in cell wall synthesis has shown that the modification is required to recognize the stem peptide as a substrate. Interestingly, in this particular species, the amidation on the second amino acid of the peptide (D-glu) is mediated by the combined activity of MurT and GatD (Münch *et al*., 2012).

For *B. subtilis,* AsnB has been identified as an essential gene for the amidation as in other species. The AsnB is a cytoplasmic protein that amidated the *m*DAP on PG precursors inside the cell. Dajkovic *et al*., 2017 reported that a strain lacking *asnB* was conditionally viable, but in this work, this proved to be problematic in the 168CA background. However, in some way consistent with that publication a conditional allele of *asnB* could be constructed in this study (sAM202). This strain exhibited a lethal phenotype in PAB media unless xylose or $MgSO_4$ was added to the media. In contrast, on a nutrient agar (NA) plate or in the NA supplemented with either xylose or 25 mM of $MgSO_4$, the sAM202 strain grew quite happily. However, the addition of glucose to NA resulted in a phenotype similar to that seen in a PAB plate. This suggested that the levels of $MgSO_4$ and glucose play a critical role in the PG amidation. Previously, it was reported that the degree of amidation was decreased in the presence of excess $MgSO_4$ in PAB media (Dajkovic *et al*., 2017b) and so fits with the results obtained. Thus, the requirement for AsnB is curious as it seems to provide an essential function

Previous studies have suggested that the presence or absence of amidation did not affect the cell wall synthesis enzymes in *B. subtilis*, *L. plantarum*, and *C. glutamicum* (Bernard *et al*., 2011; Dajkovic *et al*., 2017b; Levefaudes *et al*., 2015). Consequently, the possibility that the hydrolysis enzymes in *B. subtilis* were affected by the absence of the amidation seems logical, as previously suggested (Dajkovic *et al*., 2017). In this study, the role of the amidation was examined in various genetic backgrounds to determine whether the AsnB mediated modification was required for CwlO or LytE activities, as they are the key autolytic enzymes. By modulating the level of the *asnB* in different genetic backgrounds, the growth of P_{xyl} regulated *asnB* in a strain lacking *cwlO* was observed to be higher compared to the *lytE* background. This suggests that the LytE might be involved in the apparent growth problems experienced by a strain lacking *asnB* mediated the cell wall modification. However, this hypothesis/observation is rather weak and could not be supported by the isolation of spontaneous suppressor mutations. Hence, the precise role of AsnB in relation to bacterial cell growth remains unclear and further research is required.

Chapter 6. Conclusions and Future Directions

This thesis has focused on studying the characteristics of the autolytic enzymes in *B. subtilis* during vegetative growth. These autolysins degrade the cell wall, allowing cells to enlarge and subsequently divide. Our data indicates that the major autolytic enzymes (LytE, LytF, LytC, and LytD) in cell wall were modulated in their abundance/stability during different growth phases. Additionally, we tried to analyse the functional importance of the carbohydrate-binding domain of the secreted enzyme, using LytE and LytC as initial model proteins with very different N-terminal domains, as well as to determine if the apparent modular structure of the autolytic proteins would permit domain-swapping as a way to determine if they were biochemically specific for substrates. Finally, but related to the autolytic activity, the functional role of the PG precursor amidation by AsnB was investigated in relation to the two major autolytic enzymes LytE and CwlO.

In *B. subtill*s genome contains 42 genes that are considered to be hydrolytic enzymes (Wilson *et al*., 2023). The functional redundancy between the hydrolase enzymes was found to be high, making it difficult to define the specific functions of most of them. Consequently, over time, many publications have identified the roles of some of the major autolytic enzymes in both specific and diverse processes. The DL-endopeptidases LytE and LytF seem to have a role in cell separation, while LytC and LytD have a role in cell motility and turnover (Blackman *et al*., 1998; R. Chen *et al*., 2009; Fukushima *et al*., 2006; Margot *et al*., 1994b). Additionally, LytE and CwlO were found to be involved in cell growth. Of the known proteins collectively described as autolysins, the importance of LytE and CwlO has been clearly defined, as deleting both results in synthetic lethality (Bisicchia *et al*., 2007). However, this raises a question about how these two proteins are functionally redundant to each other in cell wall "metabolism". They have been proposed to function in very different ways, with CwlO being functionally dependent upon an integral membrane complex composed of at least FtsE, FtsX, SweC, and SweD (Meisner *et al*., 2013; Brunet *et al*., 2019). This suggests that its activity is restricted to the inner surface layers of the cell wall. In contrast, LytE is a secreted protein and seems to function on the outer surface of the cell, in some way regulated by the teichoic acids (Kasahara *et al.*, 2016; Guyet *et al.*, 2023).

As a starting point for this study, the abundance of the hydrolysis enzymes LytE, LytF, LytC, and LytD was examined using their specific antisera under different conditions. This showed that altering the cell wall composition resulted in a change in the abundance of these enzymes (Chapter 3). This modulation needs to be further characterised and related to careful transcription studies for the encoding genes, particularly in relation to growth in the

presence of elevated magnesium or glucose. This may gain further insights into the mechanism by which exogenous magnesium can suppress the lethal effects of some genes specifically involved in cell wall synthesis. Here, there are a number of observations that in combination are to some degree contradictory and difficult to incorporate into a single model of how the systems work. During this study, Wilson *et al*., 2023 indicated that the activity of LytE may be inhibited by the elevated levels of magnesium ions. However, in Chapter 3, it was seen that the abundance of LytE was reduced in different genetic backgrounds when a medium was supplemented with magnesium. Potentially having the same effect as inhibition, leading to the proposal that high $MgSO_4$ results in the dissociation of LytE from the wall and so is potentially lost from the cell. It was also suggested that LytE and CwlO compensate for the function of each other (Dobihal *et al*., 2019). Here, the concept of LytE being released from the cell wall and hence able to "move" could fit with this. It could diffuse in any direction and so could reach the inner layers and function in place of CwlO as easily as simply being lost to the environment. This concept would fit with the fact that it has been indicated that the expression of *lytE* increased in a strain deleted for *cwlO* (Dobihal *et al*., 2019) and indicated by Western blot analysis in this work. Thus, an expectation would be that the level of CwlO might increase in a strain lacking *lytE*. However, from the mass spectrometry analysis in this work, it was observed that the level of CwlO was reduced in the strain deleted for *lytE*. However, this data has its limitations, and it was not possible to determine the abundance of CwlO by Western blot as antisera were not available at that time. However, the work by Meisner *et al*., 2013 combined with structural studies of the FtsEX complex, suggest that CwlO may have a "dual existence", where the enzyme is membrane associated and regulated or can act as a free catalytic domain that is active away from them membrane.

An independent approach to understanding how LytE and CwlO might be able to functionally compensate for each other was through domain-swapping. A previous study suggested that the synthetic lethality of the *lytE cwlO* double mutant was due to the lack of DL-endopeptidase activity. Therefore, the idea was to construct a protein chimera, or domain-swapped construct, assuming that the proteins were composed of an interaction domain and a catalytic domain, as indicated by structural predictions (Table 4.1-Chapter 4). The C-terminal region of either LytE or LytF was replaced with the C-terminal portion of CwlO, and this was assessed to determine whether it could functionally complement the null mutation of the other. However, neither domain-swapped construct, $N_{LytE}C_{CwlO}$ nor

$N_{LytF}C_{CwlO}$, could recuse the lethality observed in the double mutant *lytE cwlO* or correct the phenotype of the *lytE lytF* double mutant. This result suggested that the catalytic domain of the CwlO did not have the necessary activity to suppress the lethality, or the chimeric proteins were not enzymatically active, due to miss-folding of the protein. However, this then raises the question of how the activities of these enzymes are modulated *in vivo.*

Another part of this study was in line with a previous work by Hashimoto *et al*.,2012, which indicated that the N-terminal region (CBD) of the secreted autolytic enzymes was important for maintaining the proteins sub-cellular localisation. To investigate the localisation mechanisms of the CBD of LytE and LytC, as they contain different CBDs, a pull-down assay was used in Chapter 4 to characterise the CBD interaction within the cell wall. For LytC, the XkdG, XkdK, and XkdM (secreted bacteriophage proteins) were found to be more abundant in their interaction with LytC. The phage proteins have been observed to interact with the cell wall predominantly at the polar region (Jakutytė *et al*., 2011). However, for LytE, it was difficult to determine the interaction as the fusion construct protein was trapped in the cytoplasm. Although some of the results obtained in this study by manipulating the expression of *lytE* have raised some interesting points. The most curious being the fact that overexpression of LytE seems to result in the accumulation of the protein in the vicinity of the membrane, although it is not clear if this is functional. However, it is possible that this might provide a way for LytE to compensate for the dysfunction of CwlO.

At the onset of the project, it was suggested that the absence of the amidation in *B. subtill*s disrupted the cell wall hydrolysis (Dajkovic *et al*., 2017). Additionally, it was shown that the presence of magnesium in some way mediated a reduction in the level of the amidation, and yet the amidation of a small proportion of the cell wall precursors is still required for growth under normal conditions. AsnB has been shown to have a role in amidated the *meso*-diaminopimelic acid at the third position in the PG stem peptide, and the cell becomes wider and shorter in the deletion strain (Dajkovic *et al*., 2017). Here, it seems that glucose plays a role in the amidation, as the presence of glucose in the growth medium inhibited the growth, as shown in Chapter 5. Interestingly, this work was very strain-dependent and was only easily has been done in a specific genetic background, BSB1 (Dajkovic *et al*., 2017). Construction of equivalnet strains in the 168CA background was problematic, but eventually, it was possible to generate a conditionally expressed allele of *asnB*, which permitted the isolation of strains where the requirement for AsnB activity was

reduced. However, after exmining the impact of the AsnB on the background of the two critical enzymes, *lytE* and *cwlO,* no obvious change was observed. This seems to suggest that the amidation is not related to the activity of these enzymes, but has some other important function, perhaps more related to an aspect of PG synthesis. Future work is needed to examine the degree of amidation in these strains and to determine how glucose and elevated magnesium change the need for this modification of the PG precursors.

Questions for future work

The key questions over how controlled PG degradation can be modulated tend to revolve around how the enzymes are located correctly to enable coordinated cell wall modification. For *E. coli,* this seems to have been solved by integrating them into the synthetic complex, ensuring that new synthesis is actively repairing the opening in the wall structure. This mechanism works well for an envelope structure where the PG is a thin sheet sandwiched between membranes that provide defined location surfaces for the proteins. However, this is impractical for Gram-positives as the PG is much thicker, and there is no defined outer surface (particularly in the case of *B. subtilis*, as there is no outer S-layer, etc.). Thus, the mechanics has to operate in a different way. The functioning of the cell wall synthetic complexes, where the proteins are similar, but interaction in different ways, indicates this to some degree. The current understanding at the level of cell wall degradation seems to show that CwlO and LytE are the major proteins in the process. The other autolytic enzymes could potentially provide a level of functional redundancy or are operating in other roles, such as separation after division, for which there is good evidence for LytC and LytD, or simply function to recycle cell wall material.

A current model from our lab seems to point to CwlO being active near the cell membrane and prevented from degrading newly synthesized material until DacA/LdcB removes the terminal D-alanine on the side chains (A Aljohani- unpublished). On the other hand, LytE is secreted and only active on the outside surface. Previous studies have revealed that in the absence of *cwlO*, *lytE* is overexpressed, resulting in an accumulation of LytE on the membrane that has sufficient activity to carry out CwlO's function (Dobihal *et al*., 2019). Based on this, in the absence of *lytE*, *cwlO* may be overexpressed, and it is processed in a way that results in the catalytic domain being released in an active form that is sufficient to compensate for the loss of LytE (Figure 6.1). To further investigate the CwlO activity, the purified catalytic domain of the CwlO should be examined for enzymatic specificity, and a

similar analysis should be done for LytE. This might help to identify and elucidate whether the catalytic domains are unique or truly functionally identical. In such a case, understating the regulation/localisation mechanisms would become an important aspect. Here, there is the potential for the development of an antibacterial agent that perturbs the regulation mechanism, resulting in loss or over function of the autolytic enzymes. The end result being cell death through blocked growth or lysis through an essential enzyme.

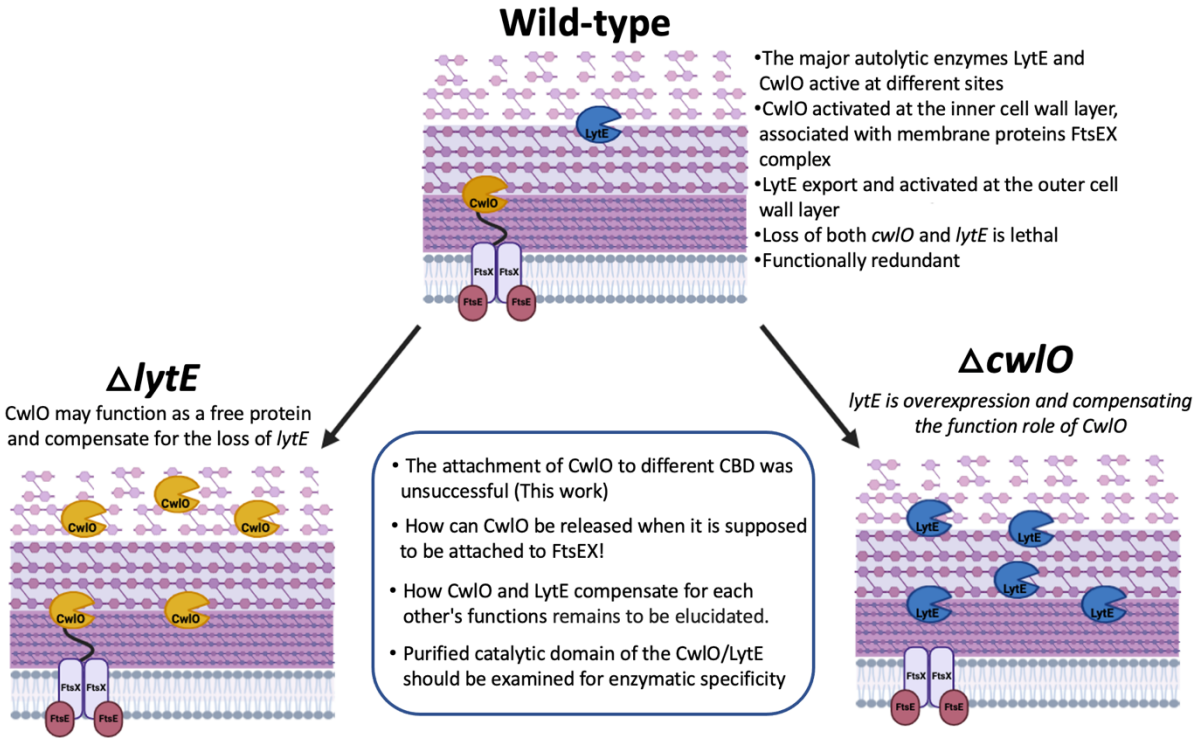

Figure 6. 1 Proposed model of the expression of major autolytic enzymes LytE and CwlO

Diagram of the *B. subtilis* cell wall showing the activation mechanism of the LytE and CwlO in wild-type, Δ*lytE*, and Δ*cwlO* backgrounds. CwlO interacts with the FtsEX and activates near the cell membrane, whereas LytE activates at the outer layer (Dobihal *et al*., 2019, Meisner *et al*., 2013). LytE and CwlO have been found to be functionally redundant (Bisicchia *et al*., 2007). Illustration generated with BioRender.

The role of cell wall amidation in autolytic enzymes remains poorly understood. It is unclear how the amidation acts to either prohibit or alter the autolytic activity. Future work is needed to examine the hydrolysis activity, and that could be a possible approach to determine the impact of amidation. Furthermore, High-performance liquid chromatography (HPLC) analysis can be useful. This method would determine whether the overexpression of the *asnB* leads to altered cell wall composition or if the modification is dependent on other processes linked to magnesium and glucose. This aspect of cell wall metabolism is poorly defined and needs further study.

References

Ad, W., & Jl, S. (1971). Structure of the peptidoglycan from vegetative cell walls of Bacillus subtilis. *Biochemistry*, *10*(24). https://doi.org/10.1021/bi00800a001

Adams, D. W., & Errington, J. (2009). Bacterial cell division: Assembly, maintenance and disassembly of the Z ring. *Nature Reviews. Microbiology*, *7*(9), 642–653. https://doi.org/10.1038/nrmicro2198

Archibald, A. R., Hancock, I. C., & Harwood, C. R. (1993). Cell Wall Structure, Synthesis, and Turnover. In *Bacillus subtilis and Other Gram-Positive Bacteria* (pp. 379–410). John Wiley & Sons, Ltd. https://doi.org/10.1128/9781555818388.ch27

Atrih, A., Bacher, G., Allmaier, G., Williamson, M. P., & Foster, S. J. (1999a). Analysis of Peptidoglycan Structure from Vegetative Cells of *Bacillus subtilis* 168 and Role of PBP 5 in Peptidoglycan Maturation. *Journal of Bacteriology*, *181*(13), 3956–3966. https://www.ncbi.nlm.nih.gov/pmc/articles/PMC93885/

Atrih, A., Bacher, G., Allmaier, G., Williamson, M. P., & Foster, S. J. (1999b). Analysis of Peptidoglycan Structure from Vegetative Cells of *Bacillus subtilis* 168 and Role of PBP 5 in Peptidoglycan Maturation. *Journal of Bacteriology*, *181*(13), 3956–3966. https://www.ncbi.nlm.nih.gov/pmc/articles/PMC93885/

Barnett, J. P., van der Ploeg, R., Eijlander, R. T., Nenninger, A., Mendel, S., Rozeboom, R., Kuipers, O. P., van Dijl, J. M., & Robinson, C. (2009). The twin-arginine translocation (Tat) systems from *Bacillus subtilis* display a conserved mode of complex organization and similar substrate recognition requirements. *The FEBS Journal*, *276*(1), 232–243. https://doi.org/10.1111/j.1742-4658.2008.06776.x

Barreteau, H., Kovač, A., Boniface, A., Sova, M., Gobec, S., & Blanot, D. (2008). Cytoplasmic steps of peptidoglycan biosynthesis. *FEMS Microbiology Reviews*, *32*(2), 168–207. https://doi.org/10.1111/j.1574-6976.2008.00104.x

Bartholomew, J. W., & Mittwer, T. (1952). The Gram stain. *Bacteriological Reviews*, *16*(1), 1–29. https://doi.org/10.1128/br.16.1.1-29.1952

Bateman, A., & Bycroft, M. (2000). The structure of a LysM domain from *E. coli* membrane-bound lytic murein transglycosylase D (MltD)1. *Journal of Molecular Biology*, *299*(4), 1113–1119. https://doi.org/10.1006/jmbi.2000.3778

Bera, A., Herbert, S., Jakob, A., Vollmer, W., & Götz, F. (2005). Why are pathogenic staphylococci so lysozyme resistant? The peptidoglycan O-acetyltransferase OatA is the major determinant for lysozyme resistance of Staphylococcus aureus. *Molecular Microbiology*, *55*(3), 778–787. https://doi.org/10.1111/j.1365-2958.2004.04446.x

Bernard, E., Rolain, T., Courtin, P., Hols, P., & Chapot-Chartier, M.-P. (2011). Identification of the Amidotransferase AsnB1 as Being Responsible for meso-Diaminopimelic Acid Amidation in *Lactobacillus plantarum* Peptidoglycan ▿. *Journal of Bacteriology*, *193*(22), 6323–6330. https://doi.org/10.1128/JB.05060-11

Bisicchia, P., Noone, D., Lioliou, E., Howell, A., Quigley, S., Jensen, T., Jarmer, H., & Devine, K. M. (2007). The essential YycFG two-component system controls cell wall metabolism in *Bacillus subtilis*. *Molecular Microbiology*, *65*(1), 180–200. https://doi.org/10.1111/j.1365-2958.2007.05782.x

Bisson Filho, A. W., Hsu, Y.-P., Squyres, G. R., Kuru, E., Wu, F., Jukes, C., Sun, Y., Dekker, C., Holden, S., VanNieuwenhze, M. S., Brun, Y. V., & Garner, E. C. (2017). Treadmilling by FtsZ Filaments Drives Peptidoglycan Synthesis and Bacterial Cell Division. *Science (New York, N.Y.)*, *355*(6326), 739–743. https://doi.org/10.1126/science.aak9973

Blackman, S. A., Smith, T. J., & Foster, S. J. (1998). The role of autolysins during vegetative growth of *Bacillus subtilis* 168. *Microbiology*, *144*(1), 73–82. https://doi.org/10.1099/00221287-144-1-73

Blount, Z. D. (2015). The unexhausted potential of E. coli. *eLife*, *4*, e05826. https://doi.org/10.7554/eLife.05826

Boylan, R. J., Mendelson, N. H., Brooks, D., & Young, F. E. (1972). Regulation of the Bacterial Cell Wall: Analysis of a Mutant of *Bacillus subtilis* Defective in Biosynthesis of Teichoic Acid. *Journal of Bacteriology*, *110*(1), 281. https://doi.org/10.1128/jb.110.1.281-290.1972

Brown, C. T., Fishwick, L. K., Chokshi, B. M., Cuff, M. A., Jackson, J. M., Oglesby, T., Rioux, A. T., Rodriguez, E., Stupp, G. S., Trupp, A. H., Woollcombe-Clarke, J. S., Wright, T. N., Zaragoza, W. J., Drew, J. C., Triplett, E. W., & Nicholson, W. L. (2011). Whole-genome sequencing and phenotypic analysis of *Bacillus subtilis* mutants following evolution under conditions of relaxed selection for sporulation. *Applied and Environmental Microbiology*, *77*(19), 6867–6877. https://doi.org/10.1128/AEM.05272-11

Brown, S., Santa Maria, J. P., & Walker, S. (2013). Wall Teichoic Acids of Gram-Positive Bacteria. *Annual Review of Microbiology*, *67*, 10.1146/annurev-micro-092412–155620. https://doi.org/10.1146/annurev-micro-092412-155620

Brunet, Y. R., Wang, X., & Rudner, D. Z. (2019a). SweC and SweD are essential co-factors of the FtsEX-CwlO cell wall hydrolase complex in *Bacillus subtilis*. *PLOS Genetics*, *15*(8), e1008296. https://doi.org/10.1371/journal.pgen.1008296

Brunet, Y. R., Wang, X., & Rudner, D. Z. (2019b). SweC and SweD are essential co-factors of the FtsEX-CwlO cell wall hydrolase complex in *Bacillus subtilis*. *PLOS Genetics*, *15*(8), e1008296. https://doi.org/10.1371/journal.pgen.1008296

Buist, G., Kok, J., Leenhouts, K. J., Dabrowska, M., Venema, G., & Haandrikman, A. J. (1995). Molecular cloning and nucleotide sequence of the gene encoding the major peptidoglycan hydrolase of *Lactococcus lactis*, a muramidase needed for cell separation. *Journal of Bacteriology*, *177*(6), 1554–1563. https://www.ncbi.nlm.nih.gov/pmc/articles/PMC176772/

Buist, G., Steen, A., Kok, J., & Kuipers, O. P. (2008). LysM, a widely distributed protein motif for binding to (peptido)glycans. *Molecular Microbiology*, *68*(4), 838–847. https://doi.org/10.1111/j.1365-2958.2008.06211.x

Cabeen, M. T., & Jacobs-Wagner, C. (2005). Bacterial cell shape. *Nature Reviews Microbiology*, *3*(8), 601–610. https://doi.org/10.1038/nrmicro1205

Candela, T., & Fouet, A. (2006). Poly-gamma-glutamate in bacteria. *Molecular Microbiology*, *60*(5), 1091–1098. https://doi.org/10.1111/j.1365-2958.2006.05179.x

Carballido-López, R., Formstone, A., Li, Y., Ehrlich, S. D., Noirot, P., & Errington, J. (2006). Actin homolog MreBH governs cell morphogenesis by localization of the cell wall hydrolase LytE. *Developmental Cell*, *11*(3), 399–409. https://doi.org/10.1016/j.devcel.2006.07.017

Chastanet, A., & Carballido-Lopez, R. (2012). The actin-like MreB proteins in Bacillus subtilis: A new turn. *Frontiers in Bioscience-Scholar*, *4*(4), Article 4. https://doi.org/10.2741/S354

Chen, J., Fu, G., Gai, Y., Zheng, P., Zhang, D., & Wen, J. (2015). Combinatorial Sec pathway analysis for improved heterologous protein secretion in *Bacillus subtilis*: Identification of bottlenecks by systematic gene overexpression. *Microbial Cell Factories*, *14*(1), 92. https://doi.org/10.1186/s12934-015-0282-9

Chen, R., Guttenplan, S. B., Blair, K. M., & Kearns, D. B. (2009). Role of the sigmaD-dependent autolysins in *Bacillus subtilis* population heterogeneity. *Journal of Bacteriology*, *191*(18), 5775–5784. https://doi.org/10.1128/JB.00521-09

Claessen, D., Emmins, R., Hamoen, L. W., Daniel, R. A., Errington, J., & Edwards, D. H. (2008). Control of the cell elongation–division cycle by shuttling of PBP1 protein in *Bacillus subtilis*. *Molecular Microbiology*, *68*(4), 1029–1046. https://doi.org/10.1111/j.1365-2958.2008.06210.x

Claessen, D., Rozen, D. E., Kuipers, O. P., Søgaard-Andersen, L., & van Wezel, G. P. (2014). Bacterial solutions to multicellularity: A tale of biofilms, filaments and fruiting bodies. *Nature Reviews Microbiology*, *12*(2), 115–124. https://doi.org/10.1038/nrmicro3178

Courtin, P., Miranda, G., Guillot, A., Wessner, F., Mézange, C., Domakova, E., Kulakauskas, S., & Chapot-Chartier, M.-P. (2006). Peptidoglycan Structure Analysis of *Lactococcus lactis* Reveals the Presence of an l,d-Carboxypeptidase Involved in Peptidoglycan Maturation. *Journal of Bacteriology*, *188*(14), 5293–5298. https://doi.org/10.1128/jb.00285-06

Dajkovic, A., Tesson, B., Chauhan, S., Courtin, P., Keary, R., Flores, P., Marlière, C., Filipe, S. R., Chapot-Chartier, M., & Carballido-Lopez, R. (2017a). Hydrolysis of peptidoglycan is

modulated by amidation of meso-diaminopimelic acid and Mg2+ in *Bacillus subtilis*. *Molecular Microbiology*, *104*(6), 972–988. https://doi.org/10.1111/mmi.13673

Daniel, R. A., Harry, E. J., Katis, V. L., Wake, R. G., & Errington, J. (1998). Characterization of the essential cell division gene ftsL (yllD) of *Bacillus subtilis* and its role in the assembly of the division apparatus. *Molecular Microbiology*, *29*(2), 593–604. https://doi.org/10.1046/j.1365-2958.1998.00954.x

Davis, K. M., & Weiser, J. N. (2011). Modifications to the Peptidoglycan Backbone Help Bacteria To Establish Infection. *Infection and Immunity*, *79*(2), 562–570. https://doi.org/10.1128/iai.00651-10

D'Elia, M. A., Millar, K. E., Beveridge, T. J., & Brown, E. D. (2006). Wall Teichoic Acid Polymers Are Dispensable for Cell Viability in *Bacillus subtilis*. *Journal of Bacteriology*, *188*(23), 8313–8316. https://doi.org/10.1128/JB.01336-06

Desvaux, M., Dumas, E., Chafsey, I., & Hébraud, M. (2006). Protein cell surface display in Gram-positive bacteria: From single protein to macromolecular protein structure. *FEMS Microbiology Letters*, *256*(1), 1–15. https://doi.org/10.1111/j.1574-6968.2006.00122.x

Dobihal, G. S., Brunet, Y. R., Flores-Kim, J., & Rudner, D. Z. (2019). Homeostatic control of cell wall hydrolysis by the WalRK two-component signaling pathway in *Bacillus subtilis*. *eLife*, *8*, e52088. https://doi.org/10.7554/eLife.52088

Domínguez-Cuevas, P., Porcelli, I., Daniel, R. A., & Errington, J. (2013a). Differentiated roles for MreB-actin isologues and autolytic enzymes in *Bacillus subtilis* morphogenesis. *Molecular Microbiology*, *89*(6), 1084–1098. https://doi.org/10.1111/mmi.12335

Duchêne, M.-C., Rolain, T., Knoops, A., Courtin, P., Chapot-Chartier, M.-P., Dufrêne, Y. F., Hallet, B. F., & Hols, P. (2019). Distinct and Specific Role of NlpC/P60 Endopeptidases LytA and LytB in Cell Elongation and Division of *Lactobacillus plantarum*. *Frontiers in Microbiology*, *10*. https://doi.org/10.3389/fmicb.2019.00713

Emami, K., Guyet, A., Kawai, Y., Devi, J., Wu, L. J., Allenby, N., Daniel, R. A., & Errington, J. (2017). RodA as the missing glycosyltransferase in *Bacillus subtilis* and antibiotic discovery for the peptidoglycan polymerase pathway. *Nature Microbiology*, *2*, 16253. https://doi.org/10.1038/nmicrobiol.2016.253

Eugster, M. R., & Loessner, M. J. (2012). Wall Teichoic Acids Restrict Access of Bacteriophage Endolysin Ply118, Ply511, and PlyP40 Cell Wall Binding Domains to the Listeria monocytogenes Peptidoglycan. *Journal of Bacteriology*, *194*(23), 6498. https://doi.org/10.1128/JB.00808-12

Fernández-Tornero, C., García, E., López, R., Giménez-Gallego, G., & Romero, A. (2002). Two New Crystal Forms of the Choline-binding Domain of the Major Pneumococcal Autolysin: Insights into the Dynamics of the Active Homodimer. *Journal of Molecular Biology*, *321*(1), 163–173. https://doi.org/10.1016/S0022-2836(02)00596-X

Figge, R. M., Divakaruni, A. V., & Gober, J. W. (2004). MreB, the cell shape-determining bacterial actin homologue, co-ordinates cell wall morphogenesis in *Caulobacter crescentus*. *Molecular Microbiology*, *51*(5), 1321–1332. https://doi.org/10.1111/j.1365-2958.2003.03936.x

Figueiredo, T. A., Sobral, R. G., Ludovice, A. M., Almeida, J. M. F. de, Bui, N. K., Vollmer, W., Lencastre, H. de, & Tomasz, A. (2012). Identification of Genetic Determinants and Enzymes Involved with the Amidation of Glutamic Acid Residues in the Peptidoglycan of *Staphylococcus aureus*. *PLOS Pathogens*, *8*(1), e1002508. https://doi.org/10.1371/journal.ppat.1002508

Formstone, A., & Errington, J. (2005a). A magnesium-dependent *mreB* null mutant: Implications for the role of *mreB* in *Bacillus subtilis*. *Molecular Microbiology*, *55*(6), 1646–1657. https://doi.org/10.1111/j.1365-2958.2005.04506.x

Fukushima, T., Afkham, A., Kurosawa, S.-I., Tanabe, T., Yamamoto, H., & Sekiguchi, J. (2006). A new D,L-endopeptidase gene product, YojL (renamed CwlS), plays a role in cell separation with LytE and LytF in *Bacillus subtilis*. *Journal of Bacteriology*, *188*(15), 5541–5550. https://doi.org/10.1128/JB.00188-06

Fukushima, T., Kitajima, T., Yamaguchi, H., Ouyang, Q., Furuhata, K., Yamamoto, H., Shida, T., & Sekiguchi, J. (2008). Identification and characterization of novel cell wall hydrolase CwlT: A

two-domain autolysin exhibiting n-acetylmuramidase and DL-endopeptidase activities. *The Journal of Biological Chemistry*, *283*(17), 11117–11125. https://doi.org/10.1074/jbc.M706626200

Fukushima, T., Yao, Y., Kitajima, T., Yamamoto, H., & Sekiguchi, J. (2007). Characterization of new l,d-endopeptidase gene product CwlK (previous YcdD) that hydrolyzes peptidoglycan in *Bacillus subtilis*. *Molecular Genetics and Genomics*, *278*(4), 371–383. https://doi.org/10.1007/s00438-007-0255-8

Garde, S., Chodisetti, P. K., & Reddy, M. (2021). Peptidoglycan: Structure, Synthesis, and Regulation. *EcoSal Plus*, *9*(2). https://doi.org/10.1128/ecosalplus.ESP-0010-2020

Green, E. R., & Mecsas, J. (2016). Bacterial Secretion Systems – An overview. *Microbiology Spectrum*, *4*(1), 10.1128/microbiolspec.VMBF-0012–2015. https://doi.org/10.1128/microbiolspec.VMBF-0012-2015

Gründling, A., & Schneewind, O. (2007). Synthesis of glycerol phosphate lipoteichoic acid in *Staphylococcus aureus*. *Proceedings of the National Academy of Sciences*, *104*(20), 8478–8483. https://doi.org/10.1073/pnas.0701821104

Guariglia-Oropeza, V., & Helmann, J. D. (2011). Bacillus subtilis σV Confers Lysozyme Resistance by Activation of Two Cell Wall Modification Pathways, Peptidoglycan O-Acetylation and d-Alanylation of Teichoic Acids. *Journal of Bacteriology*, *193*(22), 6223–6232. https://doi.org/10.1128/jb.06023-11

Guyet, A., Alofi, A., & Daniel, R. A. (2023). Insights into the Roles of Lipoteichoic Acids and MprF in *Bacillus subtilis*. *mBio*, *14*(1), e02667-22. https://doi.org/10.1128/mbio.02667-22

Han, J., Zhao, X., Zhao, X., Li, P., & Gu, Q. (2023). Insight into the structure, biosynthesis, isolation method and biological function of teichoic acid in different gram-positive microorganisms: A review. *International Journal of Biological Macromolecules*, *253*, 126825. https://doi.org/10.1016/j.ijbiomac.2023.126825

Hanahan, D., Jessee, J., & Bloom, F. R. (1991). Plasmid transformation of *Escherichia coli* and other bacteria. *Methods in Enzymology*,*204*, 63–113.https://doi.org/10.1016/0076-6879(91)04006-a

Hartl, D. L., & Dykhuizen, D. E. (1984). The population genetics of *Escherichia coli. Annual Review of Genetics*, *18*, 31–68. https://doi.org/10.1146/annurev.ge.18.120184.000335

Harwood, C. R., & Kikuchi, Y. (2022). The ins and outs of *Bacillus* proteases: Activities, functions and commercial significance. *FEMS Microbiology Reviews*, *46*(1), fuab046. https://doi.org/10.1093/femsre/fuab046

Hashimoto, M., Ooiwa, S., & Sekiguchi, J. (2012). Synthetic Lethality of the *lytE cwlO* Genotype in *Bacillus subtilis* Is Caused by Lack of d,l-Endopeptidase Activity at the Lateral Cell Wall. *Journal of Bacteriology*, *194*(4), 796–803. https://doi.org/10.1128/JB.05569-11

Helmann, J. D. (2016). *Bacillus subtilis* extracytoplasmic function (ECF) sigma factors and defense of the cell envelope. *Current Opinion in Microbiology*, *30*, 122–132. https://doi.org/10.1016/j.mib.2016.02.002

Helmann, J. D., Márquez, L. M., & Chamberlin, M. J. (1988). Cloning, sequencing, and disruption of the *Bacillus subtilis* sigma 28 gene. *Journal of Bacteriology*, *170*(4), 1568–1574. https://doi.org/10.1128/jb.170.4.1568-1574.1988

Herbold, D. R., & Glaser, L. (1975). *Bacillus subtilis* N-acetylmuramic acid L-alanine amidase. *Journal of Biological Chemistry*, *250*(5), 1676–1682. https://doi.org/10.1016/S0021-9258(19)41746-8

Hobot, J. A. (1990). New aspects of bacterial ultrastructure as revealed by modern acrylics for electron microscopy. *Journal of Structural Biology*, *104*(1), 169–177. https://doi.org/10.1016/1047-8477(90)90073-L

Hobot, J. A., Carlemalm, E., Villiger, W., & Kellenberger, E. (1984a). Periplasmic gel: New concept resulting from the reinvestigation of bacterial cell envelope ultrastructure by new methods. *Journal of Bacteriology*, *160*(1), 143–152. https://doi.org/10.1128/jb.160.1.143-152.1984

Höltje, J. V. (1996). Bacterial lysozymes. *EXS*, *75*, 65–74. https://doi.org/10.1007/978-3-0348-9225-4_4

Horsburgh, G. J., Atrih, A., & Foster, S. J. (2003). Characterization of LytH, a Differentiation-Associated Peptidoglycan Hydrolase of *Bacillus subtilis* Involved in Endospore Cortex

Maturation. *Journal of Bacteriology*, *185*(13), 3813. https://doi.org/10.1128/JB.185.13.3813-3820.2003

Horsburgh, G. J., Atrih, A., Williamson, M. P., & Foster, S. J. (2003). LytG of *Bacillus subtilis* is a novel peptidoglycan hydrolase: The major active glucosaminidase. *Biochemistry*, *42*(2), 257–264. https://doi.org/10.1021/bi020498c

Hoyland, C. N., Aldridge, C., Cleverley, R. M., Duchêne, M.-C., Minasov, G., Onopriyenko, O., Sidiq, K., Stogios, P. J., Anderson, W. F., Daniel, R. A., Savchenko, A., Vollmer, W., & Lewis, R. J. (2014). Structure of the LdcB LD-Carboxypeptidase Reveals the Molecular Basis of Peptidoglycan Recognition. *Structure(London, England:1993)*, *22*(7), 949. https://doi.org/10.1016/j.str.2014.04.015

Huang, W.-Z., Wang, J.-J., Chen, H.-J., Chen, J.-T., & Shaw, G.-C. (2013). The heat-inducible essential response regulator WalR positively regulates transcription of sigI, *mreBH* and *lytE* in *Bacillus subtilis* under heat stress. *Research in Microbiology*, *164*(10), 998–1008. https://doi.org/10.1016/j.resmic.2013.10.003

Ishikawa, S., Hara, Y., Ohnishi, R., & Sekiguchi, J. (1998a). Regulation of a new cell wall hydrolase gene, *cwlF*, which affects cell separation in *Bacillus subtilis. Journal of Bacteriology*, *180*(9), 2549–2555. https://doi.org/10.1128/JB.180.9.2549-2555.1998

Iyer, L. M., & Aravind, L. (2012). Insights from the architecture of the bacterial transcription apparatus. *Journal of Structural Biology*, *179*(3), 299–319. https://doi.org/10.1016/j.jsb.2011.12.013

Jakutytė, L., Baptista, C., São-José, C., Daugelavičius, R., Carballido-López, R., & Tavares, P. (2011). Bacteriophage Infection in Rod-Shaped Gram-Positive Bacteria: Evidence for a Preferential Polar Route for Phage SPP1 Entry in Bacillus subtilis ▿ . *Journal of Bacteriology*, *193*(18), 4893–4903. https://doi.org/10.1128/JB.05104-11

Jolliffe, L. K., Doyle, R. J., & Streips, U. N. (1981). The energized membrane and cellular autolysis in *Bacillus subtilis*. *Cell*, *25*(3), 753–763. https://doi.org/10.1016/0092-8674(81)90183-5

Jones, L. J., Carballido-López, R., & Errington, J. (2001). Control of cell shape in bacteria: Helical, actin-like filaments in Bacillus subtilis. *Cell*, *104*(6), 913–922. https://doi.org/10.1016/s0092-8674(01)00287-2

Karamanos, Y. (1997). Endo-N-acetyl-beta-D-glucosaminidases and their potential substrates: Structure/function relationships. *Research in Microbiology*, *148*(8), 661–671. https://doi.org/10.1016/S0923-2508(99)80065-5

Kasahara, J., Kiriyama, Y., Miyashita, M., Kondo, T., Yamada, T., Yazawa, K., Yoshikawa, R., & Yamamoto, H. (2016a). Teichoic Acid Polymers Affect Expression and Localization of dl-Endopeptidase LytE Required for Lateral Cell Wall Hydrolysis in *Bacillus subtilis. Journal of Bacteriology*, *198*(11), 1585–1594. https://doi.org/10.1128/JB.00003-16

Kawai, Y., Daniel, R. A., & Errington, J. (2009). Regulation of cell wall morphogenesis in *Bacillus subtilis* by recruitment of PBP1 to the MreB helix. *Molecular Microbiology*, *71*(5), 1131–1144. https://doi.org/10.1111/j.1365-2958.2009.06601.x

Kawamura, F., & Doi, R. H. (1984). Construction of a *Bacillus subtilis* double mutant deficient in extracellular alkaline and neutral proteases. *Journal of Bacteriology*, *160*(1), 442–444. https://doi.org/10.1128/jb.160.1.442-444.1984

Kiriyama, Y., Yazawa, K., Tanaka, T., Yoshikawa, R., Yamane, H., Hashimoto, M., Sekiguchi, J., & Yamamoto, H. (2014a). Localization and expression of the *Bacillus subtilis* DL-endopeptidase LytF are influenced by mutations in LTA synthases and glycolipid anchor synthetic enzymes. *Microbiology*, *160*(12), 2639–2649. https://doi.org/10.1099/mic.0.080366-0

Kj, G., Ms, S., & J, I. (1986). Nucleotide sequence of Bacillus phage phi 29 genes 14 and 15: Homology of gene 15 with other phage lysozymes. *Nucleic Acids Research*, *14*(24). https://doi.org/10.1093/nar/14.24.10001

Kleppe, G., Yu, W., & Strominger, J. L. (1982). Penicillin-binding proteins in *Bacillus subtilis* mutants. *Antimicrobial Agents and Chemotherapy*, *21*(6), 979–983. https://www.ncbi.nlm.nih.gov/pmc/articles/PMC182056/

Koch, A. L., & Doyle, R. J. (1985). Inside-to-outside growth and turnover of the wall of gram-positive rods. *Journal of Theoretical Biology*, *117*(1), 137–157. https://doi.org/10.1016/s0022-5193(85)80169-7

Koo, B.-M., Kritikos, G., Farelli, J. D., Todor, H., Tong, K., Kimsey, H., Wapinski, I., Galardini, M., Cabal, A., Peters, J. M., Hachmann, A.-B., Rudner, D. Z., Allen, K. N., Typas, A., & Gross, C. A. (2017). Construction and Analysis of Two Genome-Scale Deletion Libraries for *Bacillus subtilis*. *Cell Systems*, *4*(3), 291-305.e7. https://doi.org/10.1016/j.cels.2016.12.013

Kunst, F., Ogasawara, N., Moszer, I., Albertini, A. M., Alloni, G., Azevedo, V., Bertero, M. G., Bessières, P., Bolotin, A., Borchert, S., Borriss, R., Boursier, L., Brans, A., Braun, M., Brignell, S. C., Bron, S., Brouillet, S., Bruschi, C. V., Caldwell, B., … Danchin, A. (1997). The complete genome sequence of the Gram-positive bacterium *Bacillus subtilis*. *Nature*, *390*(6657), 249–256. https://doi.org/10.1038/36786

Kuroda, A., & Sekiguchi, J. (1991). Molecular cloning and sequencing of a major *Bacillus subtilis* autolysin gene. *Journal of Bacteriology*, *173*(22), 7304–7312. https://www.ncbi.nlm.nih.gov/pmc/articles/PMC209238/

Kuroda, A., & Sekiguchi, J. (1993). High-level transcription of the major *Bacillus subtilis* autolysin operon depends on expression of the sigma D gene and is affected by a sin (flaD) mutation. *Journal of Bacteriology*, *175*(3), 795–801. https://doi.org/10.1128/jb.175.3.795-801.1993

Laaberki, M.-H., Pfeffer, J., Clarke, A. J., & Dworkin, J. (2011). *O*-Acetylation of Peptidoglycan Is Required for Proper Cell Separation and S-layer Anchoring in *Bacillus anthracis**. *Journal of Biological Chemistry*, *286*(7), 5278–5288. https://doi.org/10.1074/jbc.M110.183236

Lazarevic, V., Abellan, F.-X., Möller, S. B., Karamata, D., & Mauël, C. (2002). Comparison of ribitol and glycerol teichoic acid genes in *Bacillus subtilis* W23 and 168: Identical function, similar divergent organization, but different regulation. *Microbiology (Reading, England)*, *148*(Pt 3), 815–824. https://doi.org/10.1099/00221287-148-3-815

Lazarevic, V., Margot, P., Soldo, B., & Karamata, D. (1992). Sequencing and analysis of the *Bacillus subtilis lytRABC* divergon: A regulatory unit encompassing the structural genes of the N-acetylmuramoyl-L-alanine amidase and its modifier. *Microbiology*, *138*(9), 1949–1961. https://doi.org/10.1099/00221287-138-9-1949

Lazarevic, V., Soldo, B., Médico, N., Pooley, H., Bron, S., & Karamata, D. (2005). *Bacillus subtilis* alpha-phosphoglucomutase is required for normal cell morphology and biofilm formation. *Applied and Environmental Microbiology*, *71*(1), 39–45. https://doi.org/10.1128/AEM.71.1.39-45.2005

Levefaudes, M., Patin, D., de Sousa-d'Auria, C., Chami, M., Blanot, D., Hervé, M., Arthur, M., Houssin, C., & Mengin-Lecreulx, D. (2015). Diaminopimelic Acid Amidation in Corynebacteriales. *The Journal of Biological Chemistry*, *290*(21), 13079–13094. https://doi.org/10.1074/jbc.M115.642843

Liu, Y., Li, J., Du, G., Chen, J., & Liu, L. (2017). Metabolic engineering of *Bacillus subtilis* fueled by systems biology: Recent advances and future directions. *Biotechnology Advances*, *35*(1), 20–30. https://doi.org/10.1016/j.biotechadv.2016.11.003

Mandelstam, J., & Waites, W. M. (1968). Sporulation in *Bacillus subtilis*. The role of exoprotease. *Biochemical Journal*, *109*(5), 793–801. https://doi.org/10.1042/bj1090793

Margot, P., Mauël, C., & Karamata, D. (1994a). The gene of the N-acetylglucosaminidase, a *Bacillus subtilis* 168 cell wall hydrolase not involved in vegetative cell autolysis. *Molecular Microbiology*, *12*(4), 535–545. https://doi.org/10.1111/j.1365-2958.1994.tb01040.x

Margot, P., Pagni, M., & Karamata, D. (1999a). *Bacillus subtilis* 168 gene *lytF* encodes a gamma-D-glutamate-meso-diaminopimelate muropeptidase expressed by the alternative vegetative sigma factor, sigmaD. *Microbiology (Reading, England)*, *145 (Pt 1)*, 57–65. https://doi.org/10.1099/13500872-145-1-57

Margot, P., Whalen, M., Gholamhoseinian, A., Piggot, P., & Karamata, D. (1998). The *lytE* Gene of *Bacillus subtilis* 168 Encodes a Cell Wall Hydrolase. *Journal of Bacteriology*, *180*(8), 2272–2272. https://doi.org/10.1128/jb.180.8.2272-2272.1998

Marks, D. S., Hopf, T. A., & Sander, C. (2012). Protein structure prediction from sequence variation. *Nature Biotechnology*, *30*(11), 1072–1080. https://doi.org/10.1038/nbt.2419

McDonnell, G. E., Wood, H., Devine, K. M., & McConnell, D. J. (1994). Genetic control of bacterial suicide: Regulation of the induction of PBSX in *Bacillus subtilis*. *Journal of Bacteriology*, *176*(18), 5820–5830. https://doi.org/10.1128/jb.176.18.5820-5830.1994

Meisner, J., Llopis, P. M., Sham, L.-T., Garner, E., Bernhardt, T. G., & Rudner, D. Z. (2013). FtsEX is required for CwlO peptidoglycan hydrolase activity during cell wall elongation in *Bacillus subtilis*. *Molecular Microbiology*, *89*(6), 1069–1083. https://doi.org/10.1111/mmi.12330

Mi, C., W, V., As, K., S, I., F, G., S, B., & A, T. (2006). Attenuation of penicillin resistance in a peptidoglycan O-acetyl transferase mutant of Streptococcus pneumoniae. *Molecular Microbiology*, *61*(6). https://doi.org/10.1111/j.1365-2958.2006.05340.x

Milohanic, E., Jonquières, R., Cossart, P., Berche, P., & Gaillard, J. L. (2001). The autolysin Ami contributes to the adhesion of *Listeria monocytogenes* to eukaryotic cells via its cell wall anchor. *Molecular Microbiology*, *39*(5), 1212–1224. https://doi.org/10.1111/j.1365-2958.2001.02208.x

Morlot, C., Straume, D., Peters, K., Hegnar, O. A., Simon, N., Villard, A.-M., Contreras-Martel, C., Leisico, F., Breukink, E., Gravier-Pelletier, C., Le Corre, L., Vollmer, W., Pietrancosta, N., Håvarstein, L. S., & Zapun, A. (2018). Structure of the essential peptidoglycan amidotransferase MurT/GatD complex from *Streptococcus pneumoniae*. *Nature Communications*, *9*(1), 3180. https://doi.org/10.1038/s41467-018-05602-w

Moynihan, P. J., & Clarke, A. J. (2010). *O*-Acetylation of Peptidoglycan in Gram-negative Bacteria. *Journal of Biological Chemistry*, *285*(17), 13264–13273. https://doi.org/10.1074/jbc.M110.107086

Münch, D., Roemer, T., Lee, S. H., Engeser, M., Sahl, H. G., & Schneider, T. (2012). Identification and in vitro analysis of the GatD/MurT enzyme-complex catalyzing lipid II amidation in *Staphylococcus aureus*. *PLoS Pathogens*, *8*(1), e1002509. https://doi.org/10.1371/journal.ppat.1002509

Murray, T., Popham, D. L., & Setlow, P. (1998). *Bacillus subtilis* Cells Lacking Penicillin-Binding Protein 1 Require Increased Levels of Divalent Cations for Growth. *Journal of Bacteriology*, *180*(17), 4555–4563. https://doi.org/10.1128/jb.180.17.4555-4563.1998

N, O., T, Y., & T, M. (1982). Identification of 2-amino-2-deoxyglucose residues in the peptidoglucan of S*treptococcus pneumoniae. Carbohydrate Research*, *107*(1). https://doi.org/10.1016/s0008-6215(00)80785-5

Neuhaus, F. C., & Baddiley, J. (2003). A Continuum of Anionic Charge: Structures and Functions of d-Alanyl-Teichoic Acids in Gram-Positive Bacteria. *Microbiology and Molecular Biology Reviews : MMBR*, *67*(4), 686–723. https://doi.org/10.1128/MMBR.67.4.686-723.2003

Nicolas, P., Mäder, U., Dervyn, E., Rochat, T., Leduc, A., Pigeonneau, N., Bidnenko, E., Marchadier, E., Hoebeke, M., Aymerich, S., Becher, D., Bisicchia, P., Botella, E., Delumeau, O., Doherty, G., Denham, E. L., Fogg, M. J., Fromion, V., Goelzer, A., … Noirot, P. (2012). Condition-Dependent Transcriptome Reveals High-Level Regulatory Architecture in *Bacillus subtilis. Science*, *335*(6072), 1103–1106. https://doi.org/10.1126/science.1206848

Ogura, M., & Asai, K. (2016). Glucose Induces ECF Sigma Factor Genes, *sigX* and *sigM*, Independent of Cognate Anti-sigma Factors through Acetylation of CshA in *Bacillus subtilis. Frontiers in Microbiology*, *7*, 1918. https://doi.org/10.3389/fmicb.2016.01918

O'Halloran, D. P., Wynne, K., & Geoghegan, J. A. (2015). Protein A Is Released into the *Staphylococcus aureus* Culture Supernatant with an Unprocessed Sorting Signal. *Infection and Immunity*, *83*(4), 1598. https://doi.org/10.1128/IAI.03122-14

Ohnishi, R., Ishikawa, S., & Sekiguchi, J. (1999). Peptidoglycan Hydrolase LytF Plays a Role in Cell Separation with CwlF during Vegetative Growth of *Bacillus subtilis*. *Journal of Bacteriology*, *181*(10), 3178–3184. https://www.ncbi.nlm.nih.gov/pmc/articles/PMC93774/

Ohno, N., Yadomae, T., & Miyazaki, T. (1982). Identification of 2-amino-2-deoxyglucose residues in the peptidoglucan of *Streptococcus pneumoniae*. *Carbohydrate Research*, *107*(1), 152–155. https://doi.org/10.1016/S0008-6215(00)80785-5

O'Toole, G. A. (2016). Classic Spotlight: How the Gram Stain Works. *Journal of Bacteriology*, *198*(23), 3128. https://doi.org/10.1128/JB.00726-16

Percy, M. G., & Gründling, A. (2014a). Lipoteichoic Acid Synthesis and Function in Gram-Positive Bacteria. *Annual Review of Microbiology*, *68*(1), 81–100. https://doi.org/10.1146/annurev-micro-091213-112949

Percy, M. G., & Gründling, A. (2014b). Lipoteichoic acid synthesis and function in gram-positive bacteria. *Annual Review of Microbiology*, *68*, 81–100. https://doi.org/10.1146/annurev-micro-091213-112949

Perkins, H. R. (2012). Microbial Cell Walls and Membranes. Springer Science & Business Media.

Pohl, S., Bhavsar, G., Hulme, J., Bloor, A. E., Misirli, G., Leckenby, M. W., Radford, D. S., Smith, W., Wipat, A., Williamson, E. D., Harwood, C. R., & Cranenburgh, R. M. (2013). Proteomic analysis of *Bacillus subtilis* strains engineered for improved production of heterologous proteins. *Proteomics*, *13*(22), 3298–3308. https://doi.org/10.1002/pmic.201300183

Popham, D. L., & Setlow, P. (1996). Phenotypes of *Bacillus subtilis* mutants lacking multiple class A high-molecular-weight penicillin-binding proteins. *Journal of Bacteriology*, *178*(7), 2079–2085. https://www.ncbi.nlm.nih.gov/pmc/articles/PMC177908/

Rajagopal, M., & Walker, S. (2017). Envelope Structures of Gram-Positive Bacteria. In F. Bagnoli & R. Rappuoli (Eds.), *Protein and Sugar Export and Assembly in Gram-positive Bacteria* (pp. 1–44). Springer International Publishing. https://doi.org/10.1007/82_2015_5021

Rashid, M. H., Kuroda, A., & Sekiguchi, J. (1993). *Bacillus subtilis* mutant deficient in the major autolytic amidase and glucosaminidase is impaired in motility. *FEMS Microbiology Letters*, *112*(2), 135–140. https://doi.org/10.1111/j.1574-6968.1993.tb06438.x

Reichmann, N. T., Cassona, C. P., & Gründling, A. (2013). Revised mechanism of D-alanine incorporation into cell wall polymers in Gram-positive bacteria. *Microbiology (Reading, England)*, *159*(Pt 9), 1868–1877. https://doi.org/10.1099/mic.0.069898-0

Rohde, M. (2019). The Gram-Positive Bacterial Cell Wall. *Microbiology Spectrum*, *7*(3). https://doi.org/10.1128/microbiolspec.GPP3-0044-2018

Salzberg, L. I., Powell, L., Hokamp, K., Botella, E., Noone, D., & Devine, K. M. (2013). The WalRK (YycFG) and σ(I) RsgI regulators cooperate to control CwlO and LytE expression in exponentially growing and stressed *Bacillus subtilis* cells. *Molecular Microbiology*, *87*(1), 180–195. https://doi.org/10.1111/mmi.12092

Sassine, J., Sousa, J., Lalk, M., Daniel, R. A., & Vollmer, W. (2020). Cell morphology maintenance in *Bacillus subtilis* through balanced peptidoglycan synthesis and hydrolysis. *Scientific Reports*, *10*(1), 17910. https://doi.org/10.1038/s41598-020-74609-5

Schallmey, M., Singh, A., & Ward, O. P. (2004). Developments in the use of *Bacillus* species for industrial production. *Canadian Journal of Microbiology*, *50*(1), 1–17. https://doi.org/10.1139/w03-076

Scheffers, D.-J., & Pinho, M. G. (2005). Bacterial Cell Wall Synthesis: New Insights from Localization Studies. *Microbiology and Molecular Biology Reviews*, *69*(4), 585–607. https://doi.org/10.1128/MMBR.69.4.585-607.2005

Schirner, K., Marles-Wright, J., Lewis, R. J., & Errington, J. (2009). Distinct and essential morphogenic functions for wall- and lipo-teichoic acids in *Bacillus subtilis*. *The EMBO Journal*, *28*(7), 830–842. https://doi.org/10.1038/emboj.2009.25

Schleifer, K. H., & Kandler, O. (1972). Peptidoglycan types of bacterial cell walls and their taxonomic implications. *Bacteriological Reviews*, *36*(4), 407–477. https://www.ncbi.nlm.nih.gov/pmc/articles/PMC408328/

Schmidt, K. L., Peterson, N. D., Kustusch, R. J., Wissel, M. C., Graham, B., Phillips, G. J., & Weiss, D. S. (2004). A predicted ABC transporter, FtsEX, is needed for cell division in *Escherichia coli*. *Journal of Bacteriology*, *186*(3), 785–793. https://doi.org/10.1128/JB.186.3.785-793.2004

Sham, L.-T., Barendt, S. M., Kopecky, K. E., & Winkler, M. E. (2011). Essential PcsB putative peptidoglycan hydrolase interacts with the essential FtsXSpn cell division protein in *Streptococcus pneumoniae* D39. *Proceedings of the National Academy of Sciences of the United States of America*, *108*(45), E1061–E1069. https://doi.org/10.1073/pnas.1108323108

Silhavy, T. J., Kahne, D., & Walker, S. (2010a). The Bacterial Cell Envelope. *Cold Spring Harbor Perspectives in Biology*, *2*(5), a000414. https://doi.org/10.1101/cshperspect.a000414

Smith, T. J., Blackman, S. A., & Foster, S. J. (2000). Autolysins of *Bacillus subtilis*: Multiple enzymes with multiple functions. *Microbiology*, *146*(2), 249–262. https://doi.org/10.1099/00221287-146-2-249

Soldo, B., Lazarevic, V., & Karamata, D. (2002). *tagO* is involved in the synthesis of all anionic cell-wall polymers in *Bacillus subtilis* 168aaThe EMBL accession number for the nucleotide sequence reported in this paper is AJ004803. *Microbiology*, *148*(7), 2079–2087. https://doi.org/10.1099/00221287-148-7-2079

Souza, B. M., Castro, T. L. de P., Carvalho, R. D. de O., Seyffert, N., Silva, A., Miyoshi, A., & Azevedo, V. (2014). σECF factors of gram-positive bacteria: A focus on *Bacillus subtilis* and the CMNR group. *Virulence*, *5*(5), 587–600. https://doi.org/10.4161/viru.29514

Sun, J., Rutherford, S. T., Silhavy, T. J., & Huang, K. C. (2022). Physical properties of the bacterial outer membrane. *Nature Reviews. Microbiology*, *20*(4), 236–248. https://doi.org/10.1038/s41579-021-00638-0

Suzuki, T., & Tahara, Y. (n.d.). Characterization of the *Bacillus subtilis* ywtD Gene, Whose Product Is Involved in ✐-Polyglutamic Acid Degradation. *J. BACTERIOL.*

Swoboda, J. G., Campbell, J., Meredith, T. C., & Walker, S. (2010). Wall Teichoic Acid Function, Biosynthesis, and Inhibition. *Chembiochem : A European Journal of Chemical Biology*, *11*(1), 35–45. https://doi.org/10.1002/cbic.200900557

Takahashi, Y., Takechi, K., Takio, S., & Takano, H. (2016a). Both the transglycosylase and transpeptidase functions in plastid penicillin-binding protein are essential for plastid division in Physcomitrella patens. *Proceedings of the Japan Academy. Series B, Physical and Biological Sciences*, *92*(10), 499–508. https://doi.org/10.2183/pjab.92.499

Tesson, B., Dajkovic, A., Keary, R., Marlière, C., Dupont-Gillain, C. C., & Carballido-López, R. (2022). Magnesium rescues the morphology of *Bacillus subtilis mreB* mutants through its inhibitory effect on peptidoglycan hydrolases. *Scientific Reports*, *12*, 1137. https://doi.org/10.1038/s41598-021-04294-5

Thackray, P. D., & Moir, A. (2003). SigM, an extracytoplasmic function sigma factor of Bacillus subtilis, is activated in response to cell wall antibiotics, ethanol, heat, acid, and superoxide stress. *Journal of Bacteriology*, *185*(12), 3491–3498. https://doi.org/10.1128/JB.185.12.3491-3498.2003

Typas, A., Banzhaf, M., Gross, C. A., & Vollmer, W. (2012). From the regulation of peptidoglycan synthesis to bacterial growth and morphology. *Nature Reviews Microbiology*, *10*(2), 123–136. https://doi.org/10.1038/nrmicro2677

Uelze, L. (2022). An analysis of LysM domain function in LytE when fulfilling the D,L-endopeptidase requirement for viability in *Bacillus subtilis.* https://doi.org/10.1101/2022.01.12.475998

van Dijl, J. M., Bolhuis, A., Tjalsma, H., Jongbloed, J. D. H., de Jong, A., & Bron, S. (2001). Protein transport pathways in *Bacillus subtilis*: A genome-based road map. In A. L. Sonenshein, J. A. Hoch, & R. Losick (Eds.), *Bacillus subtilis and its closest relatives: From genes to cells* (pp. 337–355). ASM Press.

Veiga, P., Erkelenz, M., Bernard, E., Courtin, P., Kulakauskas, S., & Chapot-Chartier, M.-P. (2009a). Identification of the Asparagine Synthase Responsible for d-Asp Amidation in the Lactococcus lactis Peptidoglycan Interpeptide Crossbridge. *Journal of Bacteriology*, *191*(11), 3752–3757. https://doi.org/10.1128/jb.00126-09

Visweswaran, G. R. R., Leenhouts, K., van Roosmalen, M., Kok, J., & Buist, G. (2014). Exploiting the peptidoglycan-binding motif, LysM, for medical and industrial applications. *Applied Microbiology and Biotechnology*, *98*(10), 4331–4345. https://doi.org/10.1007/s00253-014-5633-7

Voigt, B., Antelmann, H., Albrecht, D., Ehrenreich, A., Maurer, K.-H., Evers, S., Gottschalk, G., Van Dijl, J. M., Schweder, T., & Hecker, M. (2009). Cell Physiology and Protein Secretion of *Bacillus licheniformis* Compared to *Bacillus subtilis*. *Microbial Physiology*, *16*(1–2), 53–68. https://doi.org/10.1159/000142894

Vollmer, W., Joris, B., Charlier, P., & Foster, S. (2008). Bacterial peptidoglycan (murein) hydrolases. *FEMS Microbiology Reviews*, *32*(2), 259–286. https://doi.org/10.1111/j.1574-6976.2007.00099.x

von Heijne, G. (1986). A new method for predicting signal sequence cleavage sites. *Nucleic Acids Research*, *14*(11), 4683–4690. https://www.ncbi.nlm.nih.gov/pmc/articles/PMC311474/

Waligora, A. J., Hennequin, C., Mullany, P., Bourlioux, P., Collignon, A., & Karjalainen, T. (2001). Characterization of a cell surface protein of *Clostridium difficile* with adhesive properties. *Infection and Immunity*, *69*(4), 2144–2153. https://doi.org/10.1128/IAI.69.4.2144-2153.2001

Walter, A., Unsleber, S., Rismondo, J., Jorge, A. M., Peschel, A., Gründling, A., & Mayer, C. (2020). Phosphoglycerol-type wall- and lipoteichoic acids are enantiomeric polymers differentially cleaved by the stereospecific glycerophosphodiesterase GlpQ (p. 2020.01.08.899310). bioRxiv. https://doi.org/10.1101/2020.01.08.899310

Warth, A. D., & Strominger, J. L. (1971). Structure of the peptidoglycan from vegetative cell walls of *Bacillus subtilis*. *Biochemistry*, *10*(24), 4349–4358. https://doi.org/10.1021/bi00800a001

Webb, A. J., Karatsa-Dodgson, M., & Gründling, A. (2009). Two-enzyme systems for glycolipid and polyglycerolphosphate lipoteichoic acid synthesis in *Listeria monocytogenes*. *Molecular Microbiology*, *74*(2), 299–314. https://doi.org/10.1111/j.1365-2958.2009.06829.x

Wecke, J., Madela, K., & Fischer, W. (1997). The absence of D-alanine from lipoteichoic acid and wall teichoic acid alters surface charge, enhances autolysis and increases susceptibility to methicillin in *Bacillus subtilis*. *Microbiology*, *143*(9), 2953–2960. https://doi.org/10.1099/00221287-143-9-2953

Weidel, W., Frank, H., & Martin, H. H. (1960). The rigid layer of the cell wall of *Escherichia coli* strain B. *Journal of General Microbiology*, *22*, 158–166. https://doi.org/10.1099/00221287-22-1-158

Weidel, W., & Pelzer, H. (1964). Bagshaped macromolecules--a new outlook on bacterial cell walls. *Advances in Enzymology and Related Subjects of Biochemistry*, *26*, 193–232. https://doi.org/10.1002/9780470122716.ch5

Whisstock, J. C., & Lesk, A. M. (1999). SH3 domains in prokaryotes. *Trends in Biochemical Sciences*, *24*(4), 132–133. https://doi.org/10.1016/S0968-0004(99)01366-3

Wilson, S. A., Tank, R. K. J., Hobbs, J. K., Foster, S. J., & Garner, E. C. (n.d.). An exhaustive multiple knockout approach to understanding cell wall hydrolase function in *Bacillus subtilis*. *mBio*, *14*(5), e01760-23. https://doi.org/10.1128/mbio.01760-23

Wilson, S. A., Tank, R. K. J., Hobbs, J. K., Foster, S. J., & Garner, E. C. (2023). An Exhaustive Multiple Knockout Approach to Understanding Cell Wall Hydrolase Function in *Bacillus subtilis* (p. 2021.02.18.431929). bioRxiv. https://doi.org/10.1101/2021.02.18.431929

Wood, H. E., Dawson, M. T., Devine, K. M., & McConnell, D. J. (1990). Characterization of PBSX, a defective prophage of *Bacillus subtilis*. *Journal of Bacteriology*, *172*(5), 2667–2674. https://doi.org/10.1128/jb.172.5.2667-2674.1990

Work, E. (1961). The mucopeptides of bacterial cell walls. A review. *Journal of General Microbiology*, *25*, 169–189. https://doi.org/10.1099/00221287-25-2-167

Wörmann, M. E., Corrigan, R. M., Simpson, P. J., Matthews, S. J., & Gründling, A. (2011). Enzymatic activities and functional interdependencies of *Bacillus subtilis* lipoteichoic acid synthesis enzymes. *Molecular Microbiology*, *79*(3), 566–583. https://doi.org/10.1111/j.1365-2958.2010.07472.x

Xu, Q., Abdubek, P., Astakhova, T., Axelrod, H. L., Bakolitsa, C., Cai, X., Carlton, D., Chen, C., Chiu, H.-J., Chiu, M., Clayton, T., Das, D., Deller, M. C., Duan, L., Ellrott, K., Farr, C. L., Feuerhelm, J., Grant, J. C., Grzechnik, A., … Wilson, I. A. (2010). Structure of the γ-d-glutamyl-l-diamino acid endopeptidase YkfC from *Bacillus cereus* in complex with l-Ala-γ-d-Glu: Insights into substrate recognition by NlpC/P60 cysteine peptidases. *Acta Crystallographica Section F: Structural Biology and Crystallization Communications*, *66*(Pt 10), 1354. https://doi.org/10.1107/S1744309110021214

Yamada, S., Sugai, M., Komatsuzawa, H., Nakashima, S., Oshida, T., Matsumoto, A., & Suginaka, H. (1996). An autolysin ring associated with cell separation of Staphylococcus aureus. *Journal of Bacteriology*, *178*(6), 1565–1571. https://www.ncbi.nlm.nih.gov/pmc/articles/PMC177839/

Yamaguchi, H., Furuhata, K., Fukushima, T., Yamamoto, H., & Sekiguchi, J. (2004). Characterization of a new *Bacillus subtilis* peptidoglycan hydrolase gene, yvcE (named cwlO), and the enzymatic properties of its encoded protein. *Journal of Bioscience and Bioengineering*, *98*(3), 174–181. https://doi.org/10.1016/S1389-1723(04)00262-2

Yamamoto, H., Kurosawa, S., & Sekiguchi, J. (2003a). Localization of the Vegetative Cell Wall Hydrolases LytC, LytE, and LytF on the *Bacillus subtilis* Cell Surface and Stability of These Enzymes to Cell Wall-Bound or Extracellular Proteases. *Journal of Bacteriology*, *185*(22), 6666–6677. https://doi.org/10.1128/JB.185.22.6666-6677.2003

Yang, D. C., Peters, N. T., Parzych, K. R., Uehara, T., Markovski, M., & Bernhardt, T. G. (2011). An ATP-binding cassette transporter-like complex governs cell-wall hydrolysis at the bacterial cytokinetic ring. *Proceedings of the National Academy of Sciences of the United States of America*, *108*(45), E1052–E1060. https://doi.org/10.1073/pnas.1107780108

Yang, D. C., Tan, K., Joachimiak, A., & Bernhardt, T. G. (2012). A conformational switch controls cell wall-remodelling enzymes required for bacterial cell division. *Molecular Microbiology*, *85*(4), 768–781. https://doi.org/10.1111/j.1365-2958.2012.08138.x

Zendy, T. M. |, Zendy, D. L. P. |, & Zendy, P. S. |. (1998). *Bacillus subtilis* Cells Lacking Penicillin-Binding Protein 1 Require Increased Levels of Divalent Cations for Growth | Zendy. *Journal of Bacteriology | Zendy*, *180 | Zendy*. https://zendy.io/pdf-viewer/10.1128/jb.180.17.4555-4563.1998

Appendix1. Media and Buffer compositions

Supplementary Table 1.1 Media compotation used throughout this study

Media name	Compositions
LB	10 Tryptone (Oxoid) 5 g Yeast Extract (Difco) 10 g/L NaCl (VWR) pH 7.0 and make up to 1 L H_2O
NB	5 g/L Peptone 2 g/L Yeast Extract 5 g/L Sodium Chloride (NaCl) 15 g/L Agar 1 L H_2O
PAB **(Antibiotic Assay Medium No. 3)**	5 g/L Peptone 1.5 g/L Yeast extract 1 g/L Dextrose 3.5 g/L Sodium chloride 3.67 g/L Dipotassium hydrogen 1.3 g/L Potassium dihydrogen
Minimal media / competent media	10 ml SMM salt 125 µl Glucose (40%), 100 µl Tryptophan 2 mg/ml 60 µl $MgSO_4$ (1 M) 10 µl Casamino acid (20%) 5 µl Iron Ammonium Citrate
Starvation media	10 ml SMM, 125 µl Glucose (40%), 60 µl $MgSO_4$ (1 M)

Supplementary Table 1.2 Buffer component used in this study.

Buffer name	Components
Buffer Solution 1	50 mM Tris (pH 8), 300 mM NaCl, 10 mM Imidazole
Buffer Solution 2	50 mM Tris (pH 6), 300 mM NaCl, 10 mM Imidazole
Buffer Solution 3	50 mM Tris (pH 7), 300 mM NaCl, 10 mM Imidazole
Buffer Solution 4	50 mM Tris (pH 9), 300 mM NaCl, 10 mM Imidazole

Buffer Solution 5	50 mM Tris (pH 8), 600 mM NaCl, 10 mM Imidazole
Buffer Solution 6	8 M urea, 1 tablet PBS dissolve in 100 ml Milli-Q Water
Buffer Solution 7	8 M urea, 1 tablet PBS dissolve in 100 ml Milli-Q Water, 5 mM imidazole.
Wash Buffer 1	50 mM Tris (pH 8), 300 mM NaCl
Wash Buffer 1	50 mM Tris (pH 8), 300 mM NaCl, 5 mM of imidazole
Elution Buffer 1	50 mM Tris, 300 mM NaCl, (5 mM, 10 mM, 25 mM, 50 mM, 100 mM, 150 mM 200 mM 250 mM) Imidazole.
Elution Buffer 2	8M urea, 1 tablet PBS dissolve in 100 ml Milli-Q Water, 100mM imidazole.
Elution Buffer 3	8 M urea, 1 tablet PBS dissolve in 100 ml Milli-Q Water, and 50 mM EDTA.
SDS-loading buffer	10% SDS, 0.125 M Tris-HCL (pH 6.8), 0.01% Bromophenol blue, 40% glycerol, 400 mM DTT in Deionized water
1X Saline sodium citrate (SSC)	1 L distal water, 0.15 M Sodium chloride and 0.01 M Sodium tri-citrate at pH 7.0
Gel loading dye	0.01% Bromophenol blue in 50% glycol
GTE buffer	50 mM glucose, 25 mM Tris, 10 mM EDTA-pH 8
1X Tris-Acetate-EDTA (TAE) buffer	2 M Tris/HCl pH 8.3, 50 mM sodium acetate, 5.7 % acetate
Transfer Buffer	300 mM Tris, 300 mM glycine, 140 mM Tricine, 0.05% SDS, 2.5 mM EDTA.
PBS-T	1 L distal water,10 tablets of Phosphate-buffered saline, 0.5 ml, or 1 ml of Tween 20 0.1%.

Blocking Buffer	5% semi skimmed in PBS-T
Protoplasting buffer	50 mM Tris,100 mM NaCl, 0.5% sucrose-4 mg/ml lysozyme
1.5 M Lithium Chloride	6.36 g Lithium Chloride anhydrase in 100 ml H2O.
100% Trichloroacetic acid	Dissolve 20 g of TCA in 9 ml in Milli-Q® Ultrapure water

Supplementary Table 2.1 Oligonucleotides used in this study

Name	Sequence
oAM001	5'TGCCGCGCGGCAGCCATATGCAAAGCATTAAGGTGAAAAAAGGCGACACG'3
oAM002	5'TTGTTAGCAGCCGGATCTCAATTAGAATCTTTTCGCACCGAGGTAAC'3
oAM003	5'TGCCGCGCGGCAGCCATATGCAAAGCATTAAGGTGAAAAAAGGCGACACG'3
oAM004	5'TGTTAGCAGCCGGATCTCAAGCTTGTTCCTTTCACCTTCAATACT'3
oAM005	5'GGTGCGAAAAGATTCTAATTGAGATCCGGCTGCTAACAAAG'3
oAM006	5'CACCTTAATGCTTTGCATATGGCTGCCGCGCGGCAC'3
oAM007	5'CACCTTAATGCTTTGCATATGGCTGCCGCGCGGCAC'3
oAM008	5'CACCTTAATGCTTTGCATATGGCTGCCGCGCGGCAC'3
oAM009	5'TAAGAAGGAGATATACCATGCAAAGCATTAAGGTGAAAAAAGGCGAC'3
oAM010	5'CAGTGGTGGTGGTGGTGGTGGAATCTTTTCGCACCGAGGTAACG'3
oAM011	5'TAAGAAGGAGATATACCATGCAAAGCATTAAGGTGAAAAAAGGCGAC'3
oAM012	5'CAGTGGTGGTGGTGGTGGTGCACCTTCAATACTTGGTTGACATAGATTACAT'3
oAM013	5'ACCTCGGTGCGAAAAGATTCCACCACCACCACCACCACT'3
oAM014	5'TTTTTCACCTTAATGCTTTGCATGGTATATCTCCTTCTTAAAGTTAAACAAAATTATTTCTAGAGG'3
oAM015	5'TCAACCAAGTATTGAAGGTGCACCACCACCACCACCACT'3
oAM016	5'TTTTTCACCTTAATGCTTTGCATGGTATATCTCCTTCTTAAAGTTAAACAAAATTATTTCTAGAGG'3
oAM017	5'TGCCGCGCGGCAGCCATATGGATAACTCAGTGAAAAGAGTTGGGGGAAG'3
oAM018	5'TTGTTAGCAGCCGGATCTCATTATCTGTAATAAGATACTGTGCCGTCATGAA'3
oAM019	5'TGCCGCGCGGCAGCCATATGGATAACTCAGTGAAAAGAGTTGGGGGAAG'3
oAM020	5'TTGTTAGCAGCCGGATCTCACGGATCAATAAAGATTGTTTCACCTACAACT'3
oAM021	5'CAGTATCTTATTACAGATAATGAGATCCGGCTGCTAACAAAG'3
oAM022	5'TCTTTTCACTGAGTTATCCATATGGCTGCCGCGCGGCACCAG'3
oAM023	5'AAACAATCTTTATTGATCCGTGAGATCCGGCTGCTAACAAAGC'3
oAM024	5'TCTTTTCACTGAGTTATCCATATGGCTGCCGCGCGGCACCAG'3
oAM025	5'TAAGAAGGAGATATACCATGGATAACTCAGTGAAAAGAGTTGGGGGAAG'3
oAM026	5'CAGTGGTGGTGGTGGTGGTGTCTGTAATAAGATACTGTGCCGTCATGAATAGC'3
oAM027	5'TAAGAAGGAGATATACCATGAGAGTTGGGGGAAGCAATAGATACG'3
oAM028	5'CAGTGGTGGTGGTGGTGGTGTACAACTGGATTCTTTAGCTGATTAGCAACCT'3
oAM029	5'GCACAGTATCTTATTACAGACACCACCACCACCACCACT'3

oAM030	5’ACTCTTTTCACTGAGTTATCCATGGTATATCTCCTTCTTAAAGTTAAACAAAATTATTTCTAGAG’3
oAM031	5’AGCTAAAGAATCCAGTTGTACACCACCACCACCACCACT’3
oAM032	5’CTATTGCTTCCCCCAACTCTCATGGTATATCTCCTTCTTAAAGTTAAACAAAATTATTTCTAGAGG’3
oAM033	5’TGCCGCGCGGCAGCCATATGGCCGCGTATACCGACTACTCACTATATAAAGTAGAGCCG’3
oAM034	5’TTGTTAGCAGCCGGATCTCATTATCGATATTCCGGAACATCAAAATAAAGTGTATAACC’3
oAM035	5’ATGTTCCGGAATATCGATAATGAGATCCGGCTGCTAACAAAG’3
oAM036	5’GTAGTCGGTATACGCGGCCATATGGCTGCCGCGCGGCACCAG’3
oAM037	5’TGCCGCGCGGCAGCCATATGGCAACGATTAAGGTCAAAAGCGGAG’3
oAM038	5’TTGTTAGCAGCCGGATCTCATTAGAAATATCGTTTTGCACCGAGATAGC’3
oAM039	5’GTGCAAAACGATATTTCTAATGAGATCCGGCTGCTAACAAAG’3
oAM040	5’GCTTTTGACCTTAATCGTTGCCATATGGCTGCCGCGCGGCACCAG’3
oAM041	5’TAAGAAGGAGATATACCATGGAAACATTAGATGAAAAGAAACAAAAAATCGAAAGC’3
oAM042	5’CAGTGGTGGTGGTGGTGGTGTTGAACAACACGTCTTACAACACCTTTAAATG’3
oAM043	5’TTGTAAGACGTGTTGTTCAACACCACCACCACCACCAC’3
oAM044	5’TTCTTTTCATCTAATGTTTCCATGGTATATCTCCTTCTTAAAGTTAAACAAAATTATTTCTAGAG’3
oAM045	5’GGTGCGAAAAGATTCTCCGGATCAGGCAGCGGA’3
oAM046	5’GATTTGCTTTTTCATAGATGCATTTTATGTCATATTGTAAGTAAGTTGCAC’3
oAM047	5’GTGAAAGGAACAAGCTCCGGATCAGGCAGCGGA’3
oAM048	5’ACATAAAATGCATCTATGAAAAAGCAAATCATTACAGCTACGACA’3
oAM049	5’GCTGCCTGATCCGGAGAATCTTTTCGCACCGAGGTAACG’3
oAM050	5’GCTGCCTGATCCGGAGCTTGTTCCTTTCACCTTCAATAC’3
oAM051	5’ACAGTATCTTATTACAGATCCGGATCAGGCAGCGGA’3
oAM052	5’TTTTATATAAGAACGCAAAGATGCATTTTATGTCATATTGTAAGTAAGTTGCAC’3
oAM053	5’GTAGGTGAAACAATTCCGGATCAGGCAGCGGA’3
oAM054	5’ATGACATAAAATGCATCTTTGCGTTCTTATATAAAAGTCCTAACAATGTGTTTT’3
oAM055	5’TCCGCTGCCTGATCCGGATCTGTAATAAGATACTGTGCCGTCATG’3
oAM056	5’GCTGCCTGATCCGGAATTGTTTCACCTACAACTGG’3
oAM057	5’TGGTGAACTACTATGTTGAAAAAGAAAAACATTTATTCAATTCGTAAACTAGGTG’3
oAM058	5’ACCTGACTGCCGCTATTATAGTTCGCGACGACGTCCAG’3
oAM059	5’ACCTGACTGCCGCTAGACATGTACTCCGTTGCCGTCTTCTTTACC’3
oAM060	5’CATAGTAGTTCACCACCTTTTCC’3
oAM061	5’TAGCGGCAGTCAGGTGGCACTTTTC’3
oAM062	5’ATTATATAGGGAAAAGGTGGGAGTTAACATTTGGGGAGGAAAATATGAAAAAGC’3

oAM063	5’TGTTGAGCTTCATCGTGTTGCACCTTCAATACTTGGTTGACATAGATTACAT’3
oAM064	5’TCAACCAAGTATTGAAGGTGCAACACGATGAAGCTCAACAAAATGCTTTTTATCA’3
oAM065	5’TCCTCCCCAAATGTTAACTCCCACCTTTTCCCTATATAATTGTGAGC’3
oAM066	5’CAATTATATAGGGAAAAGGTGAGTTAACATTTGGGGAGGAAAATATGAAAAAGC’3
oAM067	5’TGAGCTTCATCGTGTTGCGCCACCTTCAATACTTGGTTGACATAGATTACAT’3
oAM071	5’CATATTTTCCTCCCCAAATGTTAACTCACCTTTTCCCTATATAATTGTGAG’3
oAM072	5’TCAACCAAGTATTGAAGGTGGCGCAACACGATGAAGC’3
oAM073	5’ATTATATAGGGAAAAGGTGGGCCATTTAAGGAGGAAATCAATTGCG’3
oAM074	5’TGTTGAGCTTCATCGTGTTGGATTGTTTCACCTACAACTGGATTCTTTAGCT’3
oAM075	5’CAGTTGTAGGTGAAACAATCCAACACGATGAAGCTCAACAAAATGCTTTT’3
oAM076	5’TGATTTCCTCCTTAAATGGCCCACCTTTTCCCTATATAATTGTGAGCG’3
oAM077	5’AATTATATAGGGAAAAGGTGGCCATTTAAGGAGGAAATCAATTGCG’3
oAM078	5’TGAGCTTCATCGTGTTGCGCCGGATCAATAAAGATTGTTTCACCTACAAC’3
oAM079	5’AAACAATCTTTATTGATCCGGCGCAACACGATGAAGCT’3
oAM080	5’TGATTTCCTCCTTAAATGGCCACCTTTTCCCTATATAATTGTGAGCG’3
oAM081	5’GATAACAATTAAGCTTAGTCGAAATTAAAAGGAGGTCATCAGCCATGAAAAAGCAAATCATTACAGCTACG’3
oAM082	5’TGCGGCTAGCTGTCGACTAAGCTTTTAGAATCTTTTCGCACCGAGGTAACG’3
oAM083	5’GATAACAATTAAGCTTAGTCGAAATTAAAAGGAGGTCATCAGCCATGAAAAAGAAATTAGCAGCA’3
oAM084	5’TGCGGCTAGCTGTCGACTAAGCTTTTAGAAATATCGTTTTGCACCGAG’3
oAM085	5’GATAACAATTAAGCTTAGTCGAAATTAAAAGGAGGTCATCAGCCGTGAGAAAGAGTTTAATTACACTTG’3
oAM086	5’TGCGGCTAGCTGTCGACTAAGCTTTTATTGAACAACACGTCTTACAACACC’3
oAM087	5’ACGTCATCTACATCAGGCGGAATTGAAGGCGCGATCAGCG’3
oAM088	5’GGTGTTGTAAGACGTGTTGTTCAATAACACTGTAGGGATAGTGGAAAGAGTG’3
oAM089	5’CGCTGATCGCGCCTTCAATTCCGCCTGATGTAGATGACGTTTTGCTGCTT’3
oAM090	5’GGTGTTGTAAGACGTGTTGTTCAACACTGTAGGGATAGTGGAAAGAGTG’3
oAM091	5’TGATGTAGATGACGTGGTGTTTGAAGAACCGGATGA’3

oAM092	5’CTCCGGCAAATCCTTCGAAAACAAACAG’3
oAM093	5’TAAGCGAGATCTGCTATAAAATTATTCTCC’3
oAM094	5’CTGTGATCTAGAAACCAAATACTATTCACAGCG’3
oAM095	5’GACTACTCGAAAGCCTTGTTGTCTGTTACAC’3
oAM096	5’ACAACTTCAGGCTTTGACAGCAGCGGATTCATTTGG’3
oAM097	5’CGTTCCGCCCCATTTATATGGCGTTCC’3
oAM098	5’AACACGATATTCACGGTTTAC’3
oAM099	5’CGTCAACGTAATGCATTCTCTCG’3

Appendix 3. Mass spectrometry analysis for pull-down

This section was written by Dr.Pawel Palmowski/ Experimental Scientific Officer

Sample preparation

To permit MS analysis of the pull-down samples, the protein was digested on S-Trap micro spin columns (Protifi). Sample volumes were reduced in a centrifugal concentrator to a final volume of ~20 ml and mixed with an equal volume of 2x concentrated S-trap lysis buffer (10% SDS in 100 mM triethylammonium bicarbonate (TEAB) pH 8.5). Proteins were the chemically reduced with dithiothreitol (DTT) at final concentration of 20 mM (65ºC, 30 min) and cysteines were alkylated by incubation with iodoacetamide (40 mM final concentration) for 30min at room temperature in dark. The samples were then acidified by adding 27.5% phosphoric acid to a final concentration of 2.5% (v/v). This processed material was then loaded onto spin columns by dilution into 6 volumes of loading buffer (90% methanol 100 mM TEAB pH 8) and centrifugation at 4000 x g for 30s. The columns were then washed with loading buffer (three times) and the flow through discarded. Protein on the column were then digested with 1ug of trypsin (Worthington) in 50 mM TEAB pH 8.5 for 1. 5h at 47ºC. This resulted in the production of peptides that were eluted with three washes of the trap: first 50 ml 50 mM TEAB, second 50 ml 0.2% formic acid and finally with 50 ml 50% acetonitrile with 0.2% formic acid. The solution was then frozen then dried in a centrifugal concentrator before being reconstituted in 10 ml of 0.2% formic acid

Data Independent Acquisition (DIA)

For each sample, 2.5 ml was loaded per LCMS run (using an UltiMate 3000 RSLCnano HPLC), initially onto an Acclaim PepMap100 C18 LC Column (5 mm Ã…~ 0.3 mm i.d., 5 Î¼m, 100 Ã…, Thermo Fisher Scientific) at a flow rate of 10 Î¼L min-1 maintained at 45°C and then separated on a 50 cm RP-C18 ÂµPACâ„¢ column (PharmaFluidics) using a 60 min gradient from 97 % A (0.1 % FA in 3 % DMSO) and 3% B (0.1 % FA in 80 % ACN 3 % DMSO), to 35 % B, at a flow rate of 400 nL min-1. The separated peptides were then injected into Exploris 480 via Thermo Scientific Î¼PAC compatible EasySpray emitter and analysed using data independent (DIA) acquisition. at a temperature of 320ºC, spray voltage 1500 V. The total LCMS run time was 90 min. Orbitrap full scan resolution was 60,000, RF lens 50%, Normalised ACG Target 300 %, scan range 390-1600 m/z. DIA MSMS were acquired with 49 variable m/z windows covering 390- 1671

m/z, at 30000 resolution, dynamic maximum injection time with ACG target set to 3000, and normalized collision energy level of 30%.

Data processing

The acquired data was analysed in DIA-NN version 1.8 (DIA-NN: neural networks and interference correction to enable deep proteome coverage in high throughput (Nature Methods, 2020) against B. subtilis proteome database (Uniprot UP000001570-2023_10_22) combined with common Repository of Adventitious Proteins (cRAP) with the settings: Fragment m/z: 200-1800, enzyme: Trypsin, allowed missed-cleavages: 1, peptide length: 6-30, precursor m/z 300-1250, precursor charge: 2 -4, Fixed modifications: carbamidomethylation (C), Variable modifications:Oxidation (M), no normalisation, Match Between Runs: off. With the report was generated and exported into text file. Protein information was extracted using an in-house R script and further processed in Perseus software package (version 1.6.15.0, https://maxquant.net/perseus/).The date was transformed into Log 2 and proteins containing too many missing values were filtered out (at least one experimental group with no missing values required). The remaining missing values were imputed by random selection from the left tale of the normal distribution (1.8 SD form the samples mean and 0.3 SD wide). After this processing the differences between groups have been assessed using ANOVA followed by a Tukey's PostHoc test. Additionally, LytC expression profile has been extracted from the dataset along with top 3 best correlating proteins.

Appendix 4. Autolytic enzymes abundance in different growth phase

In this study, the specific antisera were used to examine the level of LytE, LytF, and LytC throughout the various growth phases under different media conditions (magnesium/ glucose) and genetic backgrounds (168CA, Δ*ponA*, Δ*mprF,* Δ*sigI,* and Δ*sigM).* Strains were incubated at 37°C, and the cell samples were collected at 30-minute intervals. The growth curve of these strains is shown in Figure 3.20. Samples were then analysed by Western blot, and the results indicate a remarkable consistency in the protein abundance throughout the growth curve as shown in Supplementary Figure 1, 2, and 3. Therefore, we decide to be focused on samples collected at the mid-explorational phase as shown in Figure 3.21, 3.22, and 3.23.

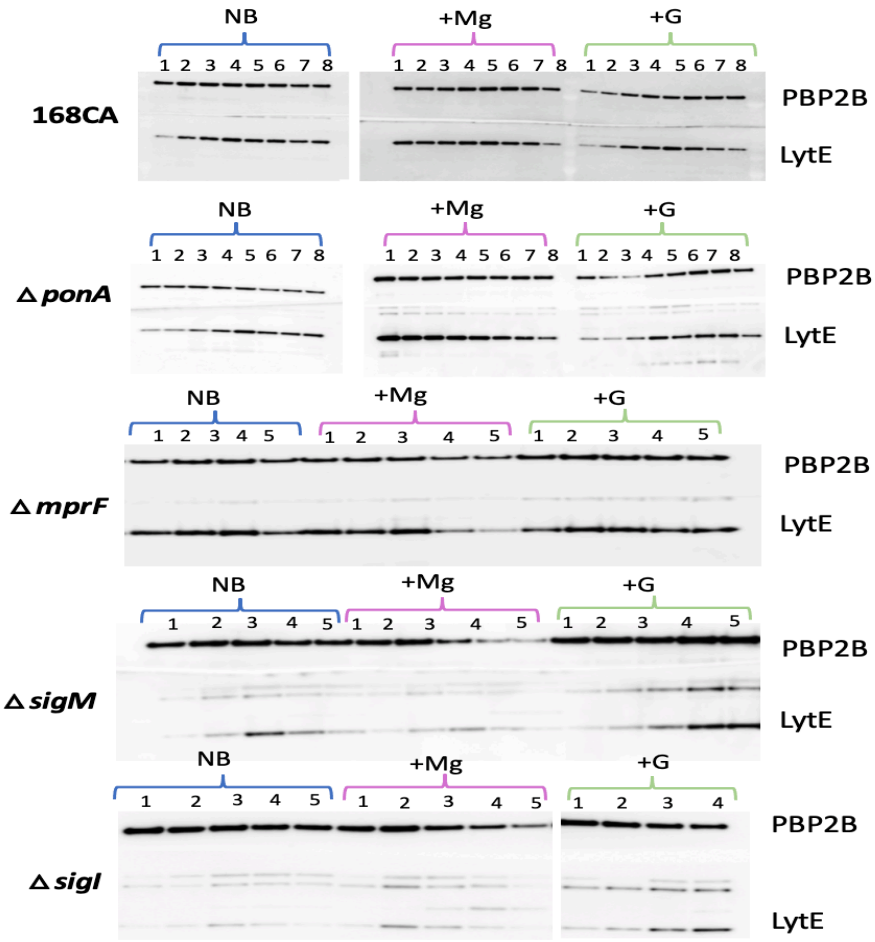

Supplementary Figure 4.1. Abundance of LytE across different growth phases

Samples were collected each 30-minute intervals then running in SDS-PAGE to subjected to Western blot analysis. LytE-antiserum (1/5000) and the loading control PBP2B (1/10,000) were used.

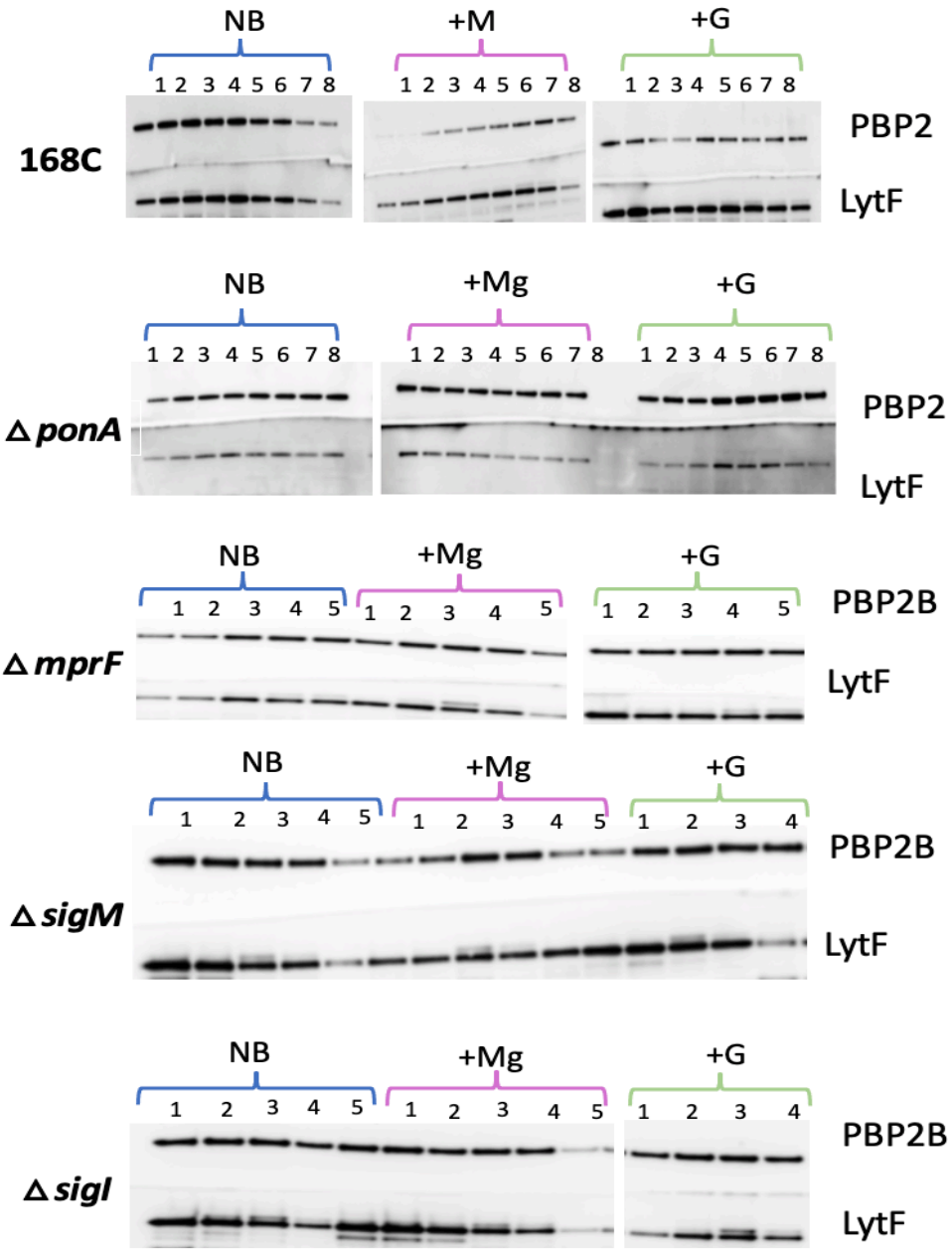

Supplementary Figure 4.1. Abundance of LytF across different growth phases

Samples were collected each 30-minute intervals then running in SDS-PAGE to subjected to Western blot analysis. LytF-antiserum (1/2000) and the loading control PBP2B (1/10,000) were used.

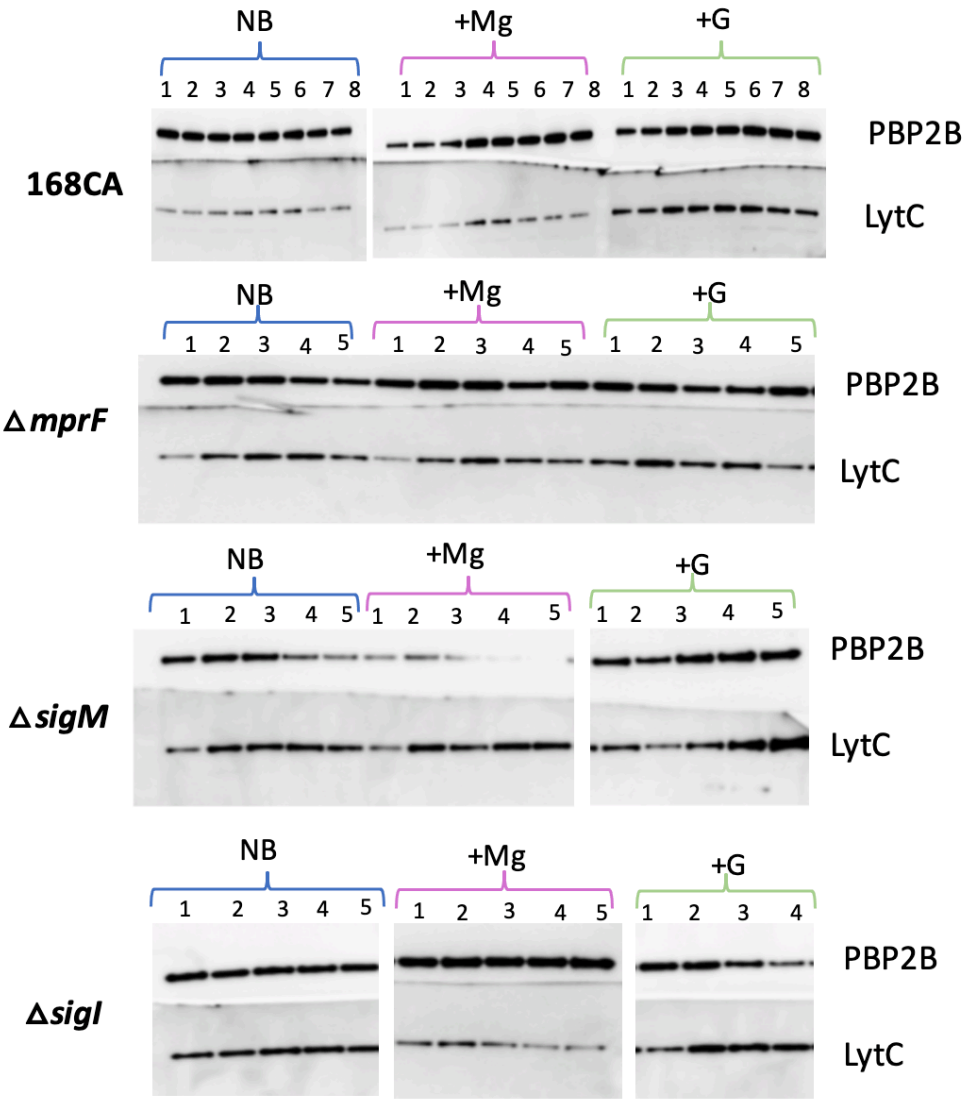

Supplementary Figure 4.3. Abundance of LytC across different growth phases

Samples were collected each 30-minute intervals then running in SDS-PAGE to subjected to Western blot analysis. LytC-antiserum (1/2000) and the loading control PBP2B (1/10,000) were used.

Appendix 5. Extracellular proteases intensity in *lytE* and *cwlO* background

Previously, it has been found that a double mutant of *lytE cwlO* is lethal, even though it is believed that these two protein are activated at different localisations of the cell wall (Bisicchia *et al*., 2007; Carballido-López *et al*., 2006; Meisner *et al*., 2013). LytE might be active at the outer surface, while CwlO might be active close to the cell membrane. Meisner *et al.,* 2013 showed that CwlO remained at the outer surface of the cytoplasmic membrane via an interaction that requires its coiled-coil domain. Therefore, in the absence of LytE activity, CwlO might be able to able to compensate for LytE activity, and to do that, it is believed that CwlO must cleave off and release from the inner layer. From the mass spectrometry data shows significant changes in abundance in some of the extracellular proteases, either in lacking cwlO or lytE background (Supplementary figure 4). Based on this, the hypothesis here is the extracellular proteases cleave the *cwlO*, and then the *cwlO* be able to perform the function of *lytE* at the outer surface.

From our mass spectrometry data, in either *lytE* or *cwlO* background, we noticed significant changes in abundance in some of the extracellular proteases (Epr-Bpr-NprE-Mpr) (Supplementary figure 4). Based on this, we hypothesized that the extracellular proteases are needed to cleave and release CwlO, allowing cwlO be able to perform the function of LytE at the outer surface of the cell wall.

Supplementary Table 5.1 Extracellular proteases in *B. subtilis.*

Name	Describe
AprE	major extracellular/serine protease (subtilisin E)
Bpr	serine protease (bacillopeptidase F)
Mpr	metalloprotease
Epr	minor extracellular serine protease
NprB	metalloprotease
NprE	Metalloprotease/ second major extracellular/ ΔaprE nprE reduce the activity of protease
Vpr	minor extracellular protease/serine protease
WprA	wall-associated serine protease/ Secreted protein quality control

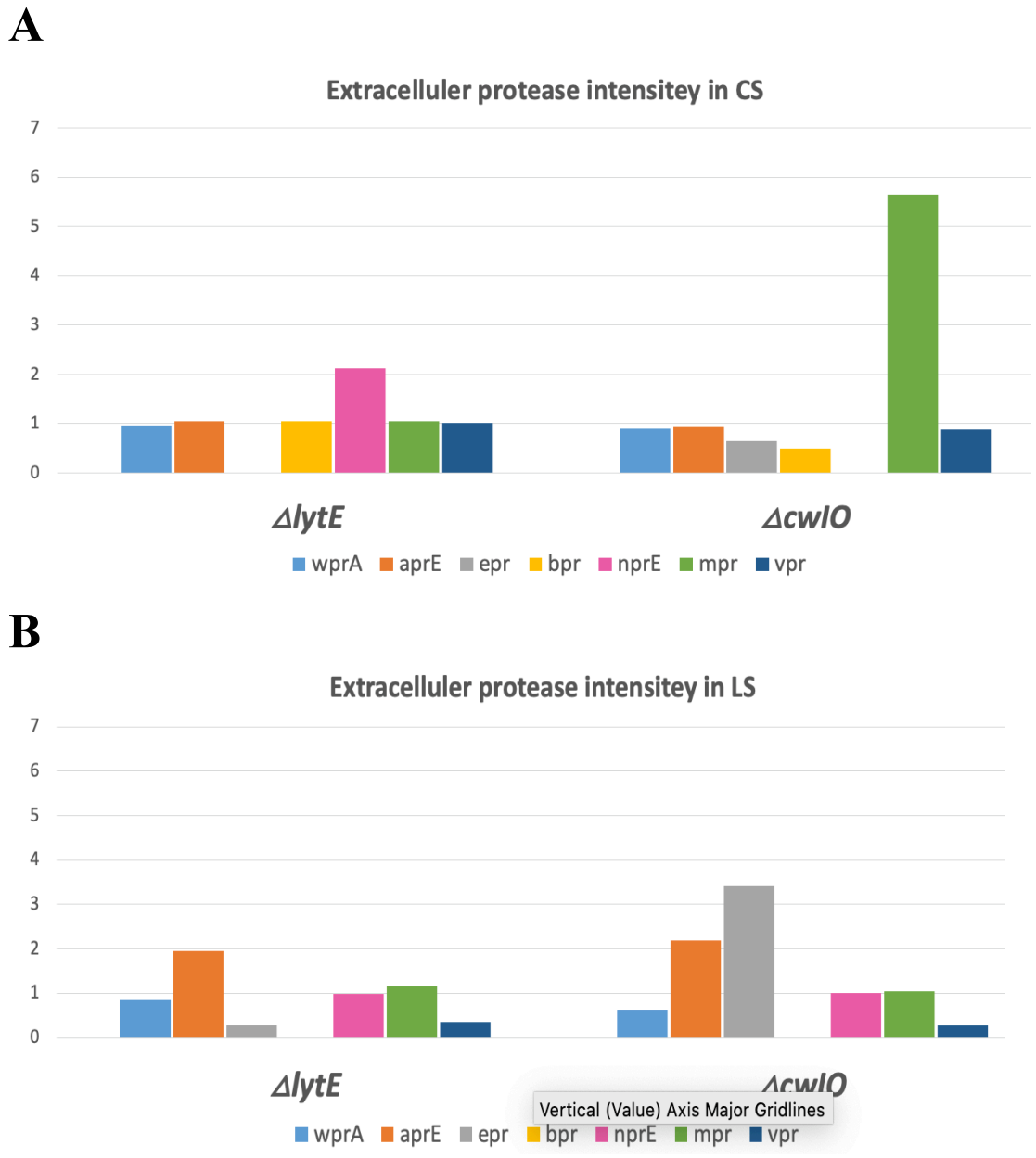

Supplementary Figure 5.1. Extracellular proteases intensity in *ΔlytE and ΔcwlO.*

Strains were grown overnight in LB media at 30°C. On a flowing day, the strains were diluted in minimal media for 2h at 37°C, then diluted back to OD_{600}-o.05 in fresh minimal media and incubated at 37°C until they reached OD_{600}-0.7. Samples were collected and separated into two groups; one was the culture supernatants (CS) (A), and the other pellet was treated with 1.5M LiCl (LS) (B). All samples were then precipitated in TCA and sent to mass spectrometry for analysis. The intensity of the AprE, NprE, Bpr, Epr, Mpr, NprB, Vpr, and WprA, in Δ*lytE* and Δ*cwlO* was normalized and compared to the wild-type strain 168CA. the Extracellular proteases intensity in 168CA as indicated as 1 on the graph.

In order to examine the role of the extracellular protease in the functional redundancy between lytE and cwlO, the BRB08 strain from Pohl *et al*., 2013 was used, which had the

eight extracellular proteases deleted (*trpC2 ΔnprB, ΔaprE, Δepr, Δbpr, ΔnprE, Δmpr, Δvpr*, *ΔwprA*). Either LytE or CwlO were then knocked into the BRB08 background strain to generate sAM023 (BRB08-Δl*ytE*) and sAM024 (BRB08-ΔcwlO), respectively. It was expected that these newly generated strains, sAM023 and sAM024, would be lethal according to the hypothesis. However, both strains (BRB08-Δl*ytE* and BRB08-Δ*cwlO*) were grown normally. It was found that LytF is partially redundant for LytE (A. Aljohani, unpublished); however, deleting *lytF* from the BRB08-Δl*ytE* strain was still viable. The morphological phenotype of these strains was detected under a fluorescence microscopy using FM dye. Cells in the BRB08 strain seem to have division defects; however, introducing either Δ*lytE* or Δ*lytE* Δ*lytF* to BRB08 strain showed no significant difference. In BRB08-Δ*cwlO,* cells gained the Δ*cwlO* phenotype, becoming shorter and wider compared to the BRB08. These results suggest that the extracellular protease do not play a role in the synthetic lethality of the double mutant *lytE cwlO*.

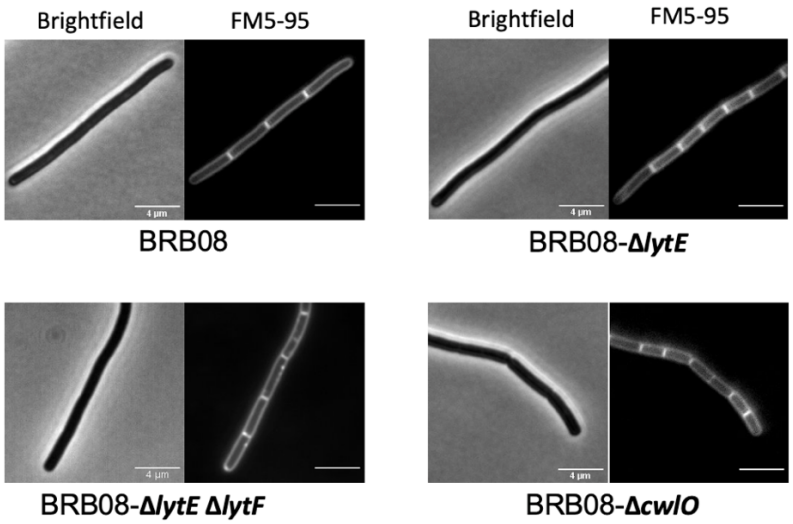

Supplementary Figure 5.2 Extracellular protease morphology in the deletion of *lytE, lytE lytF,* and *cwlO*

BRB08, BRB08-ΔlytE, BRB08-ΔlytE ΔlytF, and BRB08-ΔcwlO strains were grown in minimal media at 37°C. Cells at the mid-exponential phase were stained with FM5-95 and imaged taken by the fluorescent microscopy. Scale bar is 4 microns.